

UC Irvine

UC Irvine Electronic Theses and Dissertations

Title

CO₂ Binding by a Bifunctional Guanidine and Bifunctional Alcohol Employing Chelate Cooperativity AND Palladium-Catalyzed Enantioselective Carbene Insertion into the N-H Bonds of Aromatic Amine Heterocycles and Non-Conjugated Amines

Permalink

<https://escholarship.org/uc/item/9q21g80q>

Author

Hiew, Stanley C.

Publication Date

2019

Peer reviewed|Thesis/dissertation

UNIVERSITY OF CALIFORNIA,
IRVINE

CO₂ Binding by a Bifunctional Guanidine and Bifunctional Alcohol
Employing Chelate Cooperativity

and

Palladium-Catalyzed Enantioselective Carbene Insertion into the N–H Bonds
of Aromatic Amine Heterocycles and Non-Conjugated Amines

DISSERTATION

submitted in partial satisfaction of the requirements
for the degree of

DOCTOR OF PHILOSOPHY

in Chemistry

by

Stanley C. Hiew

Dissertation Committee:
Professor David Van Vranken, Chair
Professor Elizabeth R. Jarvo
Professor Zhibin Guan

2019

Chapter 1 is reproduced in part with permission from:
Rachel Steinhardt, Stanley C. Hiew, Hemakesh Mohapatra, Du Nguyen, Zachary Oh, Richard
Truong, and Aaron Esser-Kahn. "Cooperative CO₂ Absorption Isotherms from a Bifunctional
Guanidine and Bifunctional Alcohol." *ACS Central Science*, **2017**, 3, 1271-1275.
url: <https://pubs.acs.org/doi/abs/10.1021%2Facscentsci.7b00418>
Copyright 2017 American Chemical Society.

Chapter 2 is reproduced in part with permission from:
Vanessa Arredondo, Stanley C. Hiew, Eugene S. Gutman, Iilandari Udara Premachandra, and
David L. Van Vranken. *Angewandte Chemie International Edition*, **2017**, 56, 4156-4159.
Copyright 2017 Wiley-VCH Verlag GmbH & Co. KGaA.

All other materials © 2019 Stanley C. Hiew

Table of Contents

	Page
List of Figures	v
List of Tables	ix
Acknowledgements	x
Curriculum Vitae	xii
Abstract of the Dissertation	xvi
Chapter 1: CO₂ Binding by a Bifunctional Guanidine and Bifunctional Alcohol Employing Chelate Cooperativity	
Effect of CO ₂ on Climate	1
Political Barriers to Reducing CO ₂ Emissions	2
Carbon Capture and Sequestration	2
Synthesis and Evaluation of CO ₂ Binding by a Solution Phase Bifunctional System	5
Molecular Dynamics Simulations	14
Thermodynamic Model	16
<i>Monofunctional System</i>	16
<i>Bifunctional System</i>	20
<i>Bifunctional System with Precipitation</i>	27
Conclusion	33
Experimental Section	34
References	41

	Page
Chapter 2: Palladium-Catalyzed Enantioselective Carbene Insertion into the N–H Bonds of Aromatic Amine Heterocycles	
Introduction	43
Key Advances in Transition Metal Catalyzed Carbene Insertion into N–H Bonds	43
<i>N</i> -Substituted Heterocycles and Aliphatic Amines as Common Pharmacophores	46
Carbazole Reaction Optimization, Substrate Scope, and Pharmacophore Synthesis	48
Indole Reaction Optimization and Substrate Scope	54
Conclusion	58
Experimental Section	59
References	89
Chapter 3: Palladium-Catalyzed Enantioselective Carbene Insertion into the N–H Bonds of Cyclic Aliphatic and Non-Conjugated Amines	
Introduction	92
Optimization of Reaction Conditions for Aliphatic and Non-Conjugated Amines	93
Mechanistic Model of Palladium-Catalyzed Carbene N–H Insertion	99
Further Reaction Optimization and Development of a Parallel Slow-Addition Procedure	101
Kinetic Model of Palladium-Catalyzed N–H Insertion Reaction	108
Derivation of Rate Expressions from the Kinetic Model	111

	Page
Conclusion	112
Experimental Section	113
References	140

List of Figures

	Page
Chapter 1: CO₂ Binding by a Bifunctional Guanidine and Bifunctional Alcohol Employing Chelate Cooperativity	
Figure 1-1: Global primary energy consumption by fuel (1965-2017).	2
Figure 1-2: Processes for reversible CO ₂ capture.	3
Figure 1-3: Comparison of hyperbolic and sigmoidal binding isotherms.	4
Figure 1-4: Concept for CO ₂ binding illustrated with a bifunctional alcohol (AA) and bifunctional guanidine (GG)	5
Figure 1-5: Synthesis of a bifunctional amidine with three-carbon linker	6
Figure 1-6: Side products obtained from competing cyclization	7
Figure 1-7: Incomplete reaction of an <i>N,N</i> -dimethyl substituted diamine to obtain a mixture of difunctionalized and monofunctionalized guanidines	7
Figure 1-8: Successful two-step synthesis of a bifunctional guanidine	8
Figure 1-9: Absorption isotherms of bifunctional guanidine 1.7 and 1,5-pentanediol. <i>(a) Experimentally measured absorption isotherms in bis(2-methoxyethyl) ether</i> <i>(b) Example output of a thermodynamic model based on chelate cooperativity</i>	9
Figure 1-10: Comparison of infrared spectra of the bifunctional guanidine, 1,5-pentanediol, and the precipitated viscous phase.	10

	Page
Figure 1-11: Comparison of bifunctional and monofunctional systems in solvents of differing polarity	11
Figure 1-12a: Alkylcarbonate species formed after equilibration under 1 atm CO ₂	13
Figure 1-12b: ¹ H NMR spectra before and after 1 atm CO ₂ exposure	
Figure 1-12c: Change in relative peak areas	
Figure 1-12d: Ratio of bisalkylcarbonate A ⁻ A ⁻ to monoalkylcarbonate A ⁻ A versus solvent composition.	
Figure 1-13: Docking between a bisalkylcarbonate molecule and bisguanidinium molecule.	15
Figure 1-14: Snapshot of example MD simulation at 50 ns, with dimeric aggregates highlighted.	15
Figure 1-15: Coupled equilibrium model for the monofunctional system	16
Figure 1-16: Example outputs of equation 1.3.	20
Figure 1-17: Coupled equilibrium model for bifunctional system	21
Figure 1-18: Example plots of equation 3 for various values of AA _i , K ₀ , and EM	26
Figure 1-19: Example plot of equation 7 for a low-to-high affinity transition, bounded by corresponding low-affinity and high-affinity cases.	27
Figure 1-20: Coupled equilibrium model for the bifunctional system accounting for phase separation.	28
Figure 1-21: Comparison of solution phase concentrations of unreacted bifunctional alcohol (AA) and bifunctional guanidine (GG)	31
Figure 1-22: Component of CO ₂ saturation contained in the precipitated and solution phases.	32

	Page
Figure 1-23: Example plots of total saturation varying K_0 , K_{sp} , and both variable simultaneously.	33
Figure 1-24: Selective precipitation of bisguanidinium chloride salt.	37
Chapter 2: Palladium-Catalyzed Enantioselective Carbene Insertion into the N–H Bonds of Aromatic Amine Heterocycles	
Figure 2-1: Generation and reactivity of late transition metal carbene towards an amine nucleophiles	43
Figure 2-2: Early examples of transition metal-catalyzed carbene insertion into N–H bonds	44
Figure 2-3: Early examples of stereoselective cyclizations employing carbene insertion into N–H bonds	45
Figure 2-4: First example of enantioselective intermolecular carbene insertion into an aniline N–H bonds and subsequent optimization	45
Figure 2-5: Examples of enantioselective insertion using chiral acid and base additives	46
Figure 2-6: Biologically active <i>N</i> -substituted heterocyclic and aryl amines with chiral C(sp ³) centers	47
Figure 2-7: Scope of reaction with various carbazole substrates	50
Figure 2-8: C–H insertion observed when insertion at nitrogen is blocked	51
Figure 2-9: Ligand screen for insertion into 1-methoxycarbazole	52
Figure 2-10: Palladium catalyzed elimination of alkyl diazoacetates to alkenes	53
Figure 2-11: Synthesis of the core of 5-HT ₆ receptor antagonist	54

	Page
Figure 2-12: Alternative cyclization procedure	54
Figure 2-13: Regioselectivity of insertion with indole	55
Figure 2-14: Indole substrate scope	56
Figure 2-15: X-ray structures of carbazole and indole derivatives	56
Figure 2-16: Diminished yield and ee observed using pyrazole	57
Figure 2-17: ¹ H NMR experiments showing displacement of palladium(II)-bound (S,S)- <i>i</i> -Pr-PyBOX ligand by 4-methylpyrazole	58
Chapter 3: Palladium-Catalyzed Enantioselective Carbene Insertion into the N–H Bonds of Cyclic Aliphatic and Non-Conjugated Amines	
Figure 3-1: Optimized conditions for enantioselective insertion into aniline perform poorly with benzylamine and cyclohexylamine	92
Figure 3-2: Racemization of a carbazole derivative by piperidine	94
Figure 3-3: Testing the racemization of (<i>S</i>)-clopidogrel by the amine substrate	95
Figure 3-4: Mechanistic model for palladium-catalyzed carbene insertion into an amine N–H bond	99
Figure 3-5: Photograph of experimental setup employing parallel slow addition	104
Figure 3-6: 1,2-Stevens shift observed during reaction with benzhydrylamine	108
Figure 3-7: Kinetic model for palladium-catalyzed insertion into N–H bond	109
Figure 3-8a: Model run with Pd _i = 10 mol %, no supplemental Pd added	110
Figure 3-8b: Comparison of model run with Pd _i = 10 mol % + 10 mol % supplemental Pd versus Pd _i = 20 mol%	

List of Tables

	Page
Chapter 1: CO₂ Binding by a Bifunctional Guanidine and Bifunctional Alcohol Employing Chelate Cooperativity	
Table 1-1: Acquisition and processing parameters for solvent titration 1H NMR	38
Table 1-2: Tabulated data for the NMR solvent titration experiment	40
Chapter 2: Palladium-Catalyzed Enantioselective Carbene Insertion into the N–H Bonds of Aromatic Amine Heterocycles	
Table 2-1 Optimization of carbene insertion into carbazole	49
Chapter 3: Palladium-Catalyzed Enantioselective Carbene Insertion into the N–H Bonds of Cyclic Aliphatic and Non-Conjugated Amines	
Table 3-1: Conditions optimized for aromatic heterocycles applied to a thienopiperidine substrate	93
Table 3-2: Initial catalyst and ligand/additive combinations screened using slow amine addition.	98
Table 3-3: Further optimization using slow amine addition and chiral guanidine additive	101
Table 3-4: Solvent screen in N–H insertion	103
Table 3-5: Further optimization using the amine as the limiting reagent	104
Table 3-6: Screen against panel of chiral guanidine derivatives	105
Table 3-7: Substrate scope employing dual syringe pump addition	107

Acknowledgements

First, I thank God for the opportunity to take this journey, for the many friends and mentors I have made along the way, for personal growth, for being able to learn and to teach.

I would like to acknowledge Professor Aaron Esser-Kahn for overseeing the first part of my doctoral studies. I am grateful for the humility, perseverance, and moral steadfastness that I learned through this period in my life.

Thank you to my committee chair and Ph.D. advisor professor David Van Vranken, for always demanding the highest level of scholarship, and for compassion during challenging periods in the Ph.D. program. It was a pleasure to TA graduate courses and COSMOS with you. Thank you for your tireless consistency and always being an advocate for your students.

Thank you to my other committee members, professors Zhibin Guan and Elizabeth Jarvo. Zhibin, thank you for being one of the first to welcome me to this campus. I still remember your hospitality during the inaugural summer materials program. Thank you also for keeping in touch throughout my stay here and always greeting me with a smile. Liz, thank you for being there for me when I was transitioning labs. Your kindness made a big difference during that difficult period.

Thank you to my lab mates for being great co-workers and great friends. Gene, I won't forget spending hours together doing spectroscopy homework, and grabbing In-N-Out milkshakes after the marathon final exam. Thank you for having me over to your apartment and for making me a believer in cryptocurrencies. Vanessa, who knew deprotecting a methyl group would be so hard? Thank you for always being there to listen and putting up with my messiness. Thank you for taking me to the Anteatory and bringing me items from the \$1 menu. Your perseverance is remarkable, keep moving forward and never give up. Aaron, thanks for helping me with bioassays and getting onboard the antifungal project. I appreciate your political opinions, though I may not always agree. Thanks for taking care of safety and waste, I know they're among the least glorious of group jobs.

Thank you to the many undergraduates that have helped me in research: Zach, Richard, Marlon, Henry, Michelle, Bill, An. You've done an amazing job learning new skills and growing as critical thinkers. Thanks for working hard even though the reward might not seem tangible in the moment. I hope you all go on to do amazing things for the world, in whatever role you choose to pursue.

Thank you also Patrick, Marina, Cassidy, and Steven. I'll remember make-your-own sushi night, and pictionary telephone. Thanks for being thoughtful and saying Hi when you walk into the

lab, and for getting group meeting food when I could not. Pat, thank you for sitting with me while I got my computer fixed.

Thank you to the many students I've had the privilege to teach in classes or labs over the years. Your optimism and positivity have kept me going.

Thank you Jay for always being source of positivity at the physical sciences store.

Thank you Sach, Shwetha, Paul, Troy, for being friends through all these years. Sach, thanks for the beautiful hike to Potato Chip Rock, and letting us pilfer snacks from Google HQ.

Thank you Janine for the many memories, I hope you find peace and happiness moving forward.

Thank you to my church community, whose love and kindness restores me and helps me keep things in perspective.

Thank you Magda, for providing a welcoming environment to live, and for inviting me to your family Thanksgiving celebrations.

Thank you to my family for being present in my life. Thank you mom for showing love through home-cooked meals. Thank you dad for providing through all the years. Thanks to Amanda and David for taking time to travel to Irvine, and for hosting me when I return to the bay area.

Curriculum Vitae

Stanley C. Hiew

Education

University of California, Irvine; September 2012-June 2019

- Ph.D. in chemistry with emphasis in materials chemistry and synthetic organic methodology

Santa Clara University (Santa Clara, CA); September 2008-June 2012

- Bachelor of Science in Chemistry, summa cum laude

Teaching Experience

CHEM 51A, 51B, 51C

- Teaching assistant for introductory organic chemistry sequence.
 - *Roles:* lead discussion sections and exam review sessions, exam grading and proctoring.
- Primary instructor for CHEM 51C (2018 summer session).
 - *Roles:* Developed curriculum (lecture notes, exams, online materials) for class size of approximately 350 students. Developed worksheets for discussion sections and coordinated with teaching assistant.

CHEM 51LA, 51LB, 51LC, M51LA, M51LB, M51LC

- Teaching assistant for introductory organic chemistry laboratory sequence.
- Experience with majors (M51L sequence) and non-majors (51L) laboratory curricula.
- *Roles:* Supervised and guided students during laboratory period; graded lab reports and lab practical exams; held office hours.

CHEM 201 and 202

- Teaching assistant for graduate-level courses in organic mechanisms.
- *Roles:* Graded exams and problem sets; assisted with preparing exams; held office hours.

Undergraduate research mentorship; 2013-2019

- Mentored seven undergraduate students in the research laboratory over various periods, helping them learn laboratory techniques and encouraging them to share their work through poster and oral presentations.

Instrumental Analysis (Santa Clara University), lab and lecture teaching assistant for Dr. Steven Suljak

- Assisted undergraduate peers in learning various spectroscopic and separation techniques.

Research Experience

Van Vranken Lab; 2015-2019

- Developed palladium-catalyzed carbene insertions into the N-H bonds of nitrogen heterocycles, aliphatic amines, and non-conjugated amines.
- Identified potent phthalazinone and isoquinolone compounds that synergize with azoles against pathogenic fungal species.
- *Skills:* synthetic methodology, enantioselective catalysis, small molecule substrate synthesis, chiral HPLC for determination of ee, derivatization and assaying of biologically active compounds.

Esser-Kahn Lab; 2012-2015

- Designed small-molecule system exhibiting non-hyperbolic CO₂ absorption isotherms.
- Quantified thermodynamics of CO₂ absorption through NMR titration experiments and bulk absorption measurements.
- Simulated aggregation of CO₂-bound species using molecular mechanics modelling.
- *Skills:* small molecule and polymer synthesis, gas absorption measurements. NMR titration experiments, molecular modelling.

Fuller Lab; 2010-2012

- Synthesized oligomeric peptoids with solvatochromic dyes incorporated as side chains. Studied peptoid conformation using fluorescence and circular dichroism spectroscopy.
- *Skills:* solid-phase synthesis, reverse-phase HPLC purification, fluorescence and circular dichroism spectroscopy.

Weber Lab; 2009

- Measured spin propagation in magnetic semiconductors using ultrafast solid-state optical spectroscopy.
- *Skills:* ultra-fast lasers, optics, pump-probe spectroscopy, MATLAB.

Awards and Honors

Outstanding Contribution to the Chemistry Department Teaching Program by a TA-1st year; 2013

NSF Graduate Research Fellowship; 2013-2016

Gerald and Sally DeNardo Senior Prize in Science Research, 2012

American Chemical Society Award in Organic Chemistry, 2012

American Chemical Society Award in Analytical Chemistry, 2011

Carl H. Hayn Physics Prize, Spring 2010

Publications

Hiew, S.; Booth, M.; Mansiantima, B.; Yan, H.; Van Vranken, D. "Palladium-Catalyzed Insertion into the N-H bond of Cyclic Aliphatic and Benzylic Amines: Improved Yields and Enantioselectivity Using Parallel Slow Addition." **2019**. *In preparation*.

Arredondo, V.; **Hiew, S.;** Gutman, E.; Premachandra, D. "Enantioselective Palladium-Catalyzed Carbene Insertion into the N-H Bonds of Aromatic Heterocycles". *Angew. Chem. Int. Ed.*, **2017**, *56*, 4156-4159.

Mood, A.; Premachandra, U.; **Hiew, S.;** Fu-Qiang, W.; Scott, K.; Nathan, O.; Haoping, L.; Van Vranken, D. "Potent Antifungal Synergy of Phthalazinone and Isoquinolones with Azoles Against *Candida albicans*". *ACS Med. Chem. Lett.* **2017**, *8*, 168-173.

Steinhardt, R.; **Hiew, S.;** Mohaptra, H.; Nguyen, D.; Oh, Z.; Truong, R.; Esser-Kahn, A. Cooperative CO₂ Absorption Isotherms from a Bifunctional Guanidine and Bifunctional Alcohol. *ACS Cent Sci.* **2017**, *3*, 1271-1275.

C. Weber.; Craig A. Benko, C.; **Hiew, S.** "Measurement of Spin Diffusion in Semi-Insulating GaAs." *Journal of Applied Physics*, **2011**, *109*, 106101.

Oral Presentations

Hiew, S. "A Hemoglobin for CO₂: Designing Small Molecules to Bind Carbon Dioxide via Chelate Cooperativity." ACS National Meeting and Exposition. Denver, Co. March 24, 2016.

Hiew, S. "A Hemoglobin for CO₂: Designing Small Molecules to Bind Carbon Dioxide via Chelate Cooperativity." Materials Research Society Spring Meeting and Exhibit. San Francisco, CA. April 24, 2014.

Hiew, S. Senior Thesis Presentation. Department of Chemistry and Biochemistry Seminar, Santa Clara University, May 25, 2012.

Hiew, S. "Peptoids: An On-Resin Derivatization Strategy for Incorporating Fluorescent Dyes." ACS Undergraduate Research Symposium, Mills College, Oakland, CA. April 28, 2012.

Hiew, S. "Measuring Spin Diffusion in Dilute Magnetic Semiconductors." Physics Department Colloquium, Santa Clara University. November 5, 2010.

Poster Presentations

Hiew, S.; Fuller, A.A. "Peptoids: An On-Resin Derivatization Strategy for Incorporating Fluorescent Dyes." Sigma Xi Poster Session. Santa Clara University. May 18, 2012.

Hiew, S.; Seidl, F.S.; Plescia, M.; Fuller, A.A. "Using Solvatochromic Fluorophores to Study Peptoid Structure." Undergraduate Poster Session. Northern California Undergraduate Research Symposium, San Jose State University, May 14, 2011.

Hiew, S.; Seidl, F.; Plescia, M.; Fuller, A.A. "Using Solvatochromic Fluorophores to Study Peptoid Structure." Undergraduate Poster Session. ACS National Meeting and Exposition. Anaheim, CA. March 28, 2011.

Other Awards and Activities

Student Hosted Seminar

- Worked with fellow graduate student Jae Chung to organize seminar with professor Stephen Craig (Duke University). Coordinated meetings with student and faculty.

Sigma Xi (scientific research society), 2012

Phi Lambda Upsilon (national chemistry honors society), 2012

Phi Beta Kappa, Spring 2010

Abstract of the Dissertation

CO₂-Binding by a Bifunctional Guanidine and Bifunctional Alcohol
Employing Chelate Cooperativity

and

Palladium-Catalyzed Enantioselective Carbene Insertion into the N–H Bonds
of Aromatic Amine Heterocyclic and Non-Conjugated Amines

by

Stanley C. Hiew

Doctor of Philosophy

University of California, Irvine, 2019

Professor David L. Van Vranken, Chair

The research described herein consists of two distinct parts. The first part describes the development of a new solution phase system for binding CO₂. CO₂ capture and sequestration has been proposed as a tool for reducing global CO₂ emissions and usually involves separating CO₂ from a mixed stream of gasses, such as that encountered in the flue gas of fossil-fueled power plants. The cost of existing CO₂ capture technologies has limited their widespread deployment, motivating the search for new reagents and materials that are cheaper, scalable, and more efficient.

The design, synthesis, and CO₂-absorption properties of the new solution phase system will be discussed. The system employs a bifunctional guanidine and bifunctional alcohol pair to bind CO₂ and uses the principle of chelate cooperativity to elicit unique thermodynamic behavior. The CO₂-binding properties of the system were examined at the bulk scale using absorption isotherm measurements, and at the microscopic scale using ¹H NMR spectroscopy. Molecular dynamics simulations are presented that provide insight about the intermolecular interaction and aggregation state of the system. Finally, a thermodynamic model is proposed that rationalizes the observed CO₂ absorption isotherms.

The second section concerns the development of palladium-catalyzed carbene insertions into the N–H bonds of amines. Amine substrates for such insertion reactions have largely been confined to carbamates and anilines. This section will focus on expanding the substrate scope to include other types of amines. The section will begin by discussing enantioselective carbene insertion into aromatic heterocyclic amines, such as carbazoles and indoles. The reaction employs a palladium(II) catalyst and chiral PyBOX ligand to achieve up to 98% yield and 99% *ee*.

Next, carbene insertion into benzylic and aliphatic amines will be discussed. Historically, such substrates have proven extremely challenging owing to their tendency of coordinate and deactivate transition metal catalyst. We present a parallel slow addition procedure that permits high yields and moderate *ees* to be obtained for these types of substrates. The procedure involves simultaneous syringe pump addition of the amine substrate and supplemental palladium catalyst into a stirring solution of palladium catalyst and diazo substrate. This procedure was used to synthesize several morpholine, piperazine, and piperidine aminoester derivatives. Finally, a kinetic model is presented that provides insight into the relationship between amine addition rate, catalyst addition rate, and yield.

Chapter 1: CO₂ Binding by a Bifunctional Guanidine and Bifunctional Alcohol

Employing Chelate Cooperativity

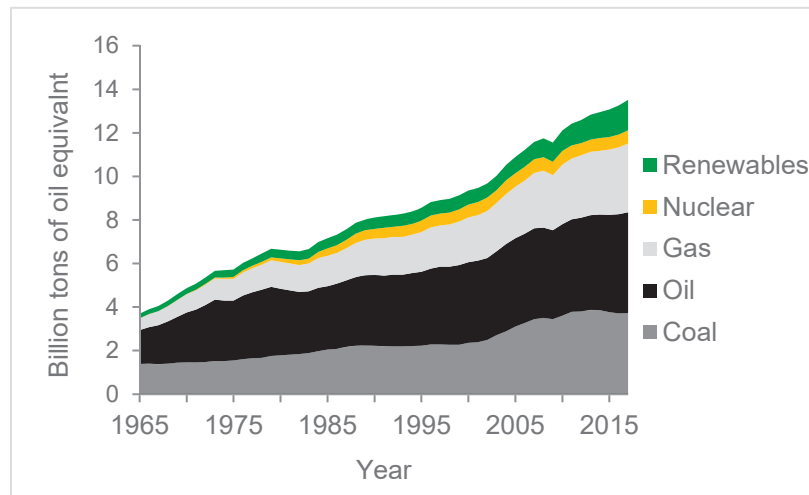
Effect of CO₂ on Climate

CO₂ is considered the primary driver of anthropogenic climate change. In 2017, CO₂ emissions totaled 36.2 billion tons, primarily due to fossil fuel combustion and cement production.¹ Due to sustained burning of fossil fuels, the current atmospheric CO₂ concentration (412 ppm) far exceeds concentrations measured over the past 800,000 years, using on ice core data.^{2,3}

In 2016, 195 nations signed the Paris Agreement, which aimed to limit the increase in global average temperature to under 2.0 °C, and ideally below 1.5 °C. Warming of 2.0 °C and above is expected to incur significantly greater economic, social, and environmental costs. For example, warming of 2.0 °C has been projected to cause sea level rise of 63 cm and \$1.4 trillion in associated flood damage; under a high emissions scenario, between \$14–27 trillion in damage is projected.⁴ Warming above 2.0 °C could also trigger positive feedback responses in earth systems that further accelerate warming. For example, a rise in temperature may accelerate thawing of Siberian permafrost⁵ or destabilization of methane hydrates,⁶ which could release large volumes of methane, a potent greenhouse gas.

Because temperature rise depends on cumulative CO₂ emissions, climate policies are often framed in terms of “carbon budgets”—the amount of CO₂ that can still be emitted before crossing a temperature threshold. An estimated 600–800 Gt CO₂ can still be emitted before crossing the 1.5 °C threshold,⁷ which translates to approximately 15–20 years assuming current emissions rates. Reducing emissions so rapidly would require a radical transformation in energy infrastructure. Currently, 85% of global primary energy consumption is still derived from coal, oil, and natural gas, despite rapid growth of renewable energy (Figure 1-1).

Figure 1-1: Global primary energy consumption by fuel (1965–2017).⁸



Political Barriers to Reducing CO₂ Emissions

Despite international agreement on the urgent need to reduce CO₂ emissions, doing so in practice has encountered significant political barriers. In 2017, the United States submitted its intent to withdraw from the Paris Agreement as soon as legally permissible.⁹ In 2018, Australia abandoned plans for a 26% emissions reduction by 2030.¹⁰ China is currently on track to add 259 GW of coal-fired power plant capacity, roughly equal to that of all existing U.S. coal-fired power plants.¹¹ In 2018, nation-wide “Yellow Vest” protests erupted in France, partly in response to a fuel tax to reduce gas and diesel consumption. These examples highlight the need for solutions that will make reducing emissions more economically and politically palatable.

Carbon Capture and Sequestration

One proposed technology to accelerate emissions reduction is Carbon Capture and Sequestration (CCS).¹² CCS aims to capture CO₂ from concentrated sources such as the flue gas of fossil-fueled power plants, or from dilute sources such as the atmosphere.¹³ The captured CO₂ would be stored underground in geological formations or converted to value-added products such

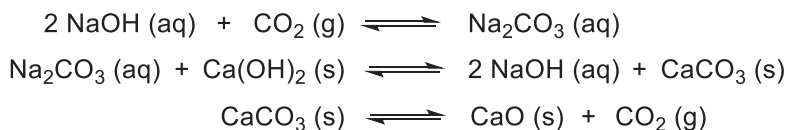
as synthetic fuels.¹⁴ Indeed, several emissions scenarios proposed by the Intergovernmental Panel on Climate Change require CCS to achieve net negative emissions in the latter half of this century.¹⁵

Currently, 17 large-scale CCS facilities are operating globally, with combined capture capacity of 37 million tons per year. This translates to approximately 0.1% of the CO₂ emitted in 2017. The Global CCS Institute has estimated that meeting the Paris 2 °C target would require 2,500 CCS facilities, each capturing 1.5 million tons per year. This is if 14% of cumulative emissions reductions come from CCS.¹⁶

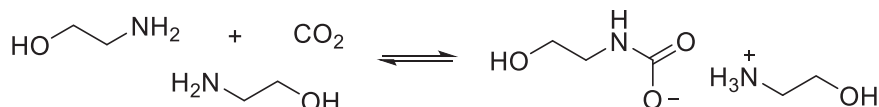
CO₂ capture typically employs an alkali mineral¹⁷ or aqueous amine solution¹⁸ to reversibly bind CO₂ (Figure 1-2). CO₂ capture processes have been patented since the 1930s,¹⁹ but their widespread deployment toward reducing emissions has been limited by high energy costs. For example, the Boundary Dam power plant in Saskatchewan, Canada consumes 45 megawatts to capture CO₂ out of an energy-generating capacity of 159 megawatts (≈ 30% parasitic load). As a result, most existing CCS operations are coupled to enhanced oil recovery or natural gas sweetening processes to offset the cost of the of the CO₂ capture.²⁰ In enhanced oil recovery, captured CO₂ is injected into an oil field to improve ultimate oil recovery. In natural gas sweetening, natural gas is refined by chemically removing CO₂ and H₂S contaminants.

Figure 1-2: Processes for reversible CO₂ capture.

a) Using alkali minerals



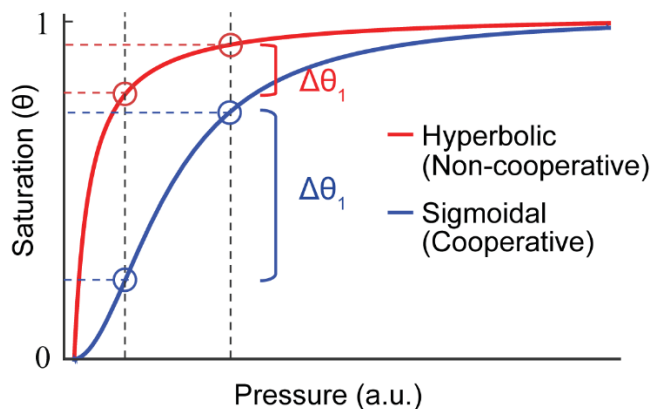
b) Using an aqueous amine solution



The high cost of traditional CO₂ capture processes has motivated research into cheaper, more efficient, and scalable alternatives. Chemists have developed a wide array of materials aimed at reducing the energy required for CO₂ capture.²¹ These materials include ionic liquids,²² metal-organic frameworks,²³ and other solid and liquid sorbents.²⁴ Such materials typically exhibit hyperbolic binding isotherms where CO₂ uptake increases quickly at lower pressures, but levels off as available binding sites become saturated. This thermodynamic behavior presents a fundamental dichotomy: materials exhibiting high CO₂ affinity are often correspondingly difficult to desorb, while materials exhibiting low affinity may show poor CO₂ uptake or lack selectivity for CO₂ over other gases.

One strategy for overcoming this dichotomy is to design a material that exhibits a sigmoidal binding isotherm, in which binding transitions between high and low affinity. In the high affinity regime, the material would bind CO₂ strongly and selectively; in the low-affinity regime, the CO₂ would readily desorb. Sigmoidal isotherms arise when substrate binding is cooperative; that is, when an initial binding event increases the binding affinity of subsequent binding events. For a sigmoidal isotherm, an intermediate pressure range can be chosen that results in greater change in the amount of CO₂ bound, relative to a hyperbolic isotherm (Figure 1-3).

Figure 1-3: Comparison of hyperbolic and sigmoidal binding isotherms.

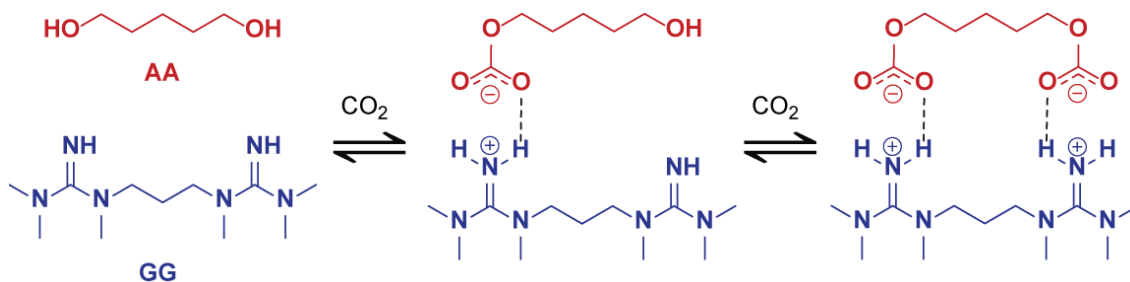


A few notable examples²⁵ demonstrate this type of thermodynamic behavior. Long and co-workers described a diamine-functionalized metal organic framework for which CO₂ uptake increases suddenly past a critical pressure, leading to isotherms that resemble a mathematical step-function. The authors illustrate how such an isotherm could improve the efficiency of CO₂ capture by allowing absorption-desorption cycles to occur over a narrower pressure range.^{25e} In another example, Brennecke and co-workers^{25f} reported an ionic liquid that melts upon CO₂ binding. The associated heat of fusion, ΔH_{fus} , contributed to the heat required for CO₂ desorption. Such examples of non-hyperbolic isotherms are scarce, highlighting the need for new strategies that can modify the thermodynamics of CO₂ binding.

Synthesis and Evaluation of CO₂ Binding by a Solution Phase Bifunctional System

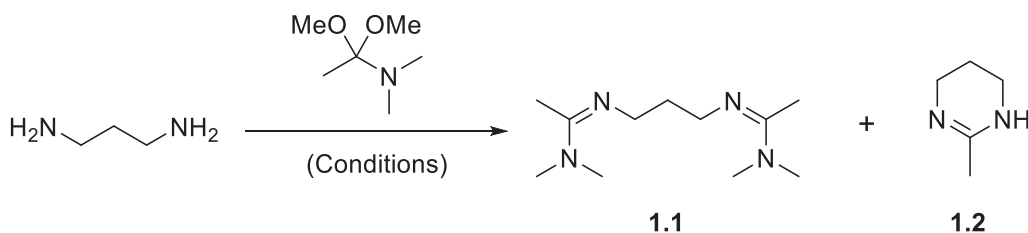
We thus set out to design a system that would exhibit cooperative CO₂ binding. We were initially inspired by chemistry developed by Jessop, Heldebrant, and co-workers²⁶ in which an alcohol and strong organic base (amidine or guanidine) react with CO₂. The reaction forms the salt of a negatively-charged alkyl carbonate species and a positively-charged, protonated base. We hypothesized that a bifunctional version of this chemistry could be used to elicit cooperative binding behavior (Figure 1-4), since binding of the first CO₂ molecule would generate an ionic interaction that facilitates binding of the second CO₂ molecule through the chelate effect.

Figure 1-4: Concept for CO₂ binding illustrated with a bifunctional alcohol (AA) and bifunctional guanidine (GG).



As a design principle, we set out to synthesize bifunctional bases with short tethers, reasoning proximity would be important for enhancing the chelate effect. We began by synthesizing a bifunctional amidine from the condensation of 1,3-diaminopropane and *N,N*-dimethylacetamide dimethyl acetal (Figure 1-5). Our initial reaction conditions gave the desired bifunctional amidine 1.1 as a minor product; the reaction mixture was instead dominated by cyclic amidine 1.2. The ratio was improved in favor of the bifunctional product by performing the reaction in neat *N,N*-dimethylacetamide dimethyl acetal. Surprisingly, we suppressed cyclization further by performing the reaction at elevated temperature, even though such conditions were expected to favor cyclization. Higher temperature apparently accelerates the condensation pathway more than the cyclization pathway. The bifunctional amidine was isolated by high-vacuum distillation (56% yield).

Figure 1-5: Synthesis of a bifunctional amidine with three-carbon linker.

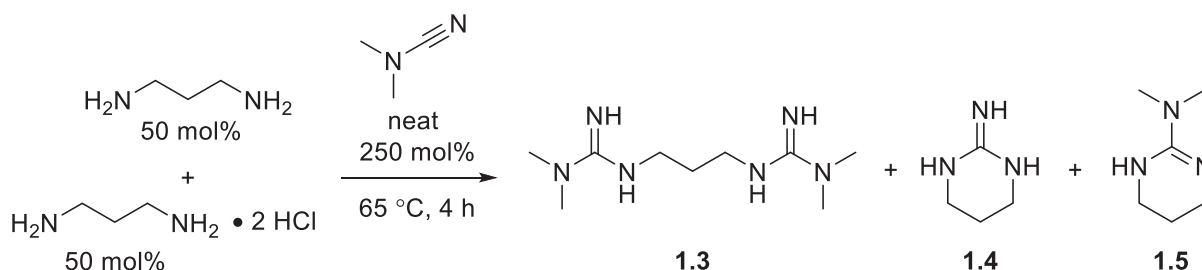


<u>Conditions</u>	<u>Ratio</u>	
0.5 M in THF w/ 2 M dimethylamine 25 °C, 18 h	10	: 90
neat, 25 °C, 20 h	51	: 49
neat, 65 °C, 4 h	91 (56%)	: 9

We next set out to synthesize a bifunctional guanidine, also with a three-carbon tether. Starting with a 1,3-diaminopropane, we hoped to obtain bifunctional guanidine 1.3 through a single-step condensation with dimethylcyanamide (Figure 1-6). While ¹H NMR and ESI-MS

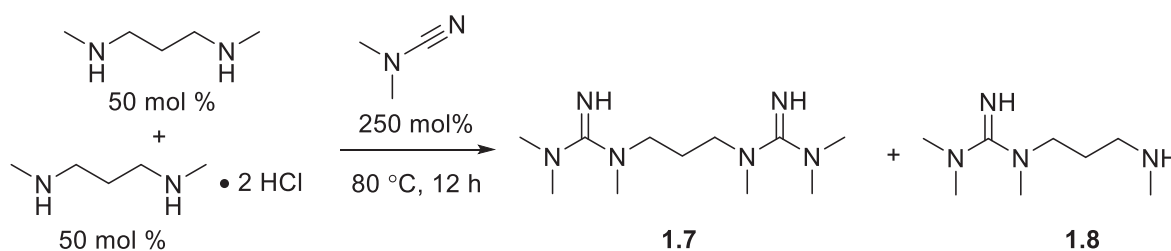
analysis of the crude reaction mixture revealed trace quantities of the desired bifunctional guanidine **1.3**, cyclic guanidines **1.4** and **1.5** were formed as the major products. Despite our best efforts, we could not find conditions to suppress cyclization.

Figure 1-6: Side products obtained from competing cyclization.



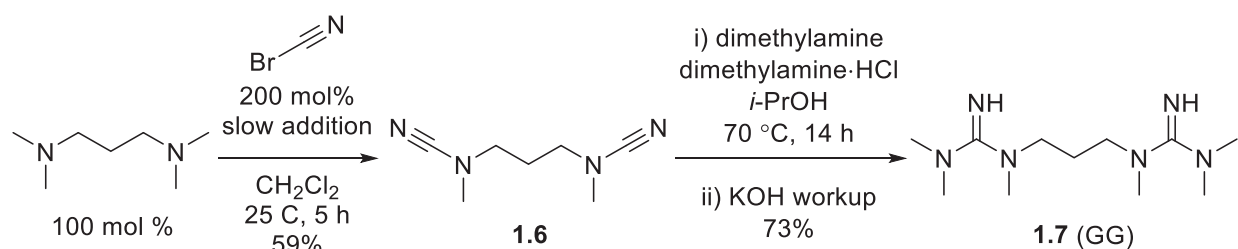
We repeated the reaction using instead an *N,N*-dimethyl-1,3-diaminopropane, reasoning that extra substitution on nitrogen would inhibit the cyclization process (Figure 1-7). While cyclization was indeed suppressed, the reaction could not be driven to the reaction to completion, resulting in an inseparable mixture of difunctional guanidine **1.7** and monofunctional guanidine **1.8**. The reaction could not be driven to completion simply by adding dimethylcyanamide. This is because protonation of the cyanamide by ammonium groups facilitates addition of the free diamine. The guanidine product formed is strongly basic and can deprotonate ammonium species, preventing further activation of dimethylcyanamide.

Figure 1-7: Incomplete reaction of a *N,N*-dimethyl substituted diamine to obtain a mixture of difunctionalized and monofunctionalized guanidines.



We reasoned that excess amine and amine-hydrochloride salt would drive the reaction to completion. Thus, we redesigned the synthetic route to pass through bis-cyanamide **1.6** as a key synthetic intermediate, allowing excess dimethylamine and its hydrochloride salt to be used in the condensation step (Figure 1-8). A solvent screen identified isopropanol as having solubility characteristics permitting selective precipitation of the bisguanidinium dichloride salt, effectively purifying it from any unreacted starting material or side products. The salt was collected by filtration and converted to bifunctional guanidine **1.7** (GG) upon treatment with concentrated aqueous KOH.

Figure 1-8: Successful two-step synthesis of a bifunctional guanidine.

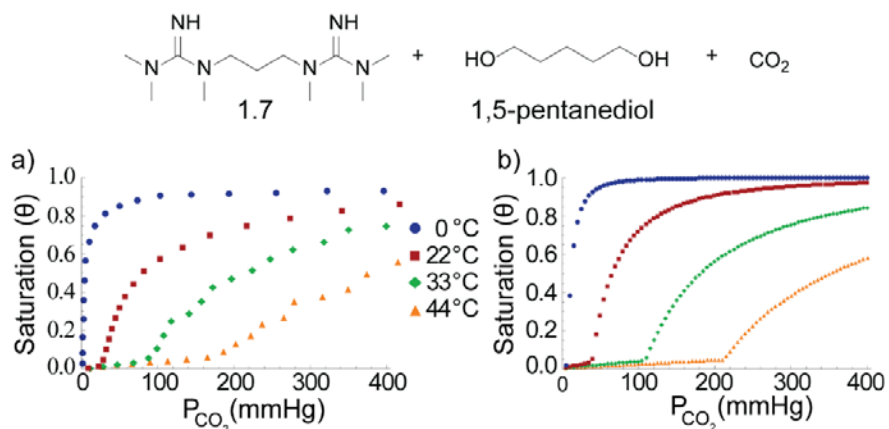


The bulk CO_2 -absorption properties of bifunctional amidine **1.1** and bifunctional guanidine **1.7**, in combination with various diols, were then measured. Absorption isotherms were measured by dissolving the bifunctional base and bifunctional alcohol in organic solvent, then introducing a fixed quantity of CO_2 into the system. The amount of CO_2 absorbed was inferred from the pressure drop due to absorption into the solution.

Bifunctional amidine **1.1** exhibited extremely high CO_2 -binding affinity, and the measured absorption isotherms had hyperbolic profiles. In contrast, bifunctional guanidine **1.7** exhibited unique isotherm profiles (Figure 1-9a). Bifunctional guanidine **1.7** and 1,5-pentane diol were dissolved in bis(2-methoxyethyl)ether²⁷ and absorption isotherms measured at four temperatures: 0 °C, 22 °C, 33 °C, and 44 °C. At 22 °C and above, CO_2 uptake is initially suppressed, but

increases abruptly past a certain pressure. For example, at 22 °C, minimal CO₂ uptake occurs below 30 mmHg ($\theta < 0.1$),²⁸ but increases rapidly by 100 mmHg ($\theta > 0.6$). The pressure at which the inflection occurs varies significantly as a function of temperature: At 33 °C, the inflection occurs near 80 mmHg, and at 44 °C, the inflection occurs near 240 mmHg. To rationalize the observed thermodynamic behavior of this system, we developed a thermodynamic model based on chelate cooperativity,²⁹ which describes the interaction between a bifunctional ligand and bifunctional receptor. The model was qualitatively consistent with the observed thermodynamic behavior (Figure 1-9b). A more detailed discussion of the model is presented later in this chapter.

Figure 1-9: Absorption isotherms of bifunctional guanidine **1.7** and 1,5-pentanediol.
 a) Experimentally measured absorption isotherms in bis(2-methoxyethyl)ether.
 b) Example output of a thermodynamic model based on chelate cooperativity.

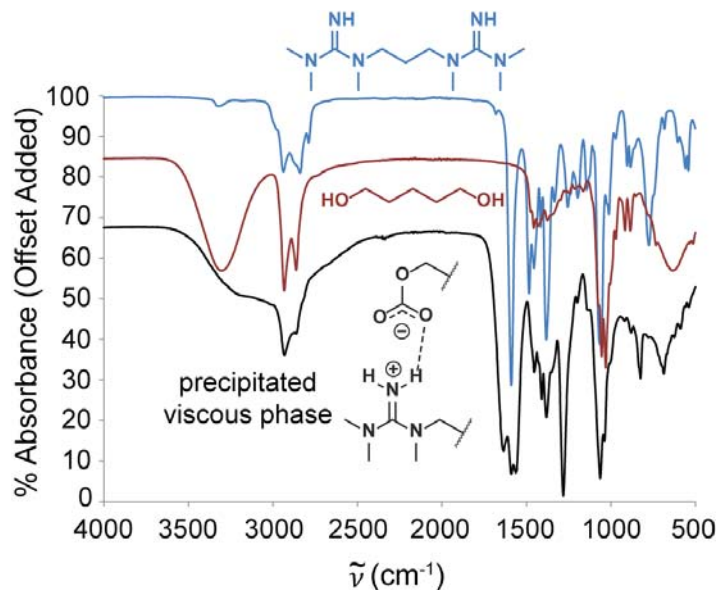


At all temperatures, the inflection coincided with visible precipitation of a secondary viscous phase. Precipitation of this CO₂-rich phase appears to act a thermodynamic sink that drives absorption of CO₂ from the gas phase. At 0 °C, precipitation occurs immediately following CO₂ uptake, and a region of suppressed CO₂ uptake is not observed.

This viscous phase was physically isolated and analyzed by infrared spectroscopy. The infrared spectrum was consistent with formation of alkylcarbonate and guanidinium functional groups (Figure 1-10). A new peak at $\tilde{\nu} = 1634 \text{ cm}^{-1}$ was consistent with alkylcarbonate asymmetric

C=O stretching.³⁰ A new peak at $\tilde{\nu} = 1563 \text{ cm}^{-1}$ was consistent with guanidinium H-N-H scissoring.³¹ Additionally, a broad peak centered around $\tilde{\nu} = 3100 \text{ cm}^{-1}$ is consistent with a hydrogen-bonded, guanidinium N-H stretch.

Figure 1-10. Comparison of infrared spectra (ATR-IR) of the bifunctional guanidine, 1,5-pentanediol, and precipitated viscous phase isolated from CO₂ absorption experiments.

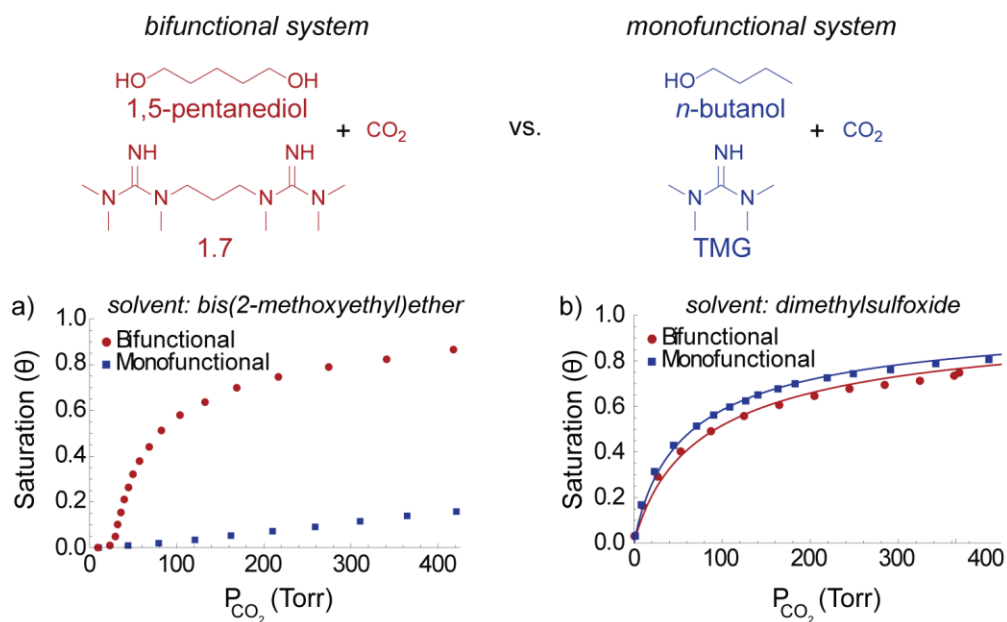


To examine the effect the aliphatic linker between the alcohol and guanidine functional groups, we next compared CO₂ absorption between the bifunctional system and an analogous monofunctional comprising *N,N,N',N'*-tetramethylguanidine and *n*-butanol (Figure 1-11). A solution comprising monofunctional components was prepared at twice the concentration as the bifunctional system, thus maintaining an equivalent functional group concentration. In bis(2-methoxyethyl)ether, CO₂ uptake for the monofunctional system was depressed across the entire pressure range tested (0-400 mmHg) and no precipitation was observed. The isotherms for the monofunctional and bifunctional systems diverge past 30 mmHg (Figure 1-11a).

The absorption isotherms of both monofunctional and bifunctional systems were strongly solvent dependent. When dimethylsulfoxide (DMSO) was used in place of bis(2-methoxyethyl)

ether, both systems exhibited closely matching, hyperbolic isotherms (Figure 1-11b). No precipitation was observed even at higher pressures when most available binding sites had reacted ($\theta > 0.6$). These observations suggest that the DMSO effectively solvates charged alkylcarbonate and guanidinium species, including any bis-cationic or bis-anionic species formed. The similarity of the isotherms suggests the aliphatic linker does not significantly influence CO₂ binding in DMSO.

Figure 1-11: Comparison of bifunctional and mono-functional systems in solvents of differing polarity.

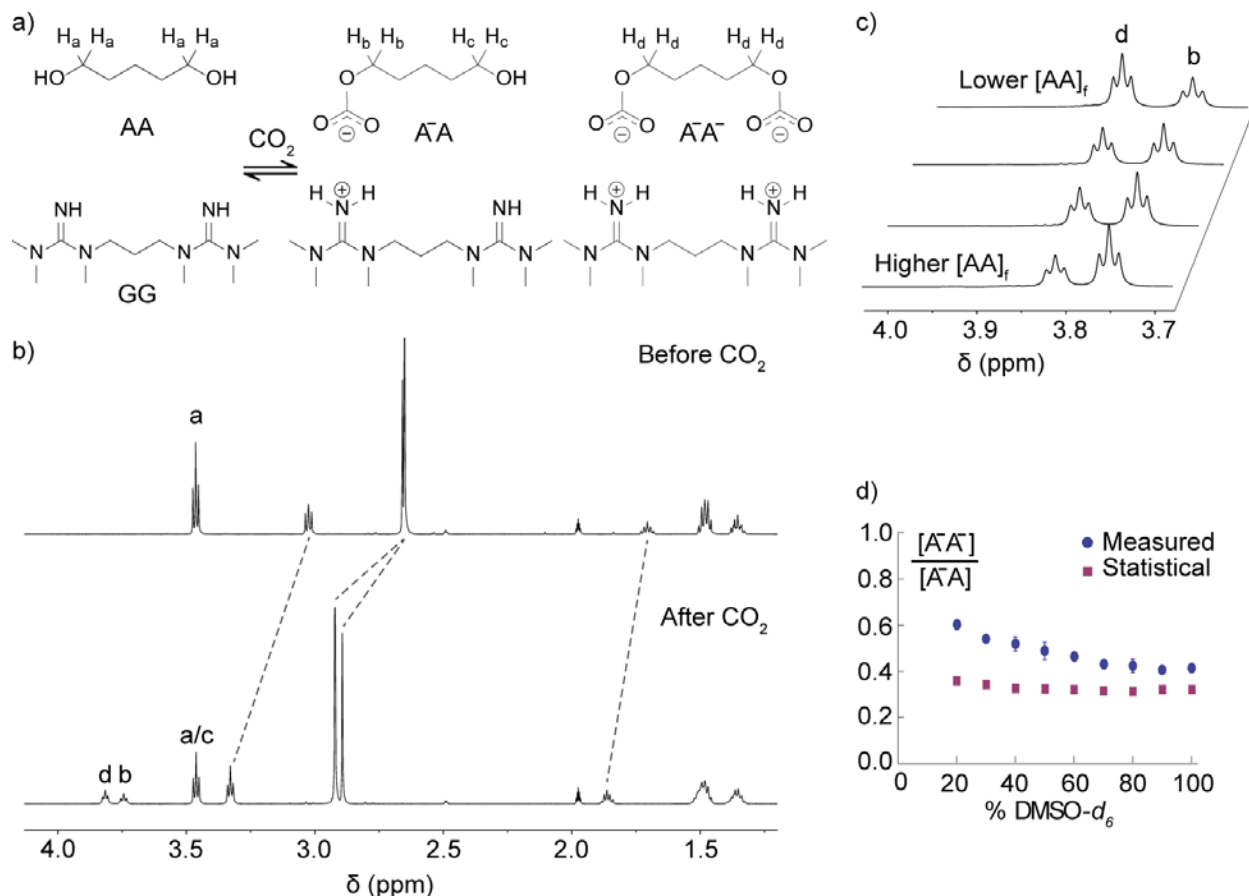


In addition to bulk absorption measurements, we investigated CO₂ binding by ¹H NMR. NMR samples of bifunctional guanidine **1.7** and 1,5-pentane diol and equilibrated under 1 atm CO₂. (For practical reasons, we used a co-solvent mixture of DMSO-*d*₆ and acetonitrile-*d*₃ to prepare NMR samples. A minimum of 20% (v/v) DMSO-*d*₆ was required to maintain a homogeneous solution, so samples were prepared ranging from 20-100% DMSO-*d*₆). Reaction with CO₂ produced two distinct alkylcarbonate species, monoalkylcarbonate A:A and

bisalkylcarbonate $A^{\cdot}A^{\cdot}$ (Figure 1-12a). These species possess well-resolved resonances in the $\delta=3.6-3.9$ ppm region corresponding to protons adjacent to the newly formed alkylcarbonate functional groups (H_b and H_d). Assignment of these species was confirmed by additional 1H TOCSY and ^{13}C NMR experiments. We also observed unreacted diol so that all three species (AA , $A^{\cdot}A$, and $A^{\cdot}A^{\cdot}$) were present simultaneously. Additionally, signals corresponding to the bifunctional guanidine **1.7** (GG) shifted downfield following reaction with CO_2 (Figure 1-12b, dashed lines), suggesting the formation of guanidinium species. Unlike the alkyl carbonate species, distinct signals from these guanidinium species likely coalesce due to acid-base exchange between guanidine and guanidinium functional groups occurring much faster than the NMR timescale. The assignment of mono-guanidinium and bis-guanidinium species by 1H NMR remains putative.

The relative concentration of monoalkylcarbonate $A^{\cdot}A$ and bisalkylcarbonate $A^{\cdot}A^{\cdot}$, which we quantified via integration of integration of H_d and H_b , varied as a function of solvent composition, as well as the concentration of unreacted diol, $[AA]_f$ (Figure 1-12c). As the proportion of DMSO is decreased, the equilibrium increasingly favors the bisalkylcarbonate species (Figure 1-12d, blue circles). DMSO is known to disrupt ionic interaction, especially by coordinating to cations,³² so decreasing the proportion $DMSO-d_6$ permits tighter interaction between charged functional groups. In other words, solvent conditions that favor a tighter interaction between charged guanidinium and alkylcarbonate functional groups also favors simultaneous binding of two CO_2 molecules per bifunctional alcohol. This observation is strong evidence of a chelate effect.

Figure 1-12. a) Alkylcarbonate species formed after equilibration under 1 atm CO₂.
 b) ¹H NMR spectra before and after 1 atm CO₂ exposure. (Dashed lines mark peaks corresponding to the bifunctional guanidine).
 c) Change in relative peak areas of H_b and H_d versus unreacted diol concentration.
 d) Ratio of bisalkylcarbonate A⁻A⁻ to monoalkylcarbonate A⁻A versus solvent composition.



Taken together, the bulk CO₂ absorption experiments and NMR experiments suggest an interdependence between CO₂ binding and the interaction of charged alkylcarbonate and guanidinium functional groups. In bis(2-methoxyethyl)ether, depressed CO₂ uptake at low pressure is consistent with observations by Heldebrant and co-workers that nonpolar solvents favor CO₂ desorption by destabilizing the charged alkylcarbonate and guanidinium species.^{8b} Above a critical CO₂ pressure, the chelate effect and precipitation bias the equilibrium toward the CO₂-bound state, leading to a rapid rise in CO₂ uptake.

Molecular Dynamics Simulations

Molecular dynamic simulations were performed to gain deeper insight into the intermolecular interaction occurring in the solution phase system. A simulation was conducted comprising all experimentally observable components, including bifunctional guanidine 1.7, 1,5-pentanediol, the various species that result from CO₂ binding (A⁻A, A⁻A⁻, G⁺G, G⁺G⁺), and solvent. Simulations were performed over 10 ns using a 1 fs time step.

Docking trajectories between bisalkylcarbonate and bisguanidinium species were observed, in which an initial interaction between one pair of guanidinium and carbonate functional groups facilitated interaction between the second pair of functional groups (Figure 1-13).

A distribution of aggregate sizes were observed in the simulations (Figure 1-14). The majority of were dimers comprising one bisguanidinium and one bisalkylcarbonate (aggregate size = 2), Most aggregates were dimeric, although higher-length oligomers were also observed. Several charged species also remained unpaired.

Figure 1-13. Docking between a bisalkylcarbonate molecule and bisguanidinium molecule. Distances plotted between guanidine nitrogen and carbonate carbon (N1-C1) and (N2-C2).

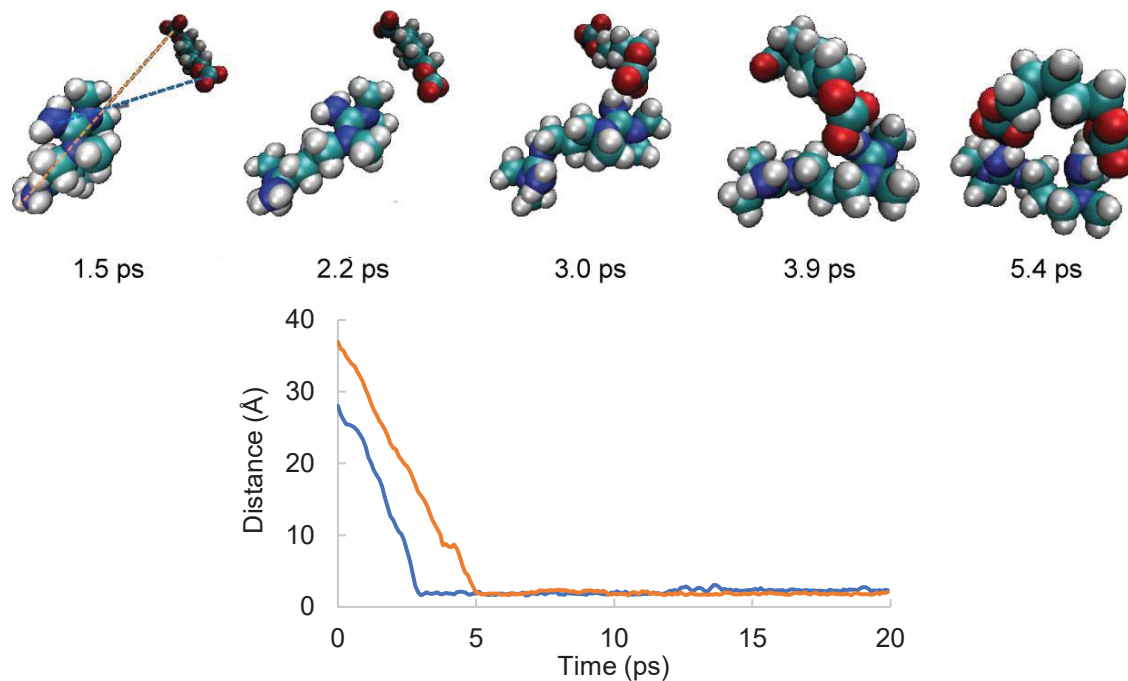
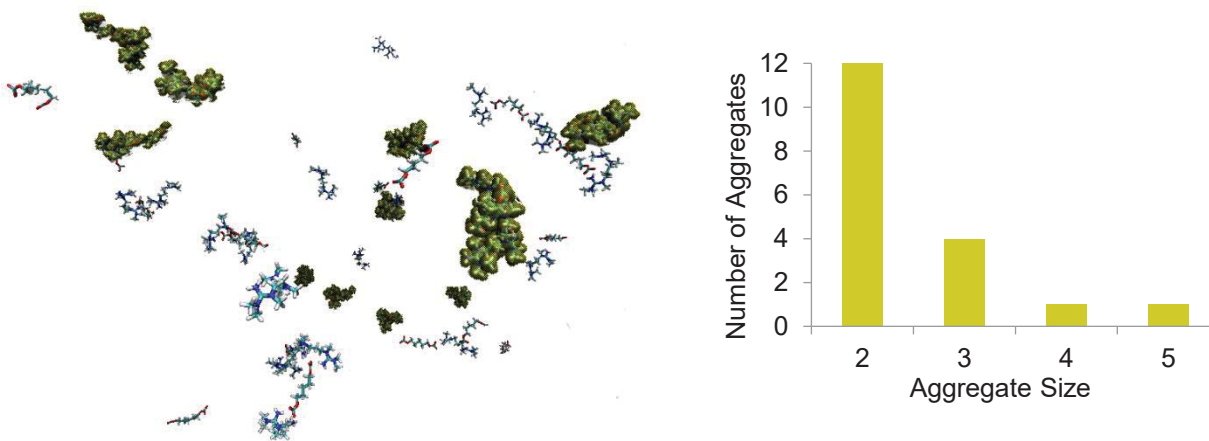


Figure 1-14. Snapshot of example simulation from at 50 ns, with dimeric aggregates highlighted. Solvent molecules are excluded for clarity.



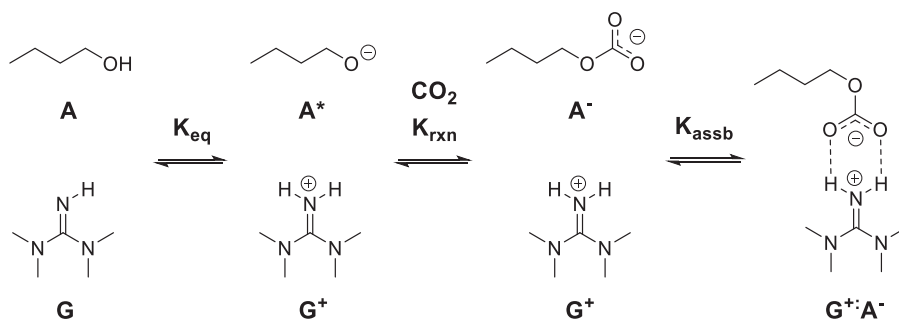
Thermodynamic Model

To better understand the interdependence between the chelate effect, solubility, and CO₂ binding affinity, we developed a thermodynamic model that builds on previous work describing the interaction between a divalent receptor and divalent ligand.¹ The model treats CO₂ binding in the initial and precipitated phases as part of a coupled equilibrium.

Monofunctional System

We first consider the monofunctional system, which provides a foundation for considering the more complex bifunctional system. Heldebrant et al. obtained thermodynamic data suggesting that, for mixtures of alcohols and strong organic bases, the binding affinity for CO₂ depends on both the strength of the base and the interaction between the protonated base and alkyl carbonate moieties.² We therefore represent CO₂ binding process as a composite of three elementary steps (Figure 1-15). In the first step, the guanidine deprotonates the alcohol to form guanidinium and alkoxide species (K_{eq}). Next, the alkoxide reacts with CO₂ to form an alkyl carbonate species (K_{rxn}). Finally, the alkylcarbonate and guanidinium assemble through an ionic interaction (K_{assb}).

Figure 1-15: Coupled equilibrium model for the monofunctional system



Mass Conservation: From this equilibrium model, the following mass conservation expression may be written:

$$G_i = G_f + G^+ + G^+:A^-$$

The expression states that the initial guanidine concentration G_i must be equal to the final unreacted guanidine concentration G_f , plus the concentrations of any guanidinium species formed. The expression may be simplified by assuming that guanidinium and alkylcarbonate species are normally complexed through an ionic interaction so that $G^+:A^- \gg G^+$:

$$G_i \approx G_f + G^+:A^-$$

The derivation may be continued without invoking this assumption, however doing so adds unnecessary complexity. We continue the derivation with the simplified expression for G_i .

Equilibrium Expressions: Next, equilibrium expressions are written for each elementary step. The symbol α_{CO_2} represents the CO_2 activity in solution.

$$K_{eq} = \frac{G^+ \cdot A^*}{G_f \cdot A_f}$$

$$K_{rxn} = \frac{A^-}{A^* \cdot \alpha_{CO_2}}$$

$$K_{assb} = \frac{G^+:A^-}{G^+ \cdot A^-}$$

With mass conservation and equilibria expressions written, we next define a parameter θ to represent the fraction of binding sites with CO_2 bound. The concentration of available binding sites is equal to the initial guanidine concentration G_i or the initial alcohol concentration A_i ,

whichever is limiting. When no CO₂ molecule is bound $\theta = 0$, and when CO₂ occupies all binding sites $\theta = 1$. If the initial guanidine concentration G_i is limiting, the expression for θ is:

$$\theta = \frac{A^- + G^+:A^-}{G_i}$$

The expression states that the fraction of binding sites with CO₂ bound is equal to the concentration of alkylcarbonate species normalized by the concentration of available binding sites. As above, we assume the guanidinium and alkylcarbonate species spend most time complexed through an ionic interaction so that $G^+:A^- \gg A^-$. Applying this assumption, the expression for θ becomes:

$$\theta = \frac{G^+:A^-}{G_i} \quad \text{eq. 1.1}$$

We substitute G_i in the denominator with the mass conservation statement written above:

$$\theta = \frac{G^+:A^-}{G_f + G^+:A^-}$$

We further substitute species concentrations with the equilibria expressions written above to obtain:

$$\theta = \frac{A_f K_{eq} K_{rxn} K_{assb} \alpha_{CO_2}}{1 + A_f K_{eq} K_{rxn} K_{assb} \alpha_{CO_2}}$$

Thus θ depends on the equilibrium constants K_{eq} , K_{rxn} , and K_{assb} , and on the CO₂ activity, α_{CO_2} .

We can further simplify the expression by defining a composite equilibrium constant K_0 :

$$K_0 = K_{eq} K_{rxn} K_{assb}$$

We substitute K_0 into the expression for θ to obtain:

$$\theta = \frac{A_f K_0 \alpha_{CO_2}}{1 + A_f K_0 \alpha_{CO_2}} \quad \text{eq. 1.2}$$

The final expression resembles that of the Langmuir equation, but also depends on the unreacted alcohol concentration A_f . Note that the unreacted alcohol concentration A_f is a function of θ , so equation 1.2 is an implicit function. The concentration of A_f decreases as it reacts to form alkylcarbonate species (as θ increases). We solve the implicit function for θ by writing a second mass conservation statement:

$$A_i = A_f + A^- + G^+ : A^-$$

Again, we assume that the alkylcarbonate exists as part of the complex $G^+ : A^-$, so:

$$A_i \approx A_f + G^+ : A^-$$

We rearrange equation 1.1 to $G^+ : A^- = \theta G_i$ and substitute this into the above equation.

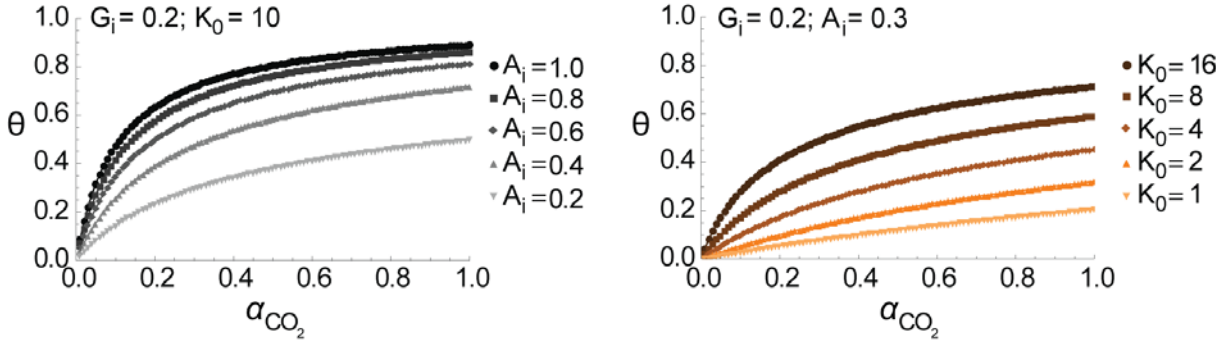
$$\begin{aligned} A_i &= A_f + \theta G_i \\ A_f &= A_i - \theta G_i \end{aligned}$$

Substituting this expression for A_f into equation 2 gives:

$$\theta = \frac{(A_i - \theta G_i) K_0 \alpha_{CO_2}}{1 + (A_i - \theta G_i) K_0 \alpha_{CO_2}} \quad \text{eq. 1.3}$$

Equation 1.3 was solved for θ at discrete values of α_{CO_2} using Wolfram Mathematica 9.0. Example outputs of equation 1.3, plotted for various values of A_i and K_0 (Figure 1-16).

Figure 1-16: Example outputs of equation 1.3.



Bifunctional System

Having derived θ for the monofunctional system (equation 1.2 explicit expression; equation 1.3 implicit expression), we next consider the more complex bifunctional system (Figure 1-17). Again, we consider the CO_2 binding process as occurring over three elementary steps: 1) guanidine functional groups deprotonate alcohol functional groups to form guanidinium and alkoxide species, 2) alkoxide species react with CO_2 to form an alkyl carbonate species, and 3) guanidinium and alkylcarbonate species assemble through ionic interactions. In contrast with the monofunctional system, the bifunctional system may conceivably form unsymmetrical species where only one of the two guanidine or alcohol functional groups reacts.

Mass Conservation: The initial bifunctional guanidine concentration GG_i must be equal to the final unreacted guanidine concentration GG_f , plus the concentrations of any monofunctional and bifunctional guanidinium species formed.

$$GG_i = GG_f + G^+G + G^+G:A^-A + G^+G^+:A^-A + G^+G^:(A^-A)_2 + G^+G^+:A^-A^* \\ + o-G^+G^+:A^-A^- + G^+G^+:A^-A^-$$

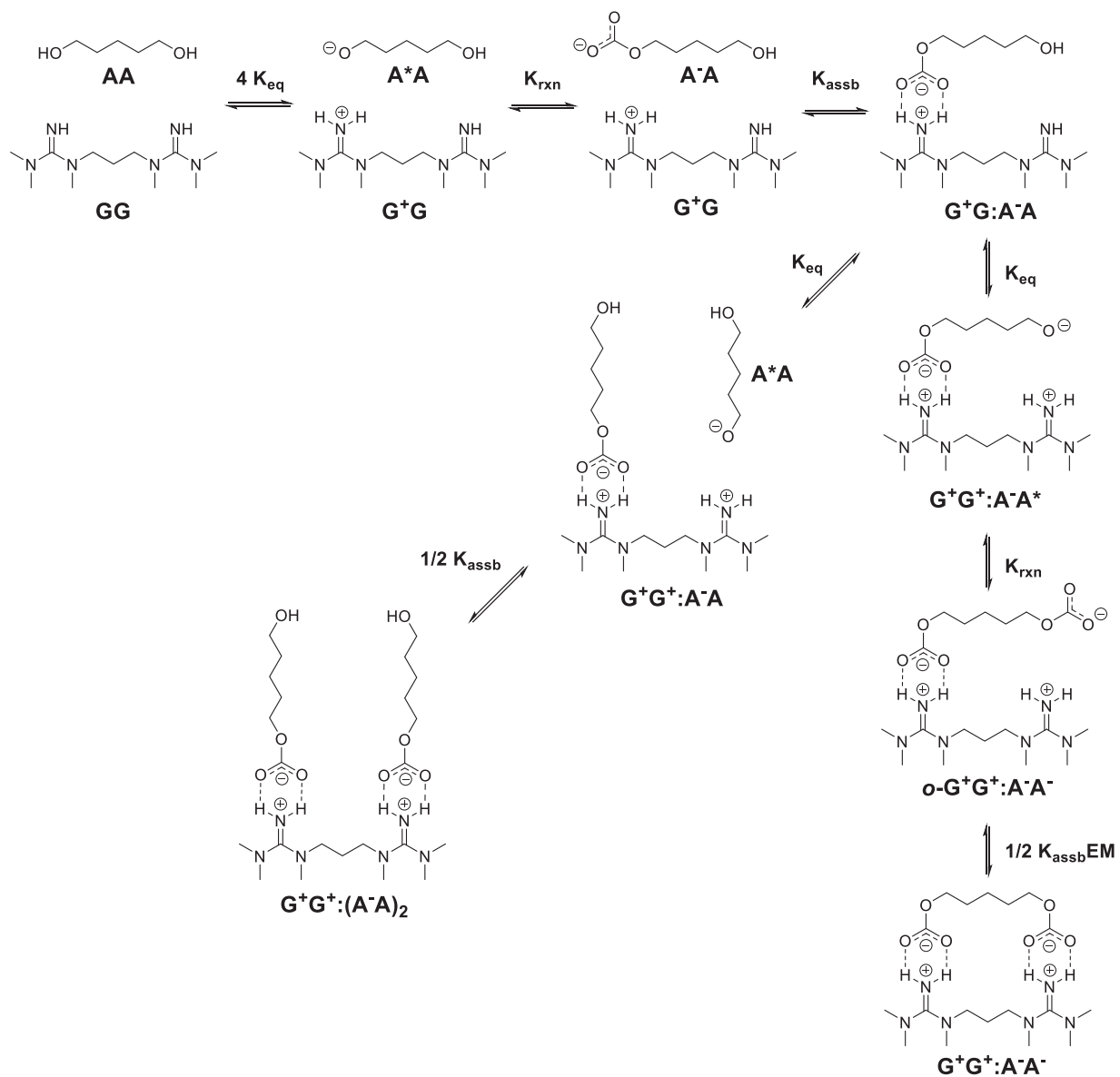
As in the monofunctional case, we assume that guanidinium and alkylcarbonate moieties are normally complexed through an ionic interaction. In this case, the concentrations of the assembled species $G^+G:A^-A$, $G^+G^:(A^-A)_2$, and $G^+G^+:A^-A^-$ are high relative to those with non-

interacting charged functional groups, including G^+G , $G^+G^+:A^-A$, $G^+G^+:A^-A^*$, and $o-G^+G^+:A^-A^-$.

Applying this assumption leads to the simplified expression:

$$GG_i \approx GG_f + G^+G:A^-A + G^+G^:(A^-A)_2 + G^+G^+:A^-A^-$$

Figure 1-17: Coupled equilibrium model for the bifunctional system.



Equilibrium Expressions: Next, we write equilibrium expressions for each step.

$$4 K_{eq} = \frac{G^+G \cdot A^*A}{GG_f \cdot AA_f}$$

$$K_{rxn} = \frac{A^-A}{A^*A \cdot \alpha_{CO_2}}$$

$$K_{assb} = \frac{G^+G : A^-A}{G^+G \cdot A^-A}$$

$$K_{eq} = \frac{G^+G^+ : A^-A^*}{G^+G : A^-A}$$

$$K_{rxn} = \frac{o-G^+G^+ : A^-A^-}{G^+G^+ : A^-A^* \cdot \alpha_{CO_2}}$$

$$\frac{1}{2} K_{assbEM} = \frac{G^+G^+ : A^-A^-}{o-G^+G^+ : A^-A^-}$$

$$K_{eq} = \frac{G^+G^+ : A^-A \cdot AA^*}{G^+G : A^-A \cdot AA_f}$$

$$\frac{1}{2} K_{assb} = \frac{G^+G^+ : (A^-A)_2}{G^+G^+ : A^-A \cdot A^-A}$$

With mass conservation and equilibria expressions in hand, we define a parameter θ to represent the fraction of binding sites with CO₂ bound. The concentration of available binding sites is equal to twice the initial concentration of the bifunctional guanidine or bifunctional alcohol, because each possesses two guanidine or alcohol functional groups, respectively. If the initial concentration GG_i is limiting, the expression for θ is:

$$\theta = \frac{G^+G + G^+G:A^-A + 2 G^+G^+:A^-A + 2 G^+G^+:(A^-A)_2 + 2 G^+G^+:A^-A^* + 2 o-G^+G^+:A^-A^- + 2 G^+G^+:A^-A^-}{2 GG_i}$$

In the above expression, certain complexes are multiplied by two because they contain two guanidinium functional groups. At complete saturation $\theta = 1$, all of guanidine functional groups have reacted to form guanidinium functional groups.

To simplify the expression for θ , we again assume that the concentrations of fully complexed species $G^+G:A^-A$, $G^+G^+:(A^-A)_2$, and $G^+G^+:A^-A^-$ are high relative to the uncomplexed species G^+G , $G^+G^+:A^-A$, $G^+G^+:A^-A^*$, and $o-G^+G^+:A^-A^-$. From this assumption, we obtain a simplified expression:

$$\theta = \frac{G^+G:A^-A + 2 G^+G^+:(A^-A)_2 + 2 G^+G^+:A^-A^-}{2 GG_i}$$

Using the mass conservation statement and equilibrium expressions above, we solve for θ in terms of AA_f , equilibrium constants, and CO_2 activity to arrive at the following expression:

$$\theta = \frac{2 AA_f K_{eq} K_{rxn} K_{assb} \alpha_{CO_2} (1 + (AA_f + EM) K_{eq} K_{rxn} K_{assb} \alpha_{CO_2})}{1 + 2 AA_f K_{eq} K_{rxn} K_{assb} \alpha_{CO_2} (2 + (AA_f + EM) K_{eq} K_{rxn} K_{assb} \alpha_{CO_2})}$$

As in the monofunctional case, the saturation depends on AA , the equilibrium constants K_{eq} , K_{rxn} , K_{assb} , and on CO_2 activity. We can further simplify the expression by defining a composite equilibrium constant K_0 .

$$K_0 = K_{eq} K_{rxn} K_{assb}$$

We substitute K_0 into the expression for θ to obtain:

$$\theta = \frac{2 AA_f K_0 \alpha_{CO_2} (1 + (AA_f + EM) K_0 \alpha_{CO_2})}{1 + 2 AA_f K_0 \alpha_{CO_2} (2 + (AA_f + EM) K_0 \alpha_{CO_2})} \quad \text{eq. 1.4}$$

Note that when $AA_f = EM$, equation 1.4 simplifies to:

$$\theta = \frac{2 AA_f K_0 \alpha_{CO_2}}{1 + 2 AA_f K_0 \alpha_{CO_2}}$$

In other words, if there is no difference between the actual concentration of AA_f and the effective molarity EM (if there is no proximity effect due complexation), the function θ becomes hyperbolic. Like the monofunctional system, the unreacted bifunctional alcohol concentration AA_f is a function of θ , so equation 1.4 is an implicit function. The concentration of AA decreases as it reacts to form alkylcarbonate species (as θ increases). We solve the implicit function for θ by writing a second mass conservation statement:

$$GG_f = GG_i - [G^+G:A^-A + G^+G^+:(A^-A)_2 + G^+G^+:A^-A^-]$$

The above equation states that the final unreacted concentration of the bifunctional guanidine GG_f is equal to the initial concentration minus that any guanidinium species formed from CO_2 binding. As above, we assume $G^+G:A^-A$, $G^+G^+:(A^-A)_2$, and $G^+G^+:A^-A^-$ predominate. We then express the species in brackets in terms of AA_f , K_0 , and EM , using the above equilibria expressions.

$$GG_f = GG_i - [4 GG_f AA_f K_0 \alpha_{CO_2} + 2 GG_f AA_f^2 K_0^2 \alpha_{CO_2}^2 + 2 GG_f AA_f EM K_0^2 \alpha_{CO_2}^2]$$

$$GG_f = \frac{GG_i}{1 + 4 AA_f K_0 \alpha_{CO_2} + 2 AA_f^2 K_0^2 \alpha_{CO_2}^2 + 2 AA_f EM K_0^2 \alpha_{CO_2}^2} \quad \text{eq. 1.5}$$

Like the bifunctional guanidine GG_f , the final concentration of bifunctional alcohol AA_f is equal to the initial concentration AA_i minus the concentration of any alkylcarbonate species:

$$AA_f = AA_i - [G^+G:A^-A + 2 G^+G^+:(A^-A)_2 + G^+G^+:A^-A^-]$$

$$AA_f = AA_i - [4 GG_f AA_f K_0 \alpha_{CO_2} + 4 GG_f AA_f^2 K_0^2 \alpha_{CO_2}^2 + 2 GG_f AA_f EM K_0^2 \alpha_{CO_2}^2] \quad \text{eq. 1.6}$$

Substituting the expression for GG_f (equation 1.5) into equation 1.6, we obtain:

$$AA_f = AA_i - \frac{4 GG_i AA_f K_0 \alpha_{CO_2}}{1 + 4 AA_f K_0 \alpha_{CO_2} + 2 AA_f^2 K_0^2 \alpha_{CO_2}^2 + 2 AA_f EM K_0^2 \alpha_{CO_2}^2} - \frac{4 GG_i AA_f^2 K_0^2 \alpha_{CO_2}^2}{1 + 4 AA_f K_0 \alpha_{CO_2} + 2 AA_f^2 K_0^2 \alpha_{CO_2}^2 + 2 AA_f EM K_0^2 \alpha_{CO_2}^2} - \frac{2 GG_i AA_f EM K_0^2 \alpha_{CO_2}^2}{1 + 4 AA_f K_0 \alpha_{CO_2} + 2 AA_f^2 K_0^2 \alpha_{CO_2}^2 + 2 AA_f EM K_0^2 \alpha_{CO_2}^2}$$

The above quadratic equation was solved using Wolfram Mathematica 9.0. Values for AA_f were calculated for discrete values of α_{CO_2} . Only solutions where $0 < AA_f < AA_i$ were kept. The values calculated for AA_f were substituted back into equation 1.6 to calculate the corresponding values of GG_f . With values of AA_f and GG_f in hand, the saturation θ was then calculated using the same expression as was used to derive equation 4 (re-written here for convenience):

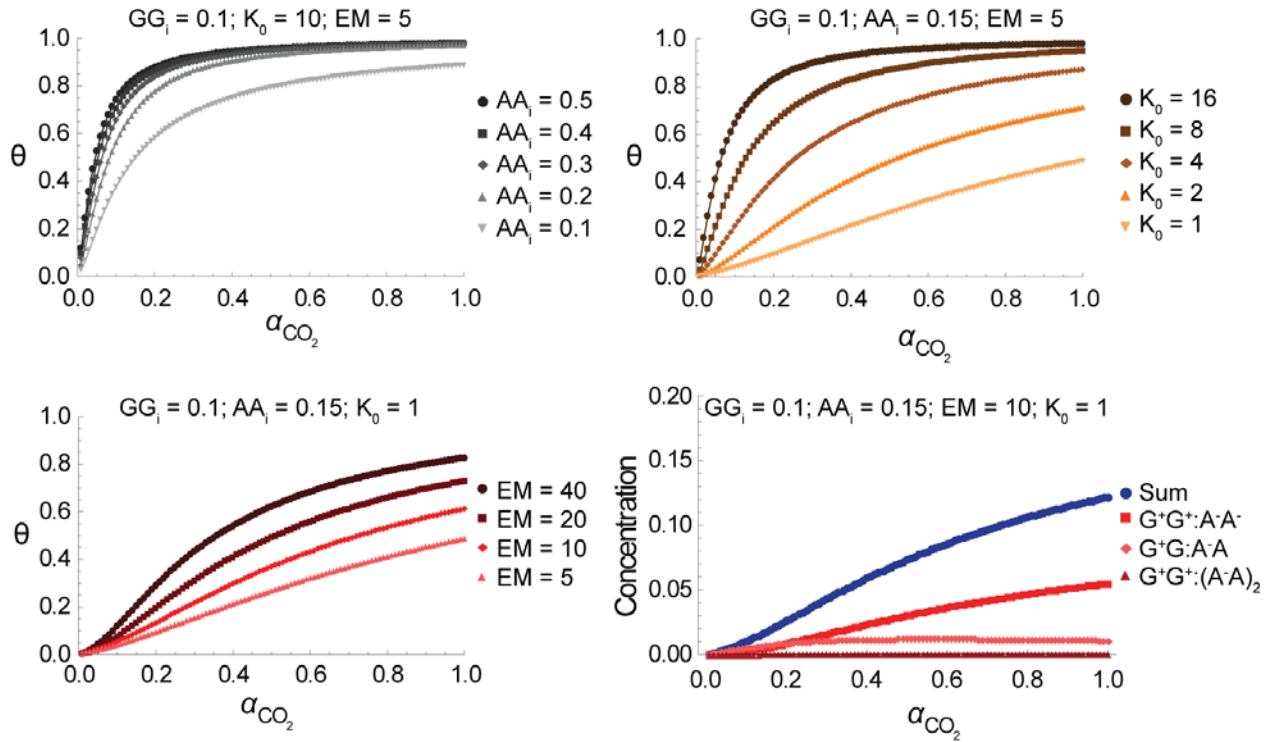
$$\theta = \frac{G^+G:A^-A + 2 G^+G^+:(A^-A)_2 + 2 G^+G^+:A^-A^-}{2 GG_i} \quad \text{eq. 1.7}$$

where

$$\begin{aligned} G^+G:A^-A &= 4 GG_f AA_f K_0 \alpha_{CO_2} \\ G^+G^+:(A^-A)_2 &= 4 GG_f AA_f^2 K_0^2 \alpha_{CO_2}^2 \\ G^+G^+:A^-A^- &= 2 GG_f AA_f EM K_0^2 \alpha_{CO_2}^2 \end{aligned}$$

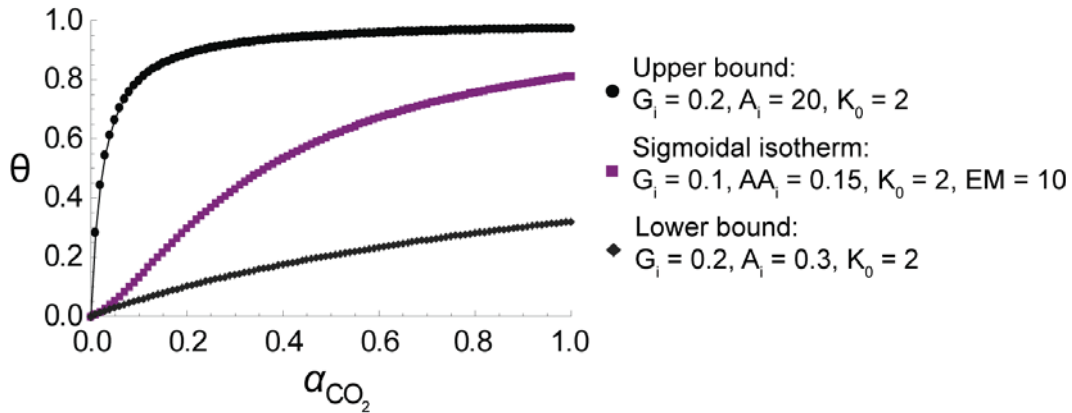
The output of equation 1.7 is plotted below (Figure 1-18) for various values of AA_i , K_0 , and EM . Also shown is concentration of complexes $G^+G:A^-A$, $G^+G^+:(A^-A)_2$, and $G^+G^+:A^-A^-$ in the regime where $EM \gg AA_i$.

Figure 1-18: Example plots of equation 1.7 for various values of AA_i , K_0 , and EM , and example plot of species concentrations



If the value of EM is large relative to AA_f , and K_0 is small, equation 1.7 generates a sigmoidal isotherm (Figure 1-19). The sigmoidal isotherm can be viewed as transitioning between a low-affinity lower bound and high-affinity upper bound. The lower bound is set by equation 1.3, where $A_f = 2 AA_f$. The upper bound is also set by equation 1.3, where $A_f = 2 EM$.

Figure 1-19: Example plot of equation 1.7 for a low-to-high affinity transition, bounded by corresponding low-affinity and high-affinity cases.



Bifunctional System with Precipitation

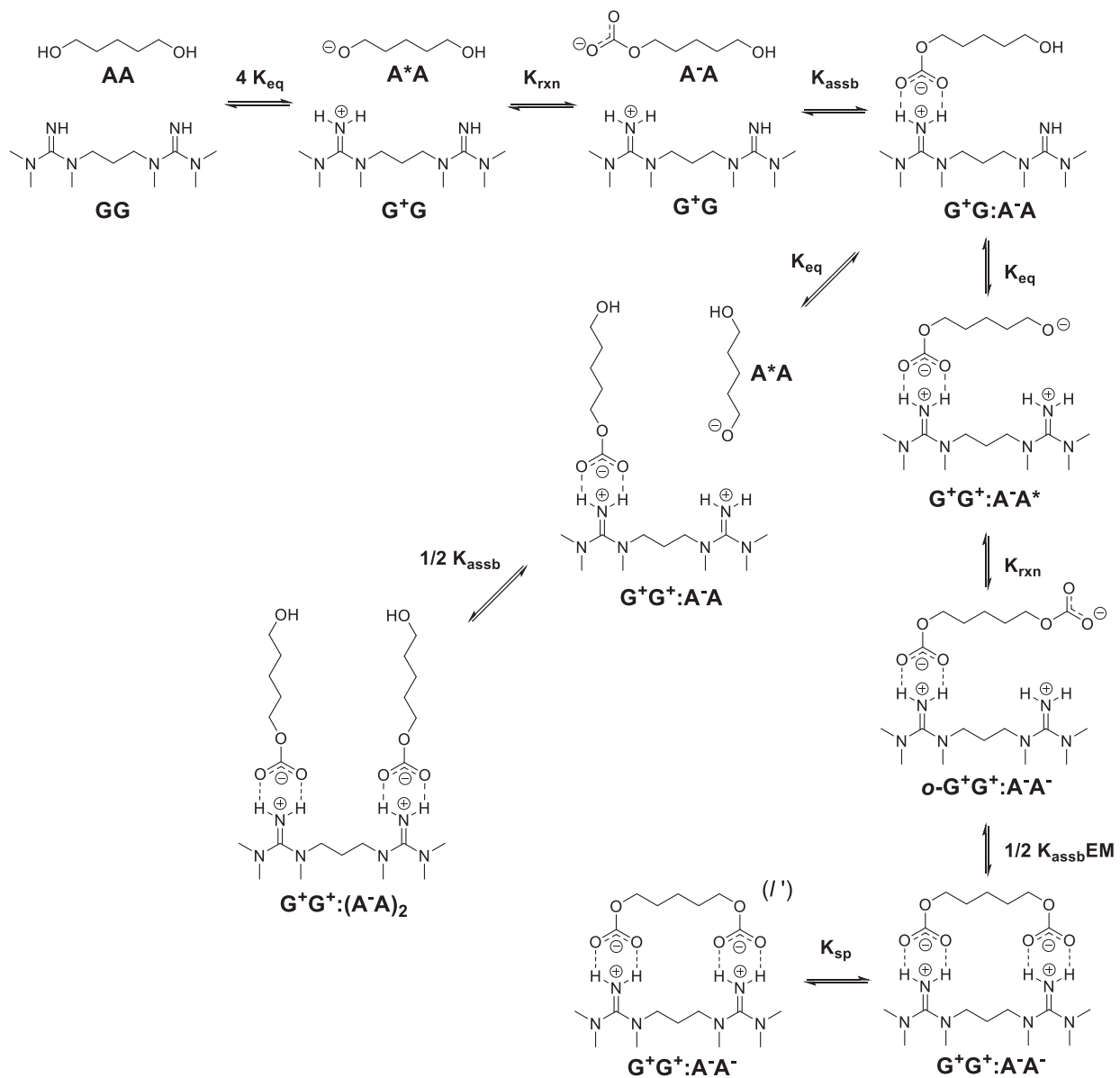
A key element of the model accounts for the formation of a secondary phase. This is accomplished by setting a limit on the concentration of bis-alkylcarbonate and bis-guanidinium species that may exist in the initial solution phase (solubility limit), so that additional formation of these species leads to a build-up of the precipitated phase. Mathematically, this is accomplished by dividing the system into two distinct cases:

Case 1: Precipitation has not occurred and the solution remains homogeneous.

Case 2: Precipitation has occurred. The total saturation is the sum of CO_2 absorbed in the original solution phase and in precipitated phase.

$$\theta = \begin{cases} \theta_{soln}, & \alpha_{\text{CO}_2} < \alpha_{sp} \\ \theta_{soln} + \theta_{ppt}, & \alpha_{\text{CO}_2} \geq \alpha_{sp} \end{cases} \quad \text{eq. 1.8}$$

Figure 1-20: Coupled equilibrium model for the bifunctional system accounting for phase separation.



In case 1, θ_{soln} is calculated in the same way as for the homogeneous bifunctional system using equation 7 (see above section).

In case 2,

$$\theta_{soln} = \frac{G^+G:A^-A_{soln} + G^+G^+:(A^-A)_{2soln} + G^+G^+:A^-A^-_{soln}}{2 GG_i}$$

$$\theta_{ppt} = \frac{G^+G^+:A^-A^-_{ppt}}{2 GG_i}$$

Hereafter, the subscript “*soln*” will be used to identify species that remain in the solution phase, and “*ppt*” the species that have left the solution phase via precipitation. The parameter α_{sp} is the CO_2 activity beyond which precipitation occurs. We assume that the bis-cationic G^+G^+ and bis-anionic A^-A^- have lower solubility than other charged species are first to phase separate. K_{sp} is the solubility product (the maximum concentration) beyond which G^+G^+ and A^-A^- precipitate:

$$K_{sp} = G^+G^+:A^-A^-_{MAX}$$

Recall from above that $G^+G^+:A^-A^-$ may be expressed in terms of equilibrium constant K_0 :

$$G^+G^+:A^-A^- = 2 GG_f AA_f EM K_0^2 \alpha_{CO_2}^2$$

when $G^+G^+:A^-A^- = G^+G^+:A^-A^-_{MAX}$ then $\alpha_{CO_2} = \alpha_{sp}$:

$$G^+G^+:A^-A^-_{MAX} = 2 GG_f AA_f EM K_0^2 \alpha_{sp}^2$$

Note that both GG_f and AA_f in the above equation are functions of α_{CO_2} , so the equation cannot be rearranged to solve for α_{sp} explicitly. In practice, we determined α_{sp} using a looping algorithm. $G^+G^+:A^-A^-$ was calculated at a discrete α_{CO_2} value and the output was compared to the maximum soluble concentration $G^+G^+:A^-A^-_{MAX}$. If $G^+G^+:A^-A^- < G^+G^+:A^-A^-_{MAX}$, the calculation is repeated with incrementally larger values of α_{CO_2} . When $G^+G^+:A^-A^- \geq G^+G^+:A^-A^-_{MAX}$, the algorithm returns $\alpha_{CO_2} = \alpha_{sp}$.

Before precipitations occurs, the concentration of $G^+G^+:A^-A^-$ is calculated in the same way as for the homogeneous case:

$$G^+G^+:A^-A^- = 2 GG_f AA_f EM K_0^2 \alpha_{CO_2}^2$$

After precipitation occurs, the equilibrium concentration of all species in the solution phase change in response to material that has precipitated. After precipitation, $G^+G^+:A^-A^- = G^+G^+:A^-A^-_{MAX}$.

$$G^+G^+:A^-A^-_{MAX} = 2 GG_{f,soln} AA_{f,soln} EM K_0^2 \alpha_{CO_2}^2 \quad \text{eq. 1.9}$$

Here, the values of $GG_{f,soln}$ and $AA_{f,soln}$ account for material that has precipitated. The final solution concentration $GG_{f,soln}$ is equal to the initial bifunctional guanidine concentration GG_i minus the sum of guanidinium species that have formed in solution and precipitated:

$$GG_{f,soln} = GG_i - [G^+G:A^-A_{soln} + G^+G^:(A^-A)_{2soln} + G^+G^+:A^-A^-_{soln} + G^+G^+:A^-A^-_{ppt}]$$

Likewise, $AA_{f,soln}$ is equal to the initial bifunctional alcohol concentration AA_i minus the sum of alkylcarbonate species that have formed in solution and precipitated:

$$AA_{f,soln} = AA_i - [G^+G:A^-A_{soln} + 2 G^+G^:(A^-A)_{2soln} + G^+G^+:A^-A^-_{soln} + G^+G^+:A^-A^-_{ppt}]$$

For the above two equations, let

$$x = G^+G:A^-A_{soln} + G^+G^:(A^-A)_{2soln} + G^+G^+:A^-A^-_{soln} + G^+G^+:A^-A^-_{ppt}$$

therefore

$$GG_{f,soln} = GG_i - x$$

$$AA_{f,soln} = AA_i - [x + G^+G^:(A^-A)_{2soln}]$$

If x is large compared to $G^+G^+:(A^-A)_{2soln}$ (valid if $EM \gg AA_i$)

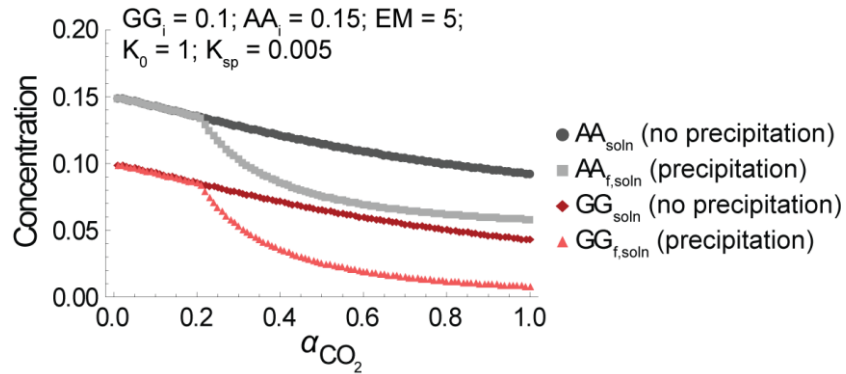
$$AA_{f,soln} \approx AA_i - x$$

We plug the expressions for $GG_{f,soln}$ and $AA_{f,soln}$ into equation 9.

$$G^+G^+:A^-A^-_{MAX} = 2(GG_i - x)(AA_i - x) EM K_0^2 \alpha_{CO_2}^2$$

The above quadratic equation was solved for x at discrete values of α_{CO_2} using Mathematica. Values of x where $0 < x < GG_i$ and $0 < x < AA_i$ were kept. The values were then used to calculate $GG_{f,soln}$ and AA_{soln} from the expressions $GG_{f,soln} = GG_i - x$ and $AA_{f,soln} \approx AA_i - x$. Below we plot the concentrations without precipitation (GG_f and AA_f) and with precipitation ($GG_{f,soln}$ and $AA_{f,soln}$). The plots diverge past $\alpha_{CO_2} = \alpha_{sp}$, which marks the onset of precipitation.

Figure 1-21: Comparison of solution phase concentrations of unreacted bifunctional alcohol (AA) and bifunctional guanidine (GG), with and without precipitation.



In region 2, θ_{soln} is calculated using $GG_{f,soln}$ and $AA_{f,soln}$ instead of GG_f and AA_f .

$$\theta_{soln} = \frac{G^+G:A^-A_{soln} + G^+G^+:(A^-A)_{2soln} + G^+G^+:A^-A^-_{soln}}{2 GG_i}$$

where

$$G^+G:A^-A_{soln} = 4 GG_{f,soln} AA_{f,soln} K_0 \alpha_{CO_2}$$

$$G^+G^+:(A^-A)_{2soln} = 4 GG_{f,soln} AA_{f,soln}^2 K_0^2 \alpha_{CO_2}^2$$

$$G^+G^+:(A^-A^-)_{soln} = 2 GG_{f,soln} AA_{f,soln} EM K_0^2 \alpha_{CO_2}^2$$

The total saturation in region 2 also includes CO₂ bound by precipitated material, θ_{ppt} :

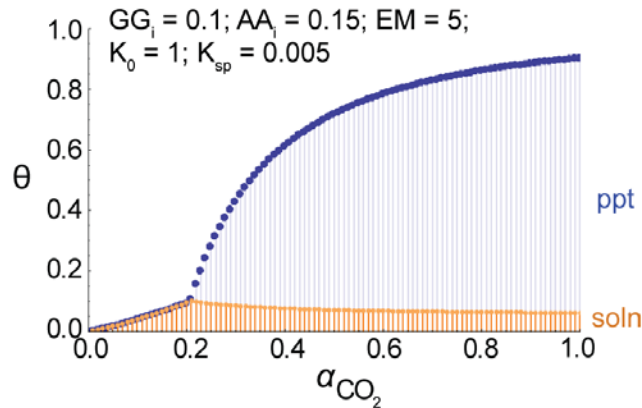
$$\theta_{ppt} = \frac{G^+G^+:(A^-A^-)_{ppt}}{2 GG_i}$$

where

$$G^+G^+:(A^-A^-)_{ppt} = x - [G^+G:A^-A_{soln} + G^+G^+:(A^-A)_{2soln} + G^+G^+:(A^-A^-)_{soln}]$$

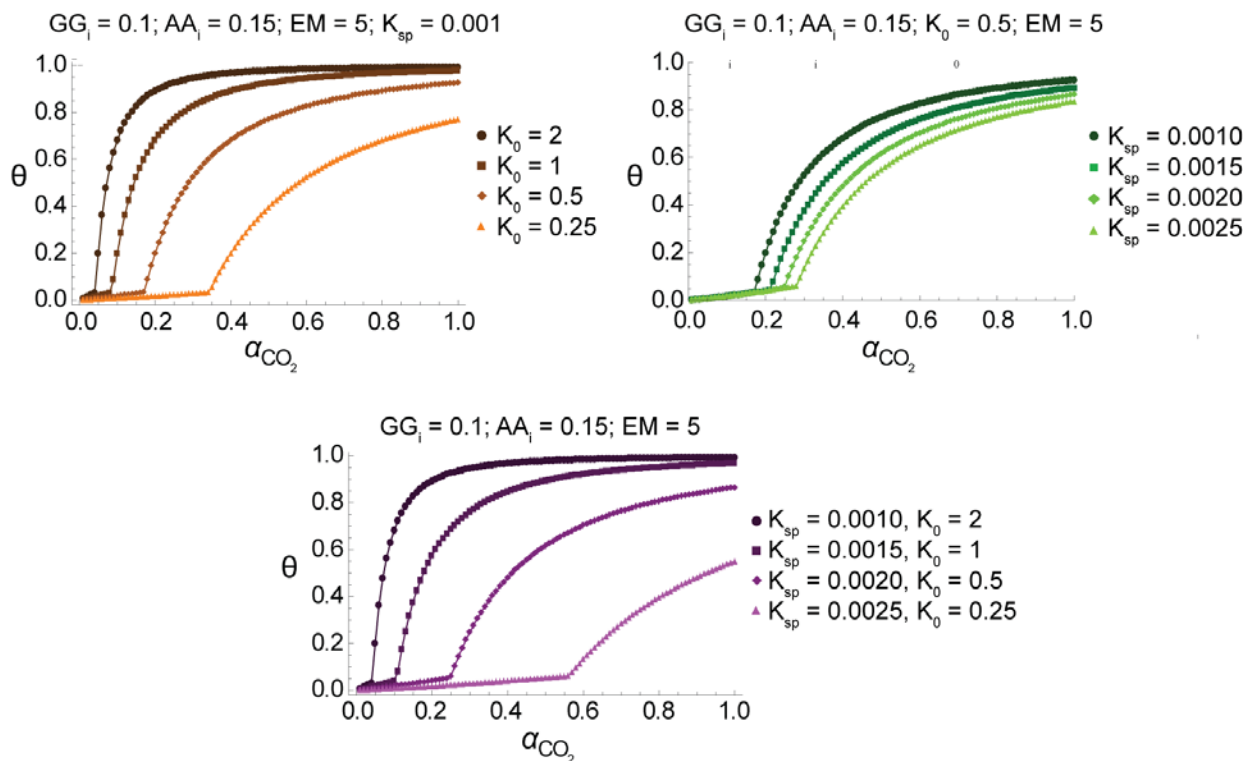
Here, x is the same used above to calculate $GG_{f,soln}$ and $AA_{f,soln}$. Below, the total saturation θ is plotted using equation 8 according to the parameters listed. Below that, the concentration of $G^+G:A^-A$, $G^+G^+:(A^-A)_2$, and $G^+G^+:(A^-A^-)$ are plotted (contrasting no precipitation versus precipitation).

Figure 1-22: Component of CO₂ saturation contained in the precipitated and solution phases.



For the chemistry used, CO_2 affinity K_0 decreases as temperature increases. Moreover, temperature likely influences the solubility K_{sp} of species formed from CO_2 binding. Below are plots of saturation θ with K_0 varied, K_{sp} varied, and K_0 and K_{sp} varied simultaneously. The final plot resembles qualitatively the experimental data and was included in the manuscript.

Figure 1-23: Example plots of total saturation ($\theta_{soln} + \theta_{ppt}$) varying K_0 , K_{sp} , and both variables simultaneously.



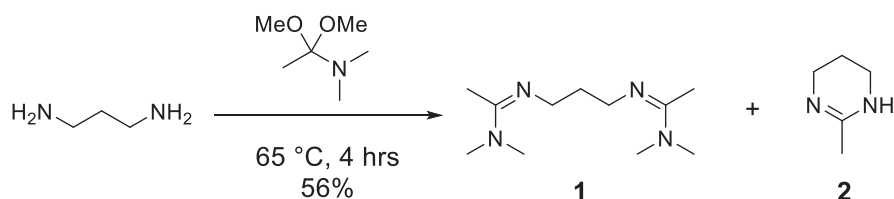
Conclusion

In summary, we have examined CO_2 binding by a system comprising a bifunctional guanidine and bifunctional alcohol. The system exhibits non-hyperbolic isotherms in bis(2-methoxyethyl)ether, where CO_2 uptake is initially suppressed, but increases abruptly following precipitation of a viscous, CO_2 -rich phase. The unique isotherm profile results from thermodynamic coupling between binding sites, and precipitation of charged alkylcarbonate and

guanidinium species as a viscous secondary phase. ^1H NMR identified the formation of distinct monoalkylcarbonate and bisalkylcarbonate species. The bisalkylcarbonate species was favored under more nonpolar solvent conditions. A thermodynamic model was constructed that rationalizes the relationship between the chelate effect, phase separation, and CO_2 binding within this solution phase system.

Experimental Section

Synthesis of bifunctional amidine **1.1**

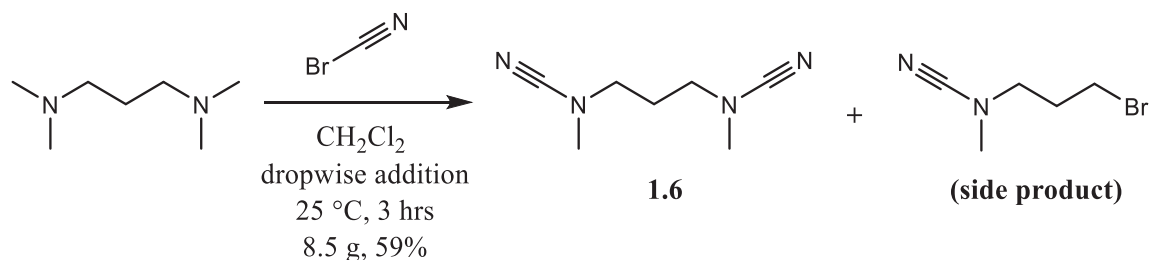


A 25 mL round-bottom flask equipped with stir bar was flame-dried under vacuum and backfilled with dry nitrogen gas. Into the flask was injected *N,N*-dimethylacetamide dimethyl acetal (7.1 mL, 53 mmol, 2.1 equiv). The flask was warmed in a 65 °C oil bath for ten minutes, then 1,3-diaminopropane (2.1 mL, 25 mmol, 1.0 equiv) added. The reaction mixture was stirred at 65 °C for 4 hours.

The mixture was concentrated by rotary evaporation to remove volatiles (methanol byproduct). The crude product was determined by ^1H NMR to comprise bifunctional amidine **1.1** and a cyclized product **1.2**. Bidentate amidine **1.1** was isolated by short-path distillation under high vacuum (91-93°C/0.3 mm Hg) as a pale-yellow oil (3.0 g, 14 mmol, 56%).

Characterization data for bifunctional amidine 1.1: ^1H NMR (500 MHz, C_6D_6): δ 3.52 (t, J = 6.7 Hz, 4 H), 2.65 (s, 12 H), 2.20 (quin, J =6.7 Hz, 2 H), 1.57 (s, 12 H), ^{13}C NMR (125 MHz, CDCl_3): δ 157.8, 48.7, 38.3, 36.2, 12.5. HRMS (ESI) m/z calcd for $\text{C}_{11}\text{H}_{24}\text{N}_4$: $[\text{M}+\text{Na}]^+$ 235.1899, found 235.1906.

Synthesis of biscyanamide **1.6**



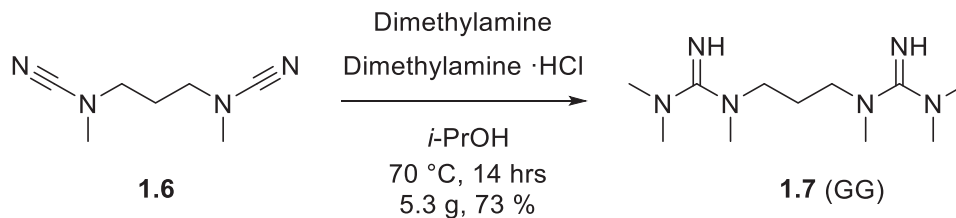
N,N,N',N'-tetramethyl-1,3-propanediamine (TMPDA) was purified prior to use by heating over CaH₂ for 3 hours at 100 °C, followed by distillation onto 4 Å molecular sieves.

In a 3-neck, 250 mL round-bottom flask a solution of cyanogen bromide (20 g, 190 mmol, 2.0 equiv) in 120 mL dry dichloromethane was prepared. Separately was prepared a solution of TMPDA (16 mL, 95 mmol, 1.0 equiv) in 35 mL dry dichloromethane. Using an addition funnel, the TMPDA solution was added dropwise into the stirring cyanogen bromide solution over 3 h, followed by an addition 15 minutes of stirring at room temperature. Throughout addition, argon was continuously bubbled through the to displace methyl bromide formed as a byproduct of the reaction.

To the reaction mixture was added excess TMPDA (4 mL diamine dissolved in 15 mL dichloromethane, added over 15 min) to quench any remaining cyanogen bromide. The reaction mixture was filtered to remove solid side products and the filtrate concentrated *in vacuo* to obtain a yellow oil.

The crude product was initially purified by dissolving in 8 mL CH₂Cl₂ and columned through 3-inch column of silica gel using EtOAc as eluent. Mixed fractions containing bis-cyanamide **1.6** and the brominated side product were combined and concentrated *in vacuo*. The product was further purified by a second round of silica gel chromatography using a gradient of 1:1 hexanes/EtOAc (*R_f* = 0.1) followed by 1:4 hexanes/EtOAc (*R_f* = 0.4). Pure fractions containing bis-cyanamide **1.6** were combined and concentrated by rotary evaporation to obtain a colorless oil (8.5 g, 56 mmol, 59%).

Characterization data for biscyanamide **1.6**: ^1H NMR (500 MHz, CDCl_3): δ 3.09 (t, $J = 6.7$ Hz, 4 H), 2.88 (s, 6 H), 1.99 (quin, $J=6.7$ Hz, 2 H), ^{13}C NMR (125 MHz, CDCl_3): δ 118.2, 49.9, 39.5, 25.4. IR (ATR): 2938.8 cm^{-1} , 2878.4 cm^{-1} , 2204.3 cm^{-1} ($\text{C}\equiv\text{N}$), HRMS (ESI) m/z calcd for $[\text{C}_7\text{H}_{12}\text{N}_4 + \text{Na}]^+$: 175.0960, found 175.0953



A 100 mL round-bottom flask was equipped with a stir bar and oven-dried. To the flask was added 50 mL isopropanol and the flask sealed with a rubber septum. While stirring, dimethylamine gas (12 g, excess) was bubbled through the solution for approximately 20 minutes, and the amount absorbed into solution was determined by weighing.

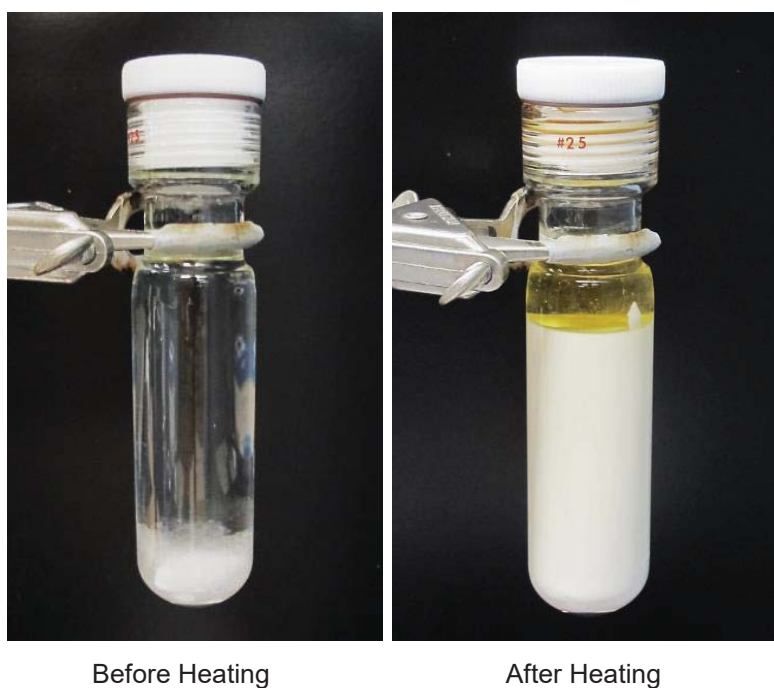
Separately, a thick-walled, pressure-safe reaction vessel (see figure XX) charged with biscyanamide **1.6** (4.5 g, 30 mmol, 1.0 equiv) and dimethylamine hydrochloride (7.2 g, 88 mmol, 3.0 equiv), followed by the isopropanol/dimethylamine solution. The vessel cap was screwed on and the vessel submerged in a 70 $^\circ\text{C}$ oil bath while stirring. After 10 minutes of heating, the dimethylamine hydrochloride dissolved completely to give a homogenous solution. After 8 hours, the dihydrochloride salt of **1.7** began to precipitate. The reaction was stirred for an additional 6 hours, for a total reaction time of 14 hours.

The reaction mixture was cooled to room temperature, and the vessel cap unscrewed. The precipitate was collected by filtration and washed with 60 mL ether. The precipitate was reacted with aqueous KOH (50 wt %, 50 g) and extracted with acetonitrile (3 x 75 mL). The extracted portions were combined and concentrated *in vacuo* to afford the product as a pale-

yellow oil with residual salts. The salts were removed by re-dissolving the product in 100 mL benzene, drying over Na₂SO₄, and filtering through a 1-inch pad of celite. The filtrate was concentrated *in vacuo* and dried under high vacuum for 3 hours to obtain bifunctional guanidine **1.7** as a pale-yellow oil (5.3 g, 22 mmol, 74%).

Characterization data for bifunctional guanidine 1.7 (GG): ¹H NMR (600 MHz, CD₃CN): δ 5.24 (br, 2 H), 3.01 (t, *J* = 7.3 Hz, 4 H), 2.64 (s, 6 H), 2.63 (s, 12 H), 1.72-1.67 (m, 2 H). ¹³C NMR (125 MHz, CD₃CN): δ 167.7, 49.5, 39.8, 37.1, 25.2. IR (ATR): 3316.8cm⁻¹, 2936.2cm⁻¹, 2838.9cm⁻¹, 1588.8 cm⁻¹. HRMS (ESI): *m/z* calcd for [C₁₁H₂₆N₆ + Na]⁺: 265.2117, found 265.2113

Figure 1-24: Selective precipitation of bisguanidinium dichloride salt.



NMR Experiments

Materials: NMR solvents were obtained from Cambridge Isotope Labs and dried over 4Å molecular sieves before use. 1,5-pentanediol (Alfa Aesar) was distilled over CaH₂. Samples were prepared in J. Young style NMR tubes (Norell, Catalog #: S-5-600-VT-8).

Solvent Titration

A series of samples were prepared with varying solvent composition, ranging from 20-100% DMSO- d_6 in 10% increments (acetonitrile- d_3 was used as the co-solvent). For all samples, the concentrations of *GG* (50 mM) and *AA* (100 mM) were held constant. To ensure accurate sample concentrations, stock solutions were prepared (*GG*, 0.5 M in DMSO- d_6 ; *AA*, 1.0 M in DMSO- d_6), then the appropriate amount dispensed into the NMR tube using a 100 μ L syringe (Hamilton). The NMR tubes were connected to a Schlenck line, subjected to 4-5 freeze-pump-thaw cycles to remove dissolved gases, then backfilled with CO₂. The samples were equilibrated at 22 \pm 2 $^{\circ}$ C under 1 atm CO₂ for ten minutes with continuous agitation. Spectra were acquired with an AVANCE 600 MHz spectrometer at 25 \pm 0.5 $^{\circ}$ C using Bruker TopSpin 3.2 software. A long duty cycle, including extended delay (D1 = 12.5 s) and acquisition time (AQ = 10 s), was used to ensure full nuclear relaxation. Spectra were processed using MestRe NOVA v. 8.1 software. NMR acquisition and processing parameters for the titration are listed in Table 1-1.

Table 1-1: Acquisition and processing parameters for solvent titration ¹H NMR

¹H NMR Acquisition Parameters	
Pulse program (pulprog)	zg30
Delay time (D1)	12.5 s
Number of scans (NS)	8
FID size (TD)	98074
Sweep width (SW)	12.82 ppm / 7692 Hz
Transmitter frequency offset (O1)	5.61 ppm / 3369 Hz
Acquisition Time (AQ)	10 s
Dwell time (DW)	65.000 μ s
FID resolution (FIDRES)	0.1 s
Filter Width (FW)	125000 Hz
Acquisition Mode (AQ_mod)	DQD
Temperature	25 $^{\circ}$ C

After the NMR spectra were recorded, the relative ratio between A^-A^- and A^-A was determined at each solvent composition. This was done by finding the relative integration of these

species, using the well-resolved resonances between 3.6 ppm and 3.9 ppm. While the chemical shift for these resonances changed with solvent composition, the resonance corresponding to A^-A^- was always observed downfield to that corresponding to A^-A . The ratio between the two species A^-A^-/A^-A was calculated, then plotted as a function of solvent composition (Fig. 9).

Next, the ratio A^-A^-/A^-A expected for a non-cooperative (no proximity effect) system was calculated. For a non-cooperative system, the ratio should be statistically determined and dependent only on the fraction of alcohols converted to alkylcarbonates. For example, consider a system in which 40% of the alcohols are converted to alkylcarbonates. There is a $(0.4)(0.4) = 0.16$ probability that both the alcohols of AA are both converted to alkylcarbonates (A^-A^-), a $(1 - 0.4)(1 - 0.4) = 0.36$ probability that neither alcohol is converted to an alkylcarbonate (AA), and a $(0.4)(1 - 0.4) + (1 - 0.4)(0.4) = 0.48$ probability that just one of the alcohols is converted to an alkylcarbonate (A^-A). The ratio A^-A^-/A^-A would then be $0.16/0.48 = 0.33$. In general, if the fraction of alcohols converted to alkylcarbonates is p , then the probability of obtaining A^-A^- is p^2 and the that of obtaining A^-A is $2(p)(1 - p)$. The ratio A^-A^-/A^-A is then $\frac{p^2}{2(p)(1-p)}$ or simply $\frac{p}{2(1-p)}$. Experimentally, p was determined by integrating signals falling between 3.6 ppm to 3.9 ppm (corresponding to protons adjacent the alkyl carbonate group), then dividing this value by the combined integration of resonances falling between 3.35 ppm to 3.9 ppm (corresponding to the protons adjacent an alkylcarbonate plus those adjacent an unreacted alcohol).

The experiment was repeated in triplicate to determine the standard error associated with the value A^-A^-/A^-A at each solvent composition. This was done for both the measured and statistical (non-cooperative) value. Species concentrations and standard errors are tabulated in Table 1-2.

Table 1-2: Tabulated data for the NMR solvent titration experiment.

%DMSO- d_6	AA _i (mM)	A-A' (mM)	A-A (mM)	AA _r (mM)	p	A-A' /A-A		A-A' /A-A (avg. ± std. dev)	
						Measured	Expected	Measured	Expected
20	102	24	38	41	0.42	0.63	0.36	0.60±0.02	0.36±0.00
	101	23	39	40	0.42	0.59	0.36		
	98	22	38	38	0.42	0.59	0.36		
30	103	22	39	42	0.40	0.55	0.34	0.54±0.01	0.34±0.00
	97	20	38	38	0.41	0.53	0.34		
	106	22	42	42	0.41	0.53	0.34		
40	96	19	37	40	0.39	0.52	0.32	0.52±0.03	0.33±0.01
	106	20	42	44	0.39	0.49	0.32		
	103	21	39	42	0.40	0.55	0.33		
50	104	19	41	43	0.38	0.47	0.31	0.49±0.04	0.32±0.01
	103	19	42	42	0.39	0.47	0.32		
	104	21	40	43	0.40	0.53	0.33		
60	99	18	39	42	0.38	0.46	0.31	0.46±0.00	0.32±0.01
	100	19	41	40	0.39	0.46	0.32		
	96	18	39	39	0.39	0.47	0.32		
70	98	17	40	41	0.38	0.43	0.31	0.43±0.01	0.31±0.01
	98	17	41	40	0.39	0.42	0.31		
	100	18	41	40	0.39	0.44	0.32		
80	100	18	40	42	0.38	0.45	0.31	0.42±0.03	0.31±0.01
	100	17	43	40	0.38	0.39	0.31		
	104	19	44	41	0.39	0.43	0.32		
90	103	18	43	43	0.38	0.41	0.30	0.40±0.01	0.31±0.01
	105	19	45	42	0.39	0.41	0.32		
	104	18	45	41	0.39	0.39	0.32		
100	108	19	46	43	0.39	0.42	0.32	0.41±0.01	0.32±0.00
	104	18	45	41	0.39	0.40	0.32		
	99	17	42	40	0.39	0.42	0.31		

References

- ¹ Jackson, R.; Quere, C.; Andrew, R. Canadell, J. Korsbakken, J., Liu, Z. Peters, G. Zheng, B. "Global Energy Growth is Outpacing Decarbonization." *Environ. Res. Lett.* **2018**, *13*, 120401.
- ² Lüthi, D., M. Le Floch, B. Bereiter, T. Blunier, J.-M. Barnola, U. Siegenthaler, D. Raynaud, J. Jouzel, H. Fischer, K. Kawamura, and T.F. Stocker. "High-Resolution Carbon Dioxide Concentration Record 650,000–800,000 Years Before Present." *Nature*, **2008**, *453*, 379–382.
- ³ Bereiter, B.; Eggleston, S.; Schmitt, J.; Nehrbass-Ahles, C.; Stocker, T.F.; Fischer, H.; Kipfstuhs, S.; Chappellaz J. "Revision of the EPICA Dome C CO₂ record from 800 to 600-kyr before present." *Geophysical Research Letters*, **2015**, *42*, 542–549.
- ⁴ Jevrejeva, S.; Jackson, L.; Grinsted, A.; Lincke, D.; Marzeion, B. "Flood Damage Costs Under the Sea Level Rise with Warming of 1.5 C and 2.0 °C." *Environ. Res. Lett.* **2018**, *13*, 074014.
- ⁵ Shakhova, N.; Semiletov, I.; Salyuk, A.; Yusupov, V.; Kosmach, D.; Gustafsson, O. "Extensive Methane Venting to the Atmosphere from Sediments of the East Siberian Arctic Shelf." *Science*, **2010**, *327*, 1246–1250.
- ⁶ Phrampus, B.; Hornbach, M. "Recent Changes to the Gulf Stream causing Widespread Gas Hydrate Destabilization." *Nature*, **2012**, *490*, 527–530.
- ⁷ Figueres, C.; Schellnhuber, H.; Hiteman, G.; Rockström, J.; Hobley, A.; Rahmstorf, S. "Three Years to Safeguard our Climate." *Nature*, **2017**, *546*, 593–595.
- ⁸ Plotted using data from: Statistical Review of World Energy 2018. *British Petroleum*. Accessed 27 May 2019. (url: <https://www.bp.com/en/global/corporate/energy-economics/statistical-review-of-world-energy.html>).
- ⁹ Valerie Volcovici. "U.S. Submits Formal Notice of Withdrawal from Paris Climate Pact." 4 August 2017. *Reuters*. Accessed 4 April 2019.
- ¹⁰ Harry Cockburn. "Australia Pulls Out of Climate Change Targets Agreed at Paris Conference." 20 August 2018. *Independent*. Accessed 14 April 2019.
- ¹¹ Mimi Nguyen Ly. "China Building New Coal Plants Equal to Entire US Capacity." 7 October 2018. *The Epoch Times*. Accessed 14 April 2018.
- ¹² International Energy Agency. *20 Years of Carbon Capture and Storage*; IEA Publications: Paris, 2016.
- ¹³ Keith, D.; Holmes, G.; Angelo, D.; Heidel, K. "A Process for Capturing CO₂ from the Atmosphere." *Joule*, **2018**, *2*, 1573–1594.
- ¹⁴ Stephen Leahy. "This Gasoline is Made of Carbon Sucked From the Air" 7 June 2018. *National Geographic*. Accessed 14 April 2018. (url: <https://news.nationalgeographic.com/2018/06/carbon-engineering-liquid-fuel-carbon-capture-neutral-science/>).
- ¹⁵ "Special Report on Global Warming of 1.5 °C." *Intergovernmental Panel on Climate Change*. Accessed 14 April 2018. (url: <https://www.ipcc.ch/sr15/>)
- ¹⁶ "The Global Status of CCS: 2018." *Global CCS Institute*. Accessed 4 April 2019. (url: <https://www.globalccsinstitute.com/resources/global-status-report/>).
- ¹⁷ Zeman, F.; Lackner, K. "Capturing Carbon Dioxide Directly from the Atmosphere." *World Resource Rev.* **2004**, *16*, 157–172.
- ¹⁸ Rochelle, G. "Amine Scrubbing for CO₂ Capture." *Science*. **2009**, *325*, 1652–1654.
- ¹⁹ R. R. Bottoms (Girdler Corp.), "Separating acid gases," U.S. Patent 1783901, 1930.
- ²⁰ (a) Rubin, E.; Davison, J.E.; Herzog, H.J. "The Cost of CO₂ Capture and Storage." *Int. J. Greenh. Gas Contr.* **2015**, *40*, 378–400. (b) Rubin, E.; Mantripragada, H.; Marks, A.; Versteeg, P.; Kitchin, J. "The Outlook for Improved Carbon Capture Technology." *Prog. Energy Combust. Sci.*, **2012**, *38*, 630–671.
- ²¹ For reviews on CO₂-capture materials, see: (a) D'Alessandro, D.M.; Smit, B.; Long, J.R. "Carbon Dioxide Capture: Prospects of New Materials." *Angew. Chem. Int. Ed.* **2010**, *49*, 6058–6082. (b) Arunkumar, S.; Zhao, A.; Shimizu, G.K.H.; Sarkar, P.; Gupta, R. "Post-Combustion CO₂ Capture Using Solid Sorbents: A Review" *Ind. Eng. Chem. Res.* **2012**, *51*, 1438–1463.
- ²² (a) Seo, S.; Quiroz-Guzman, M.; DeSilva, M.A.; Lee, T.; Huang, Y.; Goodrich, B.F.; Schneider, W.F.; Brennecke, J.F. "Chemically Tunable Ionic Liquids with Aprotic Heterocyclic Anion (AHA) for CO₂ Capture."

J. Phys. Chem. B. **2014**, *118*, 5740–5751. (b) Feng, Z.; Cheng-Gang, F.; You-Ting, W.; Yuan-Tao, W.; Ai-Min, L.; Zhi-Bing, Z. “Absorption of CO₂ in the Aqueous Solutions of Functionalized Ionic Liquids and MDEA”. *Chem. Eng. J.* **2010**, *160*, 691–697.

²³(a) Nugent, P.; Belmabkhout, Y.; Burd, S.D.; Cairns, A.J.; Luebke, R.; Forrest, K.; Pham, T.; Ma, S.; Space, B.; Wojtas, L.; Eddaoudi, M.; Zaworotko, M.J. *Nature*, **2013**, *495*, 80–84. (b) Demessence, A.; D’Alessandro, D.M.; Foo, M.L.; Long, J.R. “Strong CO₂ Binding in a Water-Stable, Triazolate-Bridged Metal-Organic Framework Functionalized with Ethylenediamine.” *J. Am. Chem. Soc.* **2009**, *131*, 8784–8786.

²⁴ (a) Dawson, R.; Adams, D.J.; Cooper, A.I. “Chemical Tuning of CO₂ Sorption in Robust Nanoporous Organic Polymers.” *Chem. Sci.* **2011**, *2*, 1173–1177. (b) Walton, K.S.; Abney, M.B.; LeVan, D. “CO₂ Adsorption in Y and X Zeolites Modified by Alkali Metal Cation Exchange.” *Microporous Mesoporous Mater.* **2006**, *91*, 78–84.

²⁵ (a) Walton, K.; Millward, A.R.; Dubbeldam, D.; Frost, H.; Low, J.; Yaghi, O.M.; Snurr, R.Q. “Understanding Inflections and Steps in Carbon Dioxide Adsorption Isotherms in Metal-Organic Frameworks.” *J. Am. Chem. Soc.* **2008**, *130*, 406–407. (b) Li, D.; Kaneko, K. “Hydrogen Bond-Regulated Microporous Nature of Copper Complex-Assembled Microcrystals.” *Chem. Phys. Lett.* **2001**, *335*, 50–56. (c) Millward, A.; Yaghi, O.M. “Metal-Organic Frameworks with Exceptionally High Capacity of Storage of Carbon Dioxide at Room Temperature.” *J. Am. Chem. Soc.* **2005**, *127*, 17998–17999. (d) McDonald, T.M.; Lee, W.R.; Mason, J.A.; Wiers, B.M.; Hong, C.S.; Long, J.R. “Capture of Carbon Dioxide from Air and Flue Gas in the Alkylamine-Appended Metal-Organic Framework mmen-Mg₂(dobpdc).” *J. Am. Chem. Soc.* **2012**, *134*, 7056–7065. (e) McDonald, T.M.; Mason, J.A.; Kong, X.; Bloch, E.D.; Gygi, D.; Dani, A.; Crocellà, V.; Giordanino, F.; Odoh, S.O.; Drisdell, W.S.; Vlasisavljevich, B.; Dzubak, A.L.; Poloni, R.; Schnell, S.K.; Planas, N.; Lee, K.; Pascal, T.; Wan, L.F.; Prendergast, D.; Neaton, J.B.; Smit, B.; Kortright, J.B.; Gagliardi, L.; Bordiga, S.; Reimer, J.A.; Long, J.R. “Cooperative Insertion of CO₂ in Diamine-Appended Metal-Organic Frameworks.” *Nature*, **2015**, *519*, 303–308. (f) Seo, S.; Simoni, L.; Ma, M.; DeSilva, M.; Huang, Y.; Stadtherr, M.A.; Brennecke, J.F. “Phase-Change Ionic Liquids for Postcombustion CO₂ Capture.” *Energy Fuels*. **2014**, *28*, 5968–5977.

²⁶ (a) Heldebrant, D.J.; Yonder, C.R.; Jessop, P.G.; Phan, L. “Organic Liquid CO₂ Capture Agents with High Gravimetric Capacity.” *Energy Environ. Sci.* **2008**, *1*, 487–493. (b) Mathias, P.M.; Afshar, K.; Zheng, F.; Bearden, M.D.; Freeman, C.J.; Andrea, T.; Koech, P.K.; Kutnyakov, I.; Zwoster, A.; Smith, A.R.; Jessop, P.G.; Nik, O.G.; Heldebrant, D.J. “Improving the Regeneration of CO₂-Binding Organic Liquids with a Polarity Change.” *Energy Environ. Sci.* **2013**, *6*, 2233–2242. (c) Koech, P.K.; Zhang, J.; Kutnyakov, I.V.; Cosimbescu, L.; Lee, S.-J.; Bowden, M.E.; Smurthwaite, T.D.; Heldebrant, D.J. “Low Viscosity Alkanolguanidine and Alkanolamidine Liquids for CO₂ Capture.” *RSC Adv.* **2013**, *3*, 566–572.

²⁷ We observed that a neat mixture of AA and GG became highly viscous upon CO₂ exposure, precluding equilibrium absorption measurements due to poor mass transfer and mixing.

²⁸ The saturation θ is defined as the fraction of available binding sites occupied, equal to twice the initial concentration of bifunctional AA or GG, whichever is limiting (GG for the isotherms shown). $\theta=1$ when all sites are occupied.

²⁹ (a) Hunter, C.A.; Anderson, H.L. “What is Cooperativity.” *Angew. Chem. Int. Ed.* **2009**, *48*, 7488–7499. (b) Ercolani, G.; Schiaffino, L. “Allosteric, Chelate, and Interannular Cooperativity: A Mise au Point.” *Angew. Chem. Int. Ed.* **2011**, *50*, 1762–1768.

³⁰ Assigned in analogy to related lithium alkylcarbonate salts: Matsuta, S.; Asada, T.; Kitaura, K. “Vibrational Assignments of Lithium Alkyl Carbonate and Lithium Alkoxide in the Infrared Spectra an *Ab Initio* MO Study.” *J. Electrochem. Soc.* **2000**, *147*, 1695–1702.

³¹ (a) Todorova, T.; Kröcher, O.; Delley, B. “DFT Study of Structural and Vibrational Properties of Guanidinium Derivatives”. *J. Mol. Struct. THEOCHEM.*, **2009**, *907*, 16–21. (b) Sension, R.J.; Hudson, B.; Callis, P.R. “Resonance Raman Studies of Guanidinium and Substituted Guanidinium Ions.” *J. Phys. Chem.* **1990**, *94*, 4015–4025.

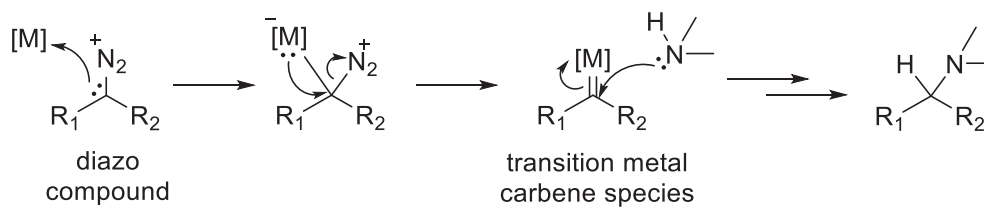
³² (a) Exner, J.H.; Steiner, E.C. “Solvation and Ion-Pairing of Alkali-Metal Alkoxides in Dimethyl Sulfoxide. Conductometric Studies.” *J. Am. Chem. Soc.* **1974**, *96*, 1782–1787. (b) Dijkstra, G.; Kruizinga, W.H.; Kellogg, R.M. “An Assessment of the Causes of the ‘Cesium Effect’.” *J. Org. Chem.* **1987**, *52*, 4230–4234.

Chapter 2: Palladium-Catalyzed Enantioselective Carbene Insertion into the N–H Bond of Aromatic Amine Heterocycles

Introduction

Transition metal carbenes are important intermediates in many modern C–C and C–heteroatom bond forming reactions. Carbene species can act as divalent synthons to generate C(sp³) stereocenters via the formation of two new σ bonds. These reactive carbene species may be generated *in situ* by the reaction of a transition metal catalyst and diazo compound. For late transition metals (e.g., Rh, Cu, Pd), the carbene is electrophilic in nature and susceptible to attack by nucleophiles (Figure 2-1). Attack by an amine at the carbene can result in formal insertion of the carbene into the amine N–H bond. This area was recently reviewed by Moody¹ and Zhou.²

Figure 2-1: Generation and reactivity of late transition metal carbene toward an amine nucleophile.

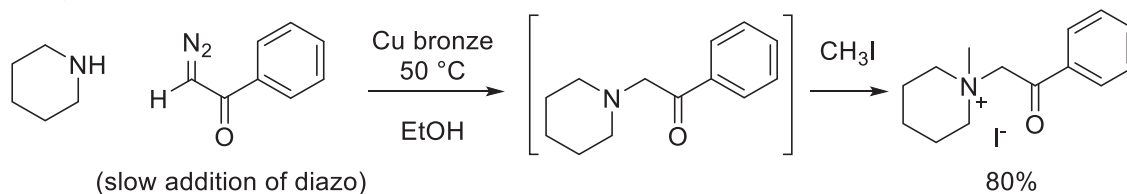


Key Advances in Transition Metal Catalyzed Carbene Insertion into N–H Bonds

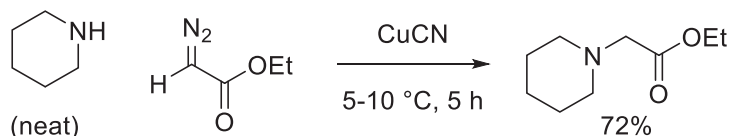
The earliest example of a transition metal catalyzed carbene insertion into an N–H bond was reported in 1952 by Yates. Yates employed heterogeneous copper bronze (“finely divided copper”) to catalyze carbene insertion into piperidine, using diazoacetophenone as the carbene precursor.³ More than a decade later, Saegusa and co-workers reported a similar transformation using CuCN and CuCl as homogeneous catalysts and ethyldiazoacetate as the carbene precursor. The authors employed piperidine and morpholine as nucleophiles (Figure 2-2).⁴

Figure 2-2: Early examples of transition metal catalyzed carbene insertion into N–H bonds.

Yates, 1952



Saegusa, 1966



In 1980, Ratcliffe and co-workers (Merck pharmaceuticals) demonstrated a diastereoselective cyclization to construct the carbapenem core of the antibiotic thienamycin (Figure 2-3).^{5,6} The example is notable as the first application of carbene insertion toward a large-scale industrial process.^{7,8,9} Later, McKervey reported an enantioselective cyclization using a chiral rhodium(II) catalyst. Intramolecular insertion into a carbamate N–H bond was achieved with moderate enantioselectivity (up to 45% ee), along with products resulting from competing C–H insertion and elimination.¹⁰

In 2004, Jørgensen and co-workers reported the first enantioselective, intermolecular insertion into an aniline N–H bond (Figure 2-4).¹¹ The authors employed CuPF_6 and a chiral bisoxazoline ligand to obtain moderate yields and enantioselectivity (28% ee). In 2007, further optimization by Zhou and co-workers dramatically improved the yield and enantioselectivity.¹²

Figure 2-3: Early examples of stereoselective cyclizations employing carbene insertion into N–H bonds.

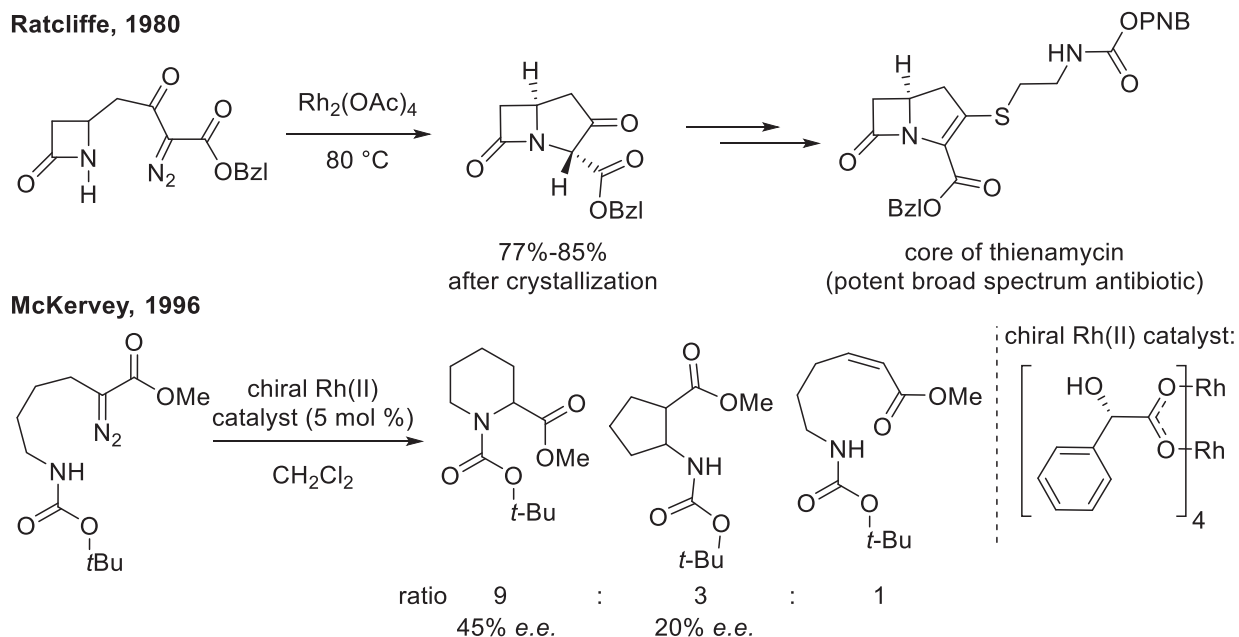
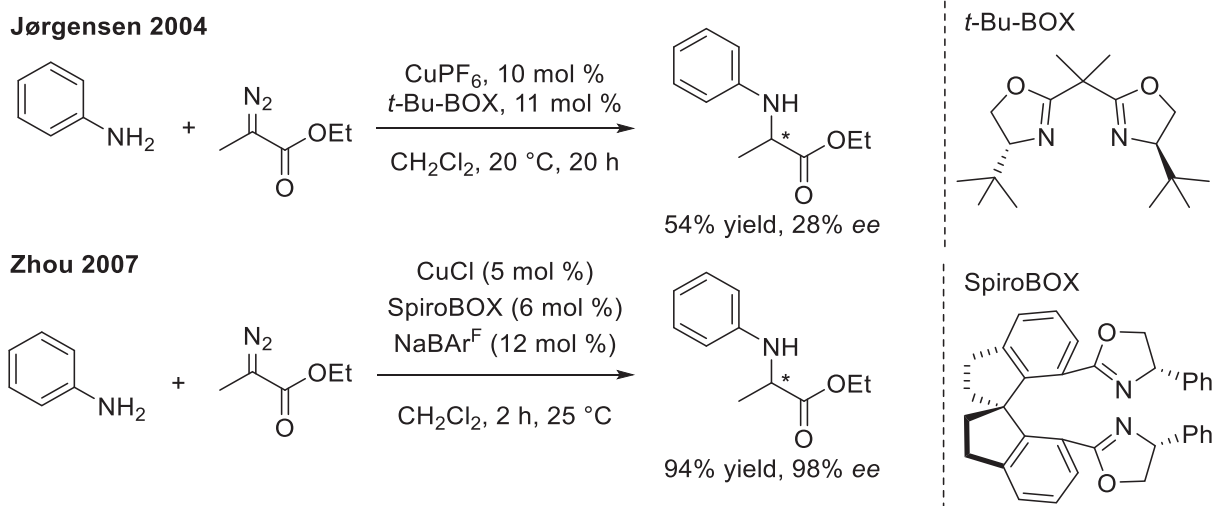


Figure 2-4: First example of enantioselective intermolecular carbene insertion into an aniline N–H and subsequent optimization.

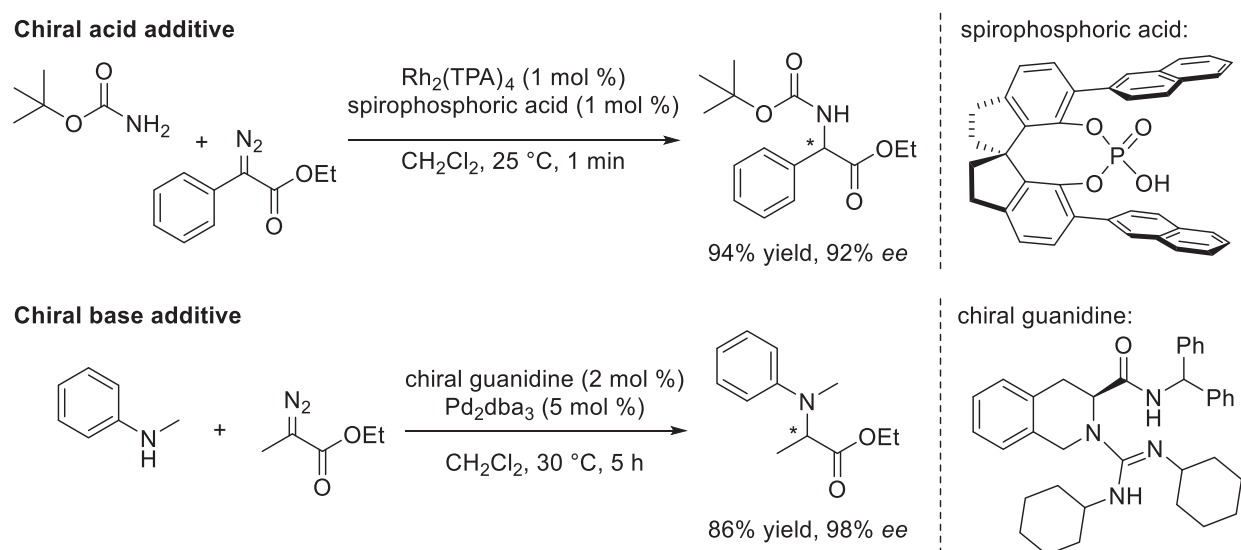


Following the reports by Jørgensen and Zhou, various conditions have been developed that catalyze enantioselective insertion. Besides chiral ligands^{13,14,15} chiral acid additives^{16,17,18} and chiral base additives^{19,20} have induced asymmetry through chiral proton transfer. For

example, chiral phosphoric acid and chiral guanidine provided excellent enantioselectivity (Figure 2-5).

The nucleophiles used in these and other enantioselective examples, however, has been limited to amides, carbamates, and anilines.^{21,22} Methods that allow other classes of amine substrates to be used would represent a valuable addition to this body of work.

Figure 2-5: Examples of enantioselective insertion using chiral acid and base additives.

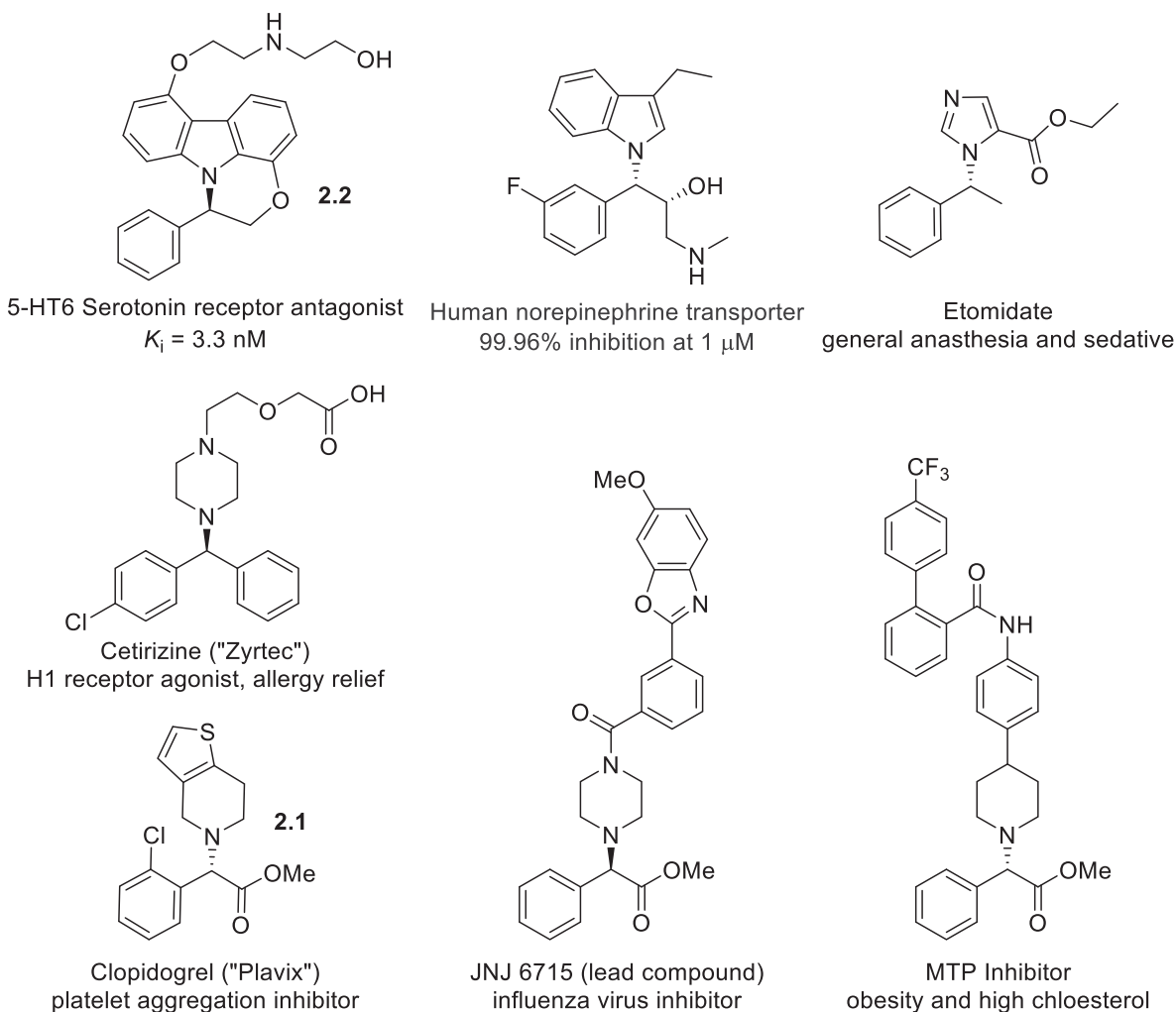


***N*-Substituted Heterocycles and Aliphatic Amines as Common Pharmacophores**

N-Substituted amines with stereocenters adjacent to nitrogen are pharmacophores for important biological targets. Selected examples include carbazole, indole, piperidine, and piperazine derivatives (Figure 2-6). For example, platelet aggregation inhibitor (*S*)-clopidogrel (PlavixTM) **2.1** was the second most prescribed drug globally in 2010 with over \$9 billion in sales.²³ *N*-Substituted arylamines are commonly accessed through inefficient and challenging substitution reactions, requiring enantioenriched starting material²⁴ or chiral resolution to obtain products with the desired stereochemistry. Other methods such as enantioselective reductive amination may be used to construct the C-N bond, but often require further manipulation to complete the amine

fragment. For example, *N*-substituted carbazole **2.2** requires a late-stage Fischer indolization to construct the heterocycle.²⁵

Figure 2-6: Biologically active *N*-substituted heterocyclic and aryl amines with chiral C(sp³) centers.^{3,26,27,28}



Carbene insertion processes are an attractive alternative to substitution reactions in forming C(sp³)–N bonds. In this and the following chapter, I describe efforts to expand the variety of amines nucleophile that can participate in carbene insertion processes. In this chapter, I discuss the application of palladium-catalyzed carbene insertions into the N–H bond of aromatic amine heterocycles. Optimization of the insertion reaction using carbazole will be discussed,

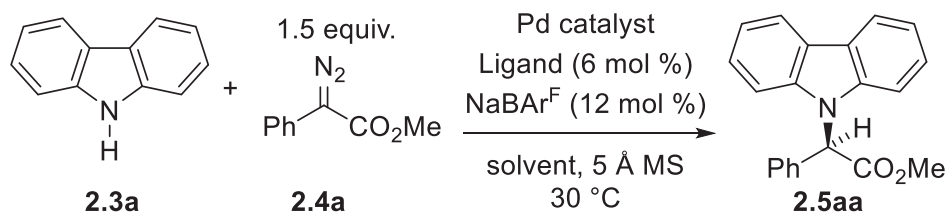
followed by application of the optimized conditions to a range of carbazole and indole substrates. The core of a potent 5-HT₆ serotonin receptor antagonist²⁵ was synthesized using the developed method. In Chapter 3, I discuss our investigation into non-conjugated (benzylic) and aliphatic amines, which have been historically challenging substrates due to their tendency to bind and deactivate transition metal catalysts. We discuss the development of a parallel addition procedure that facilitates good yields and improved *ees* for several secondary cyclic amines.

Carbazole Reaction Optimization, Substrate Scope, and Pharmacophore Synthesis

We began our optimization using carbazole as the amine nucleophile. My colleague Vanessa Arredondo performed the bulk of this optimization (Table 2-1, entries 1-10), while I performed a limited solvent screen (entries 11-13). The first conditions tested were based on existing literature precedent. Feng and co-workers employed Pd₂dba₃ and a chiral guanidine additive to catalyze carbene insertion into the N–H bonds of anilines in high yield and *ee*; the reaction used alkyldiazoacetates as the carbene precursor (Figure 2-5).²⁰ We applied Feng's conditions to carbazole **2.3a**, using methyl phenyldiazoacetate **2.4a** as the carbene precursor. The reaction was high-yielding, providing the *N*-substituted carbazole derivative **2.5aa** in quantitative yield. However, minimal *ee* was obtained. Next, reaction conditions employing Pd(PhCN)₂Cl₂ and a spiro-BOX ligand were tested and led to an encouraging improvement in *ee* up to 83% (entry 2). This was somewhat surprising given the conditions were previously optimized for carbene insertion into the O–H bond of phenols rather than the N–H bond of amines.²⁹ To test whether the improved *ee* was primarily due to using a palladium(II) source, Pd(PhCN)₂Cl₂ was tested again using the chiral guanidine additive. The resulting product was recovered in low *ee*. A further screening of Pd(PhCN)₂Cl₂ with various ligands identified (*S,S*)-*i*-Pr-PyBOX as the optimal choice, providing the carbazole derivative **2.5aa** in 99% yield and 97% *ee* (entry 8). Lower catalyst loadings still generated product in high yield and *ee*, albeit over longer reaction times

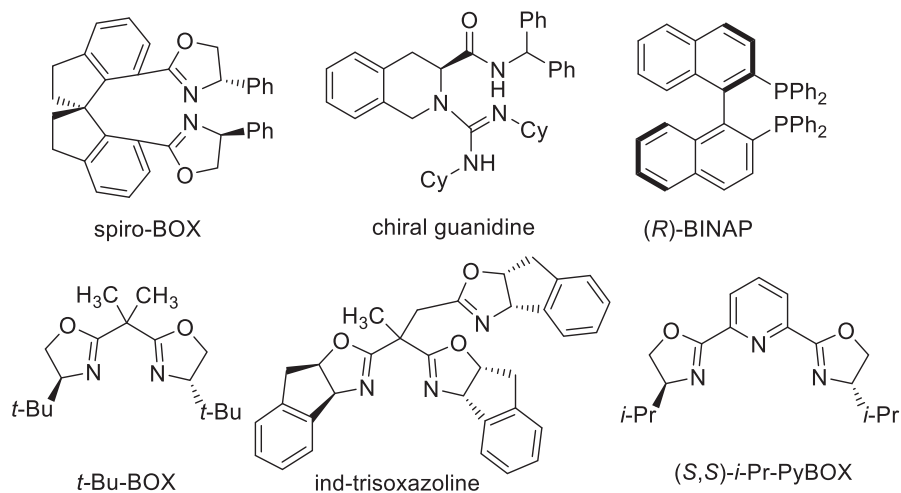
(entries 9-10). Other chlorinated solvents and toluene worked well for the reaction. The reaction did not proceed in THF.

Table 2-1: Optimization for carbene insertion into carbazole



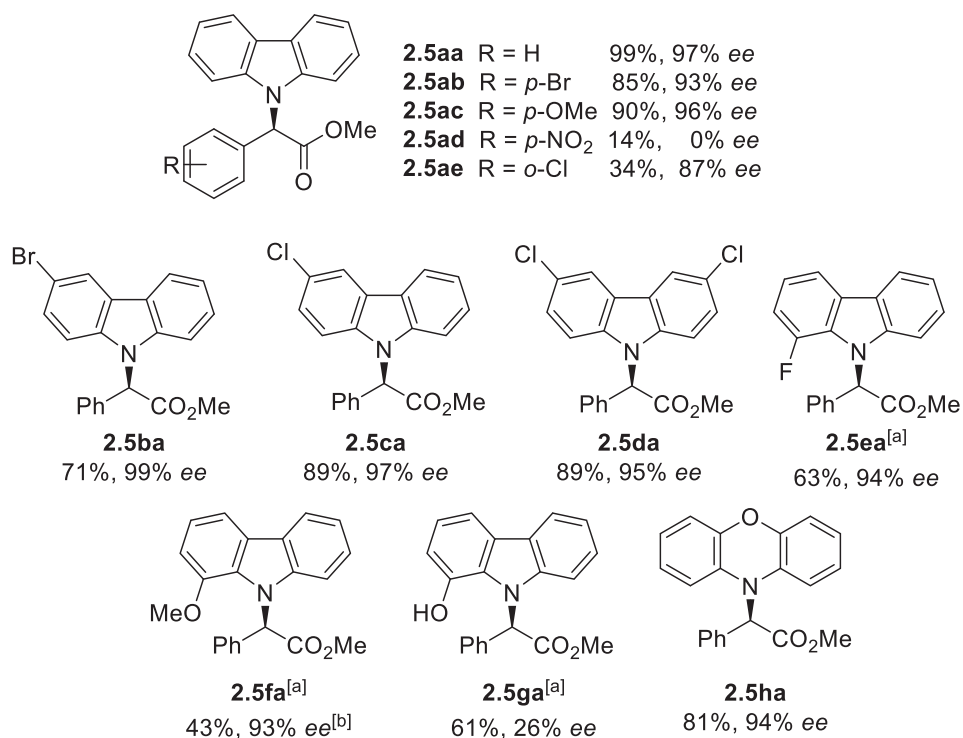
Entry	Pd	Pd (mol %)	Solvent	Ligand	t (h)	Yield (%) ^[b]	ee (%)
1	Pd ₂ dba ₃	10	CH ₂ Cl ₂	chiral guanidine	5	100	5
2 ^[a]	Pd(PhCN) ₂ Cl ₂	5	CHCl ₃	spiro-BOX	2	64	83
3	Pd(PhCN) ₂ Cl ₂	5	CHCl ₃	spiro-BOX	2	88	76
4	Pd(PhCN) ₂ Cl ₂	5	CHCl ₃	chiral guanidine	2	85	13
5	Pd(PhCN) ₂ Cl ₂	5	CHCl ₃	(<i>R</i>)-BINAP	2	0	-
6	Pd(PhCN) ₂ Cl ₂	5	CHCl ₃	<i>t</i> -Bu-BOX	2	94	15
7	Pd(PhCN) ₂ Cl ₂	5	CHCl ₃	ind-trisoxazoline	16	94	90
8	Pd(PhCN) ₂ Cl ₂	5	CHCl ₃	(<i>S,S</i>)- <i>i</i> -Pr-PyBOX	2	99	97
9	Pd(PhCN) ₂ Cl ₂	1	CHCl ₃	(<i>S,S</i>)- <i>i</i> -Pr-PyBOX	4	98	97
10	Pd(PhCN) ₂ Cl ₂	0.5	CHCl ₃	(<i>S,S</i>)- <i>i</i> -Pr-PyBOX	20	91	95
11	Pd(PhCN) ₂ Cl ₂	5	DCE	(<i>S,S</i>)- <i>i</i> -Pr-PyBOX	4	100	96
12	Pd(PhCN) ₂ Cl ₂	5	PhMe	(<i>S,S</i>)- <i>i</i> -Pr-PyBOX	4	95	95
13	Pd(PhCN) ₂ Cl ₂	5	THF	(<i>S,S</i>)- <i>i</i> -Pr-PyBOX	4	0	-

^[a]2 equiv. of diazo, no NaBAR^F, no MS. ^[b]Isolated yield.



With the optimized conditions (entry 8), we explored the scope of the reaction with other diazo compounds and *N*-heterocycles. Diazo compounds with varying substitution on the aryl ring, reacted with carbazole to form products **2.5ab-2.5ae** (Figure 2-7). I was responsible for synthesizing *para*-substituted derivatives **2.5ab-2.5ad**. *Para*-substitution with an electron-donating methoxy group accelerated the reaction, with carbazole fully consumed in 30 minutes. In contrast, an electron-withdrawing *para*-nitro group slowed the reaction significantly, affording a low yield of **2.5ad** after 24 h at 55°C. Not surprisingly, the easily enolizable *para*-nitro analogue **2.5ad** was obtained as the racemate. With an *ortho*-chloro substituent, product **2.5ae** was obtained in low yield, but good ee.

Figure 2-7. Scope of reaction with various carbazole substrates, using conditions from Table 2-1, entry 8.

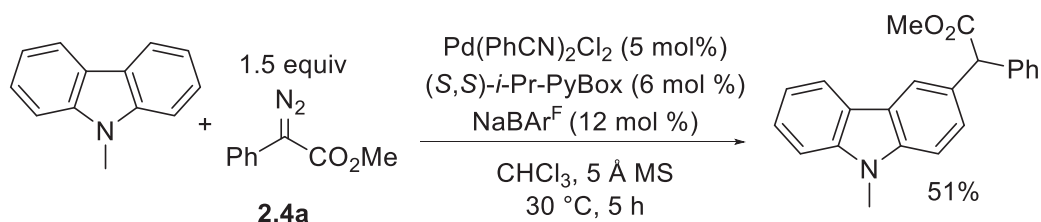


^[a]10 mol % Pd, 12 mol % (*S,S*)-*i*-Pr-PyBOX, 24 mol % NaBARF, and 8 h slow addition of diazo.

^[b]ee determined following reduction of the ester to the corresponding alcohol.

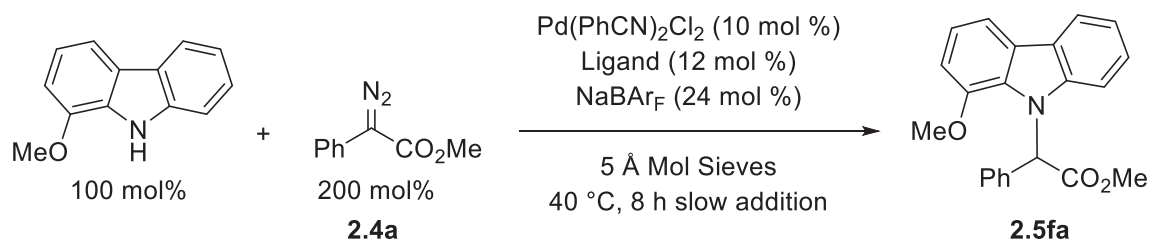
Halogen substituents on the diazo or carbazole substrate were tolerated, but bromine substituents led to slightly lower yields and incomplete conversion, possibly due to catalyst deactivation resulting from oxidative addition (**2.5ab** and **2.5ba**). My colleague Eugene Gutman was responsible for synthesizing halogenated carbazole derivatives **2.5ba–2.5da**. 1-Substituted carbazoles were challenging, affording products **2.5ea–2.5ga** in yields below 30% using the optimized conditions. We presume that substitution at the carbazole 1-position slows down nucleophilic addition to the palladium carbene primarily due to steric effects. I was responsible for synthesizing and further optimizing reaction conditions for these 1-substituted carbazole substrates. Improved yields were obtained using higher temperatures, higher catalyst loadings, and slow addition of the diazo compound. Still, up to 200 mol % of the diazo compound was required because competing dimerization or side reactions depleted the diazo starting material. With hindered 1-methoxycarbazole, the insertion product **2.5fa** was accompanied by an inseparable mixture of products resulting from insertion into the electron-rich aromatic ring. In a control experiment where the carbazole nitrogen was blocked, 9-*N*-methylcarbazole underwent C-H insertion at the aromatic ring in 51% yield (Figure 2-8).³⁰

Figure 2-8: C–H insertion observed with insertion at nitrogen is blocked.

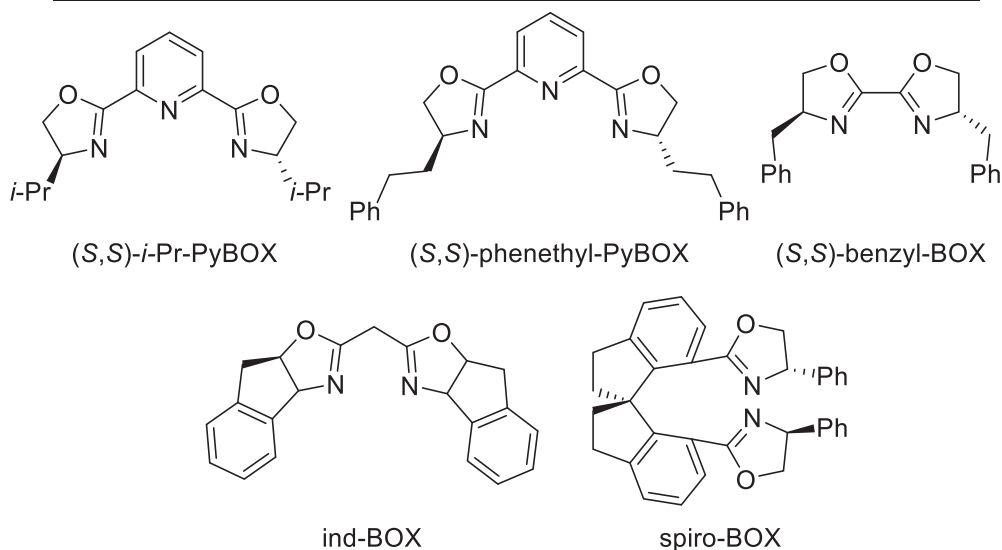


Several bisoxazoline ligands were screened to see if modifying the steric environment around palladium could improve the efficiency of insertion into 1-methoxycarbazole (Figure 2-9). None of the bisoxazoline ligands tested provided a better yield than the original (*S,S*)-*i*-Pr-PyBOX ligand.

Figure 2-9: Ligand screen for insertion into 1-methoxycarbazole.



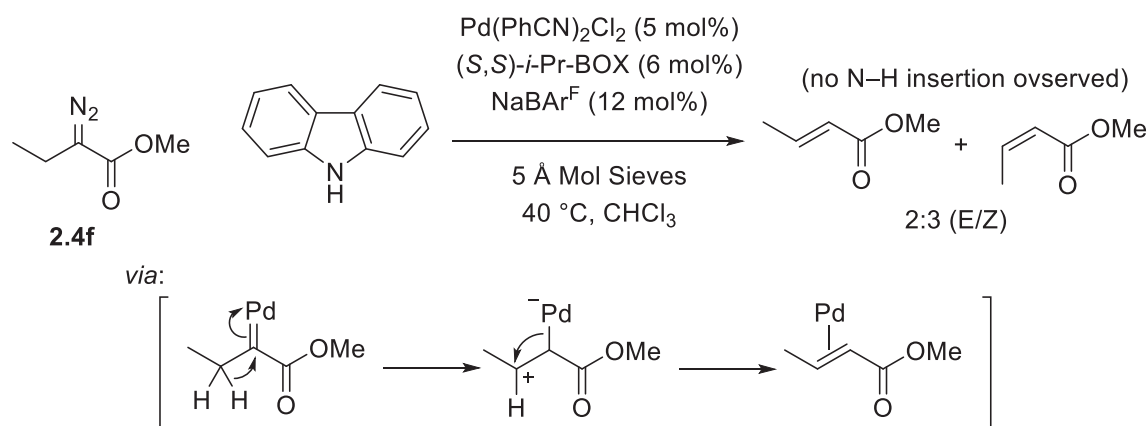
entry	ligand	yield	1-methoxycarbazole recovered
1	(<i>S,S</i>)- <i>i</i> -Pr-PyBOX	43%	8%
2	(<i>S,S</i>)-phenethyl-PyBOX	25%	40%
3	(<i>S,S</i>)-benzyl-BOX	36%	20%
4	ind-BOX	20%	34%
5	spiro-BOX	14%	25%



With 1-hydroxycarbazole, the insertion product **2.5ga** was obtained in up to 61% yield and 4:1 selectivity over the O-H insertion product.^[5e] This was surprising considering the carbazole nitrogen is more sterically hindered than the hydroxyl group, suggesting that the nitrogen lone pair is intrinsically more nucleophilic. The ee for **2.5ga** was highly variable (0 to 49%) depending on reaction conditions, possibly due to the hydroxyl group acting as an achiral proton source. Carbazole-like substrates such as phenoxazine also worked well, but some over-insertion products were observed.

α -Alkyl- α -diazoester **2.4f** was a poor substrate due to palladium-catalyzed elimination. Methyl α -diazobutanoate formed (*E*)- and (*Z*)-methylcrotonate as the sole products (Figure 2-10). Similar results with the experiment repeated excluding carbazole.

Figure 2-10: Palladium catalyzed elimination of alkyldiazoacetates to alkenes



My colleagues Vanessa Arredondo and Eugene Gutman applied the N–H insertion reaction towards synthesizing the core of 5-HT₆ receptor antagonist **2.2** (Figure 2-11). Oxazinocarbazole **2.8** was synthesized by DIBAL-H reduction of **2.5fa** to the alcohol, mesylation, and a one-step thermal cyclization-dealkylation sequence. This concise synthesis highlights the utility of the palladium-catalyzed N–H insertion reaction, avoiding a lengthy synthesis of oxazinocarbazoles that involved a late-stage Fischer indolization.¹ The last cyclization step could be performed at much lower temperature if triflic anhydride was first used to activate the primary alcohol (Figure 2-12).

Figure 2-11: Synthesis of the core of 5-HT6 receptor antagonist

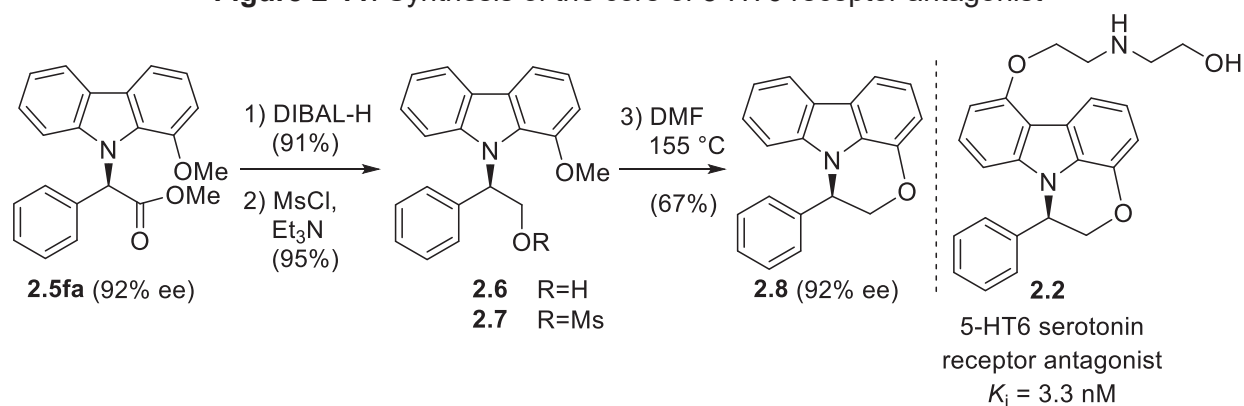
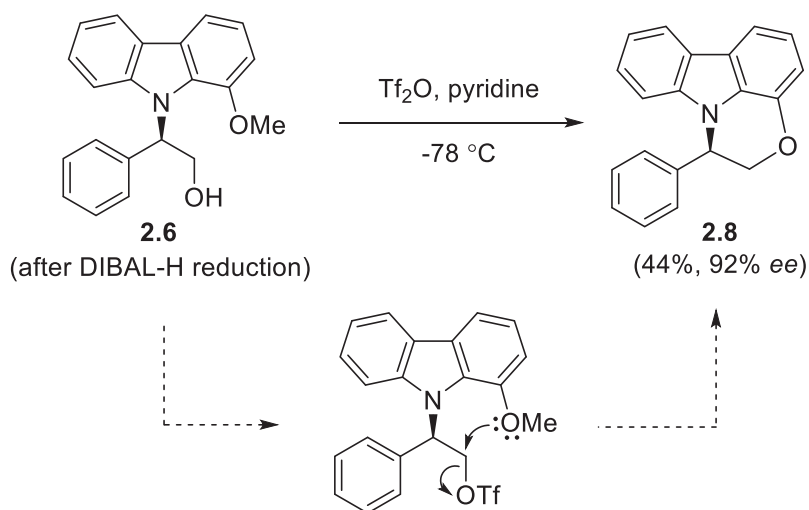


Figure 2-12: Alternative cyclization procedure



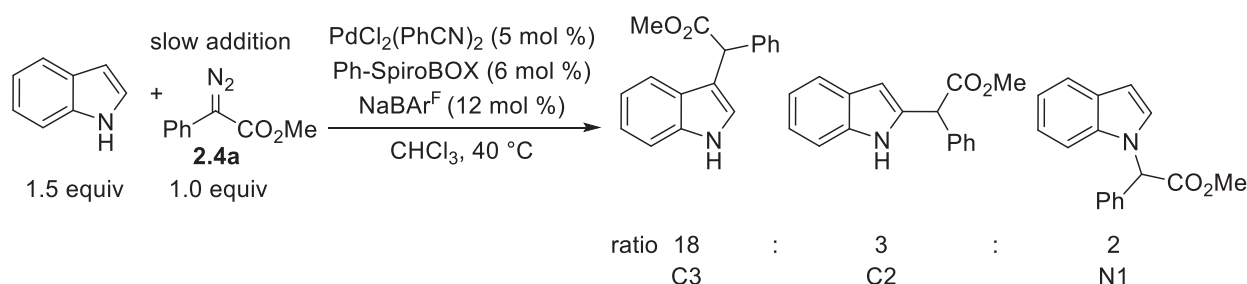
Other attempts to first deprotect the methoxy group and use the resulting alcohol to effect cyclization were unsuccessful. For example, treating reduced carbazole derivative **2.6** with HBr/AcOH at 100 °C led to cleavage of the C-N bond formed during palladium-catalyzed insertion reaction.

Indole Reaction Optimization and Substrate Scope

After examining the substrate scope for insertion into carbazoles, we turned our attention toward indoles. My colleague Vanessa Arredondo investigated the intrinsic regioselectivity of insertion with indole and found that insertion occurred primarily into the C-H bond at the C3

position, with a minor amount of insertion into the N–H bond (Figure 2-13). Zhou and co-workers had previously developed conditions for insertion at the preferred C3 position;³¹ however, it was unclear whether the selectivity could be biased toward the N1 position while maintaining asymmetric induction.

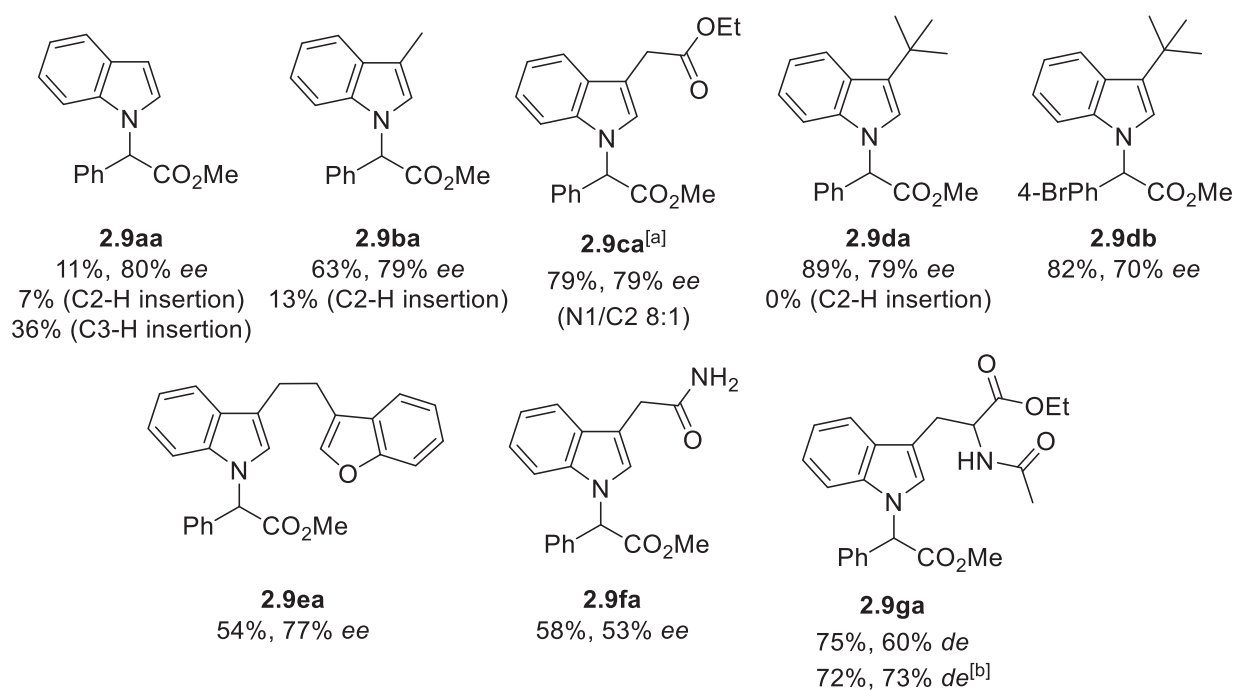
Figure 2-13: Regioselectivity of insertion with indole.



Simply blocking the C3 position led to preferential insertion at N1. We examined various indole substrates (Figure 2-14) and found that increasing bulk at the C3 position improved selectivity for N1 over C2 insertion (**2.9aa**<**2.9ba**<**2.9ca**<**2.9da**). Indoles generally exhibited lower *ees* than carbazoles. I was responsible for synthesizing *t*-butyl, benzofuran, tryptophan, and carboxamide indole derivatives **2.9da**–**2.9ga**. Substituents with hydrogen-bonding groups led to poorer *ee* (**2.9fa** and **2.9ga**). No match/mismatch effects were observed when using tryptophan ethyl ester as a substrate with either enantiomer of *i*-Pr-PyBOX ligand (**2.9ga**).

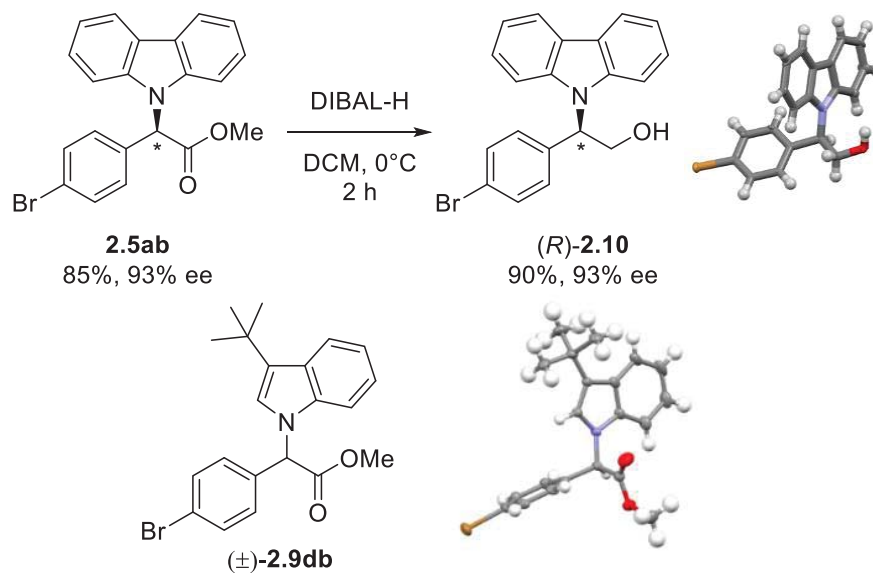
The absolute stereochemistry of reduced carbazole derivative **2.10** was secured by X-ray crystallographic analysis, which was obtained by Vanessa Arredondo after treatment of **2.5ab** with DIBAL-H (Figure 2-15). The configuration was assigned (*R*) based on the X-ray structure.³² I crystallized *t*-butyl indole derivative **2.9db** as the racemate from a scalemic sample.

Figure 2-14: Indole substrate scope.



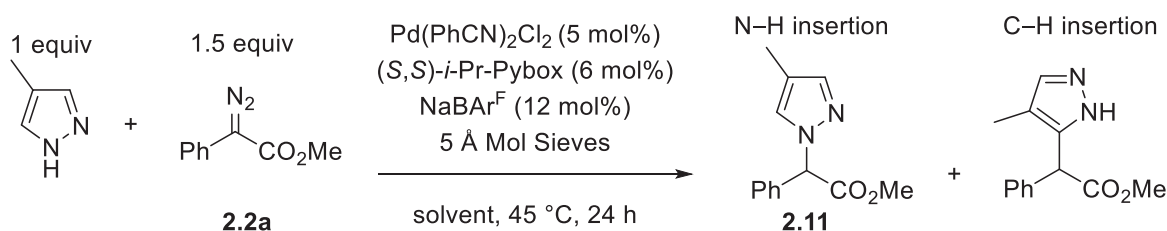
^[a]Combined yield of an inseparable mixture resulting from insertion at the N1 and C2 positions. The ratio obtained by ¹H NMR analysis. ^[b](*R,R*)-*i*-Pr-pybox.

Figure 2-15: X-ray structures of carbazole and indole derivatives.



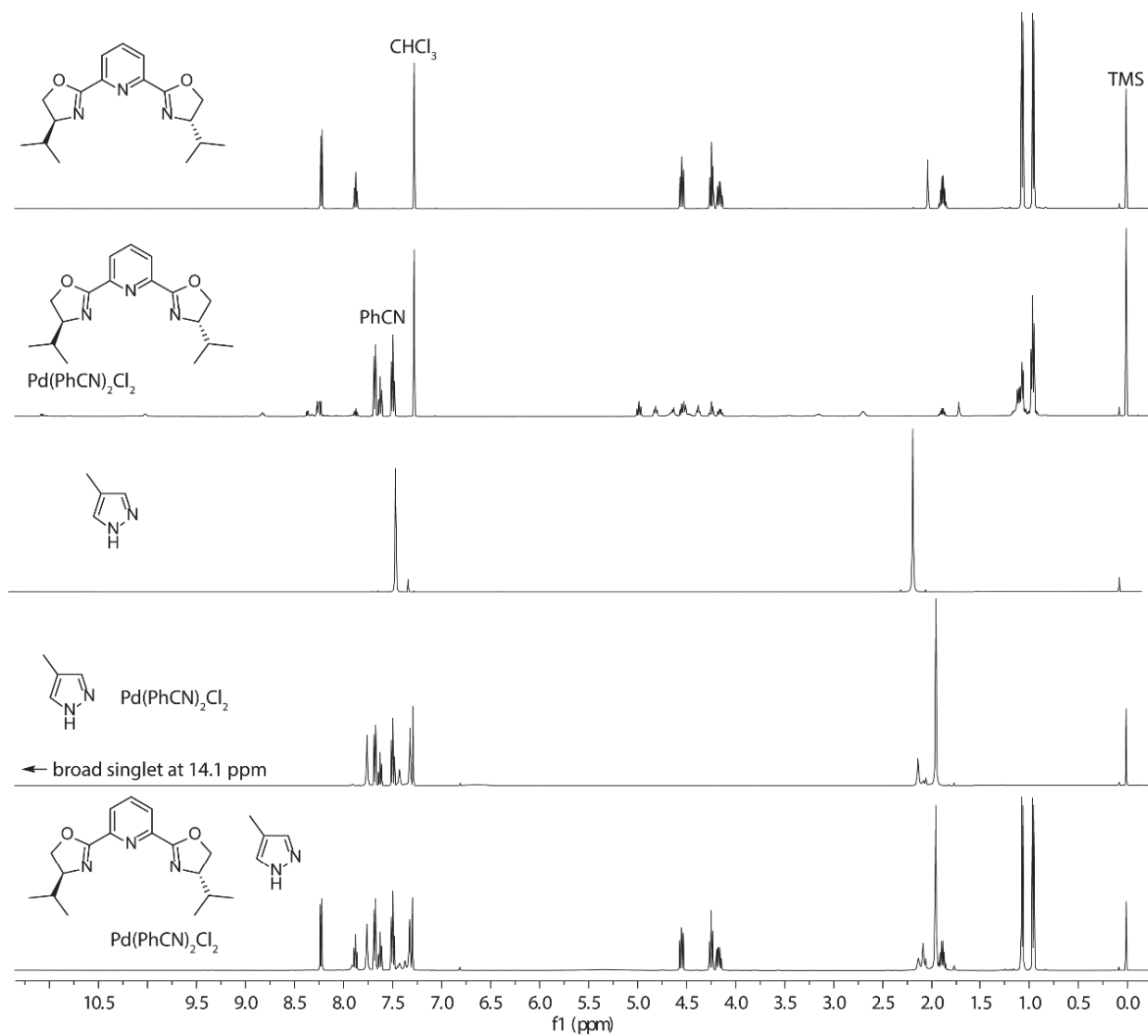
Other aromatic heterocycles with sp^2 lone pairs (e.g. imidazole, indazole, and pyrazole) were poor substrates for the reaction. For example, 4-methylpyrazole afforded racemic N–H insertion product **2.11** in 32% yield, with a small amount of product resulting from C–H insertion at the C2 position (Figure 2-16). The yield was unaffected by the presence or absence of ligand. The presence of unreacted starting material suggests catalyst deactivation due to overligation by the substrate. Moreover, ^1H NMR experiments indicated pyrazole displaces (*S,S*)-*i*-Pr-Pybox for binding to palladium. When bound to palladium, peaks corresponding to the (*S,S*)-*i*-Pr-Pybox ligand undergo a distinct change in multiplicity (particularly peaks corresponding to the oxazoline ring of in the $\delta = 4.6$ - 4.0 ppm region). Likewise, the aromatic singlet of pyrazole differentiates into several multiplets in the $\delta = 8.0$ - 7.2 ppm region. When $\text{Pd}(\text{PhCN})_2\text{Cl}_2$ was prestirred with (*S,S*)-*i*-Pr-Pybox ligand, then an equimolar amount of pyrazole added, the spectrum was most consistent with unbound (*S,S*)-*i*-Pr-Pybox and palladium-bound pyrazole (Figure 2-17).

Figure 2-16: Diminished yield and ee observed using pyrazole



Entry	Solvent	Ligand	N–H insertion	ee	C–H insertion	Pyrazole recovered	Diazo recovered
1	CHCl_3	+	32%	0%	8%	6%	18%
2	CHCl_3	-	30%	0%	5%	22%	55%
3	Toluene	+	33%	0%	3%	5%	15%
4	Toluene	-	38%	0%	8%	10%	45%

Figure 2-17: ^1H NMR experiments showing displacement of palladium(II)-bound (*S,S*)-Pybox ligand by 4-methylpyrazole



Conclusion

In summary, we report an enantioselective palladium-catalyzed carbene insertion into the N–H bonds of aromatic heterocycles using (*S,S*)-*i*-Pr-PyBOX and a palladium(II) precatalyst. Products were obtained in good to excellent yields and up to 99% ee. A product of the reaction was carried through a series of further transformations without erosion of ee to synthesize the core of a potent pharmacophore.

Experimental Section

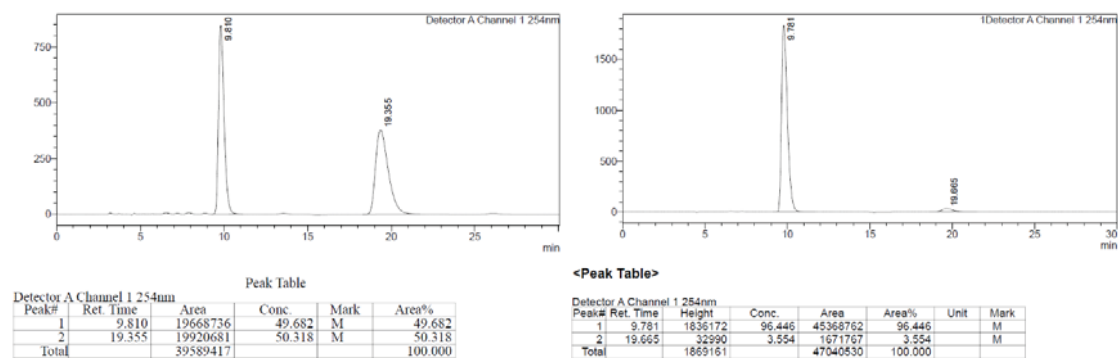
Unless otherwise noted, ^1H and ^{13}C NMR spectral data were recorded at room temperature in a Bruker 500 or 600 MHz spectrometer equipped with a cryoprobe. The NMR data are reported as follows: chemical shift in ppm, multiplicity (br = broad, app = apparent, s = singlet, d = doublet, t = triplet, q = quartet and m = multiplet), coupling constants (Hz), and integration. All spectra were calibrated to tetramethylsilane (0.00 ppm). NMR data was processed using Mestrelab Research MestReNova 11.0.2 software, using automatic phasing and baseline correction.

All reactions were monitored by thin-layer chromatography (TLC). Analytical TLC was performed using EMD Reagents 0.25 mm silica gel 60-F plates. Preparative layer chromatography (PLC) was performed using EMD Millipore PLC Plates F254, 500 μm thick, 200 \times 200 mm, 60 \AA pore size (EM1.05744.0001). KMnO_4 and *p*-anisaldehyde stains were used for TLC visualization. "Flash" chromatography on silica gel was performed using Agela Scientific Flash Silica sorbent (40-63 μm) silica gel of 230-400 mesh (CS605025-P). Infrared spectroscopic data were acquired using a PerkinElmer Spectrum Two IR Spectrometer.

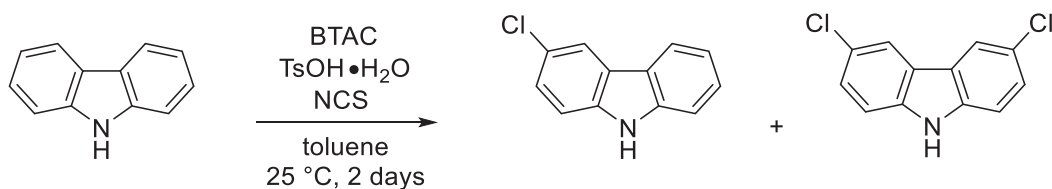
Enantiomeric excess was determined by HPLC. Waters Acrodisc filters were used to filter HPLC samples (P/N WAT200520). A Chiralcel Technologies normal phase CHIRALPAK AD (0.46cm \varnothing \times 25cm) chiral column was used on an Agilent Technologies Series 1100 HPLC instrument. Data analysis was performed using ChemStation for LC 3D systems Rev. B.04.01.

A Chiralcel Technologies normal phase CHIRALCEL OD-H (0.46cm \varnothing \times 25cm) chiral column was used on a Shimadzu Prominence Modular HPLC instrument. Analysis was performed on LabSolutions software version 5.52 copyright of Shimadzu Corporation.

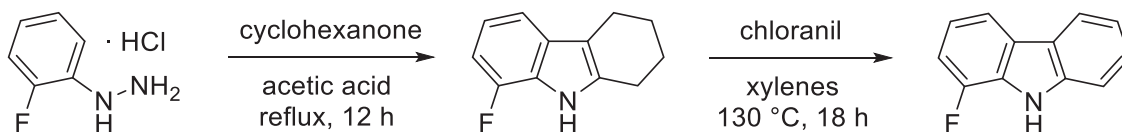
Representative HPLC traces are shown below for racemic and chiral compound **2.5ab**. Information including choice of chiral column, eluent, flow rate, and enantiomeric excess are provided in the Analytical Data section of the supporting information.



Synthesis of carbazole and indole substrates



3-chlorocarbazole and **3,6-dichlorocarbazole** were synthesized according to a previously reported procedure by Chen and co-workers, with minor modification.^[5] A flame-dried 100 mL round-bottom flask equipped with stir bar was charged with carbazole (95%, 1.0 g, 6.0 mmol), benzyltriethylammonium chloride (0.063 g, 0.30 mmol), and *p*-toluenesulfonic acid monohydrate (0.57 g, 3.0 mmol). The flask was then charged with toluene (30 mL) and allowed to stir open to air for 2 days. *N*-Chlorosuccinimide (1.6 g, 12.0 mmol) was added in four portions over two days. The reaction mixture was poured into saturated NaHCO₃ (100 mL) and the aqueous phase was extracted with ether (3 × 75 mL). The combined organic phase was washed with de-ionized water (3 × 75 mL), dried over Na₂SO₄, and concentrated *in vacuo* to obtain a yellow oil. The crude product was purified by flash chromatography on silica gel (15% EtOAc/hexanes) to afford 3-chlorocarbazole as a tan solid (92 mg, 8%) as well as 3,6-dichlorocarbazole as a tan solid (0.680 g, 48%). Spectroscopic data for both compounds matched known reported data.³³

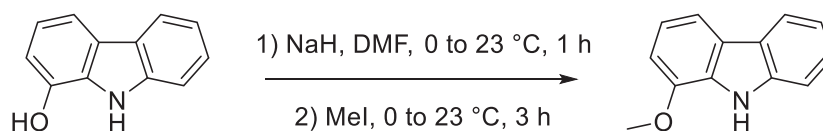


1-fluoro-9H-carbazole was synthesized in two steps according to literature procedure with minor modification.³⁴

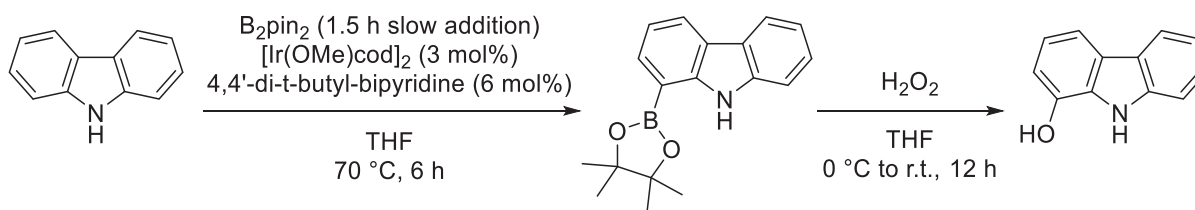
Step 1: A 100 mL round-bottom flask was charged with 2-fluorophenylhydrazine hydrochloride (3.0 g, 18.5 mmol), cyclohexanone (2.3 mL, 22.2 mmol), and acetic acid (30 mL). The flask was fitted with a reflux condenser and the reaction mixture heated at reflux for 12 h. The mixture was cooled to room temperature, diluted with H₂O (250 mL), and extracted with ether (3 × 100 mL). The combined organic layers were washed with H₂O (3 × 75 mL) and brine (75 mL), dried over Na₂SO₄, and concentrated *in vacuo*. The crude product was purified by flash chromatography on silica gel (1st column = 50% ether/hexanes; 2nd column = 10% ether/hexanes). Pure fractions were combined and concentrated *in vacuo* to obtain 8-fluoro-2,3,4,9-tetrahydro-1H-carbazole as white cubic crystals (569 mg, 3.0 mmol, 16%). $R_f = 0.81$ (50% ether/hexanes); $R_f = 0.43$ (10% ether/hexanes). ¹H NMR data agrees with previously reported values.³⁵ ¹³C NMR and IR data have not been reported. ¹H NMR (500 MHz, CDCl₃) δ 7.81 (br s, 1H), 7.21 (app d, $J = 7.8$ Hz, 1H), 7.00 – 6.92 (m, 1H), 6.86 – 6.77 (m, 1H), 2.83 – 2.58 (m, 4H), 2.00 – 1.75 (m, 4H); ¹³C NMR (125 MHz, CDCl₃) 149.2 (d, $J = 242.4$ Hz), 134.9, 131.6 (d, $J = 5.5$ Hz), 123.5 (d, $J = 12.6$ Hz), 119.3 (d, $J = 6.2$ Hz), 113.5 (d, $J = 3.1$ Hz), 111.0, 106.1 (d, $J = 16.4$ Hz), 23.2, 23.14, 23.08, 21.0; IR (ATR) 3380, 2931, 2848, 1232, 774, 725 cm⁻¹; HRMS (ESI): m/z calculated for C₁₂H₁₁FN [M – Na]⁻ 188.0876, found 188.0870.

Step 2: An oven-dried 50 mL round-bottom flask equipped with stir bar was charged with 8-fluoro-2,3,4,9-tetrahydro-1H-carbazole (500 mg, 2.61 mmol), chloranil (1.41 g, 5.74 mmol), and anhydrous xylenes (15 mL). The flask was fitted with a reflux condenser and then submerged in a 130 °C oil bath for 18 h. The reaction mixture was cooled to room temperature, diluted with ether (150 mL), and washed with aqueous NaOH (0.5 M, 2 × 75 mL), H₂O (75 mL), and brine (75

mL). The organic layer was dried over Na₂SO₄ and concentrated *in vacuo*. The crude product was purified by flash chromatography on silica gel (1st column = 25% DCM/hexanes; 2nd column = 8% ether/hexanes) to obtain 1-fluorocarbazole as a white solid (318 mg, 1.72 mmol, 66%). Spectroscopic data matched known reported data.³⁶ R_f = 0.28 (25% DCM/hexanes); R_f = 0.32 (8% ether/hexanes). ¹H NMR (500 MHz, CDCl₃) δ 8.17 (br s, 1H), 8.06 (d, *J* = 7.8 Hz, 1H), 7.85 – 7.80 (m, 1H), 7.48 – 7.41 (m, 2H), 7.30 – 7.22 (m, 1H), 7.18 – 7.10 (m, 2H); ¹³C NMR (125 MHz, CDCl₃) δ 149.1 (d, *J* = 242.8 Hz), 139.5, 127.5 (d, *J* = 13.1 Hz), 126.8 (d, *J* = 5.7 Hz), 126.5, 123.2 (d, *J* = 2.7 Hz), 120.6, 120.0, 119.7 (d, *J* = 5.9 Hz), 116.0 (d, *J* = 3.4 Hz), 111.1, 110.9 (d, *J* = 16.2 Hz); HRMS (ESI): *m/z* calculated for C₁₂H₇FN [M–Na][–] 184.0563, found 184.0555.



1-methoxy-9H-carbazole was synthesized according to a patented procedure.^[9] A 250 mL oven-dried round bottom flask was charged with carbazol-1-ol (850 mg, 4.64 mmol) and anhydrous DMF (50 mL). The flask was cooled in an ice-water bath for 10 min while stirring. To the flask was added in a single portion NaH (60 wt%, 240 mg, 6.0 mmol). The reaction was warmed to room temperature and stirred for one hour. Next, the flask was again cooled in an ice-water bath for 10 min and iodomethane (375 μL, 6.0 mmol) was added. The reaction was warmed to room temperature and stirred for 3 h. Work-up and purification according to literature procedure yielded 1-methoxycarbazole as a beige solid (801 mg, 88%). Spectroscopic data matched known reported data.^{37,38}

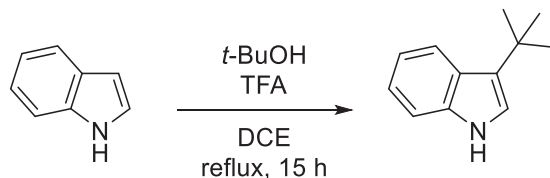


9H-carbazol-1-ol was synthesized according to a two-step procedure by Sperry and co-workers, with modifications.³⁹

Step 1: A oven-dried 500 mL round-bottom flask was charged with carbazole (6 g, 36.0 mmol), 4,4'-di-*tert*-butyl-bipyridine (193 mg, 0.72 mmol), [Ir(OMe)cod]₂ (238 mg, 0.36 mmol), and dry THF (200 mL). The mixture was stirred at room temperature for 10 minutes until a dark red, homogeneous solution was obtained. The flask was submerged in a 70 °C oil bath. Bis(pinacolato)-diboron (3.04 g, 12.0 mmol) was dissolved in dry THF (20 mL) and this solution was added over 1.5 h using a syringe pump. After addition, the reaction mixture was stirred at 70 °C for an additional 4.5 h, for a total reaction time of 6 h. The reaction mixture was cooled to room temperature and concentrated *in vacuo*. The crude product was purified by flash chromatography on silica gel using 8% EtOAc/hexanes, concentrated, and dried *in vacuo* to obtain 1-(4,4,5,5-tetramethyl-1,3,2-dioxaborolan-2-yl)-9H-carbazole as a white solid (1.86 g, 26%). *R_f* = 0.43 (8% EtOAc/hexanes); ¹H NMR¹³ and ¹³C NMR⁴⁰ spectroscopic data match previously reported data. (¹H NMR disagrees with ref. [13]). ¹H NMR (500 MHz, CDCl₃) δ 9.15 (s, 1H), 8.18 (d, *J* = 8.2 Hz, 1H), 8.07 (d, *J* = 7.8 Hz, 1H), 7.86 (dd, *J* = 7.2, 1.2 Hz, 1H), 7.49 (d, *J* = 8.1 Hz, 1H), 7.41 (ddd, *J* = 8.2, 7.1, 1.2 Hz, 1H), 7.28 – 7.18 (m, 2H), 1.42 (s, 12H); ¹³C NMR (125 MHz, CDCl₃) δ 145.1, 139.3, 132.8, 125.7, 123.7, 122.9, 122.3, 120.3, 119.1, 118.7, 110.6, 84.0, 25.0.

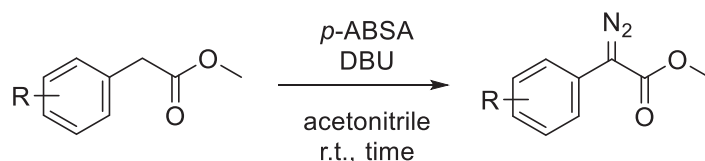
Step 2: 1-(4,4,5,5-tetramethyl-1,3,2-dioxaborolan-2-yl)-9H-carbazole (1.80 g, 6.13 mmol) was dissolved in THF (75 mL). The reaction was cooled in an ice-water bath for 10 min while stirring. Into the flask was syringed 30 wt % aqueous hydrogen peroxide (1.9 mL, 18.4 mmol). The mixture was allowed to warm to room temperature and stirred for 12 h. The mixture was

concentrated *in vacuo*, purified by flash chromatography on silica gel using 30% EtOAc/hexanes, concentrated, and dried *in vacuo* to obtain a light brown solid. The solid was recrystallized from hot benzene under nitrogen. Upon cooling to room temperature, a few drops of hexanes were added to initiate crystallization. The mother liquor was removed via syringe, and the solid washed twice with cold hexanes. The solid was dried *in vacuo* to obtain carbazol-1-ol as flaky white crystals (920 mg, 82%). $R_f = 0.28$ (30% EtOAc/hexanes). Spectroscopic data matched known reported data.³⁷ ^{13}C NMR data has not been reported. ^1H NMR (500 MHz, CDCl_3) δ 8.24 (s, 1H), 8.07 (d, $J = 8.3$ Hz, 1H), 7.70 (d, $J = 7.9$ Hz, 1H), 7.52 – 7.40 (m, 2H), 7.25 (ddd, $J = 8.0, 7.0, 1.2$ Hz, 1H), 7.09 (t, $J = 7.8$ Hz, 1H), 6.84 (dd, $J = 7.6, 0.7$ Hz, 1H), 5.00 (s, 1H); ^{13}C NMR (125 MHz, CDCl_3) 141.0, 139.4, 129.0, 126.0, 125.3, 123.6, 120.6, 119.7, 119.5, 113.3, 111.0, 110.7.

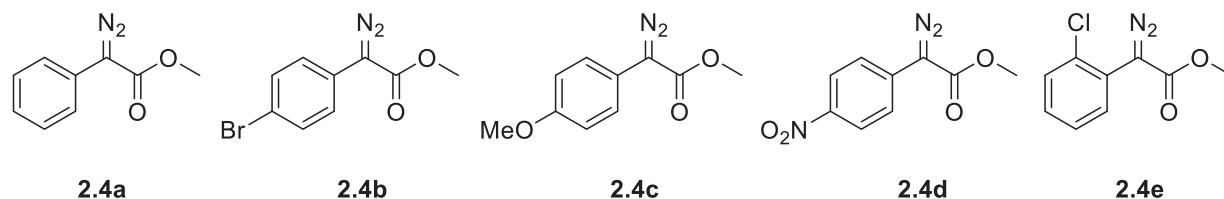


3-(tert-butyl)-1H-indole (3.6d) was synthesized according to a patented procedure.⁴¹ Indole **3.6a** (3.0 g, 25.6 mmol) was used to obtain compound **3.6d** as an amorphous pale pink solid (312 mg, 7%). Pure compound **3.6d** containing residual toluene (<5 mol %) was isolated following three rounds of flash chromatography on silica gel (1st column = 10% EtOAc/hexanes; 2nd column = gradient 5→10% EtOAc/hexanes; 3rd column = 40% toluene/hexanes). $R_f = 0.32$ (10% EtOAc/hexanes); $R_f = 0.22$ (5% EtOAc/hexanes); $R_f = 0.31$ (40% toluene/hexanes). ^1H NMR (500 MHz, CDCl_3) δ 7.82 (dd, $J = 8.0, 1.1$ Hz, 1H), 7.70 (br s, 1H), 7.30 (dd, $J = 8.1, 1.0$ Hz, 1H), 7.16 (ddd, $J = 8.1, 7.0, 1.2$ Hz, 1H), 7.09 (ddd, $J = 8.2, 7.0, 1.2$ Hz, 1H), 6.86 (d, $J = 2.5$ Hz, 1H), 1.45 (s, 9H). ^{13}C NMR (126 MHz, CDCl_3) δ 137.1, 126.7, 125.8, 121.4, 121.2, 119.2, 118.7, 111.3, 31.6, 30.7; IR (ATR): 3394, 2962, 2863, 1616, 1459, 1360, 1123, 1100, 737 cm^{-1} .

Synthesis of α -aryl- α -diazoacetates



α -aryl- α -diazoacetates 2.2a-2.2e were synthesized according to a patented procedure.⁴² An oven-dried round-bottom flask equipped with stir bar was charged with the aryl acetate (1.0 equiv) and *p*-acetamidebenzenesulfonyl azide (1.1 equiv). Dry acetonitrile was added to obtain a 0.25 M solution in aryl acetate. The flask was cooled in an ice-water bath for 10 minutes while stirring. A 1.5 M solution of DBU (1.2 equiv) in acetonitrile was syringed into the flask. The flask was allowed to warm to room temperature and stirred until aryl acetate was no longer detected by TLC. Next, the reaction mixture was diluted with three times its volume of ether, then washed sequentially with 50 mL each of saturated aqueous NH_4Cl and H_2O ($\times 2$). The organic layer was dried with Na_2SO_4 , concentrated, and purified by flash chromatography on silica gel to afford the aryl diazoacetate product.



Synthesis and characterization for **2.2a** has been previously reported.⁴³ ^1H NMR (600 MHz, CDCl_3) δ 7.48 (d, $J = 8.5$ Hz, 2H), 7.38 (t, $J = 8.0$ Hz, 2H), 7.18 (t, $J = 7.4$ Hz, 1H), 3.86 (s, 3H); ^{13}C NMR (126 MHz, CDCl_3) δ 165.6, 128.9, 125.8, 125.5, 123.9, 52.0.

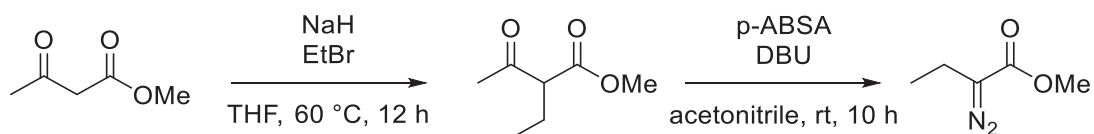
Synthesis and characterization for **2.2b** has been previously reported.¹⁸ ^1H NMR (500 MHz, CDCl_3) δ 7.50 (d, $J = 8.7$ Hz, 2H), 7.36 (d, $J = 8.7$ Hz, 2H), 3.87 (s, 3H); ^{13}C NMR (126 MHz, CDCl_3) δ 165.2, 132.0, 125.3, 124.7, 119.3, 52.1.

Synthesis and characterization for **3.2c** has been previously reported.¹⁸ ^1H NMR (500 MHz, CDCl_3) δ 7.38 (d, $J = 9.0$ Hz, 2H), 6.95 (d, $J = 9.0$ Hz, 2H), 3.85 (s, 2H), 3.81 (s, 3H).

Synthesis and characterization for **2.2d** has been previously reported.⁴⁴ ¹H NMR (500 MHz, CDCl₃) δ 8.24 (d, *J* = 9.1 Hz, 2H), 7.67 (d, *J* = 9.1 Hz, 2H), 3.91 (s, 3H); ¹³C NMR (126 MHz, CDCl₃) δ 164.1, 145.0, 133.8, 124.3, 123.1, 52.4.

Synthesis and characterization for **2.2e** has been previously reported.¹⁸ ¹H NMR (500 MHz, CDCl₃) δ 7.54 (dd, *J* = 7.8, 1.7 Hz, 1H), 7.42 (dd, *J* = 7.8, 1.6 Hz, 1H), 7.32 (td, *J* = 7.6, 1.5 Hz, 1H), 7.28 (dd, *J* = 7.9, 1.8 Hz, 1H), 3.84 (s, 3H); ¹³C NMR (126 MHz, CDCl₃) δ 165.9, 133.8, 132.3, 130.1, 129.6, 127.1, 123.9, 52.3.

Synthesis of an α -alkyl- α -diazoester



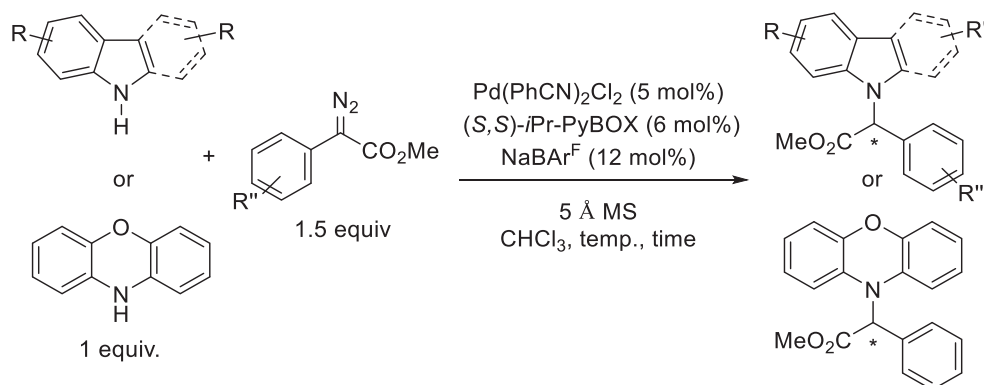
Methyl 2-ethyl-3-oxobutanoate (2.2f) was synthesized in two steps. A previously reported procedure for the first step was used with some modification.⁴⁵

Step 1: An oven-dried 100 mL round-bottom flask equipped with stir bar was evacuated and backfilled with argon. The flask was charged with NaH (60% dispersion in mineral oil, 0.48 g, 12 mmol, 1.2 equiv) and THF (25 mL). The suspension was cooled in an ice-water bath for 10 minutes while stirring. A solution of methyl acetoacetate (1.75 g, 15 mmol, 1.5 equiv) in THF (5 mL) was then added to the flask over 10 minutes. The flask was warmed to room temperature and stirred for 30 minutes. ethyl bromide (1.09 g, 10 mmol, 1.0 equiv) was then added and the flask submerged in a 60 °C oil bath for 12 h. After 12 h, the flask was cooled in an ice-water bath for 10 minutes, and saturated aqueous NH₄Cl (15 mL) was added. The mixture was diluted with ether (30 mL) and H₂O (30 mL). The resulting layers were separated and the aqueous layer extracted with additional ether (50 mL). The organic layers were combined and washed with brine, dried over Na₂SO₄, and concentrated *in vacuo*. The resulting oil was further purified by silica gel chromatography (30% ether/hexanes) to obtain methyl **2-methyl-3-oxobutanoate** as a colorless

oil (678 mg, 52%). Spectroscopic data was consistent with previous reports.⁴⁶ The product was obtained as a colorless oil (1.02 g, 71 %). ¹H NMR (500 MHz, CDCl₃) δ 3.74 (s, 3H), 3.36 (t, *J* = 7.4 Hz, 1H), 2.23 (s, 3H), 2.00 – 1.81 (m, 2H), 0.94 (t, *J* = 7.5 Hz, 3H); ¹³C NMR (125 MHz, CDCl₃) δ 203.3, 170.3, 61.2, 52.3, 28.9, 21.7, 11.9.

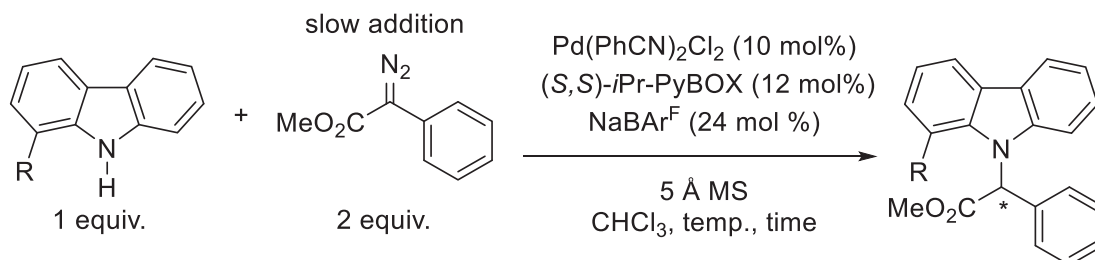
Step 2: An oven-dried round-bottom flask equipped with stir bar was charged with methyl 2-ethyl-3-oxobutanoate (912 mg, 6.33 mmol, 1.0 equiv) methyl 2-methyl-3-oxobutanoate (622 mg, 4.78 mmol, 1.0 equiv), *p*-acetamidebenzenesulfonylazide (1.67 g, 6.95 mmol, 1.1 equiv), and dry acetonitrile (20 mL). The flask was cooled in an ice-water bath for 10 minutes while stirring. A solution of DBU (1.15 g, 7.59 mmol, 1.2 equiv) in dry acetonitrile (7 mL) was then syringed into the flask. The flask was allowed to warm to room temperature and stirred for 10 h. The reaction mixture was diluted with ether (60 mL) and then washed with saturated aqueous NH₄Cl (30 mL) and brine (30 mL). The organic layer was dried over Na₂SO₄, concentrated, and purified by flash chromatography (10% ether/hexanes) to obtain **methyl 2-ethyl-3-oxobutanoate (2.2f)** as a bright yellow oil (620 mg, 76 %). The product was volatile, so was concentrated to ~2 mL *in vacuo* and the remaining solvent evaporated under a gentle stream of argon. Spectroscopic data was consistent with previous reports.⁴⁷ ¹H NMR (500 MHz, CDCl₃) δ 3.76 (s, 3H), 2.36 (q, *J* = 7.5 Hz, 2H), 1.14 (t, *J* = 7.5 Hz, 3H); ¹³C NMR (125 MHz, CDCl₃) δ 51.9, 16.6, 12.0. Resonances from C=N₂ and C=O not observed.

General Procedure A: Palladium-Catalyzed Insertion with N-Heterocycles



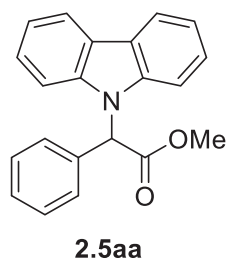
To a flame-dried round-bottom flask equipped with stirbar was added the heterocycle substrate (1 equiv), $\text{Pd}(\text{PhCN})_2\text{Cl}_2$ (5 mol %), $(S,S)\text{-}i\text{Pr-PyBOX}$ (6 mol %), NaBAR^{F} (12 mol %), and 5 Å MS (approximately 1 g/mmol of the heterocycle). To a separate flame-dried pear-shaped flask was added the diazo substrate (1.5 equiv). Both flasks were evacuated for 10 min and backfilled with nitrogen gas. Distilled CHCl_3 (stored over 4 Å MS) was added to the round-bottom flask to obtain a heterocycle concentration of 200 mM. The round-bottom flask was submerged in an oil bath of specified temperature for 5 min (see Analytical Data section below for reaction temperature). The diazo substrate was dissolved in CHCl_3 to obtain a 750 mM solution, and this solution was transferred in one portion to the round-bottom flask. Additional CHCl_3 was used to rinse the pear-shaped flask and ensure complete transfer of the diazo and to achieve a final heterocycle concentration of 75 mM. The reaction was stirred until consumption of either the heterocycle or diazo as determined by TLC (see Analytical Data section for reaction time). Upon completion, the reaction flask was cooled to room temperature and diluted with CHCl_3 . The mixture was filtered through a pad of Celite which was then washed three times with CHCl_3 . The filtrate was concentrated and the residue purified via column chromatography.

General Procedure B: Palladium-Catalyzed Insertion with 1-Substituted Carbazoles



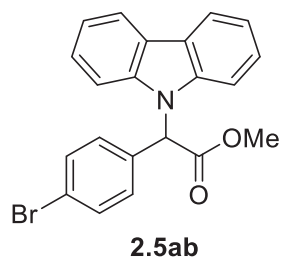
To a flame-dried round-bottom flask equipped with stir-bar was added the 1-substituted carbazole (1 equiv), Pd(PhCN)₂Cl₂ (10 mol %), (S,S)-*i*-Pr-PyBOX (12 mol %), NaBAR^F (24 mol %), and 5 Å MS (approximately 1g/mmol of carbazole). To a separate flame-dried pear-shaped flask was added the diazo substrate (2 equiv). Both flasks were evacuated for 10 min, and backfilled with nitrogen gas. To the round-bottom flask was added CHCl₃ to obtain a 100 mM solution with respect to the carbazole substrate. The diazo substrate was dissolved in CHCl₃ to obtain a 300 mM solution. The round-bottom flask was submerged in an oil bath for 5 min (see Analytical Data section below for reaction temperature) and the diazo solution added over 8 hours using a syringe pump. After addition, the reaction was stirred for some additional time (see Analytical Data section) until consumption of either the 1-substituted carbazole or diazo as determined by TLC. Upon completion, the reaction mixture was cooled to room temperature and diluted with CHCl₃. The mixture was filtered through a pad of Celite which was then washed three times with CHCl₃. The filtrate was concentrated and the residue purified via column chromatography.

Analytical Data



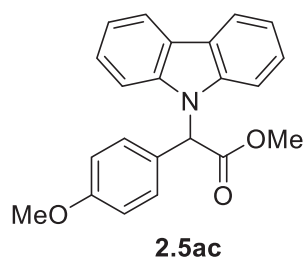
Methyl 2-(9H-carbazol-9-yl)-2-phenylacetate (2.5aa): Example using general procedure A. A flame-dried, 5 mL round-bottom flask equipped with stir bar was charged with carbazole (31.4 mg, 0.19 mmol, 1 equiv), Pd(PhCN)₂Cl₂ (3.6 mg, 0.009 mmol, 5 mol %), (S,S)-*i*-Pr-PyBOX (3.4 mg, 0.01 mmol, 6 mol %), NaBAR^F (20 mg, 0.02 mmol, 12 mol %), and 5 Å MS (190

mg). To a separate flame-dried pear-shaped flask was added methyl 2-diazo-2-phenylacetate **2.4a** (49.6 mg, 0.28 mmol, 1.5 equiv). Both flasks were evacuated for 10 min and backfilled with nitrogen gas. Distilled CHCl_3 (1.1 mL) was added to the round-bottom flask to obtain a carbazole concentration of 200 mM. The round-bottom flask was submerged in an $30\text{ }^\circ\text{C}$ oil bath for 5 min while stirring. Next, the diazo substrate was dissolved in CHCl_3 (0.4 mL) to obtain a 750 mM solution, and this solution was transferred in one portion to the round-bottom flask. Additional CHCl_3 (1.0 mL) was used to rinse the pear-shaped flask and ensure complete transfer of the diazo and to achieve a final heterocycle concentration of 75 mM. The reaction mixture was stirred for 2 h at $30\text{ }^\circ\text{C}$ at which point carbazole was no longer detected by TLC. The crude product was purified by flash chromatography on silica gel (5% ether/hexanes) to obtain compound **2.5aa** as a pale beige solid (55.6 mg, 99%, 97% ee). $R_f = 0.37$ (20% ether/hexanes); The ee was measured utilizing the Shimadzu HPLC instrument using a chiral stationary phase [Chiralcel OD-H, 2-propanol/hexanes = 8/92, 1.0 mL/min, $\lambda = 254\text{ nm}$], $t_R = 9.50\text{ min}$ (major), 19.04 min (minor); $^1\text{H NMR}$ (500 MHz, CDCl_3) δ 8.11 (dd, $J = 8.0, 1.2\text{ Hz}$, 2H), 7.36 (td, $J = 7.5, 7.1, 1.2\text{ Hz}$, 2H), 7.34 – 7.30 (m, 3H), 7.27 – 7.26 (m, 2H), 7.25 – 7.21 (m, 4H), 6.62 (s, 1H), 3.78 (s, 3H); $^{13}\text{C NMR}$ (126 MHz, CDCl_3) δ 169.8, 140.2, 134.0, 128.7, 128.3, 127.4, 125.8, 123.5, 120.3, 119.7, 110.1, 60.3, 52.8; IR (ATR) 3036, 2920, 2851, 1741, 1449, 1205 cm^{-1} . HRMS (ESI): m/z calculated for $\text{C}_{21}\text{H}_{17}\text{NO}_2\text{Na}$ [$\text{M} + \text{Na}$] $^+$ 338.1157, found 338.1144.



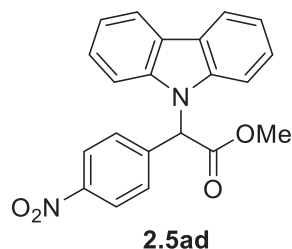
Methyl 2-(4-bromophenyl)-2-(9H-carbazol-9-yl)acetate (2.5ab): Using general procedure A, carbazole (95%, 21.1 mg, 0.12 mmol) was reacted with methyl 2-(4-bromophenyl)-2-diazoacetate **2.4b** (45.9 mg, 0.18 mmol) for 8 h. The crude product was purified by flash chromatography on silica gel (20% ether/hexanes) to obtain compound **2.5ab** as pale yellow solid (40.4 mg, 85%, 93% ee). $R_f = 0.31$ (20% ether/hexanes); The ee was measured utilizing the Shimadzu HPLC instrument using a chiral stationary phase [Chiralcel OD-H, 2-propanol/hexanes

= 8/92, 1.0 mL/min, λ = 254 nm], t_R = 9.78 min (major), 19.67 min (minor); ^1H NMR (500 MHz, CDCl_3) δ 8.11 (d, J = 7.7 Hz, 2H), 7.43 (d, J = 8.6 Hz, 2H), 7.38 (t, J = 7.2 Hz, 2H), 7.30 – 7.19 (m, 4H), 7.10 (d, J = 8.4 Hz, 2H), 6.52 (s, 1H), 3.75 (s, 3H); ^{13}C NMR (125 MHz, CDCl_3) δ 169.3, 140.0, 133.0, 131.8, 129.1, 125.9, 123.6, 122.5, 120.4, 120.0, 109.9, 59.6, 52.9; IR (ATR): 3061, 2949, 1745, 1483, 1451, 1198, 1171, 996, 749, 724 cm^{-1} ; HRMS (ESI): m/z calculated for $\text{C}_{21}\text{H}_{16}\text{BrNO}_2\text{Na}$ [$\text{M} + \text{Na}$] $^+$ 416.0262, found 416.0247.

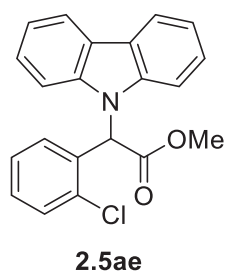


Methyl 2-(9H-carbazol-9-yl)-2-(4-methoxyphenyl)acetate (2.5ac):

Using general procedure A, carbazole (95%, 21.1 mg, 0.12 mmol) was reacted with methyl 2-diazo-2-(4-methoxyphenyl)acetate **2.4c** (37.1 mg, 0.18 mmol) for 30 min. The crude product was purified by flash chromatography on silica gel (1st column = 15% ether/hexanes; 2nd column = 25% ether/hexanes) to obtain compound **2.5ac** as a pale orange solid (37.3 mg, 90%, 96% ee). R_f = 0.15 (15% ether/hexanes); R_f = 0.29 (25% ether/hexanes); The ee was measured utilizing the Shimadzu HPLC instrument using a chiral stationary phase [Chiralcel OD-H, 2-propanol/hexanes = 12/88, 1.0 mL/min, λ = 254 nm], t_R = 11.45 min (major), 21.95 min (minor); ^1H NMR (500 MHz, CDCl_3) δ 8.10 (d, J = 7.6 Hz, 2H), 7.36 (t, J = 7.2 Hz, 2H), 7.30 – 7.20 (m, 4H), 7.16 (d, J = 8.8 Hz, 2H), 6.84 (d, J = 8.8 Hz, 2H), 6.57 (s, 1H), 3.78 (s, 3H), 3.76 (s, 3H); ^{13}C NMR (125 MHz, CDCl_3) δ 170.1, 159.5, 140.2, 128.7, 125.9, 125.8, 123.5, 120.3, 119.7, 114.0, 110.2, 59.8, 55.3, 52.7; IR (ATR): 3010, 2951, 2837, 1743, 1612, 1598, 1512, 1450, 1175, 750, 722.7 cm^{-1} ; HRMS (ESI): m/z calculated for $\text{C}_{22}\text{H}_{19}\text{NO}_3\text{Na}$ [$\text{M} + \text{Na}$] $^+$ 368.1263, found 368.1256.

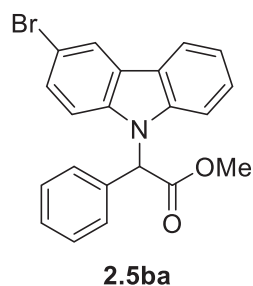


Methyl 2-(9H-carbazol-9-yl)-2-(4-nitrophenyl)acetate (2.5ad): Using general procedure A, carbazole (95%, 21.1 mg, 0.12 mmol) was reacted with methyl 2-diazo-2-(4-nitrophenyl)acetate **2.4d** (39.8 mg, 0.18 mmol) at 55 °C for 30 h. The crude product was purified by flash chromatography on silica gel using (1st column = 50% ether/hexanes; 2nd column = 70% DCM/hexanes) to obtain compound **2.5ad** as pale yellow solid (6.1 mg, 14%, 0% ee). $R_f = 0.44$ (50% ether/hexanes); $R_f = 0.39$ (70% DCM/hexanes); The ee was measured utilizing the Shimadzu HPLC instrument using a chiral stationary phase [Chiralcel OD-H, 2-propanol/hexanes = 15/85, 1.0 mL/min, $\lambda = 254$ nm], $t_R = 16.91$ min (equal), 24.08 min (equal); ^1H NMR (500 MHz, CDCl_3) δ 8.14 (t, $J = 8.0$ Hz, 4H), 7.44 – 7.35 (m, 4H), 7.29 (t, $J = 7.5$ Hz, 2H), 7.21 (d, $J = 8.3$ Hz, 2H), 6.61 (s, 1H), 3.76 (s, 3H); ^{13}C NMR (125 MHz, CDCl_3) δ 168.7, 147.8, 141.1, 139.8, 128.5, 126.2, 123.8, 123.7, 120.6, 120.3, 109.6, 59.5, 53.2; IR (ATR): 3050, 2952, 1743, 1520, 1451, 1344, 1203, 750, 723 cm^{-1} ; HRMS (ESI): m/z calculated for $\text{C}_{21}\text{H}_{15}\text{N}_2\text{O}_4$ [$\text{M} - \text{H}$] $^-$ 359.1032, found 359.1041.

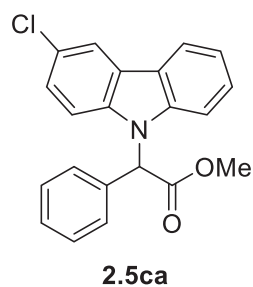


Methyl 2-(9H-carbazol-9-yl)-2-(2-chlorophenyl)acetate (2.5ae): Using general procedure A, carbazole (95%, 16.7 mg, 0.095 mmol) was reacted with methyl 2-(2-chlorophenyl)-2-diazoacetate **2.4e** (31.5 mg, 0.15 mmol) at 30 °C for 2.5 h. The crude product was purified by flash chromatography on silica gel (4% EtOAc/hexanes) to afford compound **2.5ae** as a clear oil (11.3 mg, 34%, 87% ee). $R_f = 0.65$ (25% EtOAc/hexanes); The ee was measured utilizing the Shimadzu HPLC instrument using a chiral stationary phase [Chiralcel OD-H, 2-propanol/hexanes = 1/99, 1.0 mL/min, $\lambda = 254$ nm], $t_R = 22.60$ min (major), 24.84 min (minor); ^1H NMR (500 MHz, CDCl_3) δ 8.13 (d, $J = 7.7$ Hz, 2H), 7.46 (d, $J = 8.4$ Hz, 1H), 7.41 (t, $J = 7.2$ Hz, 2H), 7.34 – 7.26 (m, 5H), 7.16 – 7.11 (m, 2H), 6.77 (s, 1H), 3.76 (s, 3H); ^{13}C NMR (125 MHz, CDCl_3) δ 168.7, 140.3, 134.1, 132.7, 129.9, 128.4, 127.0, 126.1, 123.5, 120.4, 120.0, 109.5, 59.1, 53.1; IR (ATR) 2923, 2852, 1746,

1451, 747 cm^{-1} ; HRMS (ESI): m/z calculated for $\text{C}_{21}\text{H}_{16}\text{ClNO}_2\text{Na}$ $[\text{M} + \text{Na}]^+$ 372.0767, found 372.0760.

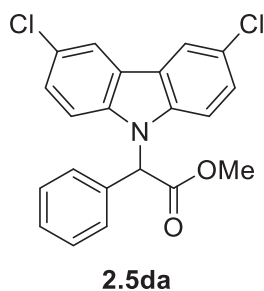


Methyl 2-(3-bromo-9H-carbazol-9-yl)-2-phenylacetate (2.5ba): Using general procedure A, 3-bromocarbazole (97%, 73.5 mg, 0.29 mmol) was reacted with methyl 2-diazo-2-phenylacetate **2.4a** (79.3 mg, 0.45 mmol) at 30 °C for 7 h. The crude product was purified by flash chromatography on silica gel (15% EtOAc/hexanes) to obtain compound **2.5ba** as a clear oil (81.9 mg, 71%, 99% ee). $R_f = 0.41$ (20% EtOAc/hexanes); The ee was measured utilizing the Shimadzu HPLC instrument using a chiral stationary phase [Chiralcel OD-H, 2-propanol/hexanes = 8/92, 1.0 mL/min, $\lambda = 254$ nm], $t_R = 8.90$ min (major), 13.75 min (minor); ^1H NMR (500 MHz, CDCl_3) δ 8.21 (d, $J = 1.9$ Hz, 1H), 8.06 (d, $J = 7.7$ Hz, 1H), 7.43 – 7.39 (m, 2H), 7.35 – 7.32 (m, 3H), 7.29 – 7.26 (m, 2H), 7.21 – 7.19 (m, 2H), 7.07 (d, $J = 8.7$ Hz, 1H), 6.58 (s, 1H), 3.79 (s, 3H); ^{13}C NMR (125 MHz, CDCl_3) δ 169.5, 140.6, 138.7, 133.6, 128.8, 128.5, 128.4, 127.3, 126.6, 125.4, 123.0, 122.5, 120.5, 120.2, 112.7, 112.1, 110.1, 60.4, 52.8; IR (ATR) 3056, 2950, 1745, 1444, 1270, 1201, 731 cm^{-1} ; HRMS (ESI): m/z calculated for $\text{C}_{21}\text{H}_{16}\text{BrNO}_2\text{Na}$ $[\text{M} + \text{Na}]^+$ 416.0262, found 416.0262.



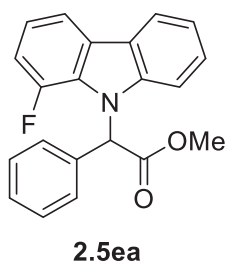
Methyl 2-(3-chloro-9H-carbazol-9-yl)-2-phenylacetate (2.5ca): Using general procedure A, 3-chlorocarbazole (24.0 mg, 0.12 mmol) was reacted with methyl 2-diazo-2-phenylacetate **2.4a** (31.4 mg, 0.18 mmol) at 30 °C for 2 h. The crude product was purified by flash chromatography on silica gel (25% ether/hexanes) to obtain compound **2.5ca** as a clear oil (33.6 mg, 89%, 97% ee). $R_f = 0.46$ (30% ether/hexanes); The ee was measured utilizing the Shimadzu HPLC instrument using a chiral stationary phase [Chiralcel OD-H, 2-propanol/hexanes = 8/92, 1.0 mL/min, $\lambda = 254$ nm], $t_R = 8.46$ min (major), 12.35 min (minor); ^1H NMR (500 MHz, CDCl_3) δ 8.09

– 8.03 (m, 2H), 7.40 (t, $J = 7.4$ Hz, 1H), 7.35 – 7.25 (m, 6H), 7.21 – 7.17 (m, 2H), 7.11 (d, $J = 8.8$ Hz, 1H), 6.58 (s, 1H), 3.78 (s, 3H); ^{13}C NMR (125 MHz, CDCl_3) δ 169.5, 140.8, 138.4, 133.6, 128.8, 128.5, 127.3, 126.5, 125.8, 125.3, 124.8, 122.6, 120.5, 120.1, 120.0, 111.6, 110.1, 60.4, 52.8; IR (ATR) 3063, 2924, 2951, 1745, 1473, 1446, 1201, 745 cm^{-1} ; HRMS (ESI): m/z calculated for $\text{C}_{21}\text{H}_{16}\text{ClNO}_2\text{Na}$ [$\text{M} + \text{Na}$] $^+$ 372.0767, found 372.0759.



Methyl 2-(3,6-dichloro-9H-carbazol-9-yl)-2-phenylacetate (2.5da):

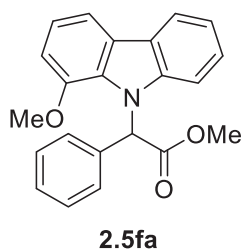
Using general procedure A, 3,6-dichlorocarbazole (22.6 mg, 0.10 mmol) was reacted with methyl 2-diazo-2-phenylacetate **2.4a** (25.3 mg, 0.14 mmol) for 30 °C at 3.5 h. The crude product was purified by flash chromatography on silica gel (30% ether/hexanes) to obtain compound **2.5da** as a clear oil (32.8 mg, 89%, 95% ee). $R_f = 0.41$ (30% ether/hexanes); The ee was measured utilizing the Shimadzu HPLC instrument using a chiral stationary phase [Chiralcel OD-H, 2-propanol/hexanes = 2/98, 1.5 mL/min, $\lambda = 254$ nm], $t_R = 9.40$ min (minor), 10.29 min (major); ^1H NMR (500 MHz, CDCl_3) δ 8.00 (d, $J = 2.1$ Hz, 2H), 7.35 – 7.31 (m, 5H), 7.19 – 7.17 (m, 2H), 7.15 (d, $J = 8.8$ Hz, 2H), 6.54 (s, 1H), 3.80 (s, 3H); ^{13}C NMR (125 MHz, CDCl_3) δ 169.3, 139.0, 133.3, 128.9, 128.7, 127.2, 126.6, 125.7, 123.8, 120.2, 111.5, 60.6, 52.9; IR (ATR) 2952, 2921, 1745, 1474, 1434, 1203, 864, 792, 734 cm^{-1} ; HRMS (ESI): m/z calcd for $\text{C}_{21}\text{H}_{15}\text{Cl}_2\text{NO}_2\text{Na}$ [$\text{M} + \text{Na}$] $^+$ 406.0378, found 406.0382.



Methyl 2-(1-fluoro-9H-carbazol-9-yl)-2-phenylacetate (2.5ea):

Example using general procedure B. A flame-dried, 5 mL round-bottom flask equipped with stir bar was charged with 1-fluorocarbazole (38.3 mg, 0.21 mmol, 1 equiv), $\text{Pd}(\text{PhCN})_2\text{Cl}_2$ (7.6 mg, 0.020 mmol, 10 mol %), (*S,S*)-*i*-Pr-PyBOX (7.2 mg, 0.024 mmol, 12 mol %), NaBAr^{F} (42.5 mg, 0.048 mmol, 24 mol %), and 5 Å MS (196 mg). To a separate flame-dried pear-shaped flask was added methyl 2-diazo-2-

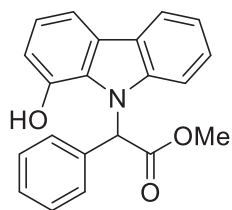
phenylacetate **2.4a** (74.0 mg, 0.42 mmol, 2 equiv). Both flasks were evacuated for 10 min and backfilled with nitrogen gas. Distilled CHCl_3 (2.1 mL) was added to the round-bottom flask to obtain a 100 mM solution with respect to 1-fluorocarbazole. The diazo substrate was dissolved in CHCl_3 (1.4 mL) to obtain a 300 mM solution. The round-bottom flask was submerged in a 43 °C oil bath and stirred for 5 min. Then, the diazo solution was added to the reaction mixture over 8 hours via syringe pump, followed by 2.5 h additional stirring. The crude product was purified by flash chromatography on silica gel (15% ether/hexanes) to obtain compound **2.5ea** as a white solid (43.1 mg, 63%, 94% ee). $R_f = 0.32$ (15% ether/hexanes); The ee was measured utilizing the Shimadzu HPLC instrument using a chiral stationary phase [Chiralcel OD-H, 2-propanol/hexanes = 8/92, 1.0 mL/min, $\lambda = 254$ nm], $t_R = 6.68$ min (major), 9.78 min (minor); ^1H NMR (500 MHz, CDCl_3) δ 8.06 (d, $J = 7.8$ Hz, 1H), 7.92 – 7.84 (m, 1H), 7.37 – 7.26 (m, 6H), 7.26 – 7.20 (m, 3H), 7.19 (m, 3H), 3.78 (s, 3H); ^{13}C NMR (125 MHz, CDCl_3) δ 169.8, 149.4 (d, $J = 241.9$ Hz), 140.3, 134.9, 128.5, 128.2, 127.9 (d, $J = 8.0$ Hz), 127.4, 127.3 (d, $J = 4.7$ Hz), 126.4, 123.7 (d, $J = 2.0$ Hz), 120.4, 120.2, 120.1 (d, $J = 6.8$ Hz), 116.1 (d, $J = 3.4$ Hz), 112.4 (d, $J = 19.6$ Hz), 111.3, 61.7 (d, $J = 7.9$ Hz), 52.8; IR (ATR): 3070, 2943, 1744, 1574, 1457, 1431, 1338, 1211, 748, 736 cm^{-1} ; HRMS (ESI): m/z calculated for $\text{C}_{21}\text{H}_{16}\text{FNO}_2\text{Na}$ [$\text{M} + \text{Na}$] $^+$ 356.1063, found 356.1081.



Methyl 2-(1-methoxy-9H-carbazol-9-yl)-2-phenylacetate (2.5fa): Using general procedure B, 1-methoxycarbazole (700 mg, 3.55 mmol) was reacted with methyl 2-diazo-2-phenylacetate (1.25 g, 7.10 mmol) at 40 °C. The diazo solution was added via syringe pump over 8 h, followed by 1 h additional stirring. The crude product was purified by flash chromatography on silica gel

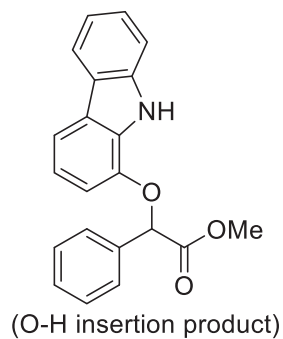
(1st column = 30% ether/hexanes; 2nd column = 30% ether/hexanes) to obtain compound **2.5fa** as a colorless oil that solidifies upon drying *in vacuo* (529 mg, 43%). $R_f = 0.31$ (toluene); $R_f = 0.38$ (30% ether/hexanes); The ee was determined by analyzing the reduced product (see next paragraph). ^1H NMR (500 MHz, CDCl_3) δ 8.05 (d, $J = 7.8$ Hz, 1H), 7.73 (d, $J = 7.8$ Hz, 1H), 7.47

(br, 1H), 7.35 – 7.23 (m, 6H), 7.21 – 7.15 (m, 2H), 7.11 (d, $J = 8.3$ Hz, 1H), 6.93 (d, $J = 7.9$ Hz, 1H), 3.86 (s, 3H), 3.71 (s, 3H); ^{13}C NMR (125 MHz, CDCl_3) δ 170.4, 146.7, 140.1, 135.9, 129.8, 128.3, 127.7, 127.5, 125.6, 125.3, 123.8, 120.2, 120.2, 119.6, 113.1, 111.2, 107.8, 61.5, 55.6, 52.5; IR (ATR): 3058, 2950, 2838, 1740, 1579, 1455, 1430, 1261, 1204, 1014, 735 cm^{-1} ; HRMS (ESI) m/z calculated for $\text{C}_{22}\text{H}_{19}\text{NO}_3\text{Na}$ $[\text{M} + \text{Na}]^+$ 368.1263, found 368.1255.

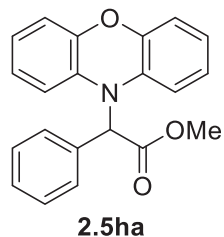


2.5ga

Methyl 2-(1-hydroxy-9H-carbazol-9-yl)-2-phenylacetate (2.5ga): Using general procedure A, 9H-carbazol-1-ol (55.0 mg, 0.30 mmol) was reacted with methyl 2-diazo-2-phenylacetate **2.4a** (79.2 mg, 0.45 mmol) at 40 °C for 5 h. The crude product was purified by flash chromatography on silica gel (1st column = 30% ether/hexanes; 2nd column = 50% ether/hexanes) to obtain compound **2.5ga** as a white solid (60.8 mg, 61%, 26% ee). $R_f = 0.15$ (30% ether/hexanes); $R_f = 0.33$ (50% ether/hexanes); The ee was measured utilizing the Shimadzu HPLC instrument using a chiral stationary phase [Chiralcel OD-H, 2-propanol/hexanes = 10/90, 1.0 mL/min, $\lambda = 254$ nm], $t_R = 12.10$ min (major), 36.38 min (minor); ^1H NMR (500 MHz, acetone- d_6) 9.08 (br, 1H), 8.08 (d, $J = 7.8$ Hz, 1H), 7.76 (s, 1H), 7.69 (dd, $J = 7.8, 0.9$ Hz, 1H), 7.38 (d, $J = 7.6$ Hz, 2H), 7.35 – 7.18 (m, 5H), 7.18 – 7.10 (m, 1H), 7.06 (t, $J = 7.7$ Hz, 1H), 6.96 (dd, $J = 7.7, 0.9$ Hz, 1H), 3.73 (s, 3H); ^{13}C NMR (125 MHz, acetone- d_6) δ 170.9, 144.5, 141.1, 137.5, 130.1, 129.0, 128.7, 128.4, 126.5, 126.2, 124.9, 121.2, 120.9, 120.2, 113.1, 112.8, 112.4, 62.1, 52.7; IR (ATR): 3413 (br), 3057, 2951, 1722, 1585, 1455, 1338, 1268, 1215, 742 cm^{-1} ; HRMS (ESI): m/z calculated for $\text{C}_{21}\text{H}_{17}\text{NO}_3\text{Na}$ $[\text{M} + \text{Na}]^+$ 354.1106, found 354.1113. The other by-product is the competitive O–H insertion product for which characterization is below.

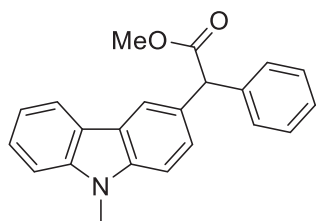


Methyl 2-((9H-carbazol-1-yl)oxy)-2-phenylacetate (O–H insertion product): Using general procedure A, carbazol-1-ol (55.0 mg, 0.30 mmol) was reacted with methyl 2-diazo-2-phenylacetate **2.4a** (79.2 mg, 0.45 mmol) at 40 °C for 5 h. The crude product was purified by flash chromatography on silica gel (1st column = 30% ether/hexanes; 2nd column = 50% ether/hexanes) to obtain the title compound as a colorless oil (14.9 mg, 15%). $R_f = 0.33$ (30% ether/hexanes); $R_f = 0.52$ (50% ether/hexanes); $^1\text{H NMR}$ (500 MHz, CDCl_3) δ 8.65 (br, 1H), 8.04 (d, $J = 7.8$ Hz, 1H), 7.72 (d, $J = 7.8$ Hz, 1H), 7.65 (d, $J = 6.6$ Hz, 2H), 7.54 – 7.36 (m, 5H), 7.24 – 7.17 (m, 1H), 7.08 (t, $J = 7.8$ Hz, 1H), 6.84 (d, $J = 7.8$ Hz, 1H), 5.82 (s, 1H), 3.75 (s, 3H); $^{13}\text{C NMR}$ (125 MHz, CDCl_3) δ 170.7, 143.3, 139.4, 135.5, 130.6, 129.2, 128.9, 127.2, 125.9, 125.0, 123.5, 120.5, 119.5, 119.4, 114.4, 111.0, 109.3, 79.7, 52.7; IR (ATR): 3414 (br), 3060, 2952, 1743, 1577, 1455, 1234, 1099, 743 cm^{-1} ; HRMS (ESI): m/z calculated for $\text{C}_{21}\text{H}_{17}\text{NO}_3\text{Na}$ $[\text{M} + \text{Na}]^+$ 354.1106, found 354.1114.



Methyl 2-(10H-phenoxazin-10-yl)-2-phenylacetate (2.5ha): Using general procedure A, phenoxazine (19.8 mg, 0.11 mmol) was reacted with methyl 2-diazo-2-phenylacetate **2.4a** (28.6 mg, 0.16 mmol) at 30 °C for 15 min. The crude product was purified by flash chromatography on silica gel (10% ether/hexanes) to obtain compound **2.5ha** as a white solid (36.5 mg, 81%, 94% ee). $R_f = 0.59$ (20% ether/hexanes); The ee was measured utilizing the Shimadzu HPLC instrument using a chiral stationary phase [Chiralcel OD-H, 2-propanol/hexanes = 2/98, 1.0 mL/min, $\lambda = 254$ nm], $t_R = 7.86$ min (major), 9.53 min (minor); $^1\text{H NMR}$ (500 MHz, CDCl_3) δ 7.43 (d, $J = 8.1$ Hz, 2H), 7.37 (t, $J = 7.4$ Hz, 2H), 7.34 – 7.31 (m, 1H), 6.79 (dd, $J = 7.8, 1.6$ Hz, 2H), 6.75 (td, $J = 7.6, 1.5$ Hz, 2H), 6.70 (td, $J = 7.6, 1.7$ Hz, 2H), 6.36 (dd, $J = 7.9, 1.4$ Hz, 2H), 5.71 (s, 1H), 3.76 (s, 3H); $^{13}\text{C NMR}$ (125 MHz, CDCl_3) δ 170.3, 146.8, 133.8, 133.3, 128.6, 128.0, 127.7, 123.4, 122.1, 115.7,

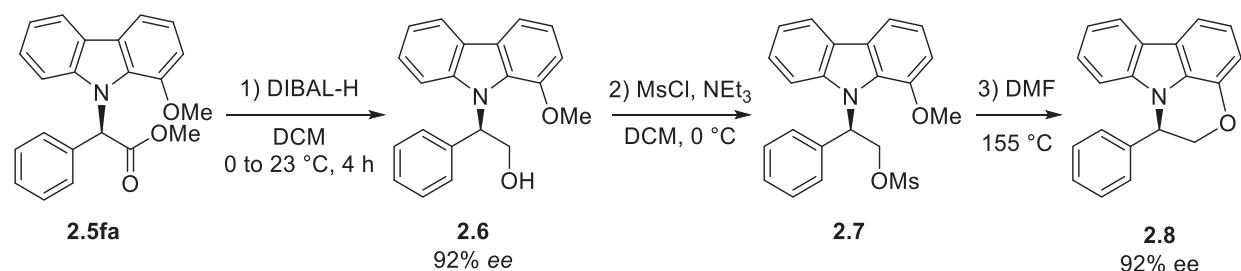
114.2, 64.0, 52.9; IR (ATR) 3056, 2922, 1744, 1484, 1207, 1131 cm^{-1} ; HRMS (ESI): m/z calculated for $\text{C}_{21}\text{H}_{17}\text{NO}_3\text{Na}$ $[\text{M} + \text{Na}]^+$ 354.1106, found 354.1113.



Methyl 2-(9-methyl-9H-carbazol-3-yl)-2-phenylacetate: Using

general procedure A, 9-methylcarbazole (36.2 mg, 0.20 mmol) was reacted with methyl 2-diazo-2-phenylacetate **2.2a** (52.8 mg, 0.30 mmol) at 30 °C for 5 h. The crude product was purified by flash chromatography on silica gel (15% EtOAc/hexanes) to obtain the title compound as a red oil (33.5 mg, 51%). R_f = 0.46(20% EtOAc/hexanes); ^1H NMR (500 MHz, CDCl_3) δ 8.06 – 8.05 (m, 2H), 7.48 – 7.43 (m, 2H), 7.38 – 7.31 (m, 6H), 7.27 – 7.24 (m, 1H), 7.21 (t, J = 7.5 Hz, 1H), 5.24 (s, 1H), 3.83 (s, 3H), 3.77 (s, 3H); ^{13}C NMR (125 MHz, CDCl_3) δ 173.6, 141.3, 140.2, 139.5, 129.0, 128.5, 127.1, 126.4, 125.8, 122.9, 122.6, 120.4, 120.3, 118.9, 108.6, 108.5, 57.0, 52.3, 29.1; IR (ATR) 3026, 2948, 1732, 1602, 1494, 1471, 1146, 730 cm^{-1} ; HRMS (ESI): m/z calculated for $\text{C}_{22}\text{H}_{19}\text{NO}_2\text{Na}$ $[\text{M} + \text{Na}]^+$ 352.1313, found 352.1326.

Synthesis and Analytical Data for 5-HT₆ Serotonin Receptor Antagonist Core



The core of 5-HT₆ receptor antagonist (**2.8**) was synthesized in three steps from methoxy carbazole derivative **2.5fa**.

Step 1: Reduction of **2.5fa** to **2-(1-methoxy-9H-carbazol-9-yl)-2-phenylethan-1-ol (2.6)**:

An oven-dried 100 mL round-bottom flask equipped with stir bar was charged with compound

2.5fa (293 mg, 0.85 mmol, 1 equiv), evacuated, backfilled with nitrogen, and sealed with a rubber septum. Through the septum was injected dry CH₂Cl₂ (20 mL). The flask was submerged in an ice-water bath for 10 min while stirring. Through the septum was injected DIBAL-H (2.6 mL, 1 M in hexanes, 2.55 mmol, 3 equiv). The ice-water bath was allowed to warm to room temperature and the reaction stirred for 4 h. Next, the flask was cooled again for 10 min in an ice-water bath. Methanol (0.5 mL) was added dropwise to quench unreacted DIBAL-H. The reaction mixture was diluted with ether (25 mL). To the mixture was added a saturated solution of sodium potassium tartrate (5 mL) and stirred vigorously at room temperature for 2 h. The ether layer was collected. Additional ether (30 mL) was added to the aqueous layer and the mixture stirred vigorously for 15 min. The ether layers were combined and concentrated. The crude product was purified by flash chromatography on silica gel (30% EtOAc/hexanes) to obtain alcohol **2.6** (246 mg, 91%, 93% ee). $R_f = 0.41$ (30% EtOAc/hexanes); The ee was measured utilizing the Shimadzu HPLC instrument using a chiral stationary phase [Chiralcel OD-H, 2-propanol/hexanes = 50/50, 0.5 mL/min, $\lambda = 254$ nm], $t_R = 14.07$ min (major), 44.20 min (minor); ¹H NMR (500 MHz, CDCl₃) δ 8.02 (d, $J = 7.9$ Hz, 1H), 7.70 (d, $J = 7.8$ Hz, 1H), 7.52 – 6.67 (m, 11H), 4.62 – 4.41 (m, 2H), 3.82 (s, 2H); ¹³C NMR (125 MHz, CDCl₃) δ 146.7, 138.8, 130.7, 128.5, 127.1, 126.4, 125.3, 124.2, 120.3, 119.9, 119.3, 113.0, 112.1, 108.1, 62.9, 60.3, 55.7; IR (ATR): 3343 (br), 3054, 2932, 2835, 1576, 1454, 1427, 1328, 1259, 1217 cm⁻¹. HRMS (ESI): m/z calculated for C₂₁H₁₉NO₂Na [M + Na]⁺ 340.1313, found 340.1325.

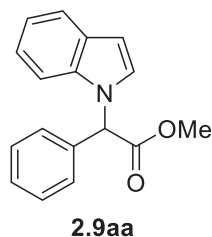
Step 2: **2-(1-methoxy-9H-carbazol-9-yl)-2-phenylethyl methanesulfonate (2.7)** was synthesized from **2.6** by adapting reaction conditions from a patented procedure.⁴⁸ A solution of 2-(1-methoxy-9H-carbazol-9-yl)-2-phenylethan-1-ol **2.6** (20 mg, 0.06 mmol, 1.0 equiv) in DCM (1.1 mL) was treated with NEt₃ (17.5 μ L, 0.13 mmol, 2 equiv) at 0 °C. Mesyl chloride (7.3 μ L, 0.09 mmol, 1.5 equiv) was then added and the resulting solution was stirred for 20 min at 0 °C. The reaction was quenched with saturated sodium bicarbonate aqueous solution (2 mL). The resulting

mixture was extracted with DCM (3 × 10 mL) and the combined organic layers were dried with Na₂SO₄. The organic layer was concentrated and purified by flash chromatography on silica gel (20% EtOAc/hexanes) to afford 2-(1-methoxy-9H-carbazol-9-yl)-2-phenylethyl methanesulfonate **2.7** as a white solid (24 mg, 95%). R_f = 0.22 (toluene); ¹H NMR (600 MHz, CDCl₃) δ 8.05 (d, *J* = 7.8 Hz, 1H), 7.72 (d, *J* = 7.8 Hz, 1H), 7.43 – 7.25 (br m, 6H), 7.20 (t, *J* = 7.8 Hz, 3H), 7.11 – 6.61 (br s, 2H), 5.52 – 4.91 (br m, 2H), 3.94 (br s, 3H), 2.31 (br s, 2H); ¹³C NMR (150 MHz, CDCl₃) δ 146.7, 137.1, 130.4, 128.80, 127.7, 126.3, 125.6, 120.5, 119.7, 113.0, 112.3, 108.2, 68.6, 57.1, 55.7, 37.0; IR (ATR) 3029, 2634, 1453, 1428, 1356, 1329, 1260, 1218, 1172 cm⁻¹; HRMS (ESI): *m/z* calculated for C₂₂H₂₁NO₄SNa [M + Na]⁺ 418.1089, found 418.1092.

Step 3: **1-phenyl-1,2-dihydro-[1,4]oxazino[2,3,4-jk]carbazole (2.8)** was synthesized by heating mesylate **2.7** (12.1 mg, 0.031 mmol, 1 equiv) at 155 °C in DMF (0.5 mL) for 8 h. After 8 h, the reaction was allowed to cool to room temperature then diluted with de-ionized H₂O (1 mL) and extracted with EtOAc (3 × 10 mL). The combined organic layers were washed with H₂O (3 × 10 mL) and dried with Na₂SO₄. The resulting organic layers were concentrated and purified using preparative layer chromatography (5% EtOAc/Hexanes) to afford the core of 5-HTC receptor antagonist **2.6** as a pale white film (6 mg, 67%, 92% ee). R_f = 0.58 (30% EtOAc/Hexanes). The ee was measured utilizing the Shimadzu HPLC instrument using a chiral stationary phase [Chiralcel OD-H, 2-propanol/hexanes = 5/95, 1.0 mL/min, λ = 254 nm], t_R = 8.57 min (major), 14.94 min (minor); ¹H NMR (600 MHz, CDCl₃) δ 8.09 (dt, *J* = 7.7, 0.9 Hz, 1H), 7.70 (dd, *J* = 7.9, 0.7 Hz, 1H), 7.38 – 7.31 (m, 3H), 7.24 – 7.20 (m, 1H), 7.20 – 7.17 (m, 3H), 7.15 (d, *J* = 7.8 Hz, 1H), 6.98 (dd, *J* = 7.8, 0.7 Hz, 1H), 6.80 (dd, *J* = 8.0, 1.0 Hz, 1H), 5.51 (dd, *J* = 5.5, 3.4 Hz, 1H), 4.63 (dd, *J* = 11.3, 3.4 Hz, 1H), 4.52 (dd, *J* = 11.3, 5.5 Hz, 1H); ¹³C NMR (150 MHz, CDCl₃) δ 142.6, 139.2, 136.9, 129.0, 128.9, 128.6, 127.1, 125.5, 123.9, 122.8, 121.2, 119.9, 119.4, 113.4,

110.3, 109.8, 71.8, 56.6; IR (ATR) 3057, 2920, 1636, 1587, 1500, 1450, 1234, 742 cm^{-1} ; HRMS (ESI): m/z calculated for $\text{C}_{20}\text{H}_{15}\text{NOH}$ [$\text{M} + \text{H}$] 286.1232, found 286.1227.

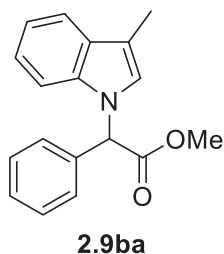
Alternative route to core of 5-HT₆ receptor antagonist **2.8** from alcohol **2.6**: A flame-dried 5 mL, single-necked, round-bottom flask equipped with a rubber septum and magnetic stir bar was charged with 2-(1-methoxy-9*H*-carbazol-9-yl)-2-phenylethan-1-ol **2.6** (20.0 mg, 0.06 mmol). The flask was purged and backfilled with nitrogen three times, charged with dry DCM (0.5 mL), cooled to -78 °C in a dry ice/acetone bath, and charged with pyridine (12 μL , 0.07 mmol) while stirring. After 10 min, TiF_2O (5.6 μL , 0.07 mmol) was added via syringe. The reaction mixture was stirred at -78 °C for 45 min and then allowed to warm to room temperature over 1 h. Half-saturated aqueous ammonium chloride (5 mL) was then added, and the resulting mixture was extracted with DCM (3 \times 5 mL). The combined organic layers were washed with brine (1 \times 25 mL), dried over Na_2SO_4 , and concentrated *in vacuo* to afford a yellow oil. The oil was purified by flash chromatography on silica gel (3% EtOAc/hexanes) to afford compound **2.6** as a pale white film (7.7 mg, 43%, 93% ee).



Methyl 2-(1*H*-indol-1-yl)-2-phenylacetate (2.9aa**)**: Using general procedure A, indole (70.2 mg, 0.60 mmol) was reacted with methyl 2-diazo-2-phenylacetate **2.4a** (158.6 mg, 0.90 mmol). The general procedure was modified so that the reaction was halted 15 minutes after adding the diazo solution, with indole only partially reacted. The reaction mixture was immediately diluted with CHCl_3 (2 mL) and filtered through a pad of celite. (Longer reaction times led to products resulting from over-insertion). The crude product was purified by flash chromatography on silica gel (8% ether/hexanes) to obtain compound **2.9aa** as a colorless oil (17.4 mg, 11%, 80% ee). The ratio of N1-H/C2-H/C3-H insertion at 15 min was 1.0:0.8:3.0 as determined by ^1H NMR analysis. $R_f = 0.49$ (20% ether/hexanes); The ee was measured utilizing

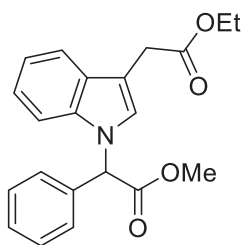
the Shimadzu HPLC instrument using a chiral stationary phase [Chiralcel OD-H, 2-propanol/hexanes = 3/97, 1.0 mL/min, λ = 254 nm], t_R = 11.29 min (major), 12.62 min (minor); ^1H NMR (600 MHz, CDCl_3) δ 7.63 (dt, J = 7.9, 0.9 Hz, 1H), 7.41 – 7.36 (m, 3H), 7.36 – 7.31 (m, 3H), 7.22 (t, J = 8.3 Hz, 1H), 7.16 – 7.10 (m, 2H), 6.53 (d, J = 3.3 Hz, 1H), 6.26 (s, 1H), 3.80 (s, 3H); ^{13}C NMR (151 MHz, CDCl_3) δ 170.1, 136.4, 134.6, 129.1, 129.0, 128.8, 128.06, 126.7, 121.9, 121.2, 120.1, 109.0, 102.5, 62.0, 52.8; IR (ATR) 3030, 952, 2923, 1745, 1457, 1310, 1197, 1168, 737 cm^{-1} ; HRMS (ESI): m/z calculated for $\text{C}_{17}\text{H}_{15}\text{NO}_2\text{Na}$ [$\text{M} + \text{Na}$] $^+$ 288.1000, found 288.1013.

Experiment analyzing insertion regioselectivity: Using Zhu's conditions,³ indole (35.2 mg, 0.30 mmol) was reacted with methyl 2-diazo-2-phenylacetate **2.4a** (35.1 mg, 0.20 mmol). Diazo solution (0.28 M in CHCl_3 , 0.35 mL/min) was added slowly via syringe pump to the reaction mixture containing indole, $\text{Pd}(\text{PhCN})_2\text{Cl}_2$ (3.8 mg, 0.01 mmol), (*S*)-Ph-SpiroBOX (6.1 mg, 0.012 mmol), NaBAR^{F} (21.3 mg, 0.024 mmol), and 5Å MS in CHCl_3 (2 mL) at 40 °C. Over-insertion products began to form within 1.5 h as determined by TLC. At this point, 0.5 mL of diazo solution had been added and the reaction was halted. The reaction mixture was immediately diluted with CHCl_3 (1 mL) and filtered through a pad of celite. The crude reaction mixture was analyzed by ^1H NMR. The ratio of N1-H/C2-H/C3-H insertion was determined to be 2:3:18.



Methyl 2-(3-methyl-1H-indol-1-yl)-2-phenylacetate (2.9ba): Using general procedure A, 3-methylindole (98%, 13.4 mg, 0.1 mmol) was reacted with methyl 2-diazo-2-phenylacetate **2.4a** (26.4 mg, 0.15 mmol) at 30 °C for 1 h. The general procedure was modified slightly so that the 3-methylindole solution was stirred at 30 °C for 15 min instead of 5 min before adding the diazo solution. The crude product was purified by flash chromatography on silica gel (5% ether/hexanes) to obtain compound **2.9ba** as an off-white oil (17.5 mg, 63%, 79% ee). R_f = 0.35 (10% ether/hexanes); The ee was measured utilizing the Agilent HPLC instrument using a chiral

stationary phase [Chiralpak AD, 2-propanol/hexanes = 5/95, 1.0 mL/min, λ = 254 nm], t_R = 6.38 min (major), 7.52 min (minor); ^1H NMR (500 MHz, CDCl_3) δ 7.57 (d, J = 7.8 Hz, 1H), 7.41 – 7.36 (m, 3H), 7.34 – 7.28 (m, 3H), 7.21 (t, J = 7.4 Hz, 1H), 7.14 (t, J = 7.4 Hz, 1H), 6.88 (s, 1H), 6.21 (s, 1H), 3.79 (s, 3H), 2.28 (s, 3H); ^{13}C NMR (126 MHz, CDCl_3) δ 170.3, 136.8, 134.9, 129.1, 129.0, 128.8, 128.0, 124.1, 121.9, 119.4, 119.2, 111.6, 108.8, 77.3, 77.0, 76.8, 61.7, 52.7, 9.7; IR (ATR) 3030, 2918, 1747, 1459, 1194, 1169 cm^{-1} ; HRMS (ESI): m/z calculated for $\text{C}_{18}\text{H}_{17}\text{NO}_2\text{Na}$ [$\text{M} + \text{Na}$] $^+$ 302.1157, found 302.1145.



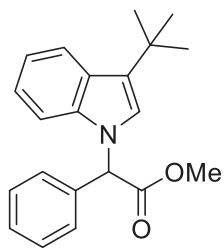
2.9ca
mixture of N1-H and C2-H
insertion products

Methyl 2-(3-(2-ethoxy-2-oxoethyl)-1H-indol-1-yl)-2-phenylacetate

(2.9ca): Using general procedure A, ethyl-3-indoleacetate (99%, 20.5 mg, 0.1 mmol) was reacted with methyl 2-diazo-2-phenylacetate **2.4a** (26.4 mg, 0.15 mmol) at 30 °C for 18 h. The general procedure was modified slightly so that the ethyl-3-indoleacetate solution was stirred at 30 °C for 15 min instead of 5 min before adding the diazo solution.

The crude product was purified by flash chromatography on silica gel (gradient 10–20% ether/hexanes) to obtain an inseparable mixture of N1-H/C2-H insertion products in an 8:1 ratio as a pale-yellow oil (28.0 mg, 79%, 79% ee); R_f = 0.23 (20% ether/hexanes); The ee was measured utilizing the Agilent HPLC instrument using a chiral stationary phase [Chiralpak AD, 2-propanol/hexanes = 30/70, 1.0 mL/min, λ = 254 nm], N1–H insertion t_R = 6.38 min (major), 7.52 min (minor); C2–H insertion t_R = 8.07 min (equal), 9.18 min (equal); Major peaks are reported for ^1H and ^{13}C NMR. See attached NMR for other peaks resulting from C2-H insertion product present in minor amounts; ^1H NMR (500 MHz, CDCl_3) δ 7.63 (d, J = 7.8 Hz, 1H), 7.41 – 7.37 (m, 3H), 7.37 – 7.28 (m, 4H), 7.23 (dd, J = 13.4, 6.1 Hz, 1H), 7.15 (t, J = 7.4 Hz, 1H), 7.09 (s, 1H), 6.22 (s, 1H), 4.12 (q, J = 7.1 Hz, 2H), 3.79 (s, 3H), 3.71 (s, 2H), 1.22 (t, J = 7.1 Hz, 3H). Note: An extra proton is reported presumably due to the C2–H insertion product overlapping in the aromatic region with

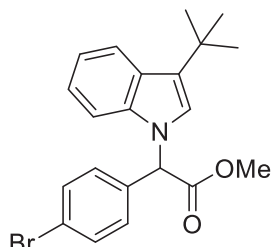
the N1–H insertion product; ^{13}C NMR (126 MHz, CDCl_3) δ 171.8, 170.0, 136.7, 134.4, 129.1, 129.0, 128.9, 128.2, 128.1, 127.7, 125.5, 122.2, 120.0, 119.5, 109.1, 108.4, 61.9, 60.7, 52.8, 31.5, 14.2; IR (ATR) 2953, 1737, 1460, 1167 cm^{-1} ; HRMS (ESI): m/z calculated for $\text{C}_{21}\text{H}_{21}\text{NO}_4\text{Na}$ [$\text{M} + \text{Na}$] $^+$ 374.1368, found 374.1379.



2.9da

Methyl 2-(3-(tert-butyl)-1H-indol-1-yl)-2-phenylacetate (2.9da): Using general procedure A, 3-(tert-butyl)-1H-indole (20.5 mg, 0.12 mmol) was reacted with methyl 2-diazo-2-phenylacetate **2.4a** (31.3 mg, 0.18 mmol) for 4 h. The crude product was purified by flash chromatography on silica gel (10% ether/hexanes) to obtain compound **2.9da** as a white solid (33.8 mg, 89%,

79% ee); $R_f = 0.33$ (10% ether/hexanes); The ee was measured utilizing the Shimadzu HPLC instrument using a chiral stationary phase [Chiralcel OD-H, 2-propanol/hexanes = 0.3/99.7, 1.0 mL/min, $\lambda = 254$ nm], $t_R = 14.27$ min (minor), 15.54 min (major); ^1H NMR (500 MHz, CDCl_3) δ 7.82 (d, $J = 8.0$ Hz, 1H), 7.41 – 7.34 (m, 3H), 7.33 – 7.29 (m, 3H), 7.18 (t, $J = 7.2$ Hz, 1H), 7.11 (t, $J = 7.2$ Hz, 1H), 6.87 (s, 1H), 6.21 (s, 1H), 3.80 (s, 3H), 1.40 (s, 9H); ^{13}C NMR (125 MHz, CDCl_3) δ 170.2, 137.6, 134.9, 129.0, 128.8, 128.0, 126.9, 126.4, 121.8, 121.6, 121.4, 119.1, 109.2, 61.8, 52.7, 31.6, 30.7; IR (ATR) 2953, 1749, 1462, 1197, 1166, 736 cm^{-1} ; HRMS (ESI): m/z calculated for $\text{C}_{21}\text{H}_{22}\text{BrNO}_2\text{Na}$ [$\text{M} + \text{Na}$] $^+$ 344.1627, found 344.1638.



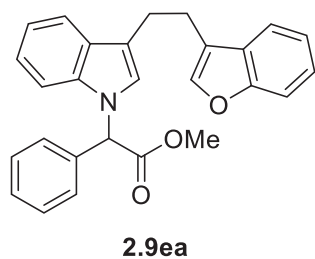
2.9db

Methyl 2-(4-bromophenyl)-2-(3-(tert-butyl)-1H-indol-1-yl)acetate (2.9db): Using general procedure A, 3-(tert-butyl)-1H-indole (153 mg, 0.88 mmol) was reacted with methyl 2-(4-bromophenyl)-2-diazoacetate **2.4b** (337 mg, 1.32 mmol) for 10 h. The crude product was purified by flash chromatography on silica gel (10% ether/hexanes) to obtain compound

2.9db as a white solid (288 mg, 82%, 70% ee); $R_f = 0.31$ (10% ether/hexanes); The ee was measured utilizing the Shimadzu HPLC instrument using a chiral stationary phase [Chiralcel OD-

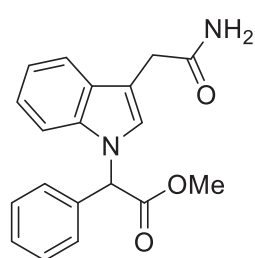
H, 2-propanol/hexanes = 1/99, 1.0 mL/min, λ = 254 nm], t_R = 7.15 min (minor), 8.07 min (major); ^1H NMR (500 MHz, CDCl_3) δ 7.82 (d, J = 8.0 Hz, 1H), 7.50 (d, J = 8.5 Hz, 2H), 7.26 (d, J = 8.3 Hz, 1H), 7.20 – 7.05 (m, 4H), 6.87 (s, 1H), 6.15 (s, 1H), 3.80 (s, 3H), 1.41 (s, 9H); ^{13}C NMR (125 MHz, CDCl_3) δ 169.7, 137.5, 134.0, 132.1, 129.5, 126.9, 126.9, 123.0, 121.7, 121.6, 121.5, 119.2, 109.2, 61.2, 52.9, 31.7, 30.7; IR (ATR) 2964, 1748, 1201, 1174, 734 cm^{-1} ; HRMS (ESI): m/z calculated for $\text{C}_{21}\text{H}_{22}\text{BrNO}_2\text{Na}$ [$\text{M} + \text{Na}$] $^+$ 422.0732, found 422.0742.

Compound **2.9db** was crystallized as the racemate from scalemic material by slow evaporation from methanol. X-ray data was uploaded to the Cambridge Crystallographic Data Centre (CCDC) Database (deposition number: 1520167).



Methyl 2-(3-(2-(benzofuran-3-yl)ethyl)-1H-indol-1-yl)-2-phenylacetate (2.9ea):

Using general procedure A, 3-(2-(benzofuran-3-yl)ethyl)-1H-indole (31.4 mg, 0.12 mmol) was reacted with methyl 2-diazo-2-phenylacetate **2.4a** (32.3 mg, 0.18 mmol) at 40 °C for 2 h. The crude product was purified by flash chromatography on silica gel (10 % ether/hexanes) to obtain compound **2.9ea** as a pale yellow oil (26.5 mg, 54%, 77% ee); R_f = 0.18 (10% ether/hexanes); The ee was measured utilizing the Shimadzu HPLC instrument using a chiral stationary phase [Chiralcel OD-H, 2-propanol/hexanes = 5/95, 1.0 mL/min, λ = 254 nm], t_R = 14.63 min (minor), 16.62 min (major); ^1H NMR (500 MHz, CDCl_3) δ 7.63 (d, J = 7.8 Hz, 1H), 7.52 (d, J = 7.7 Hz, 1H), 7.45 (d, J = 8.2 Hz, 1H), 7.40 – 7.35 (m, 3H), 7.33 (t, J = 4.1 Hz, 2H), 7.30 – 7.25 (m, 3H), 7.25 – 7.18 (m, 2H), 7.15 (t, J = 7.5 Hz, 1H), 6.88 (s, 1H), 6.22 (s, 1H), 3.79 (s, 3H), 3.14 – 3.08 (m, 2H), 3.06 – 3.00 (m, 2H); ^{13}C NMR (125 MHz, CDCl_3) δ 170.2, 155.2, 141.3, 136.9, 134.7, 129.0, 128.9, 128.24, 128.21, 127.9, 124.02, 123.99, 122.2, 122.0, 120.2, 119.7, 119.6, 119.2, 115.8, 111.4, 109.1, 61.8, 52.8, 25.1, 24.3; IR (ATR) 3055, 2949, 2852, 1746, 1452, 1195, 1169, 739 cm^{-1} ; HRMS (ESI): m/z calculated for $\text{C}_{27}\text{H}_{23}\text{NO}_3\text{Na}$ [$\text{M} + \text{Na}$] $^+$ 432.1576, found 432.1576.

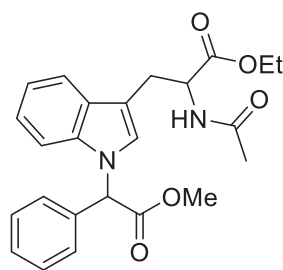


2.9fa

Methyl 2-(3-(2-amino-2-oxoethyl)-1H-indol-1-yl)-2-phenylacetate (2.9-

fa): Using general procedure A, indole-3-acetamide (21.7 mg, 0.12 mmol) was reacted with methyl 2-diazo-2-phenylacetate **2.4a** (32.9 mg, 0.19 mmol) at 40 °C for 25 h. The crude product was purified by flash chromatography on silica gel (EtOAc) to obtain compound **2.9fa** as a white solid (22.4 mg,

58%, 53% ee); $R_f = 0.37$ (EtOAc); The ee was measured utilizing the Agilent HPLC instrument using a chiral stationary phase [Chiralpak AD, 2-propanol/hexanes = 30/70, 1.0 mL/min, $\lambda = 254$ nm], $t_R = 7.21$ min (major), 9.68 min (minor); $^1\text{H NMR}$ (500 MHz, CDCl_3) δ 7.59 (d, $J = 7.9$ Hz, 1H), 7.46 – 7.40 (m, 3H), 7.39 – 7.33 (m, 3H), 7.28 (t, $J = 7.7$ Hz, 1H), 7.20 (t, $J = 7.5$ Hz, 1H), 7.04 (s, 1H), 6.24 (s, 1H), 5.62 (br s, 1H), 5.43 (br s, 1H), 3.81 (s, 3H), 3.67 (s, 2H); $^{13}\text{C NMR}$ (125 MHz, CDCl_3) δ 173.9, 170.0, 137.1, 134.1, 129.3, 128.2, 127.8, 126.1, 122.8, 120.6, 119.3, 109.28, 109.27, 61.9, 52.9, 33.0; IR (ATR) 3390, 3196, 2951, 1742, 1652, 1205, 1168, 743 cm^{-1} ; HRMS (ESI): m/z calculated for $\text{C}_{19}\text{H}_{18}\text{N}_2\text{O}_3\text{Na}$ [$\text{M} + \text{Na}$] $^+$ 345.1215, found 345.1216.



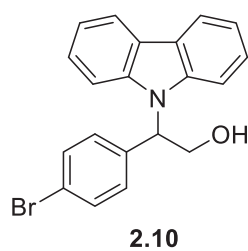
2.9ga

Ethyl *N*-acetyl-1-(2-methoxy-2-oxo-1-phenylethyl)tryptophanate

(2.9ga): Using general procedure A, *N*-acetyl-*L*-tryptophan ethyl ester (31.8 mg, 0.12 mmol) was reacted with methyl 2-diazo-2-phenylacetate **2.4a** (32.3 mg, 0.18 mmol) at 40 °C for 21 h. The crude product was purified by flash chromatography on silica gel (1st column = 60% ether/hexanes; 2nd column = 90% ether/hexanes; 3rd column = 20%

ether/DCM) to obtain compound **2.9ga** as pale yellow oil (36.9 mg, 75%, 60% de). $R_f = 0.07$ (60% ether/hexanes); $R_f = 0.28$ (90% ether/hexanes); $R_f = 0.40$ (20% ether/DCM). The diastereomeric excess was determined by $^1\text{H NMR}$ analysis of the crude product by integration of peaks at 6.86 and 6.84 ppm. $^1\text{H NMR}$ (500 MHz, CDCl_3) δ 7.53 (d, $J = 7.7$ Hz, 1H), 7.44 – 7.35 (m, 3H), 7.35 – 7.27 (m, 3H), 7.22 (ddd, $J = 8.2, 7.1, 1.1$ Hz, 1H), 7.14 (ddd, $J = 8.0, 7.1, 1.0$ Hz, 1H), 6.85 (s,

1H), 6.22 (s, 1H), 5.98 (d, $J = 7.7$ Hz, 1H), 4.87 (dt, $J = 7.9, 5.1$ Hz, 1H), 3.98 (dq, $J = 10.8, 7.2$ Hz, 1H), 3.87 (dq, $J = 10.7, 7.1$ Hz, 1H), 3.80 (s, 3H), 3.27 (qd, $J = 14.6, 4.8$ Hz, 2H), 1.95 (s, 3H), 1.08 (t, $J = 7.2$ Hz, 3H); ^{13}C NMR (125 MHz, CDCl_3) 171.7, 170.0, 169.6, 136.7, 134.6, 129.1, 129.0, 128.8, 128.1, 125.4, 122.3, 120.1, 119.2, 110.1, 109.0, 61.6, 61.4, 53.2, 52.8, 27.6, 23.2, 14.0; IR (ATR): 3300 (br), 3056, 2982, 1737, 1659, 1460, 1197, 732 cm^{-1} ; HRMS (ESI): m/z calculated for $\text{C}_{24}\text{H}_{26}\text{N}_2\text{O}_5\text{Na}$ $[\text{M} + \text{Na}]^+$ 445.1740, found 445.1721.

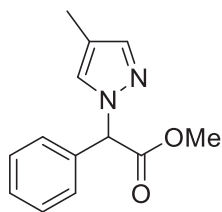


2-(4-Bromophenyl)-2-(9H-carbazol-9-yl)ethan-1-ol (2.10): was

synthesized according to a modified procedure used by Lee and co-workers.⁴⁹ Compound **2.5ab** (880 mg, 2.2 mmol, 1 equiv) was added to a round-bottom flask containing a stir bar. The flask was evacuated, backfilled with nitrogen, and capped with a septum. Through the septum was added dry DCM (15 mL). The solution was stirred and cooled to 0 °C. Upon cooling, DIBAL-H (8.9 mL, 1M in hexanes, 4 equiv) was added through the septum. The resulting solution was stirred for 25 min until consumption of starting material as determined by TLC. Upon completion, the solution was cooled to 0 °C and MeOH was added dropwise to quench unreacted DIBAL-H. The reaction was warmed to room temperature and saturated sodium potassium tartrate was added (7 mL/3.5 mmol). The reaction was stirred vigorously for 5 hours before extracting with EtOAc (3 × 20 mL). The combined organic extracts were washed with brine (3 × 30 mL) and dried with MgSO_4 . The dried organic layer was concentrated and purified by flash chromatography on silica gel (20% ether/hexanes) to afford compound **2.10** as a white solid (0.741 g, 90%, 93% ee). $R_f = 0.21$ (30% ether/hexanes); The ee was determined by utilizing the Shimadzu HPLC instrument using a chiral stationary phase [Chiralcel OD-H, 2-propanol/hexanes = 30/70, 1.0 mL/min, $\lambda = 254$ nm], $t_R = 12.03$ min (major), 18.24 min (minor); ^1H NMR (600 MHz, CDCl_3) δ 8.09 (dt, $J = 7.6, 1.1$ Hz, 2H), 7.40 (d, $J = 8.6$ Hz, 2H), 7.34 (td, $J = 7.6, 1.3$ Hz, 2H), 7.23 (td, $J = 7.5, 1.0$ Hz, 4H), 7.07 (d, $J = 8.5$ Hz, 2H), 5.90

(dd, $J = 8.6, 5.2$ Hz, 1H), 4.54 (ddd, $J = 11.5, 8.6, 4.4$ Hz, 1H), 4.46 (ddd, $J = 11.6, 8.4, 5.3$ Hz, 1H), 1.58 (dd, $J = 8.4, 4.4$ Hz, 1H); ^{13}C NMR (151 MHz, CDCl_3) δ 140.1, 136.0, 131.9, 128.4, 125.8, 123.5, 121.8, 120.4, 119.6, 110.2, 62.3, 58.8. IR (ATR) 3320, 1593, 1480, 1449, 747, 721 cm^{-1} .

Crystallization procedure for **2.10**: Alcohol **2.10** was crystallized by the vapor diffusion method using DCM and hexanes. 50 mg of **2.10** was added to a 2 dram vial and dissolved in 0.5 mL of dry DCM (filtered through a Waters Acrodisc Syringe Filter, 13 mm, 0.45 μm Nylon). The open vial was placed in a larger 20 mL vial containing 5 mL hexanes (HPLC grade). The larger vial was sealed and left undisturbed for two days. After two days, colorless cubic crystals formed, from which an X-ray structure was obtained. The absolute stereochemistry was determined as (*R*). X-ray data was uploaded to the Cambridge Crystallographic Data Centre (CCDC) Database (deposition number: 1519937).



2.11

Methyl 2-(4-methyl-1H-pyrazol-1-yl)-2-phenylacetate (2.11): Using general procedure A, 4-methyl-1H-pyrazole (22.3 mg, 0.27 mmol) was reacted with methyl 2-diazo-2-phenylacetate **2.4a** (22.3 mg, 0.41 mmol) at 55 °C for 30 h.

The crude product was purified by flash chromatography on silica gel (1st column = 20% ether/hexanes; 2nd column = 50% ether/hexanes) to obtain compound **2.11** as a white solid (20.3 mg, 32%, 0% ee); $R_f = 0.35$ (50% ether/hexanes); The ee was measured utilizing the Shimadzu HPLC instrument using a chiral stationary phase [Chiralcel OD-H, 2-propanol/hexanes = 8/92, 1.0 mL/min, $\lambda = 254$ nm], $t_R = 9.56$ min (equal), 19.38 min (equal); ^1H NMR (500 MHz, CDCl_3) δ 7.46 – 7.35 (m, 6H), 7.14 (s, 1H), 6.16 (s, 1H), 3.80 (s, 3H), 2.03 (s, 3H); ^{13}C NMR (125 MHz, CDCl_3) δ 169.7, 140.5, 134.0, 129.3, 129.2, 128.4, 127.9, 116.6, 67.8, 52.9, 890; IR (ATR) 2950, 1740, 1432, 1210, 978, 742 cm^{-1} ; HRMS (ESI): m/z calculated for $\text{C}_{13}\text{H}_{14}\text{N}_2\text{O}_2\text{Na}$ [$\text{M} + \text{Na}$]⁺ 253.0953, found 253.0957.

References

- 1 Moody, C. "Enantioselective Insertion of Metal Carbenes into N–H Bonds: A Potentially Versatile Route to Chiral Amine Derivatives". *Angew. Chem. Int. Ed.* **2007**, *46*, 9148–9150.
- 2 Zhu, S.-F.; Zhou, Q.-L. "Transition-Metal-Catalyzed Enantioselective Heteroatom–Hydrogen Bond Insertion Reactions" *Acc. Chem. Res.* **2012**, *45*, 1365–1377.
- 3 Yates, P. "The Copper-Catalyzed Decomposition of Diazoketones". *J. Am. Chem. Soc.* **1952**, *74*, 5376–5381.
- 4 Saegusa, T.; Ito, Y.; Kobayashi, S.; Hirota, K.; Shimizu, T. "Synthetic Reaction by Complex Catalyst III. Copper Catalyzed N-Alkylation of Amine with Diazoalkane". *Tetrahedron Lett.* **1966**, *49*, 1631–6134.
- 5 Ratcliffe, R.W.; Salzmann, T.N.; Christensen, B.G. "A Novel Synthesis of the Carbapen-2-em Ring System". *Tetrahedron Lett.* **1980**, *21*, 31–34.
- 6 Nobuo, I.; Hisanari, S.; Kenji, K. "Synthetic Studies of Optically Active β -Lactams. Chiral Synthesis of Carbapenam Ring System from L-Aspartic Acid." *Heterocycles.* **1980**, *14*, 1077–1080.
- 7 Christensen, B. G.; Ratcliffe, R. W. "Process for Preparing 3-Substituted-6-substituted-7-oxo-1-azabicyclo[3.2.0]hept-2-ene-2-carboxylic Acid." U.S. Patent 4745188, 1988.
- 8 Karady, S.; Amato, J. S.; Reamer, R. A.; Weinstock, L. M. "Stereospecific Conversion of Penicillin to Thienamycin. *J. Am. Chem. Soc.* **1981**, *103*, 6765–6767.
- 9 Melillo, D. G.; Cvetovich, R. J.; Ryan, K. M.; Sletzing, M. "An Enantioselective Approach to (+)-Thienamycin from Dimethyl 1,3-Acetonedicarboxylate and (+)- α -Methylbenzylamine" *J. Org. Chem.* **1986**, *51*, 1498–1504.
- 10 Garcia, C.; McKervey, A.; Ye, T. "Asymmetric Catalysis of Intramolecular N–H Insertion Reactions of α -diazocarbonyls". *Chem. Commun.*, **1996**, 1465–1466.
- 11 Bachmann, S.; Fielenbach, D.; Jørgensen, K. "Cu(I)-carbenoid- and Ag(I)-Lewis Acid Asymmetric Intermolecular Insertion of α -Diazo compounds into N–H bonds." *Org. Biomol. Chem.* **2004**, *2*, 3044–3049.
- 12 Liu, B.; Zhu, S-F.; Zhang, W.; Chen, C.; Zhou, Q-L. "Highly Enantioselective Insertion of Carbenoids into N–H Bonds Catalyzed by Copper Complexes of Chiral Spiro Bisoxazolines." *J. Am. Chem. Soc.* **2007**, *129*, 5834–5835.
- 13 Hou, Z.; Wang, J.; He, P.; Qin, B.; Liu, X.; Lin, L.; Feng, X. "Highly Enantioselective Insertion of Carbenoids into N–H Bonds Catalyzed by Copper(I) Complexes of Binol Derivatives." *Angew. Chem. Int. Ed.* **2010**, *49*, 4763–4766.
- 14 Lee, E.C.; Fu, G.C. "Copper-Catalyzed Asymmetric N–H Insertion Reactions: Couplings of Diazo Compounds with Carbamates to Generate α -Amino Acids." *J. Am. Chem. Soc.* **2007**, *129*, 12066–12067.
- 15 Maux, P.; Simonneaux, G. "Enantioselective Insertion of Carbenoids into N–H Bonds Catalyzed by Bicyclobisoxazoline Copper(I) Complexes." *Tetrahedron*, **2015**, *71*, 9333–9338.
- 16 Xu, B.; Zhu, S-F.; Xie, X-L.; Shen, J-J.; Zhou, Q-L. "Asymmetric N–H Insertion Reaction Cooperatively Catalyzed by Rhodium and Chiral Spiro Phosphoric Acids." *Angew. Chem. Int. Ed.* **2011**, *50*, 11483–11486.
- 17 Xu, B.; Zhu, S-F.; Zuo, X-P.; Zhang, Z-C.; Zhou, Q-L. "Enantioselective N–H Insertion Reaction of α -Aryl- α -Diazoketones: An Efficient Route to Chiral α -Aminoketones." *Angew. Chem.* **2014**, *126*, 3994–3997.
- 18 Guo, J-X.; Zhou, T.; Xu, B.; Zhu, S-F.; Zhou, Q-L. "Enantioselective Synthesis of α -Alkenyl α -Amino Acids via N–H Insertion Reactions." *Chem. Sci.* **2016**, *7*, 1104–1108.
- 19 Saito, H.; Morita, D.; Uchiyama, T.; Miyake, M.; Shinichi, M. "Cinchona Alkaloids Induce Asymmetry in the Insertion Reaction of Thermally Generated Carbenes into N–H Bonds". *Tetrahedron Lett.* **2012**, *53*, 6662–6664.
- 20 Zhu, Y.; Liu, X.; Dong, S.; Zhou, Y; Li, W.; Lin, L.; Feng, X. "Asymmetric N–H Insertion of Secondary and Primary Anilines Under the Catalysis of Palladium and Chiral Guanidine Derivatives." *Angew. Chem. Int. Ed.* **2014**, *53*, 1636–1640.
- 21 Zhu, S-F.; Xu, B.; Wang, G.P.; Zhou, Q-L. "Well-Defined Binuclear Chiral Spiro Copper Catalysts for Enantioselective N–H Insertion." *J. Am. Chem. Soc.* **2012**, *134*, 436–442.
- 22 Huang, W-S.; Xu, Z.; Yang, K-F.; Chen, L.; Zheng, Z-J.; Xu, L-W. "Modular Construction of Multifunctional Ligands for the Enantioselective Ruthenium-Catalyzed Carbenoid N–H Insertion Reaction: an Enzyme-Like and Substrate-Sensitive Catalyst System." *RSC Adv.* **2015**, *5*, 46455–46463.

- ²³ a) Topol, E.; Schork, N. "Catapulting clopidogrel pharmacogenomics forward". *Nature Medicine*, **2011**, *17*, 40–41. b) Winslow, R. "Plavix rival gains from studies." 30 August 2010. *Wall Street Journal*. Accessed 4 April 2019.
- ²⁴ Selected examples: a) Loakes, D.; Hill, F.; Brown, D.M.; Ball, S.; Reeve, M.; Robinson, P. "5'-Tailed Octanucleotide Primers for Cycle Sequencing." *Nucleosides and Nucleotides*, **1999**, *18*, 2685–2695. b) Wasserman, H.; Xia, M.; Carr, A.; Han, W.; Siegel, M. "Generation of Penems, Carbapenems and Aza Analogs of Cephems by the Addition of Heterocycles and Other Building Blocks to Azetionones." *Tetrahedron*, **2000**, *56*, 5621–5629.
- ²⁵ "Oxazinocarbazoles for the Treatment of CNS Diseases": R.E. Tenbrink. U.S. 6821970(B2), Nov. 23, **2004**.
- ²⁶ a) "Phenylaminopropanol Derivatives and Methods of their use": C. Kim, et al., US2005/0222148(A1), Oct. 6, 2005. b) Mahaney, P.E.; Kim, C.Y.; Coghlan, R.D.; Cohn, S.T.; Heffernan, G.D.; Huselton, C.A.; Terefenko, E.A.; Vu, A.T.; Zhang, P.; Burroughs, K.D.; Cosmi, S.A.; Bray, J.A.; Johnson, G.H.; Deecher, D.C.; Trybulski, E.J. "Structure-activity relationships of the 1-amino-3-(1H-indol-1-yl)-3-phenylpropan-2-ol series of monoamine reuptake inhibitors." *Bioorg. Med. Chem. Lett.* **2009**, *19*, 5807–5810.
- ²⁷ Dongen, M.; Kadam, R.; Juraszek, J.; Lawson, E.; Brandenburg, B.; Schmitz, F.; Schepens, W.; Stoops, B.; Diepen, H.; Jongeneelen, M.; Tang, C.; Vermond, J.; Real, A.; Blokland, S.; Garg, D.; Yu, W.; Goutier, W.; Lanckacker, E.; Klap, J.; Peeters, Danielle; Wu, J.; Buyck, C.; Jonckers, T.; Royans, D.; Roevens, P.; Vogels, R.; Koudstaal, W.; Friesen, R.; Raboisson, P.; Dhanak, D.; Goudsmit, J.; Wilson, I. "A small-molecule fusion inhibitor of influenza virus." *Science*, **2019**, *363*.
- ²⁸ "Resolution of (±)-methyl phenyl[4-[4-[[[4'-(trifluoromethyl-2-biphenyl)carbonyl]amino]phenyl]-1-piperidinyl]acetate": A.H. Copmans, J. Hoet, A. Willemsens, W. Couk, J. van Dun. WO2010/136526 (A1), Dec. 2, **2010**.
- ²⁹ Xie, X.-L.; Zhu, S.-F.; Guo, J.-X.; Cai, Y.; Zhou, Q.-L. "Enantioselective Palladium-Catalyzed Insertion of α -Aryl- α -diazoacetates into the O–H Bonds of Phenols." *Angew. Chem. Int. Ed.* **2014**, *53*, 2978–2981.
- ³⁰ a) Tayama, E.; Yanaki, T.; Iwamoto, H.; Hasegawa, E. "Copper(II) Triflate Catalyzed Intermolecular Aromatic Substitution of *N,N*-Disubstituted Anilines with Diazo Esters." *Eur. J. Org. Chem.* **2010**, *35*, 6719–6721; b) Tayama, E.; Ishikawa, M.; Iwamoto, H.; Hasegawa, F. "Copper(II)-Acid Co-Catalyzed Intermolecular Substitution of Electron-Rich Aromatics with Diazoesters." *Tetrahedron Lett.* **2012**, *53*, 5159–5161; c) Yang, J.-M.; Cai, Y.; Zhu, S.-F. "Iron-Catalyzed Arylation of α -Aryl- α -diazoesters." *Org. Biomol. Chem.* **2016**, *14*, 5516–5519.
- ³¹ Gao, X.; Wu, B.; Huang, W.-X.; Chen, M.-W.; Zhou, Y.-G. "Enantioselective Palladium-Catalyzed C–H Functionalization of Indoles Using an Axially Chiral 2,2'-Bipyridine Ligand." *Angew. Chem. Int. Ed.* **2015**, *54*, 11956–11960; *Angew. Chem.* **2015**, *127*, 12124.
- ³² For crystallographic structure and data, see the Cambridge Crystallographic Data Centre, deposition numbers CCDC 1519937 (carbazole derivative **2.10**) and CCDC 1520167 (indole derivative **2.9db**).
- ³³ a) Bonesi, S.M.; Erra-Balsells, R. "On the Synthesis of Isolation of Chlorocarbazoles Obtained by Chlorination of Carbazoles." *J. Heterocyclic Chem.* **1997**, *34*, 877–889; b) Bonesi, S.M.; Ponce, M. A., Erra-Balsells, R. "A Study of Substituent Effect on ¹H and ¹³C NMR Spectra of Mono, Di, and Poly Substituted Carbazoles." *J. Heterocyclic Chem.* **2005**, *42*, 867–875.
- ³⁴ Allen, F.L.; Suschitzky, H. "Heterocyclic Fluorine Compounds. Part I. Monofluoro-1,2,3,4-tetrahydrocarbazoles and Monofluorocarbazoles." *J. Chem. Soc.* **1953**, 3845–3849.
- ³⁵ Jing, C.; Yongzhou, H. "Microwave-Assisted One-Pot Synthesis of 1,2,3,4-Tetrahydrocarb azoles." *Synth. Commun.* **2006**, *36*, 1485–1494.
- ³⁶ G. Balasubramanian, L. A. Gharat, A. D. Lakdawala, R. R. Anupindi. "Novel Tricyclic Compounds Useful for the Treatment of Inflammatory and Allergic Disorders: Process for Their Preparation and Pharmaceutical Compositions Containing Them." WO/2004/037805 A1, May 6, **2004**.
- ³⁷ Martin, T.; Moody, C. J. "A new route to 1-oxygenated carbazoles. Synthesis of the Carbazole Alkaloids Murrayafoline-A and Murrayaquinone-A." *J. Chem. Soc. Perkin Trans. 1* **1988**, 235–240.
- ³⁸ Ackermann, L.; Althammer, A.; Mayer, P. "Palladium-Catalyzed Direct Arylation-Based Domino Synthesis of Annulated *N*-Heterocycles Using Alkenyl or (Hetero)Aryl 1,2-Dihalides." *Synthesis*, **2009**, *20*, 3493–3503; b) Ackermann, L.; Althammer, A.; Domino N–H/C–H Bond Activation: Palladium-Catalyzed Synthesis of Annulated Heterocycles Using Dichloro(hetero)arenes." *Angew. Chem. Int. Ed.* **2007**, *46*, 1627–1629.
- ³⁹ Eastabrook, A.; Wang, C.; Davison, E.; Sperry, J. "A Procedure for Transforming Indoles into Indolequinones." *J. Org. Chem.* **2015**, *80*, 1006–1017.

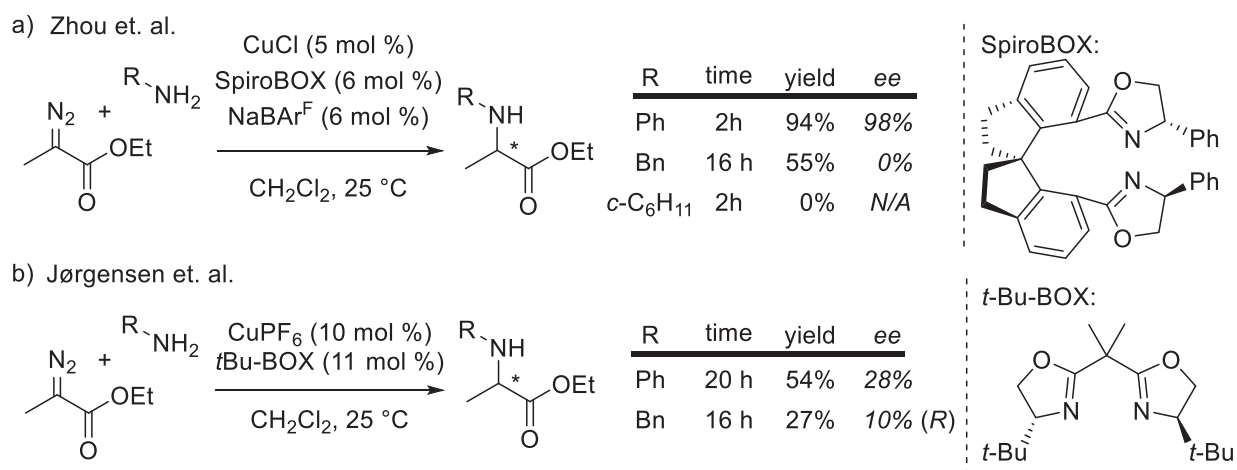
-
- ⁴⁰ Robbins, D.W.; Boebel, T.A.; Hartwig, J.F. "Iridium-Catalyzed, Silyl-Directed Borylation of Nitrogen-Containing Heterocycle." *J. Am. Chem. Soc.* **2010**, *132*, 4068–4069.
- ⁴¹ A. J. Rebecca, A. A Kudzovi, G. K Matthew, G. G. Stuart, H. S. Andrew, P. J. Hoogestraat, J. W. Dennis, Jr., S. D. Lynn. CB1 Modulator Compounds. WO/2005/066126 (A1), **2005**.
- ⁴² H. M. Davies, S. Chennamadhavuni, T. J. Martin, S. R. Childers. "Cyclopropyl Derivatives and Methods of Use." WO/2012/145234, **2012**.
- ⁴³ Yayama, E.; Saito, S. "Copper-Catalyzed Regiospecific and 1,2-Regioselective Cyclopropanation of (1Z)-1-Amino- and (1Z)-1-Oxy-1,3-butadienyl Derivatives." *Synlett* **2015**, *26*, 1880–1884.
- ⁴⁴ Chan, W.-W.; Yeung, S.-H.; Zhou, Z.; Chan, A.; Yu, W.-Y. "Ruthenium Catalyzed Directing Group-Free C2-Selective Carbenoid Functionalization of Indoles by α -Aryldiazoesters." *Org. Lett.* **2010**, *12*, 604-607.
- ⁴⁵ Gao, L.; Kang, B.; Ryu, D. "Catalytic Asymmetric Insertion of Diazoesters into Aryl-CHO Bonds: Highly Enantioselective Construction of Chiral All-Carbon Quaternary Centers". *J. Am. Chem. Soc.* **2013**, *135*, 14556–14559.
- ⁴⁶ Lee, M.; Kim, D.H.; "Syntheses and Kinetic Evaluation of Racemic and Optically Active 2-Benzyl-2-methyl-3,4-epoxybutanoic Acids as Irreversible Inactivators for Carboxypeptidase A". *Bioorg. Med. Chem.* **2002**, *10*, 913-922.
- ⁴⁷ H. E. Bartrum, D. C. Blakemore, C. J. Moody, C. J. Hayes, C.J. "Rapid Access to α -Alkoxy and α -Amino Acid Derivatives through Safe Continuous-Flow Generation of Diazoesters." *Chem. Eur. J.*, **2011**, *17*, 9586–9589.
- ⁴⁸ L. Li, C. Beaulieu, D. Guay, C. Sturino, Z. Wang. "Fluoro-Methanesulfonyl-Substituted Cycloalkanoindoles and their use as Prostaglandin d2 Antagonists." WO/2004/103970 (A1), May 18, **2004**.
- ⁴⁹ Lee, C.-L.; Loh, T.-P. "Gram-Scale Synthesis of (-)-Epibatidine." *Org. Lett.* **2005**, *7*, 2965-2967.

Chapter 3: Palladium-Catalyzed Enantioselective Carbene Insertion into the N–H bonds of Cyclic Aliphatic and Non-Conjugated Amines

Introduction

While examples of high-yielding asymmetric transition metal-catalyzed carbene insertion into carbamate and aniline N–H bonds are by now well-documented, aliphatic and non-conjugated (benzylic) amines have proven much more challenging substrates. Recall that Zhou and co-workers developed conditions for a highly enantioselective Cu(I)-catalyzed insertion between anilines and alkyldiazoacetates.¹ However, when benzylamine was used instead of aniline, the insertion required a longer reaction time and formed racemic product in diminished yield (Figure 3-1a). Moreover, no reaction was observed with cyclohexylamine. To our knowledge, the best *ee* obtained with any type of non-conjugated amine was an earlier report by Jørgensen and co-workers, who achieved 27% yield and 10% *ee* using benzylamine, CuPF₆, and a chiral bisoxazoline ligand (Figure 3-1b).²

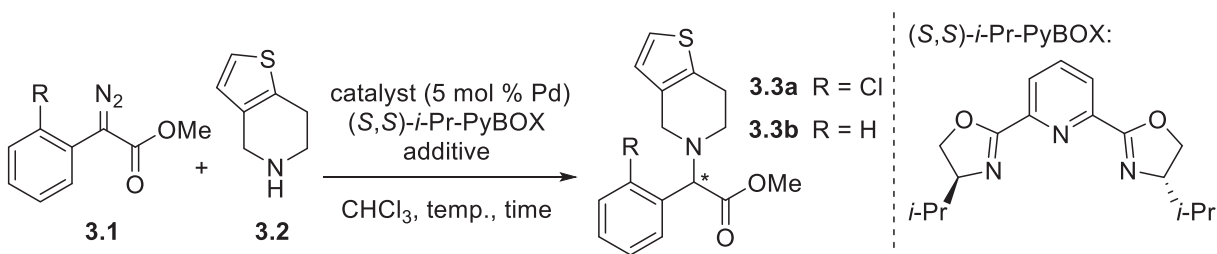
Figure 3-1: Optimized conditions for enantioselective insertion into aniline perform poorly with benzylamine and cyclohexylamine



Optimization of Reaction Conditions for Aliphatic and Non-Conjugated Amines

We sought to extend our previous success with palladium(II)-catalyzed insertion conditions—previously developed for indoles and carbazoles—to aliphatic and non-conjugated amine substrates. Our interest in these substrates arose from attempts to react chloro-substituted aryl diazoacetate **3.1** and 4,5,6,7-tetrahydrothieno[3,2-*c*]pyridine **3.2** to obtain clopidogrel **3.3a** (Table 3-1). Clopidogrel is a potent P2Y₁₂ antagonist prescribed clinically as an antithrombotic and marketed as the *S* enantiomer. However, only racemic clopidogrel **3.3a** was obtained when we applied conditions developed for enantioselective carbene insertion into carbazoles and indoles (entry 1).³ The inclusion of NaBAR^F provides a halophilic sodium cation that facilitates exchange of palladium-bound chloride anion for a non-coordinating borate anion.⁴ Unsubstituted aryl diazoacetate **3.2** also failed to provide any asymmetric induction (entry 2).

Table 3-1: Conditions optimized for aromatic heterocycles applied to a thienopiperidine substrate.

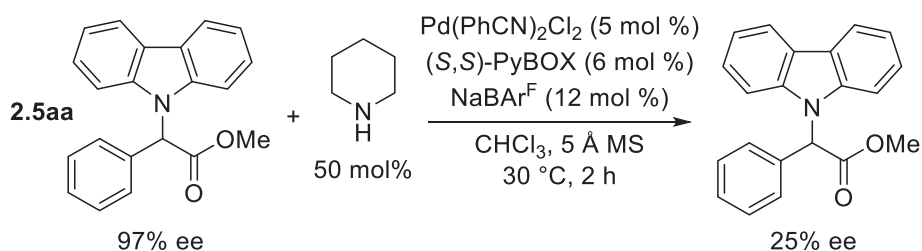


entry	catalyst	R	ligand (mol%)	additive	temp.	time	yield	ee
1	Pd(PhCN) ₂ Cl ₂	Cl	6	NaBAR ^F (12 mol%)	40 °C	15 h	79%	0%
2	Pd(PhCN) ₂ Cl ₂	H	6	NaBAR ^F (12 mol%)	35 °C	18 h	59%	0%
3	Pd(PhCN) ₂ Cl ₂	H	6	<i>p</i> -TsOH (50 mol%)	50 °C	7 h	54%	0%
4	Pd(PhCN) ₂ Cl ₂	H	20	<i>p</i> -TsOH (110 mol%)	61 °C	15 h	12%	0%

In our previous experiments with aromatic amine heterocycles, my colleague Eugene Gutman observed that carbazole derivative **2.5aa** (from previous chapter) was racemized by

piperidine under optimized reaction conditions. The ee of the carbazole product declined to 25% after 2 h when 50 mol % piperidine was added (Figure 3-2).

Figure 3-2: Racemization of carbazole derivative by piperidine.

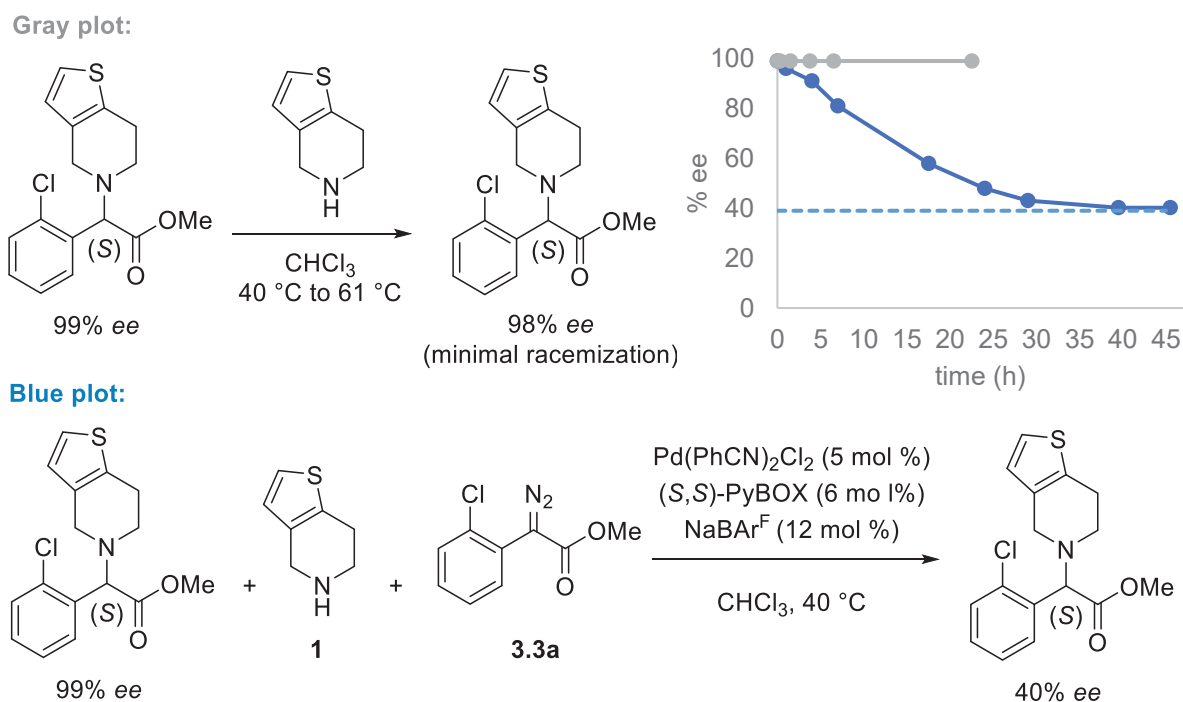


Based on the racemization experiment from above, we hypothesized that the thienopiperidine substrate might also be racemizing aminoesters **3.3a** and **3.3b** product under the present reaction conditions. A portion of *p*-toluenesulfonic acid (*p*-TsOH) was added to buffer the reaction mixture to mitigate racemization (Table 3-1, entry 3). Doing so slowed the reaction, leading to a diminished yield even with a higher reaction temperature. The addition of *p*-TsOH presumably generates an equilibrium mixture of piperidine and piperidinium species, the latter an ineffective nucleophile for addition to electrophilic carbene species. Next, we hypothesized that a protonated chiral species generated from (S,S)-*i*-Pr-PyBOX might have been responsible for the asymmetric induction observed during carbene insertion into amine heterocycles. We intentionally tried to generate such species by adding a larger quantity of ligand and *p*-TsOH (entry 4). The ensuing reaction was even more sluggish and low-yielding. Based on these initial results and existing literature precedent, it was unclear whether asymmetric induction and good yield could be achieved simultaneously for aliphatic and benzylic amine substrates.

To more directly test whether ee was eroding under the reaction conditions, optically pure (S)-clopidogrel (99% ee, obtained by basification of the commercially available bisulfate salt) was stirred with thienopiperidine **3.2** in chloroform. Aliquots of the reaction mixture were sampled periodically and the ee determined by chiral HPLC. No change in ee was observed after several

hours stirring at 40 °C, followed by heating for 16 h at reflux (Figure 3-3, gray plot). A second experiment was then devised to check for racemization under the actual reaction conditions. Chloro-substituted diazoacetate **3.1a** was reacted with thienopiperidine **3.2** in the presence of an initial amount of (*S*)-clopidogrel (99% ee, 62 mol %). Initially, the enantiomeric excess declined before asymptotically approaching 39% ee (blue plot). The result is consistent with the formation of racemic aminoester, which dilutes the ee of initially optically pure (*S*)-clopidogrel. No further erosion in ee was observed after the reaction reached full conversion. The result suggested racemization is not a key impediment to maintaining ee; instead, the reaction conditions appear to not induce any asymmetry.

Figure 3-3: Testing the racemization of (*S*)-clopidogrel by the amine substrate



We next hypothesized that the amine substrate might be causing two distinct problems: first, achiral proton transfer by the amine substrate could outcompete asymmetric induction by a chiral ligand or additive; second, over-ligation of the catalyst by the amine could reduce catalyst

turnover. We envisioned that both issues might be addressed by adding the amine slowly. Low concentrations would be maintained if the amine was consumed at a rate comparable to the rate of addition. It was anticipated that the hindered aminoester product would not over-ligate the transition metal catalyst. Notably, slow addition of the nucleophile is the inverse order typically employed for reactions involving metal carbene intermediates. Typically, a solution of the diazo compound is added slowly to avoid undesired dimerization processes catalyzed by the metal.⁵

We set out to apply slow amine addition using well-established catalysts for N–H insertion reactions. First, we tested CuCl, which Zhou had successfully applied toward catalyzing insertion into aniline N–H bonds.¹ When CuCl was used in combination with the *i*-Pr-PyBOX ligand and NaBAR^F additive, a large amount of unreacted diazo compound was recovered, suggesting catalyst deactivation (Table 3-2, entry 1) and no *ee* was observed. We next increased the temperature and tested the spiro-BOX ligand which Zhou had successfully applied.¹ A notable improvement in yield and a small but encouraging *ee* was observed (entry 2). Two other bisoxazoline ligands were screened. The ind-PyBOX ligand provided a comparable yield, but no *ee* (entry 3). The SaBOX ligand caused dimerization of the diazo substrate primarily to azine side products (entry 4). To slow the rate of dimerization relative to the rate of amine addition, the temperature was lowered, and the rate of amine addition increased (entries 5 and 6). The attempt to match those relative rates yielded little improvement. Further attempts were made to combine ind-PyBOX, which gave the highest yield so far, with a chiral guanidine additive (entry 7). We hoped to maintain the yield while improving asymmetric induction; instead, a drop in yield and no *ee* was observed. Chiral phosphoramidite ligand (*R*)-monophos gave poor results (entry 8).

Having little success with copper as a catalyst, we next screened rhodium. Although rhodium(II) catalysts such as Rh₂(OAc)₄ are common choice for carbene insertion processes, they are known to rapidly dimerize the diazo compounds when present in high concentration. Therefore, we screened two rhodium(I) catalysts, [Rh(CO)₂Cl]₂ (entry 9) and [Rh(cod)Cl]₂ (entry 10), which gave low to moderate yield, and no *ee*.

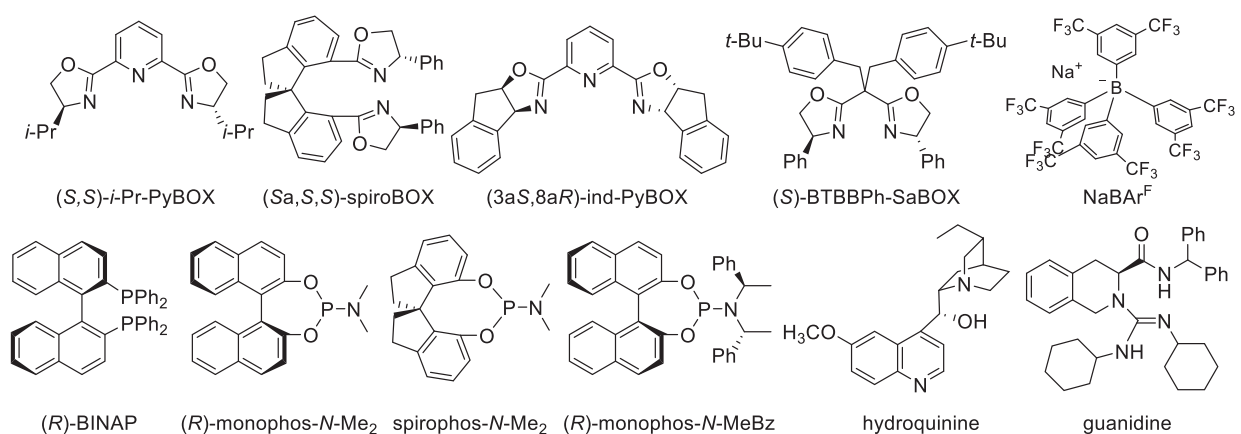
Previously, Feng and co-workers demonstrated that a palladium(0) source like Pd₂dba₃ effectively catalyzes insertion into aniline N–H bonds.⁶ We hypothesized that the effect of amine inhibition on palladium(II) might be reduced by using a palladium(0) source instead. We therefore screened Pd₂dba₃ with various ligands, including *i*-Pr-PyBOX and various chiral phosphorus-based ligands (entries 11-16). Bidentate (*R*)-BINAP seemed to slow the reaction substantially and led mostly recovered diazo compound (entry 12). Using one equivalent per palladium atom of (*R*)-monophos gave the highest *ees* so far observed (entries 13 and 14), although other phosphoramidite ligands with different backbones led to diminished yield and *ee* (entries 15 and 16). Next, I tested two chiral additives, the cinchona alkaloid derivative dihydroquinine (entry 17)⁷ and a chiral guanidine (entry 18). The chiral guanidine additive gave promising results, with *ee* comparable to that obtained with (*R*)-monophos (entry 13). This catalyst and additive combination was previously shown by Feng and coworkers to achieve highly enantioselective insertion into anilines using alkyl diazoacetates as the carbene precursor.⁵ Attempts to rescue the yield by using a different palladium(0) source with strongly-bound X-Phos or NHC ligands (entries 19-21) inhibited the reaction without improvement in *ee*. From this initial screen employing slow addition, palladium(0) seemed the most promising catalyst for further optimization. The highest *ees* with palladium(0) were obtained with (*R*)-monophos and the chiral guanidine additive. Moving forward, increasing the loading of chiral guanidine seemed a better strategy than adding more of the phosphoramidite ligand.

Table 3-2: Initial catalyst and ligand/additive combinations screened using slow amine addition

syringe pump addition (1 mmol/time) + catalyst (5 mol% [M]) ligand/additive
 CHCl_3 , temperature, time

entry	catalyst	ligand	additive	temperature	time ^[b] (diazot recovered)	yield	ee
1	CuCl	(<i>S,S</i>)- <i>i</i> -Pr-PyBOX	NaBAR ^F (6 mol%)	30 °C	4 h (85%)	14%	0%
2	CuCl	(<i>Sa,S,S</i>)-SpiroBOX	NaBAR ^F (6 mol%)	40 °C	4 h (10%)	58%	7%
3	CuCl	(<i>3aS,8aR</i>)-ind-PyBOX	NaBAR ^F (6 mol%)	40 °C	4 h (14%)	60%	0%
4	CuCl	(<i>S</i>)-BTBBPh-SaBOX	NaBAR ^F (6 mol%)	40 °C	2 h (0%) ^[c]	8%	4%
5	CuCl	(<i>S</i>)-BTBBPh-SaBOX	NaBAR ^F (6 mol%)	25 °C	2 h (66%) ^[d]	12%	0%
6	CuCl	(<i>S</i>)-BTBBPh-SaBOX	NaBAR ^F (6 mol%)	25 °C	1 h (84%)	5%	3%
7	CuCl	(<i>3aS,8aR</i>)-ind-PyBOX	NaBAR ^F (6 mol%) + guanidine (6 mol%)	40 °C	4 h (55%)	36%	0%
8	CuCl	(<i>R</i>)-monophos- <i>N</i> -Me ₂ , 1 eq./Cu	NaBAR ^F (6 mol%)	50 °C ^[a]	4 h (89%)	2%	4%
9	[Rh(CO) ₂ Cl] ₂	(<i>R</i>)-monophos- <i>N</i> -Me ₂ , 1 eq./Rh	---	40 °C	4 h (58%)	3%	0%
10	[Rh(cod)Cl] ₂	(<i>R</i>)-monophos- <i>N</i> -Me ₂ , 1 eq./Rh	---	40 °C	4 h (0%)	31%	0%
11	Pd ₂ (dba) ₃	(<i>S,S</i>)- <i>i</i> -Pr-PyBOX	---	30 °C	4 h (39%)	13%	0%
12	Pd ₂ (dba) ₃	(<i>R</i>)-BINAP	---	61 °C ^[a]	4 h (6 h) (77%)	3%	0%
13	Pd ₂ (dba) ₃	(<i>R</i>)-monophos- <i>N</i> -Me ₂ , 1 eq./Pd	---	37 °C	4 h (63%)	15%	19%
14	Pd ₂ (dba) ₃	(<i>R</i>)-monophos- <i>N</i> -Me ₂ , 2 eq./Pd	---	50 °C ^[a]	4 h (7 h) (22%)	30%	16%
15	Pd ₂ (dba) ₃	spiropos- <i>N</i> -Me ₂ , 1 equiv/Pd	---	50 °C ^[a]	4 h (8 h) (79%)	1%	5%
16	Pd ₂ (dba) ₃	(<i>R</i>)-monophos- <i>N</i> -MeBz, 1 eq./Pd	---	30 °C	4 h (74%)	9%	0%
17	Pd ₂ (dba) ₃	---	dihydroquinine	30 °C	4 h (59%)	15%	4%
18	Pd ₂ (dba) ₃	---	guanidine (6 mol%)	30 °C	4 h (64%)	14%	16%
19	XPhos-Pd-G1	---	guanidine (6 mol%)	61 °C ^[a]	4 h (3 h) (68%)	3%	4%
20	Pd-IMes	---	guanidine (6 mol%)	30 °C	4 h (59%)	8%	0%
21	Pd-IMes	(<i>R</i>)-monophos, 1 eq./Pd	---	61 °C ^[a]	4 h (10 h) (68%)	3%	10%

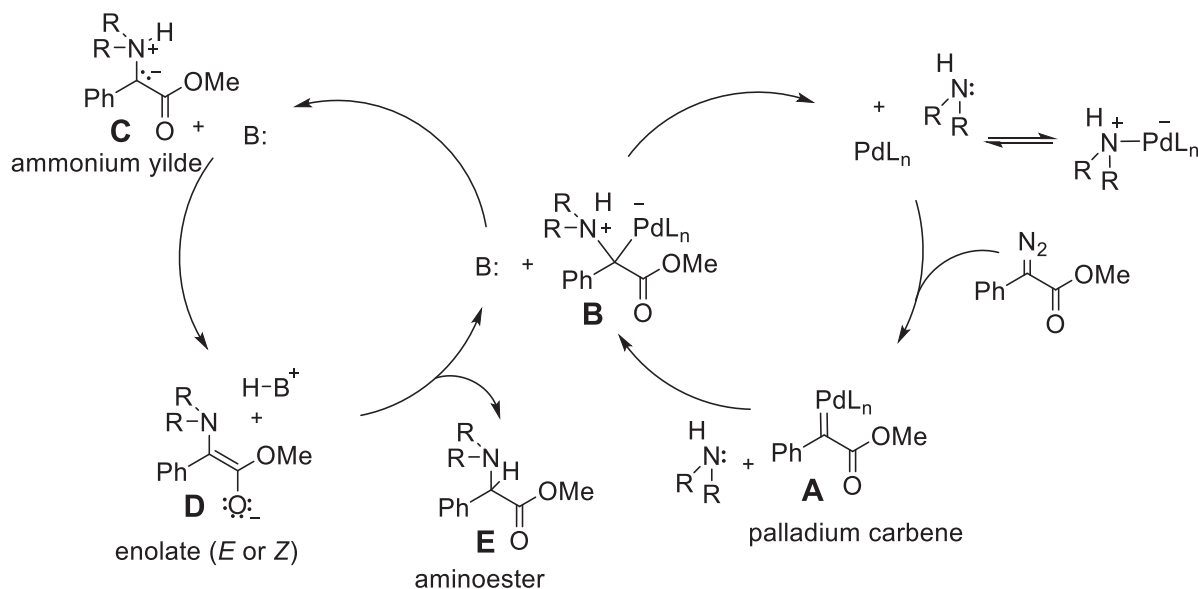
^[a]Reaction mixture heated to indicated temperature after initial syringe pump addition at 40 °C. ^[b]Number in parentheses indicates additional time heating after syringe pump addition completed ^[c]50% recovered as azine dimer ^[d]16% recovered as azine dimer



Mechanistic Model of Palladium-Catalyzed Carbene N–H Insertion

With promising results obtained with palladium(0) and a chiral base additive, we set out to develop a mechanistic model that would account for sequestration of the palladium by the amine substrate, and competition between chiral and achiral protonation pathways that could influence *ee*. The mechanism (Figure 3-4) begins with formation of an electrophilic transition-metal carbene species **A**, followed by attack of the amine nucleophile. The resulting C-bound palladium intermediate **B** could dissociate to regenerate the palladium catalyst and ammonium ylide **C**. Experimental evidence for such ammonium ylide intermediates comes from trapping by 1,2-addition into imines⁸ and aldehydes⁹ or 1,4-addition into unsaturated ketoesters¹⁰ and azodicarboxylates.¹¹ A computational study on related oxonium ylides suggests that dissociation of the metal-bound ylide depends on the particular metal catalyst.¹²

Figure 3-4: Mechanistic model for palladium-catalyzed carbene insertion into an amine N-H bond.



Deprotonation of the ammonium group by an external base would generate enolate intermediate **D**, which, upon protonation at carbon would form aminoester **E**. Asymmetric induction could result from facially selective protonation of the enolate intermediate.

In the mechanistic model, the amine substrate could act as an achiral proton transfer agent for protonation of the enolate intermediate. Due to their greater basicity relative to aniline, benzylic and aliphatic amines would interfere more strongly with enantioselective protonation by a chiral base additive.

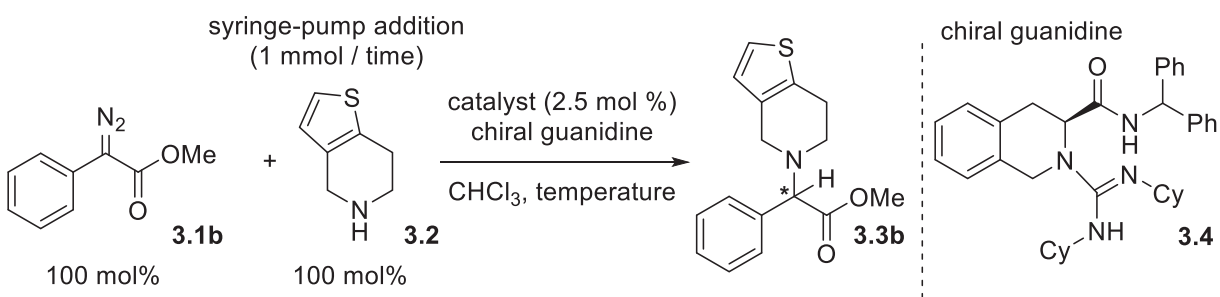
Also in the model, we propose that palladium(0)-enone complexes are easily saturated by coordination to amines. The saturation of palladium(0) olefin complexes by amines is supported by the work of Elsevier and coworkers.¹³ They showed binding of aliphatic dialkylamines to palladium(0)-enone complexes inhibits additional sigma-donors from binding. Addition to palladium by the diazo substrate is required to form a carbene intermediate, so prior amine complexation would prevent palladium from entering the catalytic cycle. Aliphatic amines bind more strongly to transition metals than arylamines. For example, Widenhoefer and Buchwald estimated the binding affinity of *N*-methylbenzylamine to an arylpalladium(II) complex to be $\geq 10^3$ greater than that of *N*-methylaniline.¹⁴ Yet, binding of aliphatic amines to palladium(II) generally does not inhibit catalysis. For example, the palladium-catalyzed Buchwald cross-coupling between amines and aryl halides is not inhibited by stoichiometric quantities of aliphatic amine. Likewise, the PdCl₂-catalyzed polymerization of ethyl diazoacetate uses triethylamine as an initiator, indicating the aliphatic amine does not stop the polymerization process.¹⁵ In our own experiments, using Pd(PhCN)₂Cl₂ as a palladium(II) pre-catalyst provided good yields of insertion into the N-H bond into aliphatic amines in good yield without slow addition (Table 3-1, entry 1).

In short, owing to strong sigma donor ability and basicity, aliphatic and benzylic amines present several obstacles to metal-catalyzed carbene insertion not encountered with carbamates, anilines, or aromatic amine heterocycles.

Further Reaction Optimization and Development of a Parallel Slow-Addition Procedure

The mechanistic model provided a useful framework for further optimization. Successive doubling of the guanidine (“B:” in Figure 3-4) loading led to a monotonic increase in ee up to 24 mol % but increasing loading further to 48 mol % provided only marginal further improvement (Table 3-3, entries 1-4). The trend was consistent with chiral protonation favored by higher concentrations of the guanidine. Even if all proton transfer events involve the chiral guanidine, the ee will be limited by the shape complementary between the guanidinium and the enolate intermediate.

Table 3-3: Further optimization using the slow amine addition and chiral guanidine additive.



entry	catalyst	guanidine (mol %)	temperature	time	(diazo recovered)	yield	ee
1	Pd ₂ dba ₃	6	30 °C	4 h	(64%)	14%	16%
2	Pd ₂ dba ₃	12	30 °C	4 h	(73%)	15%	28%
3	Pd ₂ dba ₃	24	30 °C	4 h	(68%)	24%	37%
4	Pd ₂ dba ₃	48	30 °C	4 h	(53%)	24%	38%
5	Pd ₂ dba ₃	24	40 °C	4 h	(38%)	38%	34%
6	Pd ₂ dba ₃	24	50 °C	4 h	(24%)	32%	24%
7	Pd ₂ dba ₃	24	40 °C	6 h	(38%)	33%	31%
8	Pd ₂ dba ₃	24	40 °C	2 h	(61%)	27%	39%
9 ^b	Pd ₂ dba ₃	24	40 °C	4 h	(79%)	12%	9%
10 ^c	Pd ₂ dba ₃	24	40 °C	4 h	(42%)	30%	30%
11	Pd ₂ dba ₃	0	40 °C	4 h	(50%)	42%	0%
12	Rh ₂ (OAc) ₄	6	20 °C	5 min	(0%)	0%	N/A
13	CuCl ^[a]	6	30 °C	4 h	(74%)	21%	3%

^[a] 5 mol % ^[b] Amine added at outset of reaction. ^[c] Reaction seeded with 40 mol % racemic aminoester previously obtained to test for product inhibition

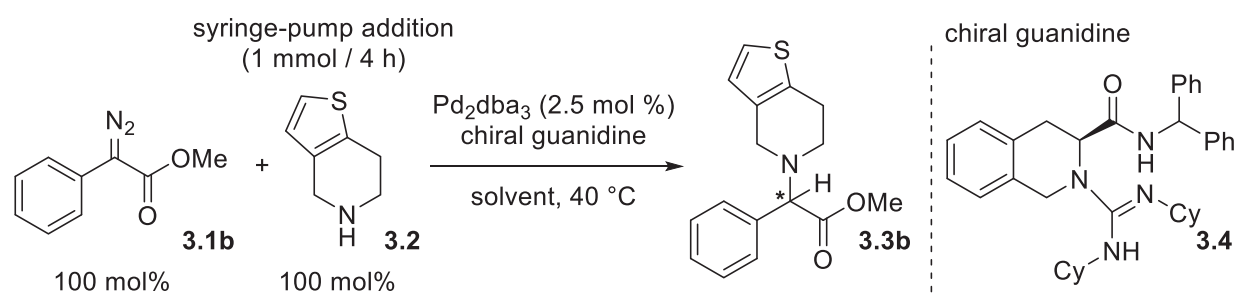
We reasoned that balancing the rate of amine addition with the rate of aminoester formation might be an important factor. Too fast an addition rate would lead to build-up of the amine and sequestration of the catalyst; too slow an addition rate would allow reactive palladium carbene species to undergo side reactions. We therefore increased the temperature and varied the amine addition rate. Increasing the temperature to 40 °C improved the yield, but raising the temperature further was detrimental (entries 5 and 6). No improvement was observed by slowing down or speeding up the amine addition (entries 7 and 8). To verify that the improved yield and ee were due to syringe pump addition, and not an artifact of the higher temperature and guanidine loading, the amine substrate was added at the beginning of the reaction (entry 9). A significant reduction in the yield and ee confirmed the importance of slow amine addition.

At this stage of the optimization, it was unclear what was limiting the yield of the reaction. TLC analysis consistently showed unreacted diazo and amine starting material at the end of the reaction, suggesting catalyst deactivation. To rule out product inhibition of the catalyst, the reaction was seeded at the outset with 40 mol % racemic aminoester product (entry 10). The presence of 70 mol % product at the end of the reaction implied a 30% yield and 30% ee for the newly formed aminoester; the result was similar enough to previous entries to suggest that product inhibition was not the primary cause of the limited yield. Next, omission of the chiral guanidine did not affect the yield materially, so a side reaction involving the guanidine also did not seem a plausible explanation for the low yield (entry 11). A large portion of the mass balance (for example, from entry 11) could be recovered as a complex mixture of slower-eluting side products. The ¹H NMR spectrum of the mixture showed peaks in the aromatic and methyl ester regions without aliphatic signals from the thienopiperidine group. Since the palladium catalyst is being continuously stirred with the diazo substrate, it is plausible that the palladium carbene (Figure 3-4, intermediate **A**) is engaging in competitive oligomerization processes.

Now with the amine addition rate optimized and higher guanidine loadings, I returned to rhodium and copper catalysts. $\text{Rh}_2(\text{OAc})_4$ catalyzed rapid dimerization the diazo substrate to a mixture of azine and fumarate side products, making slow addition of the amine impractical (entry 12). CuCl provided a low yield of the aminoester and negligible ee (entry 13).

Next, a solvent screen was performed (Table 3-4) using conditions identified from Table 3-3, entry 5. Toluene provided a slightly higher yield, but inferior to chlorinated solvents in terms of enantioselection, possibly due to disruption of π -stacking interactions.

Table 3-4: Solvent screen in N–H insertion

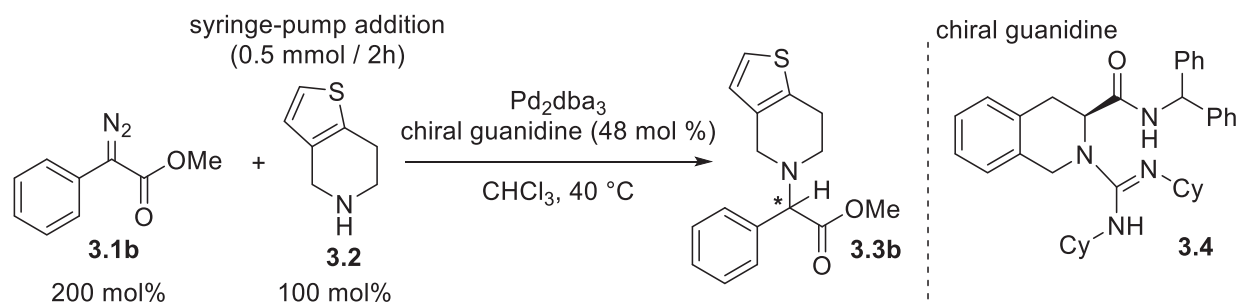


entry	solvent	(diazo recovered)	yield	ee
1	CHCl_3	(38%)	38%	34%
2	1,2-dichloroethane	(18%)	39%	33%
3	toluene	(17%)	58%	22%
4	acetonitrile	(45%)	11%	5%
5	MTBE	(39%)	16%	5%

Progress in improving yield was finally made by replicating a previous experiment (Table 3-3, entry 5) except using the amine as the limiting reagent (Table 3-5). Adding half as much thienopiperidine **3.2** effectively doubled the loading of the other components of the reaction and improved the yield of aminoester (Table 3-5, entry 1). Adding additional catalyst to the flask at the beginning of the reaction did not improve the yield significantly (entry 2); from TLC analysis, we ascribe this to early depletion of the diazo substrate. The yield did, however, improve significantly when aliquots of supplemental palladium catalyst were added at regular intervals alongside the

amine substrate (entry 3). A more reproducible version of this procedure was established by adding both the amine and supplemental palladium catalyst independently via syringe pumps (entries 4 and 5).

Table 3-5: Further optimization using the amine as the limiting reagent.



entry	initial Pd_2dba_3 in flask (mol %)	suppl. Pd_2dba_3 added (mol %)	(diazot recovered)	yield ^[a]	ee
1	5	0	(104%)	55%	40%
2	10	0	(14%)	60%	28%
3	5	5 (manual) ^[b]	(78%)	96%	33%
4	5	5 (syringe pump)	(42%)	97%	35%
5	2	5 (syringe pump)	(122%)	49%	29%

^[a] Calculated based on thienopiperidine **3.2** as the limiting reagent.

^[b] Added manually in 1 mol % increments every twenty minutes.

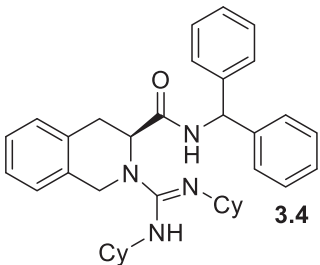
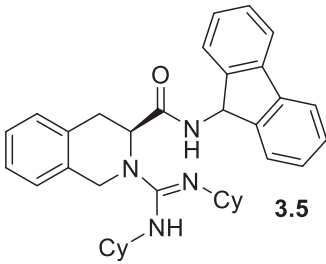
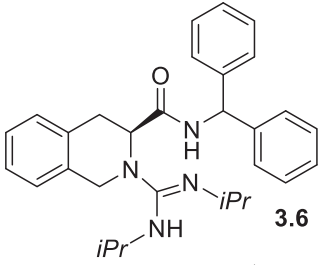
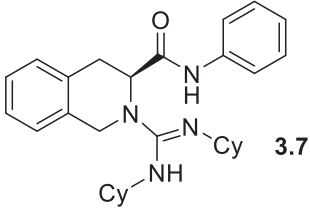
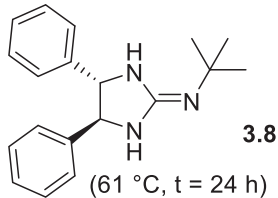
^[c] Added by syringe pump addition over 2 h.

Figure 3-5: Photograph of experimental setup employing parallel slow addition.



In parallel to this last stage of yield of optimization, we attempted to further improve ee by designing, synthesizing and testing a panel of novel chiral guanidine derivatives **3.5-3.7**, using a previously established four-step route.¹⁶

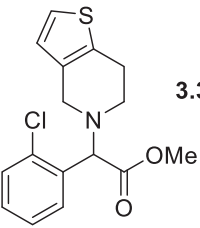
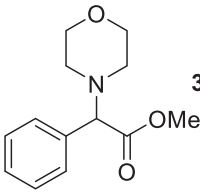
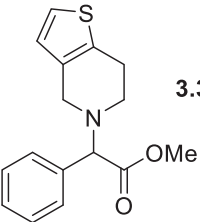
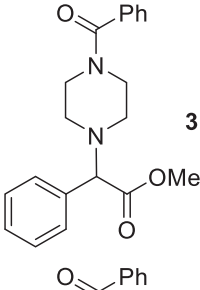
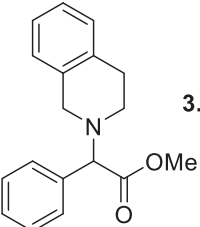
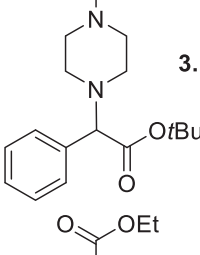
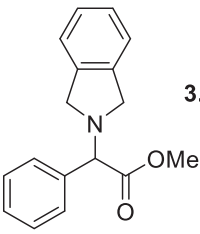
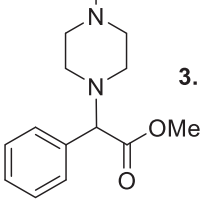
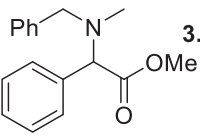
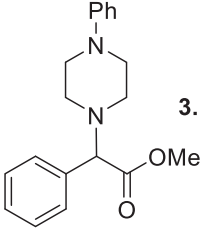
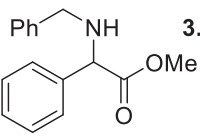
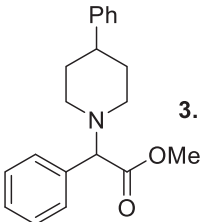
Table 3-6: Screen against panel of chiral guanidine derivatives.

entry	guanidine additive	yield	ee
1	 3.4	55%	40%
2	 3.5	42%	13%
3	 3.6	37%	29%
4	 3.7	50%	16%
5	 3.8 (61 °C, t = 24 h)	24%	10%

Modifications were made to either the benzhydryl amide or dicyclohexyl portions of the molecule (Table 3-6). Conditions from Table 3-5, entry 1 were used as a starting point. None of the new derivatives gave superior ee to the originally tested guanidine **3.4**. Guanidine **3.8**, possessing a pseudo C2-symmetric diphenyl backbone, was synthesized through a different four-step route¹⁷ and tested. This guanidine derivative, lacking a hydrogen-bonded amide group, seemed to inhibit the reaction; prolonged heating was required to obtain even a modest yield.

We therefore settled on using the original guanidine **3.4** and the newly developed “dual syringe-pump addition” procedure to examine substrate scope. The optimized conditions were applied to several piperidine, morpholine, piperazine, and piperidine substrates (Table 3-7). Disappointingly, only a moderate yield and low ee were obtained in the synthesis of clopidogrel (entry 1). The absolute stereochemistry was assigned by comparison of the HPLC trace to that of commercially available (*S*)-clopidogrel. Most secondary cyclic amines gave yields between 81-98% yield, and 31-53% ee. Not surprisingly, isoindoline-derived aminoester **3.10** (entry 4) decomposed by autoxidation at room temperature.¹⁸ Interestingly, *N*-methylbenzylamine (entry 5) and benzylamine (entry 6) provided lower yields and ees, which may explain why previous attempts to optimize for asymmetric induction using aliphatic and benzylic amines has been discouraged. *N*-Benzoylpiperazine provided the highest enantioselectivity (53% ee, entry 8). Related *N*-benzoylpiperazines (see Figure 2–6) have been shown to exhibit activity against histone deacetylase,¹⁹ Na_v1.7 channels,²⁰ and influenza hemagglutinin.²¹ Attempts to further enhance steric differentiation with a large *t*-butyl ester group did not improve the yield or ee (entry 10).

Table 3-7: Substrate scope employing dual syringe pump addition^[a]

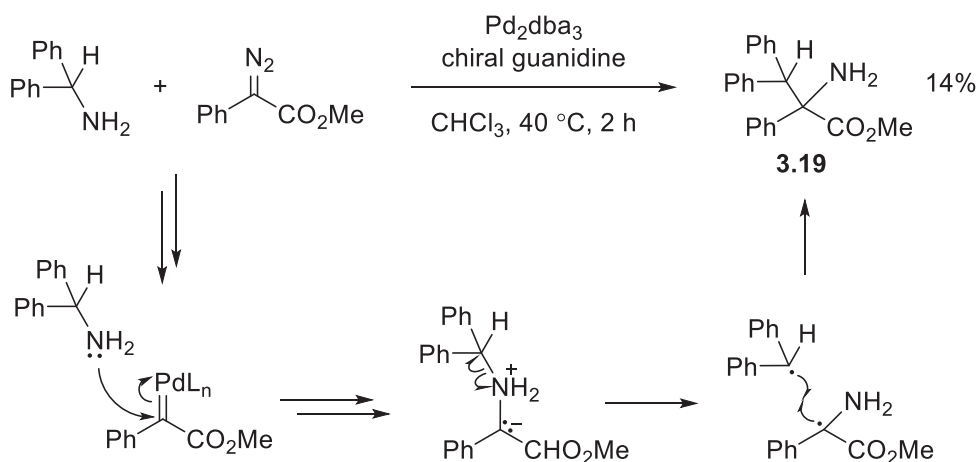
entry	aminoester	yield	ee	entry	aminoester	yield	ee
1	 3.3a	47%	12% (S)	7	 3.13	98%	40%
2	 3.3b	97%	35%	8	 3.14	86%	53%
3	 3.9	92%	33%	9	 3.15	61%	28%
4	 3.10^[b]	21%	28%	10	 3.16	89%	43%
5	 3.11	72%	6%	11	 3.17	96%	31%
6	 3.12	41%	6%	12	 3.18	81%	N/A ^[d]

^[a] Using conditions from Table 3-5, entry 4. ^[b] Decomposes gradually at room temperature over the course of several hours. ^[c] Only 2 mol % Pd₂dba₃ added initial to the reaction flask.

^[d] Unable to resolve enantiomers by HPLC

When benzhydrylamine was tested as an amine substrate, the expected aminoester was not recovered, but a rearrangement product was isolated (Figure 3-6). The product could be explained by a 1,2-Stevens shift,²² in which the ammonium ylide intermediate undergoes homolytic dissociation to a benzhydryl radical and a captodatively-stabilized methyl phenylacetate radical. Radical recombination to form a new C-C bond would generate the observed primary amine product. Davies and co-workers reported a similar rearrangement resulting from trapping of a thermally generated carbene.²³

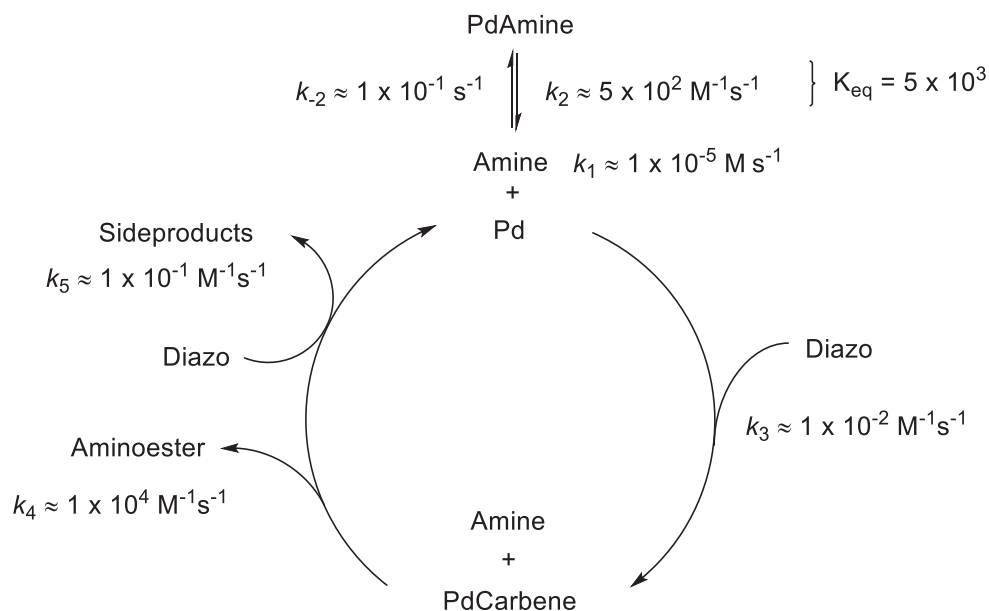
Figure 3-6: 1,2-Stevens shift observed during reaction with benzhydrylamine.



Kinetic Model of Palladium-Catalyzed N-H Insertion Reaction

Finally, a kinetic model is presented (Figure 3-7) that is consistent with the amine addition rate, supplemental catalyst addition rate, and the observed time course of diazo consumption and product formation. The model was constructed using COPASI.²⁴ The model matches the rate at which the amine was added experimentally under optimized conditions ($k_1=1.38 \times 10^{-5} \text{ M s}^{-1}$), corresponding to 100 mol % over 2 h. Under a steady-state assumption, the rate of aminoester formation is first-order in [Pd] and first-order in [Diazo]. The amine can react to form aminoester or bind reversibly to Pd ($K_{\text{eq}} = 5 \times 10^3$), sequestering it as the inactive Pd·amine complex.²⁵

Figure 3-7: Kinetic model for palladium-catalyzed carbene insertion into amine N-H bond.



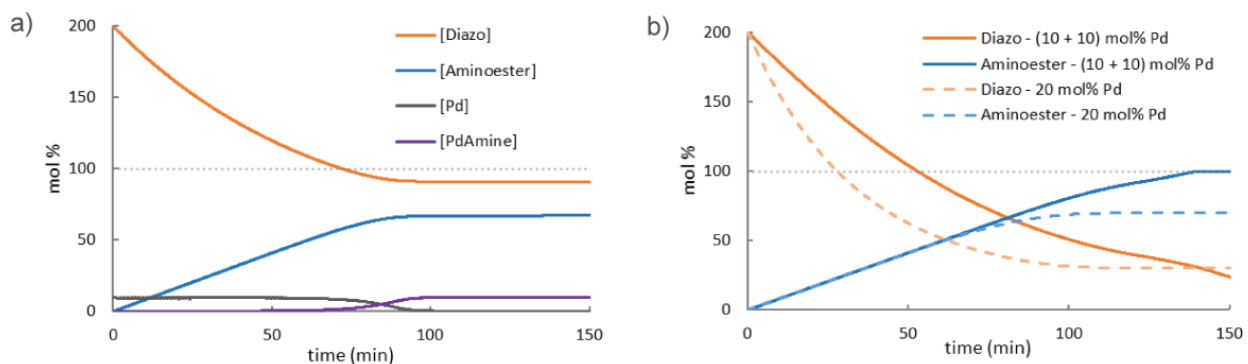
In a model run where $[\text{Pd}]_i = 0.01 \text{ M}$ (10 mol %) and no supplemental Pd is added (Figure 3-8a), formation of the aminoester occurs steadily at first ($t_{1/2} \approx 45$ minutes) but stalls around 1.5 h. This stalling occurs as the amine addition rate begins to outpace the rate at which the amine is consumed. The excess amine sequesters the Pd catalyst, which slows the rate of aminoester formation and further accelerates the buildup of amine. This feedback loop causes a precipitous decline in the concentration of active Pd catalyst at approximately 1.5 h, limiting the final yield of aminoester. Deactivation of the Pd catalyst also causes consumption of the diazo compound to stall. These features of the model run were consistent with experimental TLC observations, which showed buildup of the amine toward the middle or later stages of syringe pump addition. Moreover, diazo compound was often recovered despite the presence of unreacted amine, which is consistent with catalyst deactivation.

The model also rationalizes why the addition of supplemental Pd catalyst boosts the observed yield (Figure 3-8b). Based on the model, the overall reaction rate is first order in $[\text{Diazo}]$ and consumption of the diazo compound should lead over time to a decrease in the rate of

aminoester formation. Therefore, addition of supplemental Pd catalyst is expected to compensate for this decrease, since the reaction is also first order in [Pd] (see below). In the model run, gradual addition of Pd delays sequestration as the Pd·amine complex and allows a higher yield of the aminoester to be achieved. Such improvement is only observed when the supplemental catalyst is added over time; adding it at the beginning of the model run results in early depletion of diazo due to side product formation.

Other variations of the kinetic model (Figure 3-7), including alterations of rate constants and species were not consistent with experimental observations.

Figure 3-8: a) Model run with $Pd_i = 10$ mol %, no supplemental Pd added. b) Comparison of model run with $Pd_i = 10$ mol % + 10 mol % supplemental Pd added versus $Pd_i = 20$ mol %.



Derivation of Rate Expressions from the Kinetic Model

The above kinetic model (Figure 3-7) was used to derive rate expressions for the rate of aminoester formation and rate of amine buildup. We begin by deriving an expression relating the concentration of active palladium catalyst to the amine concentration.

$$\begin{aligned}
 [PdAmine] &= K_{eq}[Pd][Amine] \\
 [Pd] &= [Pd]_i - ([PdAmine] + [PdCarbene])
 \end{aligned}
 \tag{eq. 3.1}$$

Assuming $[PdAmine] \gg [PdCarbene]$:

$$[Pd] = [Pd]_i - [PdAmine] \quad \text{eq. 3.2}$$

Substituting eq. 3.1 into eq. 3.2, we obtain an expression for $[Pd]$ in terms of the initial catalyst concentration $[Pd]_i$, and $[Amine]$ (eq. 3):

$$[Pd] = [Pd]_i - K_{eq}[Pd][Amine] \quad \text{eq. 3.3}$$

$$[Pd] = \frac{[Pd]_i}{1 + K_{eq}[Amine]}$$

Next, we apply a steady state assumption that $[PdCarbene]$ is consumed as quickly as it is generated:

$$k_3[Pd][Diazo] = k_4[PdCarbene][Amine] + k_5[PdCarbene][Diazo]$$

$$k_3[Pd][Diazo] = \frac{d[Aminoester]}{dt} + k_5[PdCarbene][Diazo]$$

$$\frac{d[Aminoester]}{dt} = k_3[Pd][Diazo] - k_5[PdCarbene][Diazo]$$

If $k_3[Pd][Diazo] \gg k_5[PdCarbene][Diazo]$,

$$\frac{d[Aminoester]}{dt} = k_3[Pd][Diazo]$$

Substituting eq. 3.3 for $[Pd]_i$:

$$\frac{d[Aminoester]}{dt} = k_3 \frac{[Pd]_i}{1 + K_{eq}[Amine]} [Diazo] \quad \text{eq. 3.4}$$

According to equation 3.4, the rate of amino ester formation is first order in $[Pd]$, and first order in $[Diazo]$. The rate of amine buildup can be expressed as the rate at which amine is added

to the solution minus how quickly it is converted to aminoester and the rate at which the amine binds to and dissociates from palladium.

$$\frac{d[Amine]}{dt} = k_1 - \frac{d[Aminoester]}{dt} + k_2[Pd][Amine] - k_{-2}[PdAmine]$$

If the amine-palladium complexation is at equilibrium, the last two terms cancel, and the expression becomes:

$$\frac{d[Amine]}{dt} = k_1 - \frac{d[Aminoester]}{dt} \quad \text{eq. 3.5}$$

Eq. 3.4 and eq. 3.5 create a feedback loop that leads to a nonlinear decrease in the amount of active Pd, and buildup of inactive PdAmine, once the rate of amine addition begins to outpace the rate at which it is converted to Aminoester.

Conclusion

In summary, when cyclic aliphatic and benzylic amines and additional palladium catalyst are added slowly to a solution of an α -aryldiazoester, good yields and moderate ees can be obtained for carbene insertion into the N-H bond. A kinetic model was presented that examines the relationship between various parameters such as amine addition rate and supplemental catalyst addition; the output of the model was qualitatively consistent with our experimental results. At present, the current method uses a relatively high loading of palladium catalyst and guanidine additive, but the results suggest that it may be possible to formulate flow-based procedures for highly efficient asymmetric insertion into aliphatic amine N-H bonds.

Experimental Section

General Methods

All reactions were evacuated, backfilled with nitrogen, and carried out under an atmosphere of nitrogen. All reactions were monitored by thin-layer chromatography (TLC). Analytical TLC was performed using EMD Reagents 0.25 mm silica gel 60-F plates. KMnO_4 and p-anisaldehyde stains were used for TLC visualization. Silica gel chromatography was performed using Agela Scientific Flash Silica sorbent (40-63 μM) silica gel of 230-400 mesh (CS605025-P).

^1H and ^{13}C NMR spectra were recorded at room temperature using a Bruker 500 MHz spectrometer equipped with a cryoprobe. The NMR data are reported as follows: chemical shift in ppm, multiplicity (br = broad, app = apparent, s = singlet, d = doublet, t = triplet, q = quartet, m = multiplet), coupling constants (Hz), and integration. All spectra were calibrated to tetramethyl silane (0.00 ppm). NMR data were processed using Mestrelab Research MestReNova 12.0.2 software, using automatic phasing and baseline correction.

Infrared spectra were acquired using a Nicolet iS5 FT-IR spectrometer equipped with a Nicolet iD5 attenuated total reflectance (ATR) accessory.

Enantiomeric excess was determined by HPLC using a CHIRALPAK OD-H (0.46 cm x 25 cm) column on a Shimadzu Prominence Modular HPLC instrument. The instrument comprises two solvent delivery units (LC-20AD), a UV-VIS detector (SPD-20AV), and an on-line degassing unit (DGU-20A-5R). In cases where enantiomers could be fully separated, peak analysis was performed using LabSolutions software version 5.52 copyright of Shimadzu Corporation. In cases where peaks exhibited partial overlap, the data was imported into Wolfram Mathematica 9.0 and the ee determined by curve-fitting. Peaks were fit using a log-normal probability density function (PDF) of the form:

$$PDF = \frac{A}{\sqrt{2\pi}(x-t)\sigma} e^{-\frac{[-\mu + \ln(x-t)]^2}{2\sigma^2}}$$

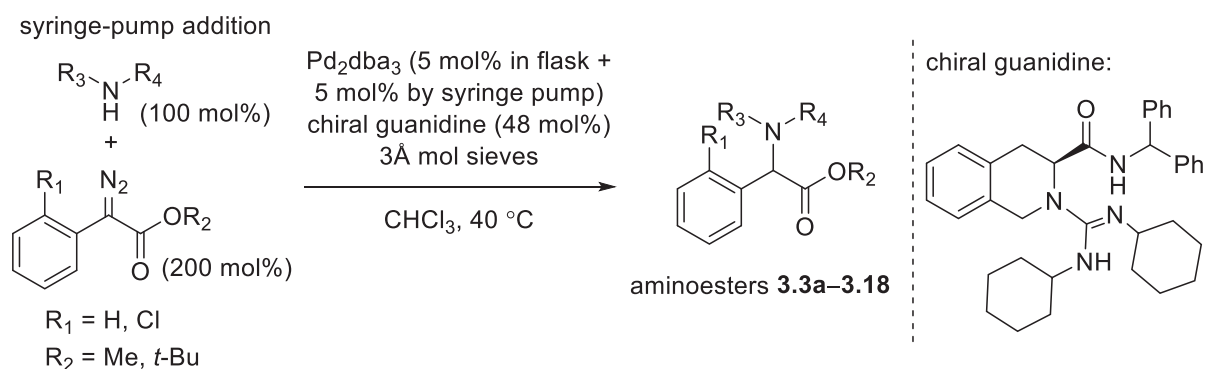
Fitted parameters (t , A , μ , and σ) are provided in this experimental section where appropriate. (Note that the parameter t does not equal the retention time R_T). The % peak areas and ee were calculated from the fitted parameter A using the following equations:

$$\% \text{ Peak Area } 1 = \frac{A_1}{A_1 + A_2}$$

$$\% \text{ Peak Area } 2 = \frac{A_2}{A_1 + A_2}$$

$$\% ee = |\% \text{ Peak Area } 1 - \% \text{ Peak Area } 2|$$

Parallel slow-addition procedure for synthesis of aminoesters 3.3a-3.18



In a 5 mL pear-shaped flask was prepared a 1 mL solution of tris(dibenzylideneacetone)-dipalladium(0) (22.9 mg, 2.5 mmol, 5 mol %) in chloroform.* The solution was withdrawn by syringe and fit into a syringe pump apparatus.

In another 5 mL pear-shaped flask was prepared a 1 mL solution of the amine (0.5 mmol, 100 mol %) in chloroform. The solution was withdrawn by syringe and fit into a second syringe pump apparatus.

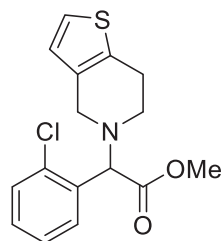
In still another 5 mL pear-shaped flask was prepared a 1 mL solution of the diazo compound (1.0 mmol, 200 mol %) in chloroform.

Finally, A 10 mL round bottom flask was charged with tris(dibenzylideneacetone) dipalladium(0) (22.9 mg, 2.5 mmol, 5 mol %), chiral guanidine (132 mg, 0.24 mmol, 48 mol %),

and 3 Å molecular sieves (approx. 250 mg). To the mixture was added 3 mL chloroform to obtain a deep purple solution. The flask was lowered into a 40 °C oil bath. After stirring for 10 minutes, the solution of methyl phenyldiazoacetate was added. An additional 0.5 mL chloroform was used to ensure complete transfer of the diazo compound.

Within one minute of finishing addition of the diazo compound, syringe pump addition of the palladium catalyst solution and amine solution were begun. Both the catalyst and amine solutions were added at a rate of 0.008 mL/min over 2 h. After addition was completed, the reaction was stirred at 40 °C for an additional 20 min. The flask was then removed from the oil bath and the crude reaction mixture filtered through a 1-inch pad of celite using dichloromethane. The filtrate was concentrated by rotary evaporation. The residue was purified by column chromatography to isolate the aminoester product.

*Chloroform was purified prior to use: chloroform (200 mL) was washed with saturated aqueous sodium bicarbonate (2 x 100 mL) and dried over sodium sulfate. The solvent was decanted and purified by distillation under nitrogen gas onto activated 3 Å molecular sieves. The chloroform was stored in sealed flask under nitrogen gas and kept in the dark when not in use.

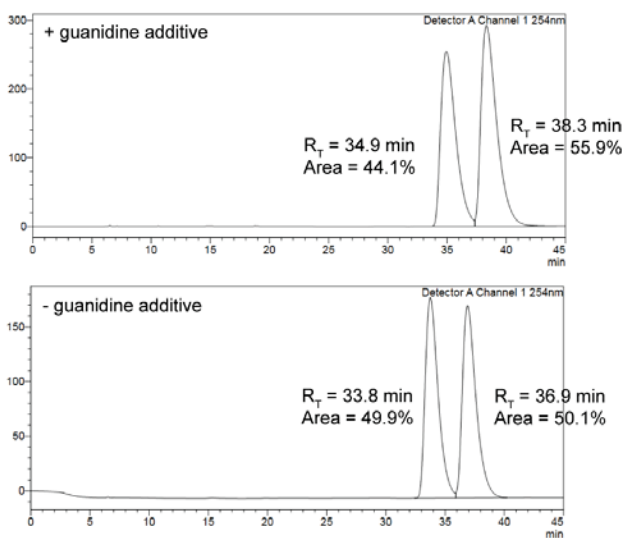


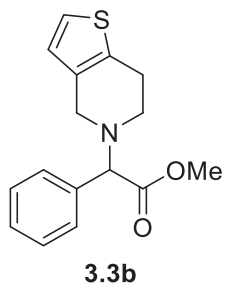
3.3a

methyl 2-(2-chlorophenyl)-2-(6,7-dihydrothieno[3,2-c]pyridin-5(4H)-yl)acetate (3.3a, clopidogrel) was synthesized according to the general procedure using methyl 2-(2-chlorophenyl)-2-diazoacetate **3.1a** (211 mg, 1.0 mmol, 200 mol %) and 4,5,6,7-tetrahydrothieno[3,2-c]pyridine (70 mg, 0.5 mmol, 100 mol %). The crude residue was purified by two rounds of silica gel

column chromatography: first column using 4:1 hexanes/Et₂O ($R_f = 0.24$), second column using 9:1 hexanes/acetone ($R_f = 0.28$) to obtain a colorless oil (76 mg, 47% yield, 12% ee).

¹H NMR (500 MHz, CDCl₃) δ 7.70 (dd, $J = 7.4, 2.1$ Hz, 1H), 7.40 (dd, $J = 7.6, 1.8$ Hz, 1H), 7.34 – 7.21 (m, 2H), 7.05 (d, $J = 5.1$ Hz, 1H), 6.67 (d, $J = 5.1$ Hz, 1H), 4.92 (s, 1H), 3.74 (s, 1H), 3.72 (d, $J = 1.0$ Hz, 3H), 3.63 (d, $J = 14.2$ Hz, 1H), 2.96 – 2.81 (m, 4H). ¹³C NMR (125 MHz, CDCl₃) δ 171.33, 134.71, 133.87, 133.33, 133.28, 129.98, 129.80, 129.41, 127.15, 125.24, 122.74, 67.89, 52.15, 50.70, 48.30, 25.54. IR (ATR): 3066.8, 2949.2, 1737.9, 1433.1, 1163.1, 752.2, 733.0, 700.2 cm⁻¹ HRMS (ESI): Calculated [M+H]⁺ 344.0488; Found 344.0480 HPLC: 0.3:99.7 IPA/Hex, 45 min, 0.5 mL/min, $R_T = 34.9$ min (44.1%), 38.3 min (55.9%).

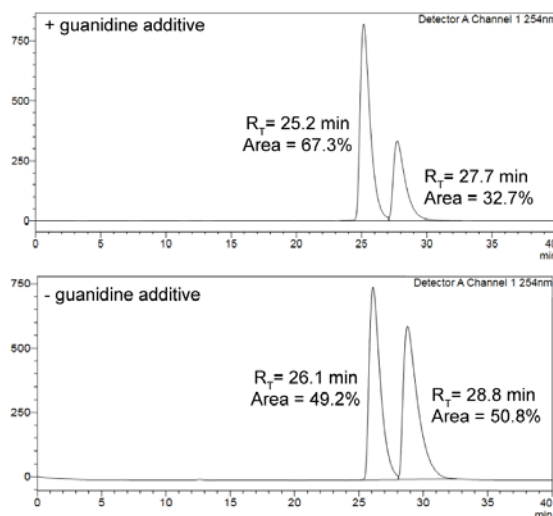


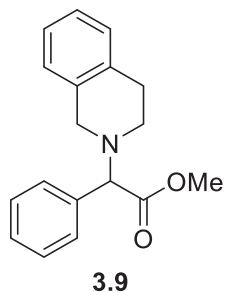


methyl 2-(6,7-dihydrothieno[3,2-c]pyridin-5(4H)-yl)-2-phenylacetate

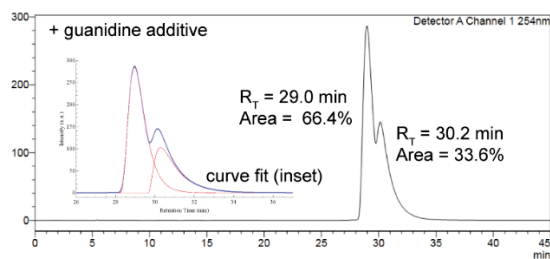
(3.3b) was synthesized according to the general procedure using methyl phenyldiazoacetate **3.1b** (176 mg, 1.0 mmol, 200 mol %) and 4,5,6,7-tetrahydrothieno[3,2-c]pyridine (70 mg, 0.5 mmol, 100 mol %). The crude residue was purified by two rounds of silica gel column chromatography: first column using 6:4:1 hexanes/CH₂Cl₂/Et₂O (R_f = 0.33), second column using 4:1 hexanes/Et₂O (R_f

= 0.21) to obtain a colorless oil (140 mg, 97% yield, 35% ee). ¹H NMR (500 MHz, CDCl₃) δ 7.54 – 7.43 (m, 2H), 7.43 – 7.29 (m, 3H), 7.05 (d, J = 5.1 Hz, 1H), 6.65 (d, J = 5.1 Hz, 1H), 4.31 (s, 1H), 3.72 (d, J = 0.9 Hz, 3H), 3.65 (d, J = 14.3 Hz, 1H), 3.60 (d, J = 14.3 Hz, 1H), 2.91 – 2.83 (m, 3H), 2.83 – 2.64 (m, 1H). ¹³C NMR (125 MHz, CDCl₃) δ 172.12, 136.04, 133.39, 133.32, 128.85, 128.76, 128.57, 125.33, 122.81, 72.94, 52.15, 51.02, 48.35, 25.34. IR (ATR): 3028.2, 2949.2, 1732.1, 1452.4, 1433.1, 1161.2, 731.0, 696.3 cm⁻¹ HRMS (ESI): Calculated [M+H]⁺ 288.1058; Found 288.1048. HPLC: 0.5:99.5 IPA/Hex, 40 min, 0.5 mL/min, R_T = 25.2 min (67.3%), 27.7 min (32.7%).

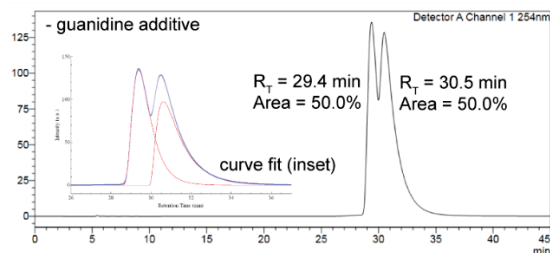




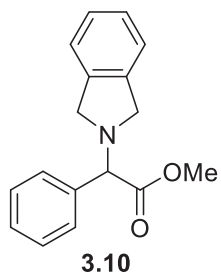
methyl 2-(3,4-dihydroisoquinolin-2(1H)-yl)-2-phenylacetate (3.9) was synthesized according to the general procedure using methyl phenyldiazoacetate **3.1b** (176 mg, 1.0 mmol, 200 mol %) and 1,2,3,4-tetrahydroisoquinoline (67 mg, 0.5 mmol, 100 mol %). The crude residue was purified by two rounds of silica gel column chromatography: first column using 9:1 hexanes/EtOAc ($R_f = 0.24$), second column using 7:3:1 hexanes/ CH_2Cl_2 /Et₂O ($R_f = 0.26$) to obtain a pale yellow oil (130 mg, 92% yield, 33% ee). ¹H NMR (500 MHz, CDCl_3) δ 7.50 (d, $J = 8.0$ Hz, 2H), 7.44 – 7.28 (m, 3H), 7.16 – 7.03 (m, 3H), 6.93 (d, $J = 8.1$ Hz, 1H), 4.25 (s, 1H), 3.74 – 3.69 (m, 4H), 3.67 (d, $J = 14.7$ Hz, 1H), 2.88 (t, $J = 6.1$ Hz, 2H), 2.85 – 2.79 (m, 1H), 2.76 – 2.68 (m, 1H). ¹³C NMR (125 MHz, CDCl_3) δ 172.03, 135.99, 134.28, 134.24, 128.78, 128.66, 128.65, 128.44, 126.64, 126.18, 125.62, 73.48, 53.85, 52.05, 48.31, 28.87. IR (ATR): 3026.6, 2949.9, 2805.1, 2755.3, 1738.1, 1162.8, 731.7, 697.5 cm^{-1} . HRMS (ESI): Calculated $[\text{M}+\text{H}]^+$ 282.1494; Found 282.1502. HPLC: 0.3:99.7 IPA/hexanes, 45 min, 0.6 mL/min, $R_T = 29.0$ min (66.4%), 30.2 min (33.6%).



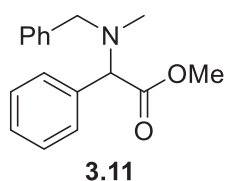
Fit Parameters					
	t	A	μ	σ	Area
+ guanidine additive	28.0	314	0.114	0.431	66.4%
	29.6	159	0.12	0.700	33.6%



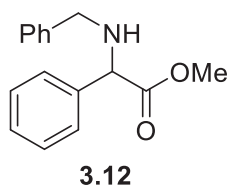
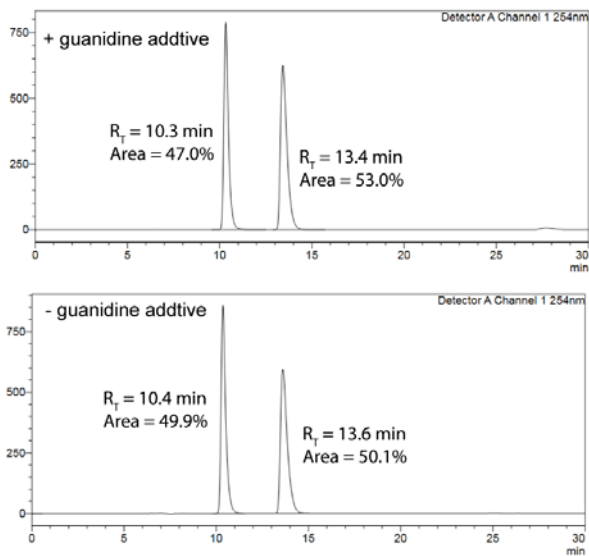
Fit Parameters					
	t	A	μ	σ	Area
- guanidine additive	28.5	165	0.153	0.471	50.0%
	29.9	165	0.21	0.700	50.0%



methyl 2-(isoindolin-2-yl)-2-phenylacetate (3.10) was synthesized according to the general procedure using methyl phenyldiazoacetate **3.1b** (176 mg, 1.0 mmol, 200 mol %) and isoindoline (60 mg, 0.5 mmol, 100 mol %). ¹H NMR (500 MHz, CDCl₃) δ 7.57 – 7.51 (m, 2H), 7.41 – 7.32 (m, 3H), 7.20 – 7.10 (m, 4H), 4.40 (s, 1H), 4.01 (d, J = 10.8 Hz, 2H), 3.89 (d, J = 11.0 Hz, 2H), 3.72 (s, 3H). ¹³C NMR (125 MHz, CDCl₃) δ 171.95, 139.33, 136.95, 128.76, 128.60, 128.59, 128.52, 126.80, 122.31, 72.66, 57.35, 52.17. IR (ATR): 3028.2, 2949.2, 2773.6, 1737.9, 1454.3, 1433.1, 1149.6, 1003.0, 738.7, 696.3 cm⁻¹. HRMS (ESI): Calculated [M+H]⁺ 268.1338; Found 268.1327, HPLC: RT=14.9 min, 15.2 min, 28% ee, 2:98 IPA/Hex, 30 min, 0.5 mL/min (unstable on HPLC).

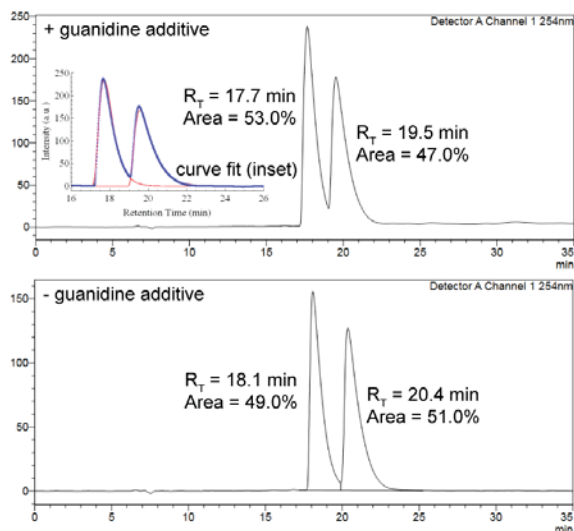


methyl 2-(benzyl(methyl)amino)-2-phenylacetate (3.11) was synthesized according to the general procedure using methyl phenyldiazoacetate **3.1b** (176 mg, 1.0 mmol, 200 mol %) and *N*-methylbenzylamine (61 mg, 0.5 mmol, 100 mol %). The crude residue was purified by silica gel column chromatography using 85:15 hexanes/Et₂O (R_f = 0.31) to obtain a colorless oil (96 mg, 72% yield, 6% ee). ¹H NMR (500 MHz, CDCl₃) δ 7.51 – 7.44 (m, 2H), 7.37 – 7.28 (m, 7H), 7.25 – 7.19 (m, 1H), 4.33 (s, 1H), 3.72 (s, 3H), 3.65 (d, J = 13.4 Hz, 1H), 3.51 (d, J = 13.4 Hz, 1H), 2.21 (s, 3H). ¹³C NMR (125 MHz, CDCl₃) δ 172.35, 138.88, 136.61, 128.86, 128.80, 128.50, 128.22, 128.16, 127.01, 72.11, 58.53, 51.74, 39.12. IR (ATR): 3062.2, 3028.2, 2949.8, 2846.8, 2792.2, 1734.5, 1453.4, 1162.3, 733.6, 696.2 cm⁻¹ HRMS (ESI): Calculated [M+Na]⁺ 292.1313; Found 292.1313. 2:98 IPA/Hex, 30 min, 0.5 mL/min, R_T= 10.3 min (47.0 %), 13.4 (53.0%) min.

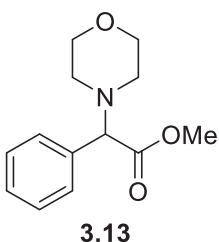


methyl 2-(benzylamino)-2-phenylacetate (3.12) was synthesized according

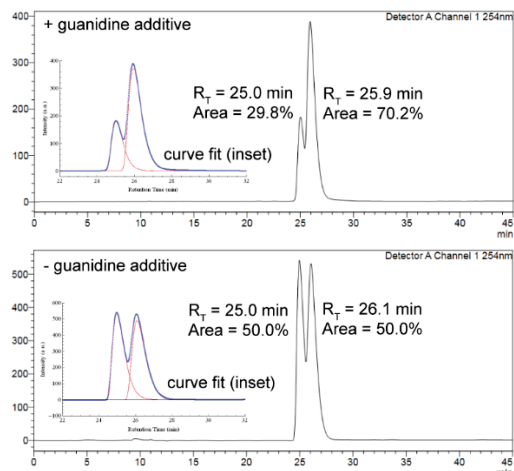
to the general procedure using methyl phenyldiazoacetate **3.1b** (176 mg, 1.0 mmol, 200 mol %) and benzylamine (54 mg, 0.5 mmol, 100 mol %). The crude residue was purified by silica gel column chromatography using 4:1 hexanes/EtOAc ($R_f = 0.29$) to obtain a colorless oil (53 mg, 41% yield, 6% ee). ^1H NMR (500 MHz, CDCl_3) δ 7.41 – 7.33 (m, 4H), 7.31 (d, $J = 4.5$ Hz, 5H), 7.25 (q, $J = 4.2$ Hz, 1H), 4.39 (s, 1H), 3.78 – 3.69 (m, 2H), 3.68 (s, 3H), 2.36 (s, 1H). ^{13}C NMR (125 MHz, CDCl_3) δ 173.42, 139.47, 138.05, 128.71, 128.43, 128.32, 128.11, 127.58, 127.15, 64.35, 52.22, 51.34. IR (ATR): 3340, 3028.4, 2950.8, 2847.2, 1734.9, 1454.5, 1201.0, 1169.3, 697.8 cm^{-1} . HPLC: 2:98 IPA/Hex, 35 min, 0.5 mL/min, $R_T = 17.7$ min (53.0%), 19.5 min (47.0%).



Fit parameters					
	t	A	μ	σ	Area
+ guanidine additive	16.9	228	0.0001	0.423	53.0%
	18.9	202	0.0001	0.560	47.0%

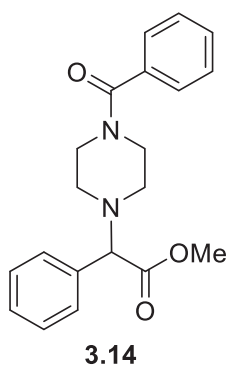


methyl 2-morpholino-2-phenylacetate (3.13) was synthesized according to the general procedure using methyl phenyldiazoacetate **3.1b** (176 mg, 1.0 mmol, 200 mol %) and morpholine (44 mg, 0.5 mmol, 100 mol %). The crude residue was purified by silica gel column chromatography using a gradient of 4:1 hexanes/EtOAc ($R_f = 0.17$) followed by 2:1 hexanes/EtOAc ($R_f = 0.29$) to obtain a pale-yellow oil (115 mg, 98% yield, 40% ee). ^1H NMR (500 MHz, CDCl_3) δ 7.46 – 7.41 (m, 2H), 7.37 – 7.29 (m, 3H), 3.98 (s, 1H), 3.72 (t, $J = 4.0$ Hz, 4H), 3.68 (s, 3H), 2.52 – 2.38 (m, 4H). ^{13}C NMR (125 MHz, CDCl_3) δ 171.68, 135.32, 128.89, 128.66, 128.53, 74.44, 66.82, 52.06, 51.62. IR (ATR): 2953.7, 2915.7, 2853.5, 2815.4, 1743.8, 1450.2, 1151.8, 1114.9, 877.1, 730.4, 698.0 cm^{-1} . HRMS (ESI): Calculated $[\text{M}+\text{Na}]^+$ 258.1106; Found 258.1101. HPLC: 2:98 IPA/Hex, 45 min, 0.5 mL/min, $R_T = 25.0$ min (29.8%), 25.9 min (70.2%).



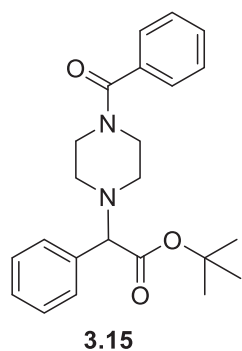
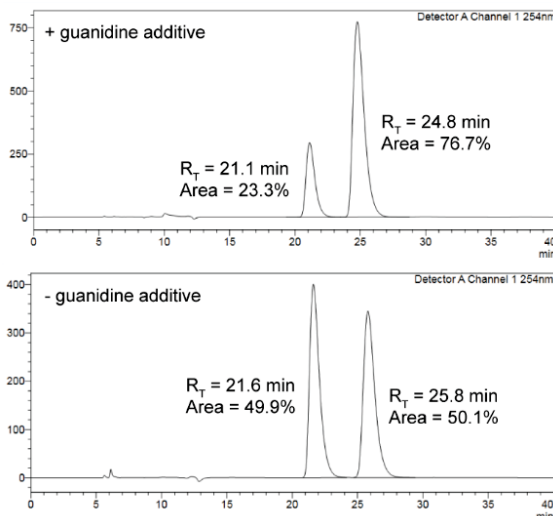
Fit parameters					
	t	A	μ	σ	Area
+ guanidine additive	24.1	139	0.0001	0.322	29.8%
	25.08	328	0.0001	0.379	70.2%

Fit parameters					
	t	A	μ	σ	Area
- guanidine additive	24.1	457	0.0001	0.360	50.0%
	25.2	457	0.0001	0.404	50.0%



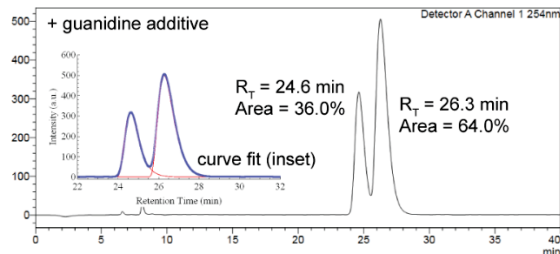
methyl 2-(4-benzoylpiperazin-1-yl)-2-phenylacetate (3.14) was synthesized according to the general procedure using methyl phenyldiazoacetate **3.1b** (176 mg, 1.0 mmol, 200 mol %) and 1-benzoylpiperazine (95 mg, 0.5 mmol, 100 mol %). The crude residue was purified by silica gel chromatography using 1:1 hexanes/EtOAc ($R_f = 0.20$) to obtain a yellow oil (145 mg, 86% yield, 53% *ee*). $^1\text{H NMR}$ (500 MHz, CDCl_3)

δ 7.48 – 7.28 (m, 10H), 4.08 (s, 1H), 3.81 (br, 2H), 3.69 (s, 3H), 3.44 (br, 2H), 2.65 – 2.26 (m, 4H). $^{13}\text{C NMR}$ (125 MHz, CDCl_3) δ 171.60, 170.19, 135.70, 135.16, 129.66, 128.77, 128.72, 128.61, 128.42, 127.03, 73.51, 52.08, 51.04, 50.81, 47.65, 42.01. IR (ATR): 3057.6, 3002.2, 2818.4, 2362.0, 1739.0, 1628.7, 1430.8, 1158.3, 1011.8, 730.3, 697.3 cm^{-1} HRMS (ESI): Calculated $[\text{M}+\text{Na}]^+$ 361.1528; Found 361.1527. HPLC: 15:85 IPA/Hex, 40 min, 0.5 mL/min, $R_T=21.1$ min (23.3%), 24.8 min (76.7%).

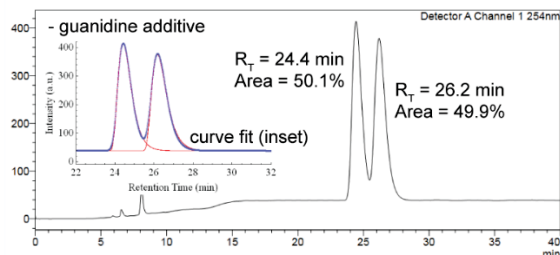


tert-butyl 2-(4-benzoylpiperazin-1-yl)-2-phenylacetate (3.15) was synthesized according to the general procedure using *t*-butyl phenyldiazoacetate **3.1d** (218 mg, 1.0 mmol, 200 mol %) and 1-benzoylpiperazine (95 mg, 0.5 mmol, 100 mol %). The crude residue was purified by silica gel chromatography using a gradient of 2:1 hexanes/EtOAc ($R_f = 0.21$) followed by 1:1 hexanes/EtOAc ($R_f = 0.34$) to obtain a pale yellow

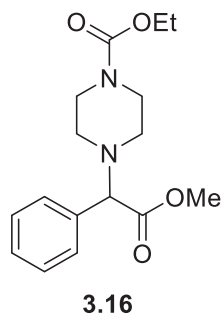
oil that upon storage at $-20\text{ }^\circ\text{C}$ formed a beige solid (145 mg, 86% yield, 53% ee). mp: 96-98 $^\circ\text{C}$. ^1H NMR (500 MHz, CDCl_3) δ 7.65 – 7.10 (m, 10H), 3.95 (s, 1H), 3.85 (s, 1H), 3.76 (s, 1H), 3.43 (s, 2H), 2.58 (s, 2H), 2.44 (s, 2H), 1.38 (s, 9H). ^{13}C NMR (125 MHz, CDCl_3) δ 170.37, 170.18, 135.82, 135.80, 129.59, 128.68, 128.50, 128.41, 128.23, 127.02, 81.55, 74.02, 50.91, 50.67, 47.77, 42.12, 27.92. IR (ATR): 3057.2, 2978.1, 2816.1, 1732.1, 1633.7, 1427.3, 1139.9, 1006.8 cm^{-1} . HPLC: 5:95 IPA/Hex, 40 min, 0.5 mL/min, $R_T = 24.6$ min (36.0%), 26.3 min (64.0%).



	Fit parameters				
	t	A	μ	σ	Area
+ guanidine additive	23.7	284	0.06	0.36	36.0%
	25.3	505	0.12	0.385	64.0%

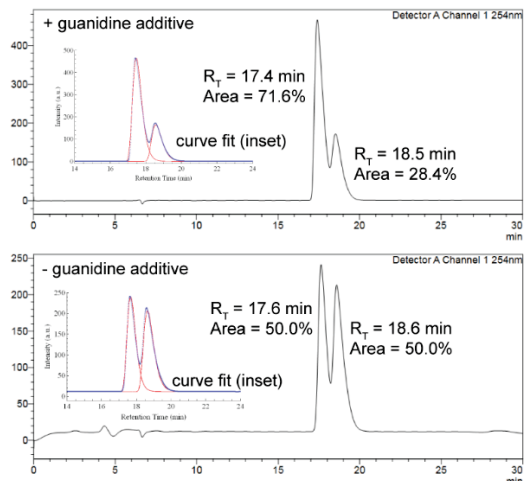


	Fit parameters				
	t	A	μ	σ	Area
- guanidine additive	23.5	336	0.05	0.360	50.1%
	28.5	334	0.10	0.385	49.9%



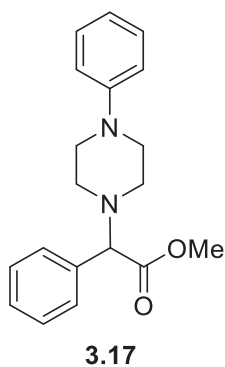
ethyl 4-(2-methoxy-2-oxo-1-phenylethyl)piperazine-1-carboxylate (3.16)

was synthesized according to the general procedure using methyl phenyldiazoacetate **3.1b** (176 mg, 1.0 mmol, 200 mol %) and ethyl 1-piperazinecarboxylate (79 mg, 0.5 mmol, 100 mol %). The crude residue was purified by silica gel chromatography using 5:2:2 hexanes/ CH_2Cl_2 /EtOAc ($R_f = 0.30$) to obtain a colorless oil (136 mg, 89% yield, 43% ee). ^1H NMR (500 MHz, CDCl_3) δ 7.45 – 7.39 (m, 2H), 7.39 – 7.30 (m, 3H), 4.11 (q, $J = 6.9$ Hz, 2H), 4.04 (s, 1H), 3.69 (s, 3H), 3.49 (t, $J = 5.2$ Hz, 4H), 2.52 – 2.33 (m, 4H), 1.24 (t, $J = 7.1$ Hz, 3H). ^{13}C NMR (125 MHz, CDCl_3) δ 171.71, 155.40, 135.34, 128.80, 128.68, 128.54, 73.76, 61.31, 52.05, 50.69, 43.57, 14.65. HRMS (ESI): Calculated $[\text{M}+\text{Na}]^+$ 375.1685; Found 375.1684. HPLC: 5:95 IPA/Hex, 30 min, 0.5 mL/min, $R_T = 17.4$ min (71.6%), 18.5 min (28.4%).



Fit parameters					
	t	A	μ	σ	Area
+ guanidine additive	16.5	305	0.0001	0.272	71.6%
	17.7	121	0.0001	0.308	28.4%

Fit parameters					
	t	A	μ	σ	Area
- guanidine additive	16.7	144	0.0001	0.260	50.0%
	17.7	144	0.0001	0.310	50.0%



methyl 2-phenyl-2-(4-phenylpiperazin-1-yl)acetate (3.17) was synthesized

according to the general procedure using methyl phenyldiazoacetate **3.1b**

(176 mg, 1.0 mmol, 200 mol %) and 1-phenylpiperazine (81 mg, 0.5 mmol,

100 mol %). The crude residue was purified by silica gel chromatography

using 4:1 hexanes/Et₂O ($R_f = 0.29$) to obtain a pale-yellow oil (149 mg, 96%

yield, 31% ee). ¹H NMR (500 MHz, CDCl₃) δ 7.47 (dd, $J = 8.0, 1.7$ Hz, 2H),

7.40 – 7.29 (m, 3H), 7.29 – 7.19 (m, 2H), 6.89 (d, $J = 7.7$ Hz, 2H), 6.84 (t, $J = 7.3$ Hz, 1H), 4.05

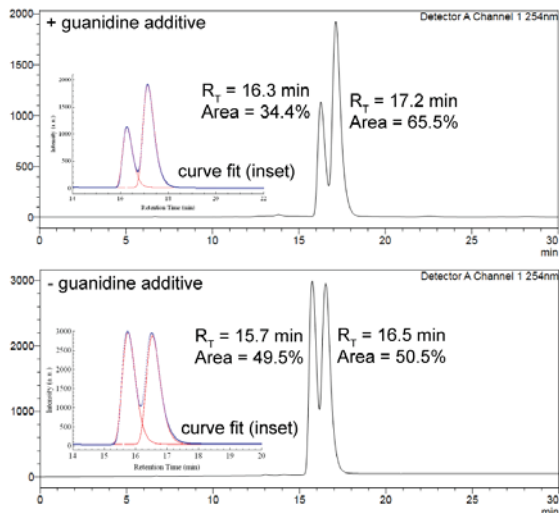
(s, 1H), 3.70 (s, 3H), 3.21 (dd, $J = 6.9, 3.9$ Hz, 4H), 2.66 – 2.57 (m, 4H). ¹³C NMR (125 MHz,

CDCl₃) δ 171.84, 151.21, 135.63, 129.08, 128.85, 128.66, 128.49, 119.73, 116.06, 74.12, 52.07,

51.13, 49.02. IR (ATR): 3027.6, 2950.7, 2823.4, 1742.6, 1598.7, 1495.0, 1232.4, 1144.1, 731.4,

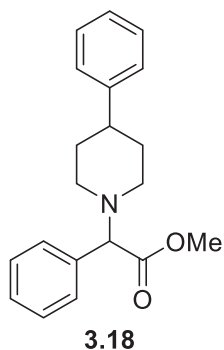
692.7 cm⁻¹. HRMS (ESI): Calculated [M+H]⁺ 311.1760; Found 311.1762. HPLC: 4:96 IPA/Hex, 30

min, 0.5 mL/min, $R_T = 16.3$ min (34.4%), 17.2 min (65.5%).



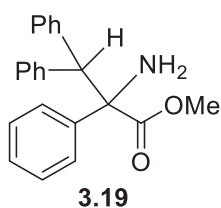
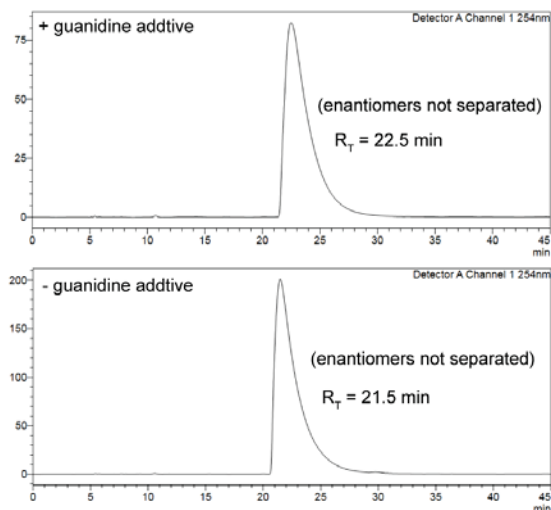
Fit parameters					
	t	A	μ	σ	Area
+ guanidine additive	15.3	580	0.0001	0.211	34.4%
	16.2	1108	0.0001	0.240	65.6%

Fit parameters					
	t	A	μ	σ	Area
- guanidine additive	14.8	1530	0.0001	0.212	49.5%
	15.6	1560	0.0001	0.225	50.5%



methyl 2-phenyl-2-(4-phenylpiperidin-1-yl)acetate (3.18) was synthesized according to the general procedure using methyl phenyldiazoacetate **3.1b** (176 mg, 1.0 mmol, 200 mol %) and phenylpiperidine (81 mg, 0.5 mmol, 100 mol %). The crude residue was purified by two rounds of silica gel column chromatography: first column using 9:1 hexanes/EtOAc ($R_f = 0.21$) followed by 7:3:1 hexanes/ CH_2Cl_2 /Et₂O ($R_f = 0.29$) to obtain a white solid (126 mg, 81%

yield, ee not determined). ¹H NMR (500 MHz, CDCl₃) δ 7.46 (d, $J = 6.6$ Hz, 2H), 7.39 – 7.31 (m, 3H), 7.28 (t, $J = 7.6$ Hz, 2H), 7.22 (d, $J = 6.9$ Hz, 2H), 7.18 (t, $J = 7.2$ Hz, 1H), 4.06 (s, 1H), 3.70 (s, 3H), 3.09 (d, $J = 11.0$ Hz, 1H), 2.88 (d, $J = 11.0$ Hz, 1H), 2.49 (tt, $J = 12.0, 4.1$ Hz, 1H), 2.28 (td, $J = 11.5, 2.8$ Hz, 1H), 1.99 (td, $J = 11.2, 2.6$ Hz, 1H), 1.91 (qd, $J = 12.1, 3.8$ Hz, 1H), 1.87 – 1.79 (m, 2H), 1.79 – 1.70 (m, 1H). ¹³C NMR (125 MHz, CDCl₃) δ 172.28, 146.26, 136.11, 128.82, 128.55, 128.40, 128.29, 126.87, 126.14, 74.62, 52.59, 51.99, 51.83, 42.70, 33.30. IR: 3027.8, 2935.1, 2804.4, 2757.7, 1734.2, 11162.3, 730.2, 696.7 cm⁻¹. HRMS (ESI): Calculated [M+H]⁺ 310.1807; Found 310.1805. HPLC: 5:95 IPA/Hex, 45 min, 0.5 mL/min, $R_T=22.5$ min.

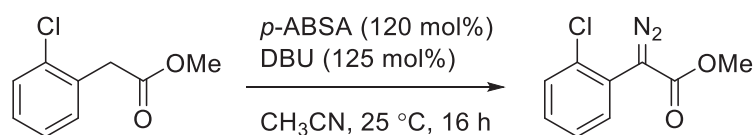


methyl 2-amino-2,3,3-triphenylpropanoate (3.19) was synthesized according to the general procedure using methyl phenyldiazoacetate **3.1b** (176 mg, 1.0 mmol, 200 mol %) and benzhydrylamine (92 mg, 0.5 mmol, 100 mol %). The crude residue was purified by silica gel chromatography using

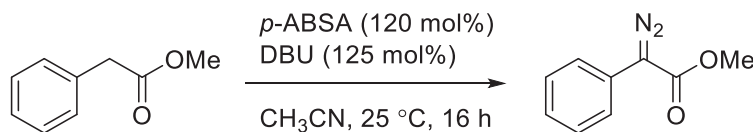
4:1 hexanes/Et₂O ($R_f = 0.28$) to obtain a white solid (39 mg, 12% yield).

¹H NMR (500 MHz, CDCl₃) δ 7.60 (d, $J = 8.2$ Hz, 2H), 7.53 (d, $J = 7.7$ Hz, 2H), 7.28 (t, $J = 7.7$ Hz, 2H), 7.26 – 7.16 (m, 6H), 7.07 – 7.00 (m, 3H), 5.24 (s, 1H), 3.59 (s, 3H), 2.10 (s, 2H). ¹³C NMR (125 MHz, CDCl₃) δ 175.27, 142.00, 141.36, 139.77, 130.39, 129.70, 128.33, 127.99, 127.61, 127.28, 126.64, 126.27, 126.18, 67.37, 57.90, 52.55. HRMS (ESI): Calculated [M+H]⁺ 332.1650; Found 332.1653. IR (ATR): 3382.2, 3323.9, 3060.8, 3025.2, 2948.0, 1724.3, 1493.4, 1446.7, 1077.7, 694.4 cm⁻¹

Synthesis and characterization of diazo compounds 3.1a-3.1d:

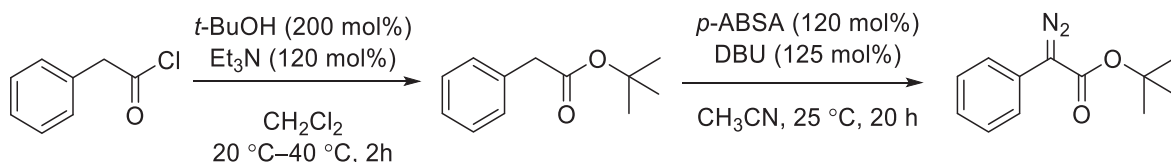


methyl 2-(2-chlorophenyl)-2-diazoacetate 3.1a: To a 100 mL round-bottom flask equipped with stir bar was charged *p*-acetamidobenzenesulfonyl azide (2.88 g, 12 mmol, 120 mol %) and 30 mL dry acetonitrile. To the resulting solution was added methyl 2-(2-chlorophenyl)acetate (1.84 g, 10 mmol, 100 mol %); the solution was cooled in an ice-water bath for 15 minutes. Separately, a 10 mL solution of DBU (1.90 g, 12.5 mmol, 125 mol %) in dry acetonitrile was prepared, then added to the reaction mixture over 5 minutes. The solution was warmed gradually to room temperature and stirred for 16 h. The resulting yellow solution was diluted with 50 mL Et₂O, and washed half-saturated ammonium chloride solution (aq, 2 x 50 mL), water (50 mL), and brine (50 mL). The organic layer was dried over sodium sulfate, filtered, and concentrated by rotary evaporation. The residue was purified by column chromatography using 4:1 hexanes/Et₂O (*R*_f = 0.38) to obtain a yellow oil that upon drying under high vacuum formed a yellow solid (1.74 g, 8.3 mmol, 83%). ¹H NMR (500 MHz, CDCl₃) δ 7.54 (dd, *J* = 7.8, 1.7 Hz, 1H), 7.42 (dd, *J* = 7.8, 1.6 Hz, 1H), 7.32 (td, *J* = 7.6, 1.5 Hz, 1H), 7.28 (dd, *J* = 7.9, 1.8 Hz, 1H), 3.84 (s, 3H); ¹³C NMR (126 MHz, CDCl₃) δ 165.9, 133.8, 132.3, 130.1, 129.6, 127.1, 123.9, 52.3.



methyl 2-diazo-2-phenylacetate 3.1b: To a 250 mL round-bottom flask equipped with stirbar was charged *p*-acetamidobenzenesulfonyl azide (5.76 g, 24 mmol, 120 mol %) and 60 mL dry acetonitrile. To the resulting solution was added methyl phenylacetate (3.00 g, 20 mmol, 100 mol %); the solution was cooled in an ice-water bath for 15 minutes. Separately, a 20 mL solution of

DBU (3.81 g, 25 mmol, 125 mol %) in dry acetonitrile was prepared, then added to the reaction mixture over 5 minutes. The solution was warmed gradually to room temperature and stirred for 16 h. The resulting orange solution was diluted with 100 mL Et₂O, and washed half-saturated ammonium chloride solution (aq, 2 x 100 mL), water (100 mL), and brine (100 mL). The organic layer was dried over sodium sulfate, filtered, and concentrated by rotary evaporation. The residue was purified by column chromatography using 92:8 hexanes/Et₂O (R_f = 0.31) to obtain a red-orange oil (1.89 g, 10.7 mmol, 54%). IR: 3025.7, 2952.9, 2080.7, 1698.3, 1286.2, 1151.4, 752.7, 689.5 cm⁻¹

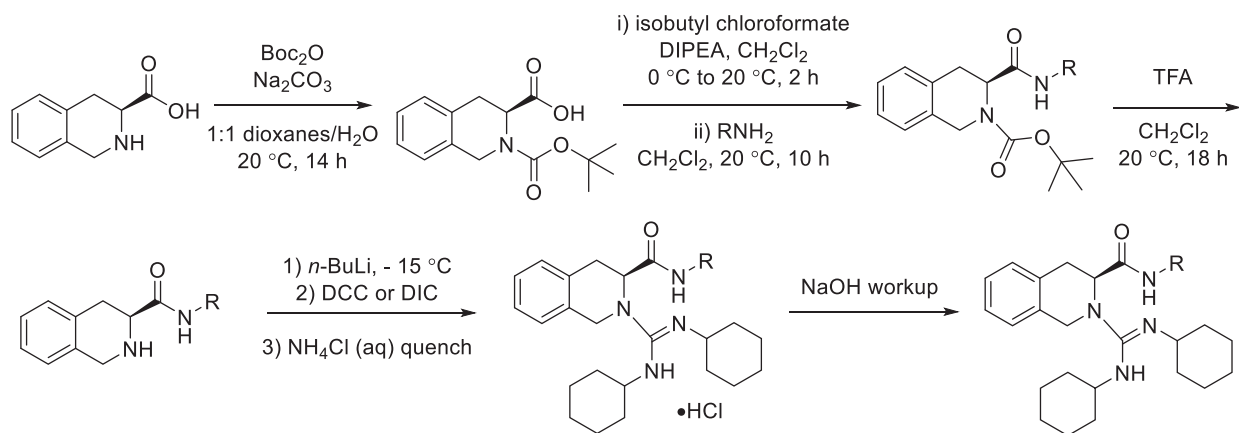


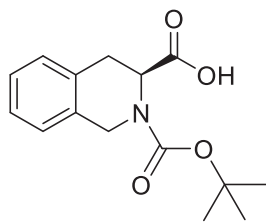
tert-butyl 2-phenylacetate: A 250 mL round-bottom flask equipped with stirbar was charged 100 mL dry CHCl₃, *tert*-butanol (3.70 g, 50 mmol, 200 mol %), and triethylamine (3.04 g, 30 mmol, 120 mol %), and the mixture stirred for 5 minutes. Separately was prepared a 20 mL solution of phenylacetyl chloride (3.87 g, 25 mmol, 100 mol %) in dry CH₂Cl₂. The phenylacetyl chloride solution was added to the reaction mixture over 10 minutes. The round-bottom flask was then equipped with a condenser and heated at reflux for 2 h. The reaction was cooled to room temperature and washed successively with 1M KHSO₄ (aq, 2 x 100 mL), water (100 mL), and brine (50 mL). The organic layer was dried over Na₂SO₄, filtered, and concentrated by rotary evaporation. The crude residue was purified by silica gel chromatography using 8:92 Et₂O/Hex (R_f = 0.35, stains blue by *p*-anisaldehyde) to obtain *tert*-butyl 2-phenylacetate as a colorless oil (1.68 g, 35% yield). ¹H NMR (500 MHz, CDCl₃) δ 7.46 – 7.17 (m, 5H), 3.52 (s, 2H), 1.44 (s, 9H). ¹³C NMR (125 MHz, CDCl₃) δ 170.93, 134.73, 129.19, 128.44, 126.82, 80.77, 42.67, 28.04. IR (ATR): 3031.3, 2978.2, 2931.8, 1730.1, 1136.0, 694.7 cm⁻¹.

tert-butyl 2-diazo-2-phenylacetate: A 25 mL round-bottom flask equipped with stirbar was charged *p*-acetamidobenzenesulfonyl azide (864 mg, 3.60 mmol, 120 mol %) and 10 mL dry acetonitrile. To the resulting solution was added tert-butyl phenylacetate (576 mg, 3.0 mmol, 100 mol %); the solution was cooled in an ice-water bath for 15 minutes. Separately, a 2 mL solution of DBU (571 mg, 3.75 mmol, 125 mol %) in dry acetonitrile was prepared, then added to the reaction mixture over 5 minutes. The solution was warmed gradually to room temperature and stirred for 20 h. The resulting orange solution was diluted with 20 mL Et₂O, and washed half-saturated ammonium chloride solution (aq, 2 x 20 mL), water (20 mL), and brine (20 mL). The organic layer was dried over sodium sulfate, filtered, and concentrated by rotary evaporation. The residue was purified by column chromatography 95:5 hexanes/Et₂O (*R*_f = 0.40) to obtain a red-orange oil (461 mg, 70% yield). IR (ATR): 2977.0, 2077.5, 1695.7, 1348.9, 1245.0, 1139.2, 754.1, 689.4 cm⁻¹.

Synthesis and characterization of chiral guanidine additives

Guanidine additives **3.4-3.6** were synthesized according to a reported literature procedure¹⁶ with minor modification. The following general synthetic system was used:

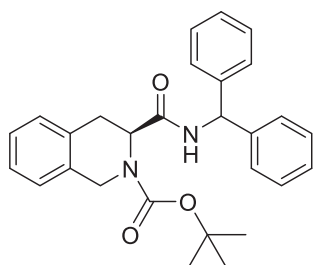




(S)-2-(tert-butoxycarbonyl)-1,2,3,4-tetrahydroisoquinoline-3-carboxy-

lic acid (Boc-Tic-OH): *Example procedure:* A 250 mL round bottom flask was charged with a 100 mL solution of 1:1 H₂O/*p*-dioxane mixture, followed by (S)-1,2,3,4-tetrahydroisoquinolinecarboxylic acid (7.08 g, 40 mmol, 100

mol %) and Na₂CO₃ (8.48 g, 80 mmol, 200 mol %). The mixture was stirred for 5 minutes at room temperature, then Boc anhydride (10.5 g, 48 mmol, 120 mol %) added. The mixture was stirred over 14 h. The mixture was concentrated to half-volume by rotary evaporation, then adjusted to pH ≈ 2 using 1 N HCl (aq). The mixture was extracted with Et₂O (2 x 100 mL). The organic layers were combined, washed with 1 N HCl (aq, 100 mL), water (100 mL), and brine (100 mL). The organic layer was dried over Na₂SO₄, then concentrated *in vacuo* to obtain a colorless, viscous oil. Methanol (40 mL) was added and a white crystalline solid began to form. The mixture was stored at -20 °C for several hours, then the solid collected by filtration and washed with cold methanol (20 mL). A white powder was obtained (4.53 g, 16.3 mmol, 41%).

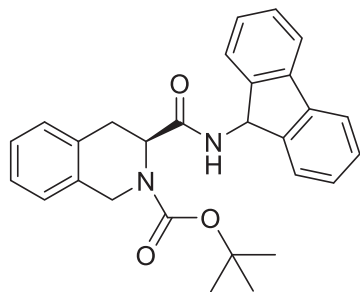


tert-butyl (S)-3-(benzhydrylcarbamoyl)-3,4-dihydroisoquinoline-2-(1H)-carboxylate. *Example procedure:* In a 50 mL round bottom flask

Boc-Tic-OH (1.66 g, 6.0 mmol, 100 mol %) was dissolved in 25 mL CH₂Cl₂. DIPEA (2.32 g, 18.0 mmol, 300 mol %) was added, then the

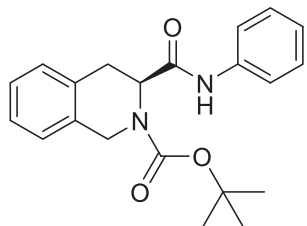
solution cooled to 0 °C in an ice-water bath for 15 minutes. To the solution was added isobutyl chloroformate (900 mg, 6.6 mmol, 110 mol %) and stirring continued at 0 °C for 2 h. Benzhydrylamine (2.18 g, 12.0 mmol, 200 mol %) was then added, and the solution allowed to warm gradually to room temperature and stirred for 10 h. The reaction mixture was diluted with 100 mL CH₂Cl₂ and washed with 1 M KHSO₄ (aq, 100 mL) and water (50 mL). The organic layer was collected, dried over Na₂SO₄, and concentrated by rotary evaporation. The residue was purified by silica gel chromatography using a gradient of 2:1 hexanes/EtOAc (R_f = 0.16) followed by 1:1 hexanes/EtOAc (R_f = 0.28). Column fractions were concentrated *in vacuo* and dried under

high vacuum to obtain a white foam (2.18 g, 4.93 mmol, 82%). mp: 48-51 °C. ¹H NMR (500 MHz, CDCl₃) δ 7.64 – 6.58 (m, 13H), 6.58 – 6.13 (m, 2H), 6.07 (d, *J* = 8.5 Hz, 1H), 5.11 – 4.18 (m, 3H), 3.37 (dd, *J* = 15.1, 3.0 Hz, 1H), 3.25 – 2.92 (m, 1H), 1.66 – 1.06 (m, 8H). ¹³C NMR (125 MHz, CDCl₃) δ 170.68, 155.34, 141.48, 140.53, 134.15, 133.83, 128.66, 128.61, 128.32, 128.26, 128.19, 128.02, 127.80, 127.60, 127.47, 127.30, 127.26, 127.12, 127.08, 126.96, 126.57, 81.37, 57.04, 56.22, 45.01, 32.48, 28.14. IR (ATR): 3306.4, 3028.4, 2975.6, 1694.0, 1494.0, 1364.9, 1161.4, 697.3 cm⁻¹.



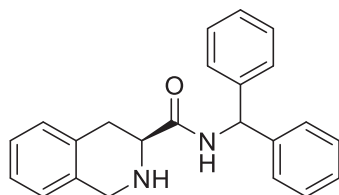
tert-butyl (S)-3-((9H-fluoren-9-yl)carbamoyl)-3,4-dihydroisoquinoline-2(1H)-carboxylate was synthesized and extracted according to the above example procedure from Boc-TIC-OH (555 mg, 2 mmol, 100 mol %) and aminofluorene•HCl (485 mg, 2.25 mmol, 112 mol %). All other reagents were scaled proportionally to

the Boc-TIC-OH starting material. The product was purified by column chromatography using a gradient of 2:1 hexanes/EtOAc (*R_f* = 0.15) followed by 1:1 hexanes/EtOAc (*R_f* = 0.25) to obtain the title compound as a white solid (580 mg, 1.32 mmol, 66%). mp: 66-74 °C ¹H NMR (500 MHz, CDCl₃) δ 7.61 (dd, *J* = 12.7, 7.6 Hz, 2H), 7.49 (d, *J* = 7.6 Hz, 1H), 7.42 – 7.16 (m, 6H), 7.05 (d, *J* = 7.6 Hz, 2H), 6.91 – 5.69 (m, 3H), 5.14 – 4.71 (m, 1H), 4.65 – 4.16 (m, 2H), 3.48 (dd, *J* = 15.0, 3.2 Hz, 1H), 3.23 – 3.06 (m, 1H), 1.39 (s, 9H). ¹³C NMR (125 MHz, CDCl₃) δ 172.39, 144.16, 140.43, 140.35, 128.64, 128.51, 128.06, 127.79, 127.50, 127.06, 126.51, 125.12, 124.42, 119.93, 119.79, 81.39, 56.95, 54.26, 44.77, 32.63, 28.26. HRMS (ESI): Calculated [M+H]⁺ 463.1998; Found 463.1995.



tert-butyl-(S)-3-(phenylcarbamoyl)-3,4-dihydroisoquinoline-2(1H)-carboxylate was synthesized from Boc-Tic-OH (500 mg, 1.8 mmol, 100 mol %) and aniline (335 mg, 3.6 mmol, 200 mol %). The product was purified by column chromatography using 1:2 hexanes/EtOAc (R_f

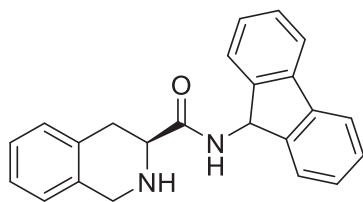
=0.35) to obtain the title compound as white cubic crystals (542 mg, 1.54 mmol, 86%). All other reagents were scaled proportionally to the BOC-TIC-OH starting material. ^1H NMR (500 MHz, CDCl_3) δ 8.91 – 6.75 (m, 10H), 5.31 – 4.21 (m, 3H), 3.40 (s, 1H), 3.20 (s, 1H), 1.59 (s, 9H). ^{13}C NMR (125 MHz, CDCl_3) δ 170.27, 137.90, 133.81, 128.89, 127.97, 127.03, 126.56, 126.00, 124.37, 119.84, 81.61, 57.69, 54.59, 45.06, 44.60, 31.97, 29.90, 28.36. IR (ATR): 3288.6, 3203.8, 3142.0, 2976.2, 1315.5, 1550.8, 1410.0 cm^{-1} . HRMS (ESI): Calculated $[\text{M}+\text{Na}]^+$ 375.1685; Found 375.1684.



(S)-N-benzhydryl-1,2,3,4-tetrahydroisoquinoline-3-carboxamide

Example procedure: In a 100 mL round bottom flask, *tert*-butyl (S)-3-(benzhydrylcarbamoyl)-3,4-dihydroisoquinoline-2(1H)-carboxylate (2.18 g, 4.93 mmol) was dissolved in 25 mL CH_2Cl_2 . Trifluoroacetic acid (3 mL) was added and the solution stirred at 20 °C for 18 h. The solution was diluted with 25 mL CH_2Cl_2 and cooled to 0 °C in an ice-water bath. Saturated NaHCO_3 (aq, 25 mL) was added and the resulting biphasic mixture stirred vigorously for 1 h until gas evolution subsided. The layers were separated and the aqueous layer further extracted with CH_2Cl_2 (25 mL). The organic layers were combined, dried over Na_2SO_4 , and filtered. The filtrate was concentrated *in vacuo* to approx. 10 mL volume, diluted with 50 mL hexanes, and stored at -20 °C overnight. The product crystallized as fine white needles collected by filtration filtered and washed with cold hexanes (1.61 g, 4.7 mmol, 95%). mp: 141-142 °C. Spectroscopic data was consistent with reported literature values: ^1H NMR (500 MHz, CDCl_3) δ 7.95 (d, J = 8.7 Hz, 1H), 7.37 – 7.21 (m, 8H), 7.20 – 7.08 (m, 5H), 7.09 – 7.01 (m, 1H), 6.25 (d, J = 8.7 Hz, 1H), 4.02 (d, J = 15.9 Hz, 1H), 3.96 (d, J = 15.9 Hz, 1H), 3.65 (dd, J = 9.8, 5.3

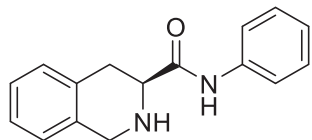
Hz, 1H), 3.24 (dd, $J = 16.3, 5.3$ Hz, 1H), 2.90 (dd, $J = 16.3, 9.8$ Hz, 1H), 1.66 (s, 1H). ^{13}C NMR (125 MHz, CDCl_3) δ 172.29, 141.76, 141.62, 136.02, 134.41, 129.15, 128.66, 128.60, 127.53, 127.43, 127.28, 127.17, 126.73, 126.26, 125.60, 56.38, 56.29, 47.43, 31.05. IR: 3291.5, 3060.7, 2924.9, 1643.2, 1537.3, 731.4, 696.3 cm^{-1}



(S)-N-(9H-fluoren-9-yl)-1,2,3,4-tetrahydroisoquinoline-3-carb-

oxamide was obtained after TFA deprotection of the corresponding Boc-protected amine (500 mg, 1.13 mmol) to obtain a white powder (350 mg, 91%). All other reagents were scaled

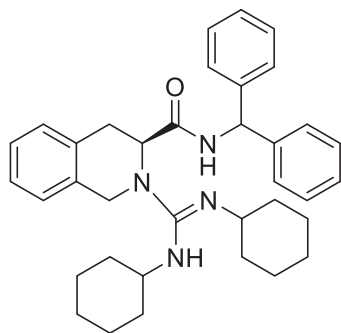
proportionally to the Boc-protected amine starting material. ^1H NMR (500 MHz, CDCl_3) δ 7.72 – 7.66 (m, 2H), 7.57 (dd, $J = 7.5, 1.0$ Hz, 1H), 7.50 (d, $J = 9.2$ Hz, 1H), 7.42 – 7.35 (m, 3H), 7.31 (td, $J = 7.5, 1.1$ Hz, 1H), 7.28 – 7.23 (m, 1H), 7.23 – 7.19 (m, 2H), 7.19 – 7.13 (m, 1H), 7.00 (d, $J = 7.4$ Hz, 1H), 6.20 (d, $J = 9.1$ Hz, 1H), 4.04 – 3.79 (m, 2H), 3.72 (dd, $J = 9.8, 5.3$ Hz, 1H), 3.32 (dd, $J = 16.3, 5.3$ Hz, 1H), 3.00 (dd, $J = 16.3, 9.8$ Hz, 1H), 1.65 (br, 2H). ^{13}C NMR (125 MHz, CDCl_3) δ 174.17, 144.51, 144.43, 140.65, 140.61, 135.97, 134.30, 129.15, 128.64, 128.60, 127.75, 127.73, 126.69, 126.29, 125.60, 125.17, 124.94, 119.99, 119.96, 56.48, 54.30, 47.20, 31.27. IR (ATR) 3265.5, 3063.0, 2924.1, 2359.4, 1645.6, 1549.3, 1447.8, 733.1 cm^{-1} . HRMS (ESI): Calculated $[\text{M}+\text{H}]^+$ 341.1564; Found 341.1663.



(S)-N-phenyl-1,2,3,4-tetrahydroisoquinoline-3-carboxamide was

obtained after TFA deprotection of the corresponding Boc-protected amine (450 mg, 1.28 mmol) as a white powder (287 mg, 1.13 mmol, 89%). All other reagents were scaled proportionally to the Boc-protected amine starting material. mp: 166-168 $^{\circ}\text{C}$. ^1H NMR (500 MHz, CDCl_3) δ 9.31 (s, 1H), 7.68 – 7.53 (m, 2H), 7.32 (t, $J = 7.9$ Hz, 2H), 7.22 – 7.14 (m, 3H), 7.14 – 7.02 (m, 2H), 4.21 – 3.86 (m, 2H), 3.64 (dd, $J = 10.4, 5.4$ Hz, 1H), 3.31 (dd, $J = 16.4, 5.4$ Hz, 1H), 2.88 (dd, $J = 16.4, 10.4$ Hz, 1H), 1.73 (s, 1H). ^{13}C NMR (125

MHz, CDCl₃) δ 171.26, 137.71, 136.06, 134.37, 129.18, 129.00, 126.77, 126.33, 125.52, 124.13, 119.43, 56.82, 47.51, 30.53. IR (ATR): 3307.2, 3279.5, 3058.0, 3029.3, 2943.1, 2895.8, 1677.5, 1531.5, 1441.1, 898.8, 739.0 cm⁻¹. HRMS (ESI): Calculated [M+H]⁺ 253.1341; Found 253.1342

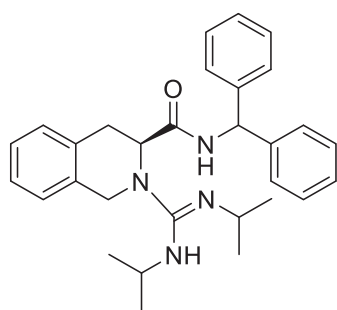


(S)-N-benzhydryl-2-(N,N'-dicyclohexylcarbamimidoyl)-1,2,3,4-tetrahydroisoquinoline-3-carboxamide (4). Example procedure:

In a 100 mL round bottom flask, (S)-N-benzhydryl-1,2,3,4-tetrahydroisoquinoline-3-carboxamide (1.37 g, 4.0 mmol, 100 mol %) was dissolved into 40 mL dry THF. The solution was cooled to -15 °C in a dry ice/ethylene glycol bath over 15 minutes. A solution of *n*-BuLi (5.37 mL, 1.6 M in hexanes, 8.4 mmol, 210 mol %) was added over ten minutes. The resulting dark red solution was stirred for at -15 °C for 1 h. A solution of *N,N'*-dicyclohexylcarbodiimide (990 mg, 4.8 mmol, 120 mol %) in 8 mL dry THF was added, the solution transferred to an ice water bath and stirred for 2 h. The reaction was quenched by adding 3 mL saturated NH₄Cl (aq). The resulting layers were separated, and the aqueous (bottom) layer extracted with an additional 25 mL CH₂Cl₂. The organic layers were combined and concentrated in vacuo. The resulting guanidinium chloride was purified by silica gel chromatography using a gradient of CH₂Cl₂ followed by 95:5 CH₂Cl₂/MeOH. Column fractions were collected and concentrated in vacuo to obtain a yellow-beige solid, which was recrystallized from CH₂Cl₂/acetone. Recrystallization procedure: The solid was transferred to a 50 mL Erlenmeyer flask equipped with stir bar. The solid was dissolved completely in 15 mL of refluxing CH₂Cl₂, then 15 mL of acetone were added while maintaining the solution at reflux. (Note: We had difficulty dissolving the guanidinium chloride if the CH₂Cl₂ and acetone were pre-mixed). Heating was continued until 10 mL of the resulting solution evaporated. The flask was removed from the hot plate and allowed to cool to room temperature and further cooled in the refrigerator to -20 °C. The guanidinium chloride crystallized

as prisms that were collected by filtration and washed with cold acetone. The prisms became a white powder after further drying.

NaOH workup: The white powder was dissolved in 15 mL CH₂Cl₂ and shaken vigorously with 2M NaOH (aq, 10 mL). The organic layer was collected and the aqueous layer extracted with an additional 15 mL CH₂Cl₂. The organic layers were combined and shaken again with 2M NaOH (aq, 10 mL). The organic layer was collected, dried over Na₂SO₄, and filtered through a 1-inch pad of celite using CH₂Cl₂. The filtrate was concentrated and dried under high vacuum to obtain a white foam (1.65 g, 3.0 mmol, 75%). Spectroscopic data was consistent with reported literature values: ¹H NMR (500 MHz, CDCl₃) δ 10.51 (d, J = 8.4 Hz, 1H), 7.34 – 7.10 (m, 14H), 7.08 (t, J = 7.3 Hz, 1H), 6.96 (d, J = 7.5 Hz, 1H), 6.17 (d, J = 8.2 Hz, 1H), 4.80 (d, J = 6.4 Hz, 1H), 4.34 (d, J = 16.5 Hz, 1H), 4.13 (d, J = 16.5 Hz, 1H), 3.48 – 3.35 (m, 2H), 3.02 – 2.87 (m, 3H), 1.85 (dd, J = 55.2, 12.5 Hz, 2H), 1.74 – 1.38 (m, 9H), 1.32 – 0.85 (m, 7H). ¹³C NMR (125 MHz, CDCl₃) δ 171.64, 155.76, 142.66, 142.49, 134.40, 132.60, 128.96, 128.33, 128.24, 127.77, 127.66, 126.93, 126.77, 126.46, 125.70, 125.39, 56.85, 55.83, 55.38, 53.73, 47.26, 35.50, 35.18, 34.56, 33.76, 29.58, 25.70, 25.47, 25.17, 25.08, 24.84. IR: 3349.8, 2923.5, 2849.7, 1667.3, 1614.5, 696.4 cm⁻¹.

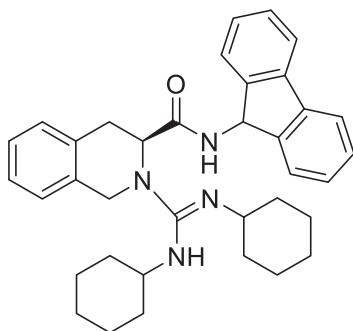


(S)-N-benzhydryl-2-(N,N-diisopropylcarbamimidoyl)-1,2,3,4-

tetra hydroisoquinoline-3-carboxamide was synthesized from the corresponding benzhydryl derivative (238 mg, 0.70 mmol) using DIC to obtain a white foam (200 mg, 0.43 mmol, 61%). All other reagents were scaled proportionally to the benzyhydryl derivative starting

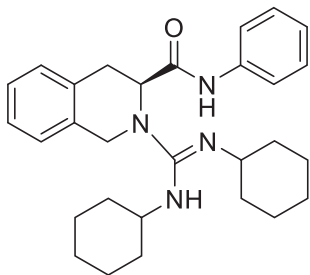
material. The product was purified by chromatography, recrystallization, and NaOH workup as described in the above example procedure. mp: 111-113 °C. ¹H NMR (500 MHz, CDCl₃) δ 10.63 (d, J = 8.6 Hz, 1H), 7.35 – 7.10 (m, 12H), 7.08 (t, J = 7.3 Hz, 1H), 6.96 (d, J = 7.6 Hz, 1H), 6.18 (d, J = 8.4 Hz, 1H), 4.82 (d, J = 6.4 Hz, 1H), 4.34 (d, J = 16.5 Hz, 1H), 4.11 (d, J = 16.5 Hz, 1H), 3.50 – 3.21 (m, 4H), 2.93 (dd, J = 16.0, 6.5 Hz, 1H), 1.13 (d, J = 6.4 Hz, 3H), 1.02 (dd, J = 12.0,

6.1 Hz, 6H), 0.89 (d, J = 6.4 Hz, 3H). ^{13}C NMR (125 MHz, CDCl_3) δ 171.53, 155.95, 142.71, 142.58, 134.44, 132.46, 129.01, 128.35, 128.26, 127.64, 126.93, 126.80, 126.56, 125.74, 125.39, 56.83, 55.32, 47.26, 47.12, 46.73, 29.51, 25.40, 24.43, 24.28, 23.04. IR (ATR): 2960.6, 2923.2, 2361.7, 1662.0, 1615.4, 1402.9, 1362.3, 738.2, 696.5, 608.4, 584.7 cm^{-1} . HRMS (ESI): Calculated $[\text{M}+\text{H}]^+$ 469.2967; Found 469.2946.



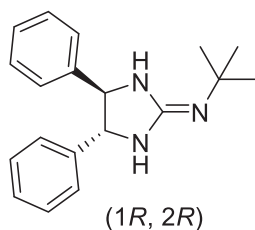
(S)-2-(*N,N'*-dicyclohexylcarbamimidoyl)-*N*-(9*H*-fluoren-9-yl)-1,2,3,4-tetrahydroisoquinoline-3-carboxamide was synthesized from the corresponding amidofluorene derivative (238 mg, 0.70 mmol) with DCC to obtain the title compound as a white powder (223 mg, 0.41 mmol, 58%). All other reagents were scaled proportionally to the amidofluorene starting material. The product

was purified by chromatography, recrystallization, and NaOH workup as described in the above example procedure. ^1H NMR (500 MHz, CDCl_3) δ 7.82 – 7.72 (m, 2H), 7.65 (d, J = 7.5 Hz, 1H), 7.58 (d, J = 9.2 Hz, 1H), 7.51 – 7.42 (m, 3H), 7.42 – 7.36 (m, 1H), 7.36 – 7.31 (m, 1H), 7.31 – 7.19 (m, 3H), 7.07 (d, J = 7.3 Hz, 1H), 6.27 (d, J = 9.1 Hz, 1H), 4.25 (s, 1H), 4.08 – 3.90 (m, 2H), 3.79 (dd, J = 9.8, 5.3 Hz, 1H), 3.56 (tdt, J = 11.2, 7.8, 3.9 Hz, 1H), 3.39 (dd, J = 16.3, 5.3 Hz, 1H), 3.07 (dd, J = 16.3, 9.8 Hz, 1H), 2.07 – 1.72 (m, 3H), 1.72 – 1.35 (m, 3H), 1.28 – 1.10 (m, 2H). ^{13}C NMR (125 MHz, CDCl_3) δ 174.16, 144.52, 144.44, 140.65, 140.61, 135.98, 134.31, 129.15, 128.64, 128.60, 127.74, 127.73, 126.69, 126.29, 125.61, 125.17, 124.94, 119.99, 119.96, 56.48, 54.30, 49.09, 47.20, 33.98, 31.27, 25.64, 24.96. IR (ATR): 3323.0, 3257.0, 3063.4, 2927.5, 2850.0, 2359.8, 1645.9, 1550.2, 1448.1, 733.4 cm^{-1} . HRMS (ESI): calculated $[\text{M}+\text{H}]^+$ 547.3437; found 547.3444.



(S)-2-(N,N'-dicyclohexylcarbamimidoyl)-N-phenyl-1,2,3,4-tetrahydroisoquinoline-3-carboxamide was synthesized from the corresponding phenyl derivative (238 mg, 0.94 mmol) and obtained as a white powder (322 mg, 0.70 mmol, 74%). All other reagents were scaled proportionally to the phenyl derivative starting material. The

product was purified by chromatography, recrystallization, and NaOH workup as described in the above example procedure. mp: 79-81 °C The ^1H NMR (500 MHz, CDCl_3) δ 12.14 (s, 1H), 7.58 – 7.50 (m, 2H), 7.28 – 7.21 (m, 4H), 7.17 (t, J = 7.1 Hz, 1H), 7.10 (t, J = 7.4 Hz, 1H), 4.90 (d, J = 6.3 Hz, 1H), 4.38 (d, J = 16.5 Hz, 1H), 4.18 (d, J = 16.6 Hz, 1H), 3.52 (d, J = 10.2 Hz, 1H), 3.45 (d, J = 16.1 Hz, 1H), 3.10 (ddt, J = 10.0, 6.3, 3.7 Hz, 1H), 3.03 – 2.90 (m, 2H), 2.05 – 1.59 (m, 9H), 1.58 – 0.95 (m, 10H). ^{13}C NMR (125 MHz, CDCl_3) δ 170.86, 156.14, 139.39, 134.30, 132.39, 128.99, 128.72, 126.65, 125.68, 125.45, 123.06, 119.53, 56.12, 55.90, 53.72, 47.44, 35.88, 35.40, 35.30, 33.64, 29.31, 25.82, 25.45, 25.25, 25.17, 25.12, 24.78. HRMS (ESI): calculated $[\text{M}+\text{H}]^+$ 459.3124; found 459.3121.



(4*R*,5*R*)-*N*-(*tert*-butyl)-4,5-diphenylimidazolidin-2-imine was synthesized over four synthetic steps according to a literature procedure.¹⁷ Starting from (1*R*,2*R*)-1,2-diphenylethane-1,2-diamine (1.06 g, 5.0 mmol) was obtained the title compound as colorless cubic crystals (167.1 mg ,

0.57 mmol, 11.4%). mp: 175-177 °C. Spectroscopic data was consisted with that previously reported: ^1H NMR (500 MHz, CDCl_3) δ 7.31 (dd, J = 8.6, 6.2 Hz, 4H), 7.28 – 7.19 (m, 6H), 4.58 (s, 2H), 1.43 (s, 9H). ^{13}C NMR (125 MHz, CDCl_3) δ 159.04, 144.17, 128.50, 127.21, 126.43, 51.07, 29.63.

Kinetic parameters used for COPASI model of palladium-catalyzed insertion into amine N–H bonds

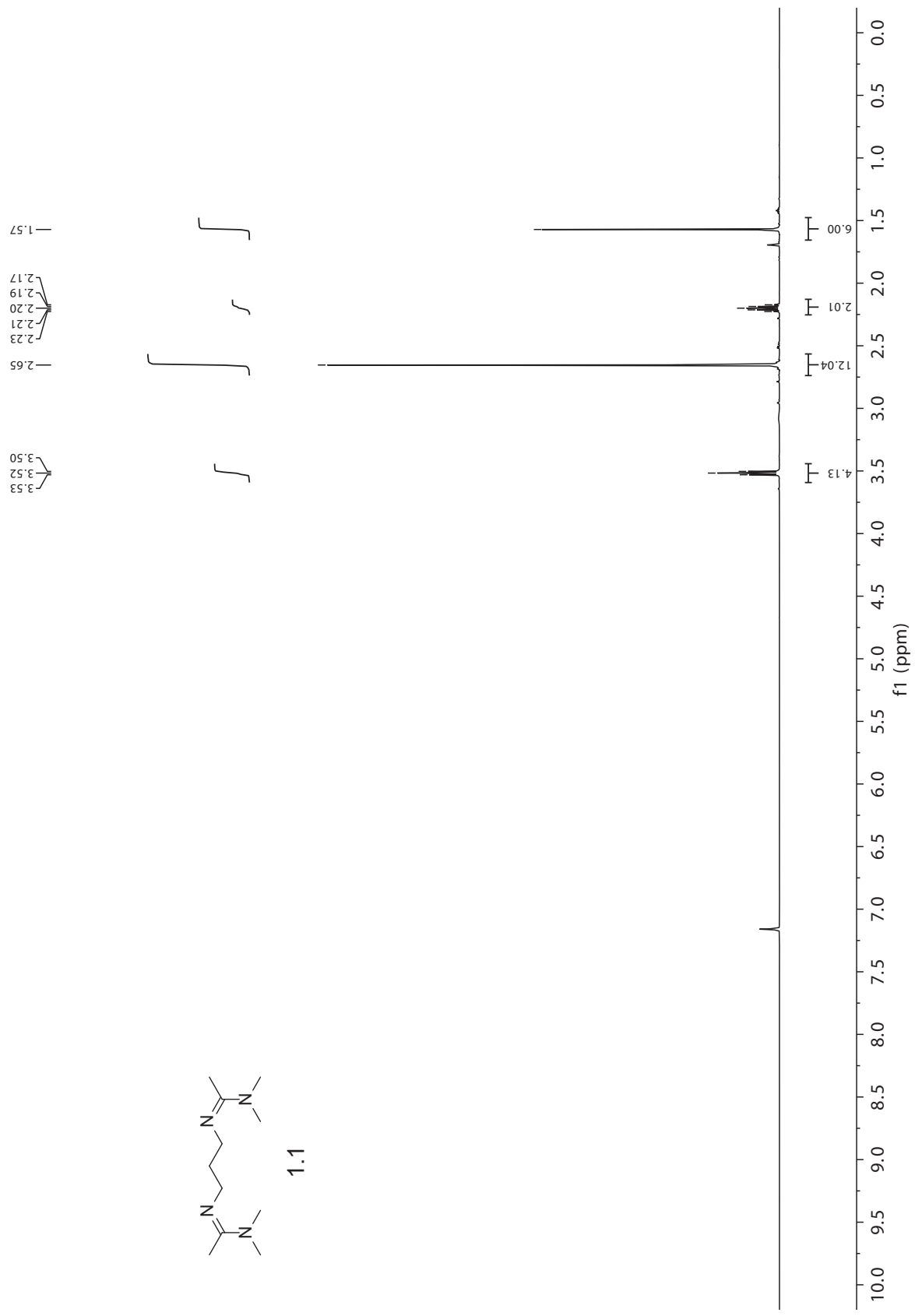
reaction	rate	unit	k_{rel}	
$\xrightarrow{k_1}$ Amine	1.38×10^{-5}	$M s^{-1}$	0.001	
$Pd + Amine \xrightleftharpoons[k_{-2}]{k_2} PdAmine$	6.88×10^2	$M^{-1}s^{-1}$	50,000	} $K_{eq} = 5 \times 10^3$
	1.38×10^{-1}	s^{-1}	10	
$Diazo + Pd \xrightarrow{k_3} PdCarbene$	1.38×10^{-2}	$M^{-1}s^{-1}$	1	
$PdCarbene + Amine \xrightarrow{k_4} Aminoester + Pd$	1.38×10^4	$M^{-1}s^{-1}$	1,000,000	
$PdCarbene + Diazo \xrightarrow{k_5} Side\ products + Pd$	1.38×10^{-1}	$M^{-1}s^{-1}$	10	

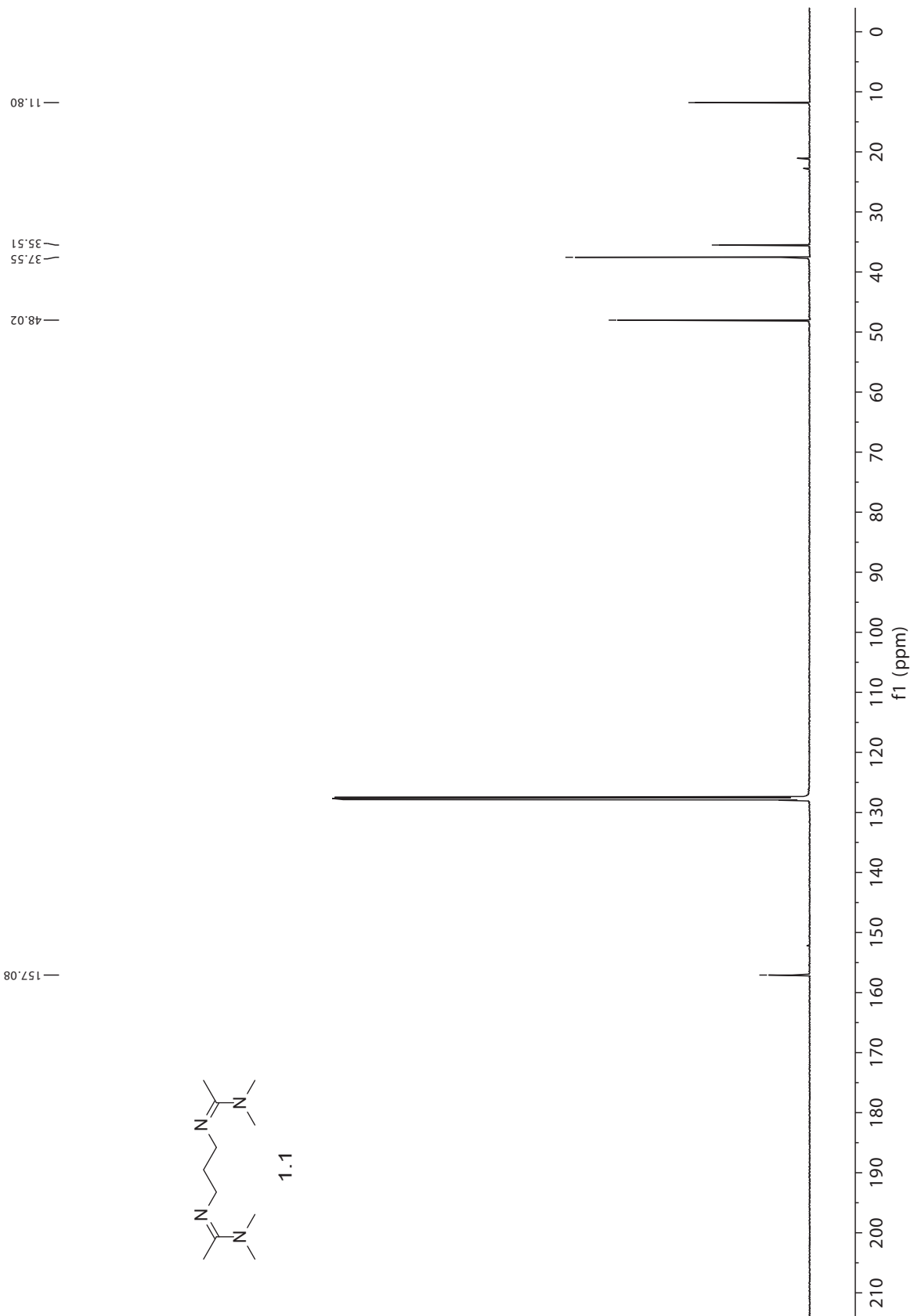
References

- ¹ Liu, B.; Zhu, S-F.; Zhang, W.; Chen, C.; Zhou, Q-L. "Highly Enantioselective Insertion of Carbenoids into N–H Bonds Catalyzed by Copper Complexes of Chiral Spiro Bisoxazolines." *J. Am. Chem. Soc.*, **2007**, *129*, 5834–5835.
- ² Bachmann, S.; Fielenbach, D.; Jørgensen, K. "Cu(I)-Carbenoid- and Ag(I)-Lewis Acid-catalyzed Asymmetric Intermolecular Insertion of α -Diazo Compounds into N–H Bonds." *Org. Biomol. Chem.* **2004**, *2*, 3044–3049.
- ³ Arredondo, V.; Hiew, S.; Gutman, E.; Premachandra, I.D.U.A.; Van Vranken, D.L. "Enantioselective Palladium-Catalyzed Carbene Insertion into the N–H Bonds of Aromatic Heterocycles." *Angew. Chem. Int. Ed.* **2017**, *56*, 4156–4159.
- ⁴ a) Crossing, I.; Raabe, I. "Noncoordinating Anions–Fact or Fiction? A Survey of Likely Candidates." *Angew. Chem. Int. Ed.* **2004**, *43*, 2066–2090; b) Nishida, H.; Takada, N.; Yoshiura, M.; Sonoda, T.; Kobayashi, H. "Tetrakis(3,5-bis(trifluoromethyl)phenyl)borate. Highly Lipophilic Stable Anionic Agent for Solvent-Extraction of Cations." *Bull. Chem. Soc. Jpn.*, **1984**, *57*, 2600–2604.
- ⁵ Doyle, M.P.; Leusen, D. V.; Tamblin, W. "Efficient Alternative Catalysts and Methods for the Synthesis of Cyclopropanes from Olefins and Diazo Compounds". *Synthesis*, **1981**, *10*, 787–789.
- ⁶ Zhu, Y.; Liu, X.; Dong, S.; Zhou, Y.; Li, W.; Lin, L.; Feng, X. "Asymmetric N–H Insertion of Secondary and Primary Anilines Under the Catalysis of Palladium and Chiral Guanidine Derivatives." *Angew. Chem. Int. Ed.* **2014**, *53*, 1636–1640.
- ⁷ Cinchona alkaloids have been shown previous to induce asymmetry in related N–H insertion processes: Saito, H.; Morita, D.; Uchiyama, T.; Miyake, M.; Shinichi, M. "Cinchona Alkaloids Induce Asymmetry in the Insertion Reaction of Thermally Generated Carbenes into N-H Bonds". *Tetrahedron Lett.* **2012**, *53*, 6662–6664.
- ⁸ Wang, Y.; Zhu, Y.; Chen, Z.; Mi, A.; Hu, W.; Doyle, M. "A Novel Three-Component Reaction Catalyzed by Dirhodium(II) Acetate: Decomposition of Phenyl diazoacetate with Arylamine and Imine for Highly Diastereoselective Synthesis of 1,2-Diamines." *Org. Lett.* **2003**, *5*, 3923–3926.
- ⁹ Wang, Y.; Chen, Z.; Mi, A.; Hu, W. "Novel C–C Bond Formation Through Addition of Ammonium Ylides to Arylaldehydes: a Facile Approach to β -Aryl- β -hydroxy α -Amino Acid Frameworks." *Chem. Commun.*, **2004**, 2486–2487.
- ¹⁰ Zhu, Y.; Zhai, C.; Yue, Y.; Yang, L. Hu, W. "One-pot Three-component Tandem Reaction of Diazo Compounds with Anilines and Unsaturated Ketoesters: a Novel Synthesis of 2,3-Dihydropyrrrole Derivatives." *Chem. Commun.*, **2009**, 1362–1364.
- ¹¹ Huang, H.; Wang, Y.; Chen, Z.; Hu, W. "Rhodium-Catalyzed, Three-Component Reaction of Diazo Compounds with Amines and Azodicarboxylates." *Adv. Synth. Catal.* **2005**, *347*, 531–534.
- ¹² Liang, Y.; Zhou, H.; Yu, Z-X. "Why is Copper(I) Complex More Competent Than Dirhodium(II) Complex in Catalytic Asymmetric O–H Insertion Reactions? A Computational Study of the Metal Carbenoid O–H Insertion into Water." *J. Am. Chem. Soc.* **2009**, *131*, 17783–17785.
- ¹³ Kluwer, A. M.; Elsevier, C. J.; Bühl, M.; Lutz, M.; Spek, A. L. "Zero-Valent Palladium Complexes with Monodentate Nitrogen σ -Donor Ligands" *Angew. Chem. Int. Ed.* **2003**, *42*, 3501–3504.
- ¹⁴ Widenhoefer, R.; Buchwald, S. "Halide and Amine Influence in the Equilibrium Formation of Palladium Tris(o-tolyl)phosphine Mono(amine) Complexes from Palladium Aryl Halide Dimers." *Organometallics*, **1996**, *15*, 2755–2763.
- ¹⁵ Ihara, E.; Haida, N.; Iio, M.; Inoue, K. "Palladium-Mediated Polymerization of Alkyl Diazoacetates To Afford Poly(alkoxycarbonylmethylene)s. First Synthesis of Polymethylenes Bearing Polar Substituents." *Macromolecules*, **2003**, *36*, 36–41.
- ¹⁶ Tang, Y.; Chen, Q.; Liu, X.; Wang, G.; Lin, L.; Feng, X. "Direct Synthesis of Chiral Allenolates from the Asymmetric C–H Insertion of α -Diazoesters into Terminal Alkynes." *Angew. Chem. Int. Ed.* **2015**, *54*, 9512–9516.
- ¹⁷ Fukada, I.; Seki, T.; Ishikawa, Y. "Modified Guanidines as Potential Chiral Superbases. @. Preparation of 1,3-Unsubstituted and 1-Substituted 2-Iminoimidazolidine Derivatives and a Related Guanidine by the 2-Chloro-1,3-dimethylimidazolinium Chloride-Induced Cyclization of Thioureas." *J. Org. Chem.* **2000**, *65*, 7774–7778.

-
- ¹⁸ Kochi, J.K.; Singleton, E.A.; "Autoxidation of *N*-Alkylisoindolines. Solvent Effects and Mechanisms". *Tetrahedron*, **24**, **1968**, 24, 4649–4665.
- ¹⁹ Tessier, P.; Leit, S.; Smil, D.; Deziel, R.; Ajamian, A.; Chantigny, Y. A. "Inhibitors of Histone Deacetylase." U.S. Patent 2009/181943. $IC_{50} < 15 \mu\text{M}$. See compound 5–42 on pages 85 and 191.
- ²⁰ Sparling, B. A.; Yi, S.; Able, J.; Bregman, H.; DiMauro, E. F.; Foti, R. S.; Gao, H.; Guzman-Perez, A.; Huang, H.; Jarosh, M.; Kornecook, T.; Ligutti, J.; Milgram, B. C.; Moyer, B. D.; Youngblood, B.; Yu, V. L.; Weiss, M. M. "Discovery and Hit-to-Lead Evaluation of Piperazine Amides as Selective, State-Dependent Nav1.7 inhibitors". *MedChemComm*, **2017**, 744–754.
- ²¹ van Dongen, M. J. P.; Kadam, R. U.; Juraszek, J.; Lawson, E.; Brandenburg, B.; Schmitz, F.; Schepens, W. B. G.; Stoops, B.; van, Diepen, H. A.; Jongeneelen, M.; Tang, C.; Vermond, J.; van Eijgen-Obregoso Real, A.; Blokland, S.; Garg, D.; Yu, W.; Goutier, W.; Lanckacker, E.; Klap, J. M.; Peeters, D. C. G.; Wu, J.; Buyck, C.; Jonckers, T. H. M.; Roymans, D.; Roevens, P.; Vogels, R.; Koudstaal, W.; Friesen, R. H. E.; Raboisson, P.; Dhanak, D.; Goudsmit, J.; Wilson, I. A. "A small-molecule fusion inhibitor of influenza virus is orally active in mice." *Science* **2019**, 363, eaar6221.
- ²² Vanecko, J.; Wan, H.; West, F. "Recent Advances in the Stevens Rearrangement of Ammonium Ylides. Application to the Synthesis of Alkaloid Natural Products." *Tetrahedron*, **2006**, 62, 1043–1062.
- ²³ Hansen, S.; Spangler, J.; Hansen, Jørn.; Davies, H. "Metal-Free N–H Insertions of Donor/Acceptor Carbenes." *Org. Lett.* **2012**, 14, 4626–4629.
- ²⁴ Hoops, S.; Sahle, S.; Gauges, R.; Lee, C.; Pahle, J.; Simus, N.; Singhal, M.; Xu, L.; Mendes, P.; Kummer, U. "COPASI: a COMplex PATHway Simulator." *Bioinformatics*, **2006**, 22, 3067–3074.
- ²⁵ Widenhoefer and Buchwald (ref. 14) measured the binding constant of benzylamine to an aryl palladium species at $K_{\text{eq}} = 6 \times 10^3$. Other rate constants were chosen based on upper and lower limits reported in previous literature, and to be consistent with experimental observations.

^1H NMR and ^{13}C NMR Spectra for Characterized Compounds



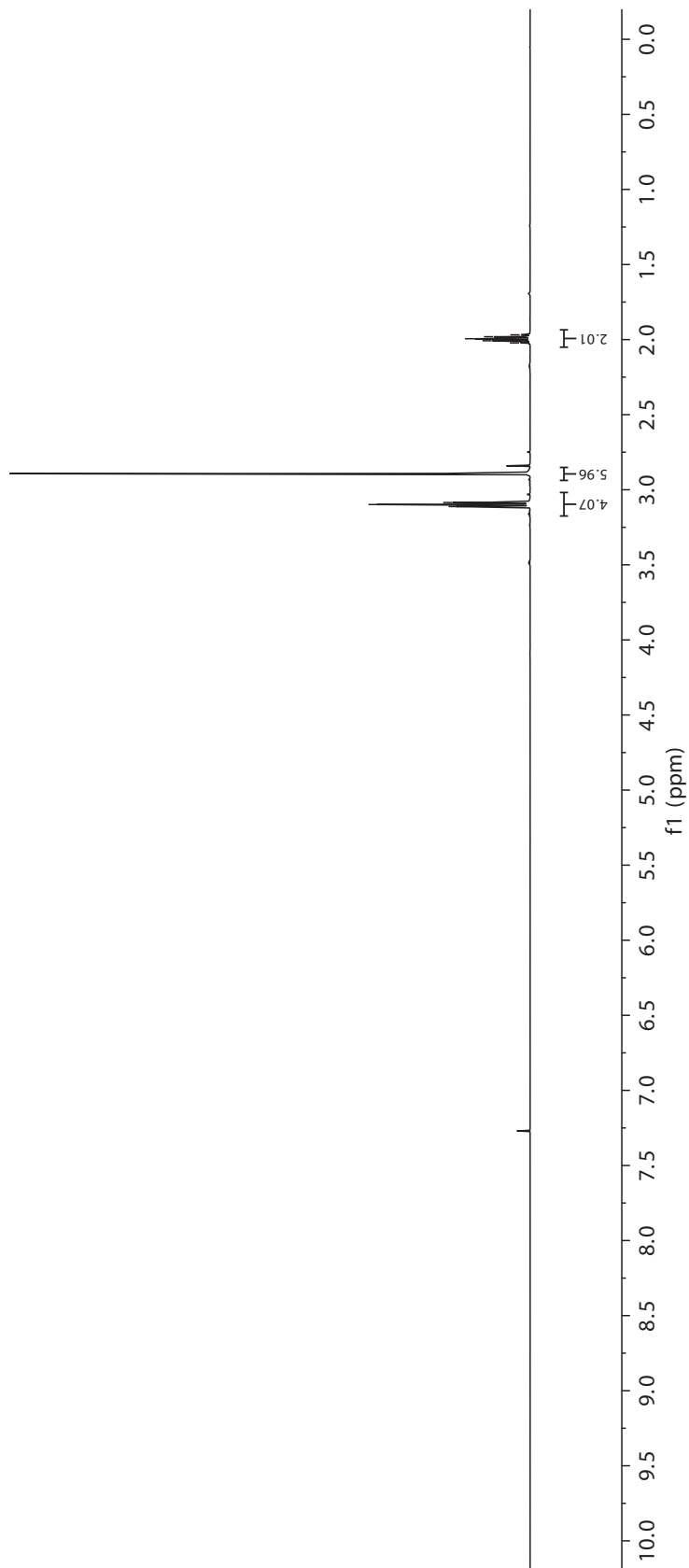


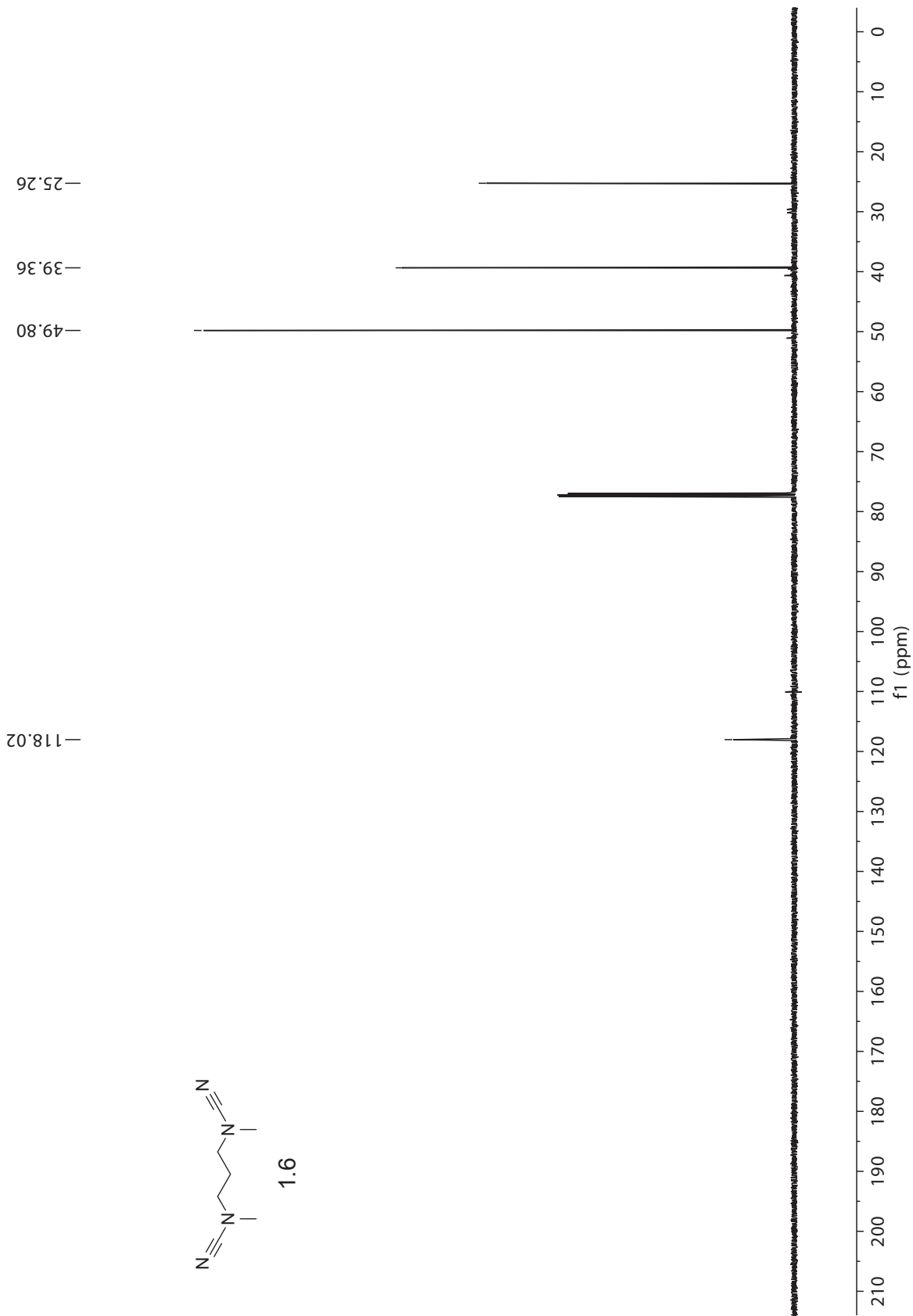
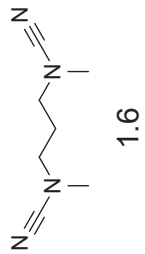


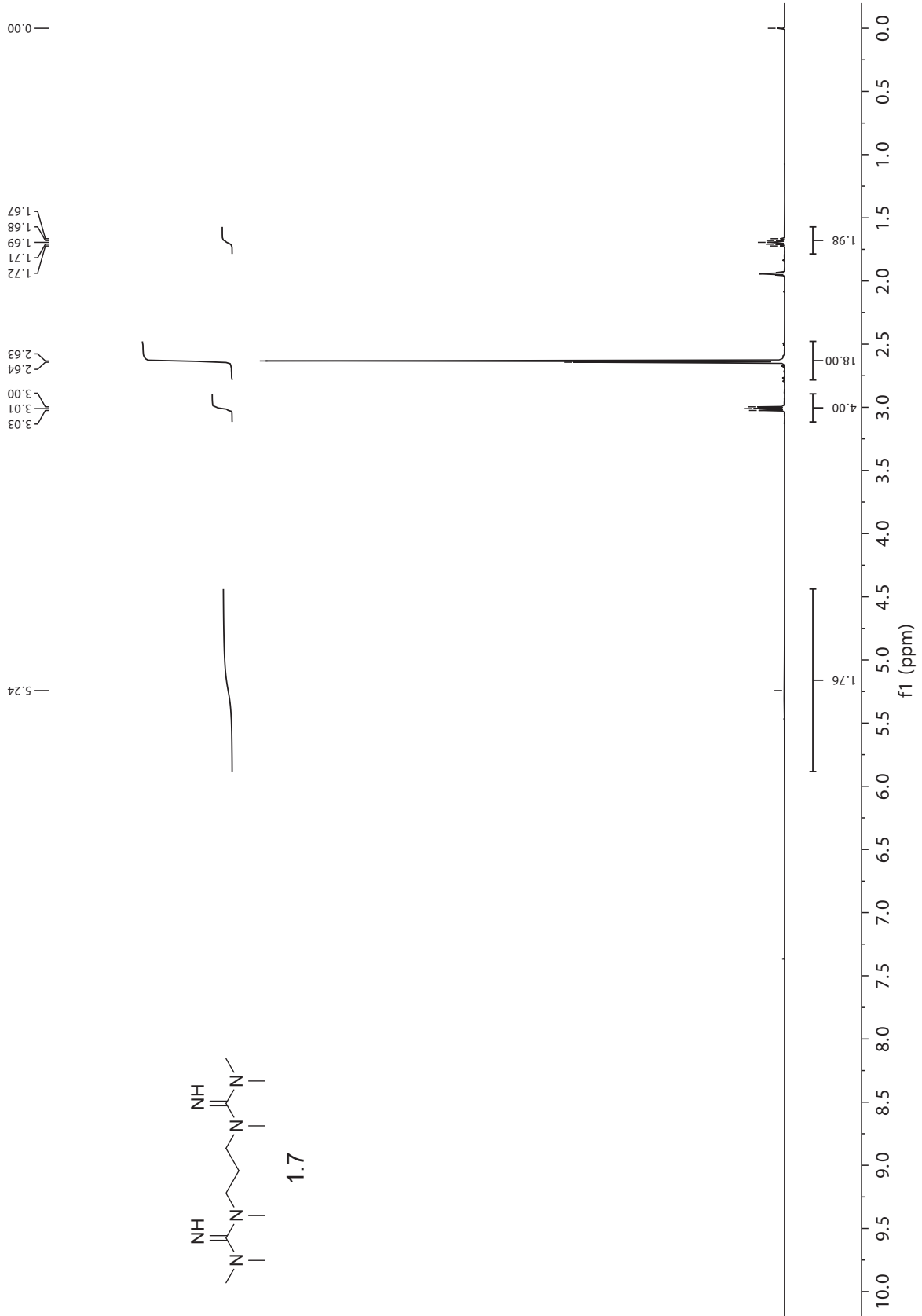
1.6

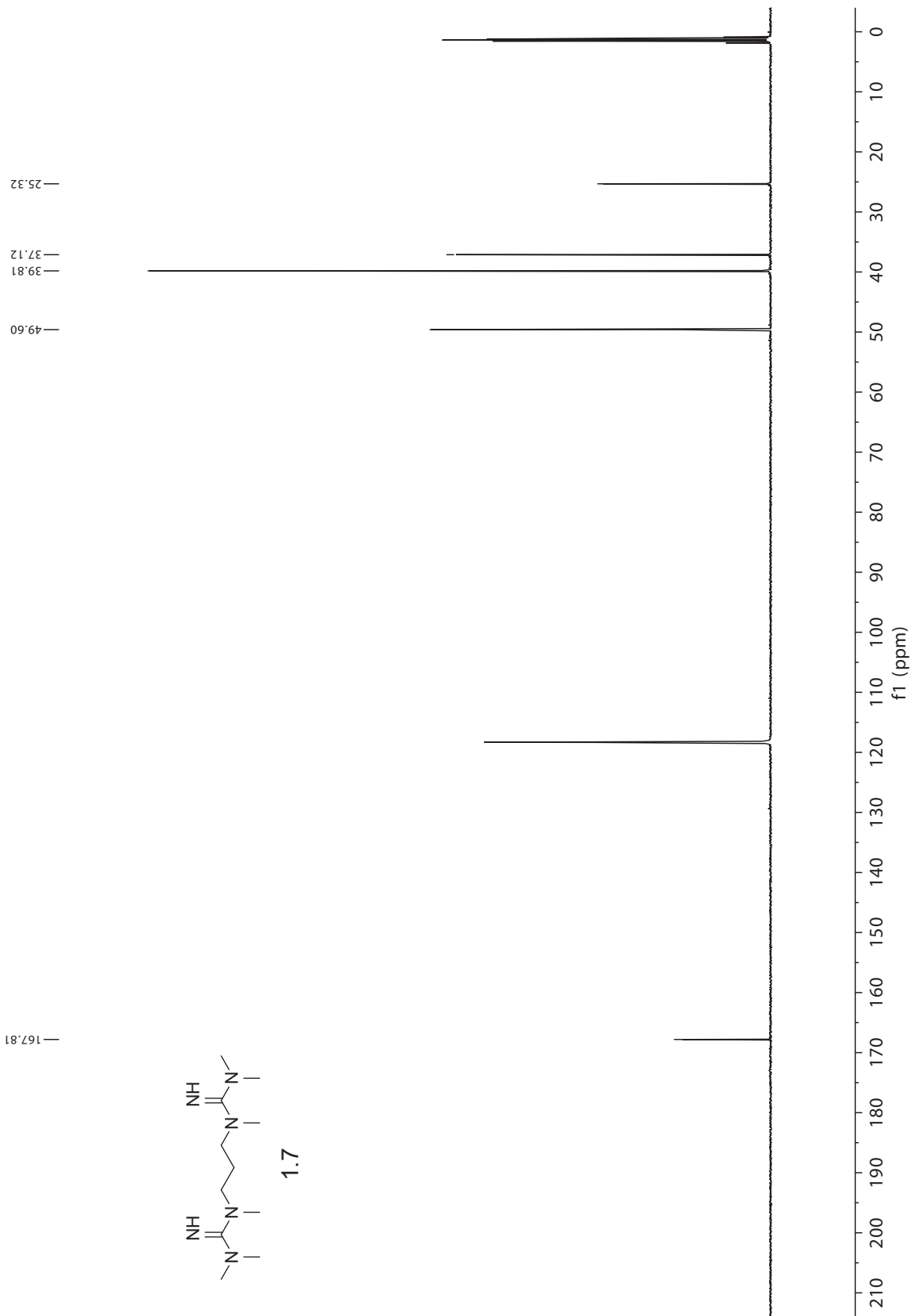
2.02
2.01
1.99
1.98
1.97

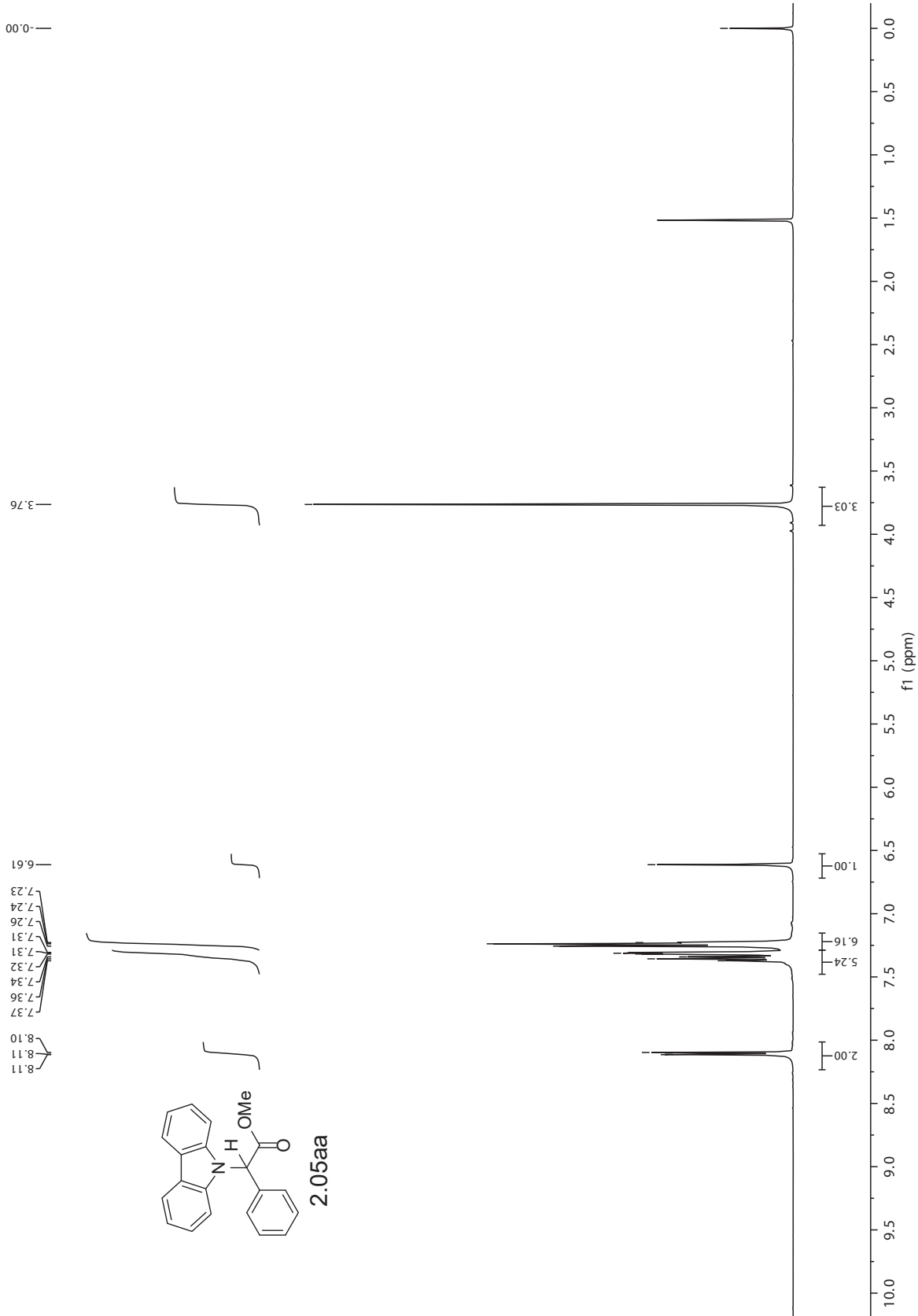
3.11
3.10
3.08
2.89

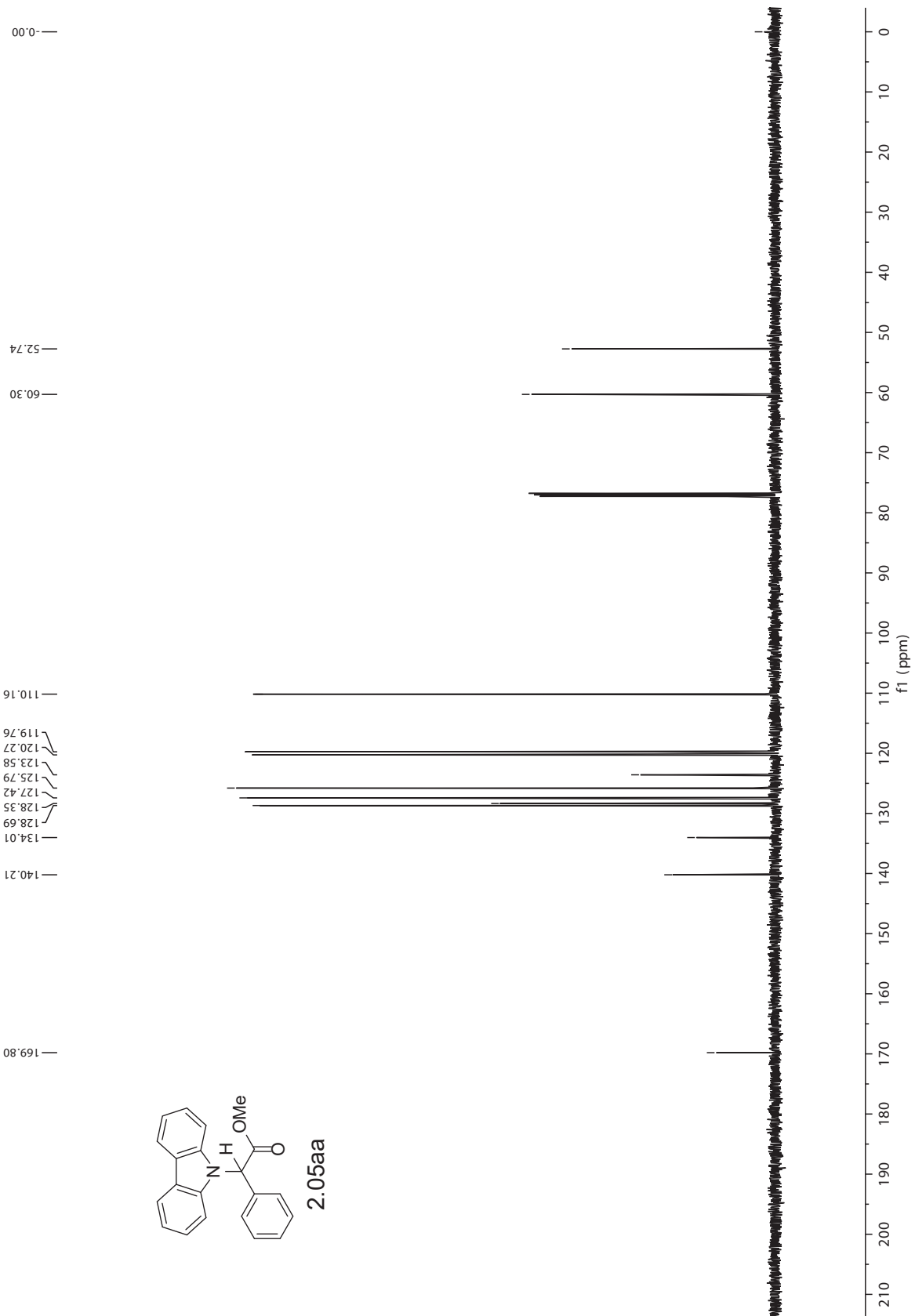


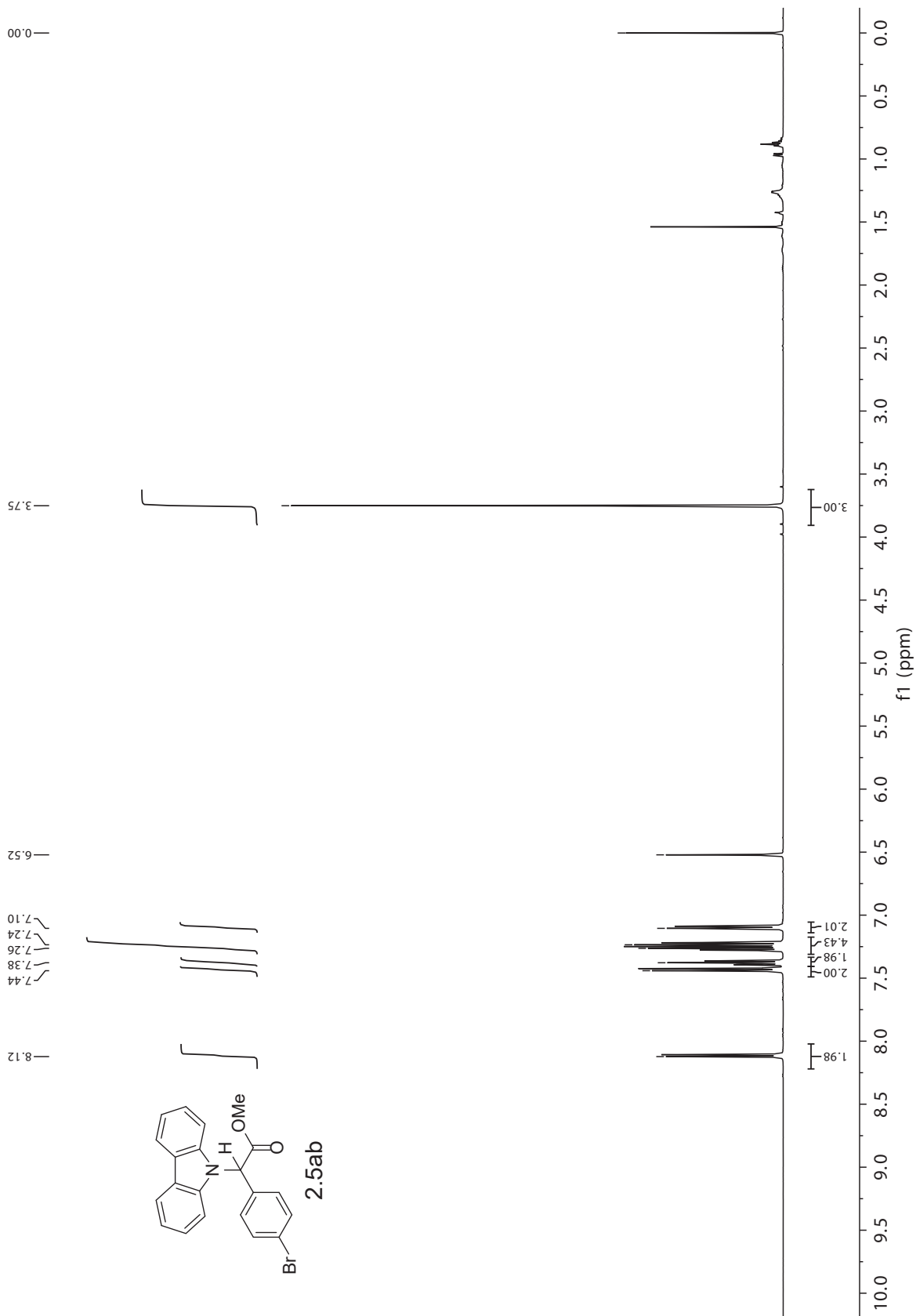


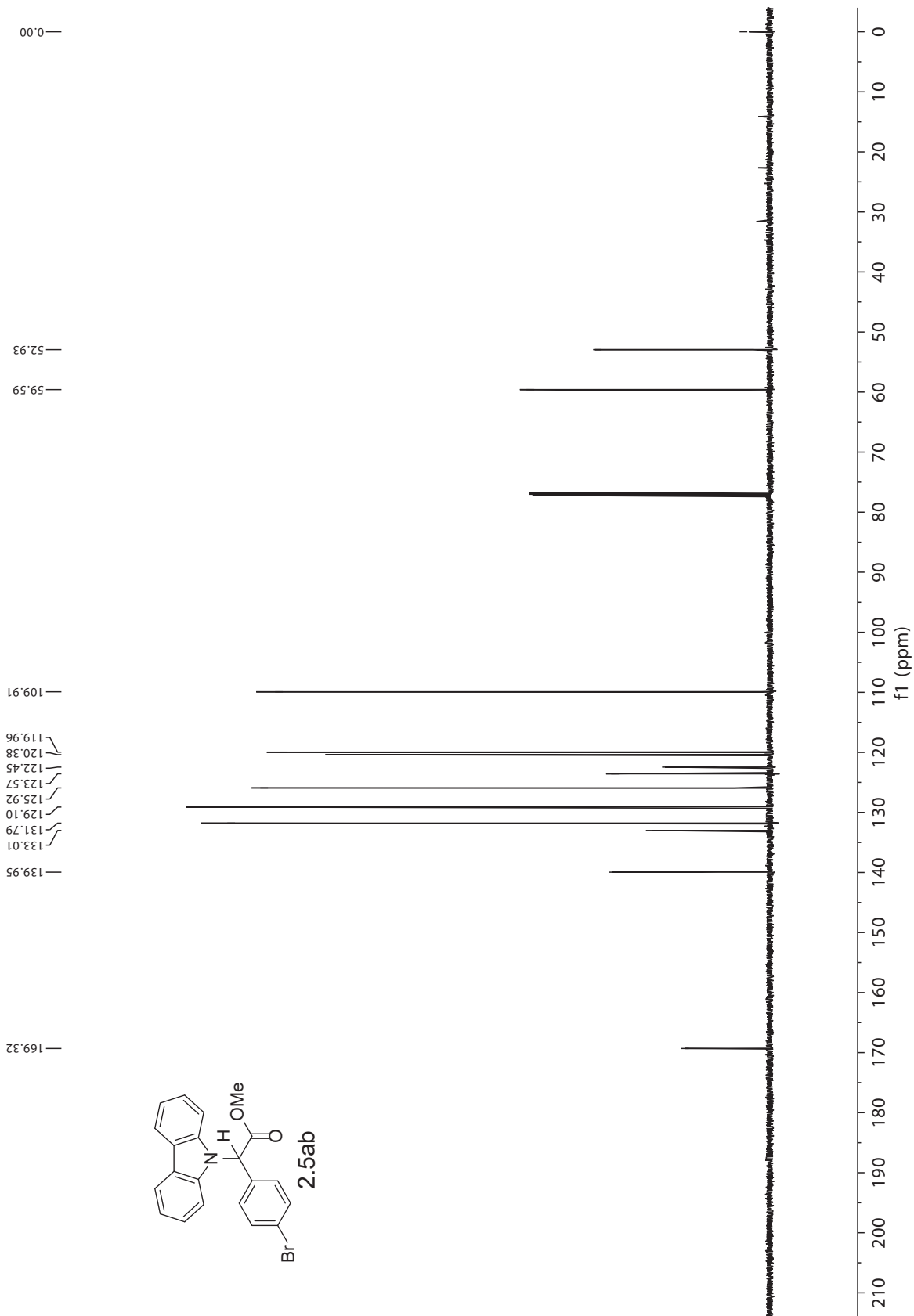


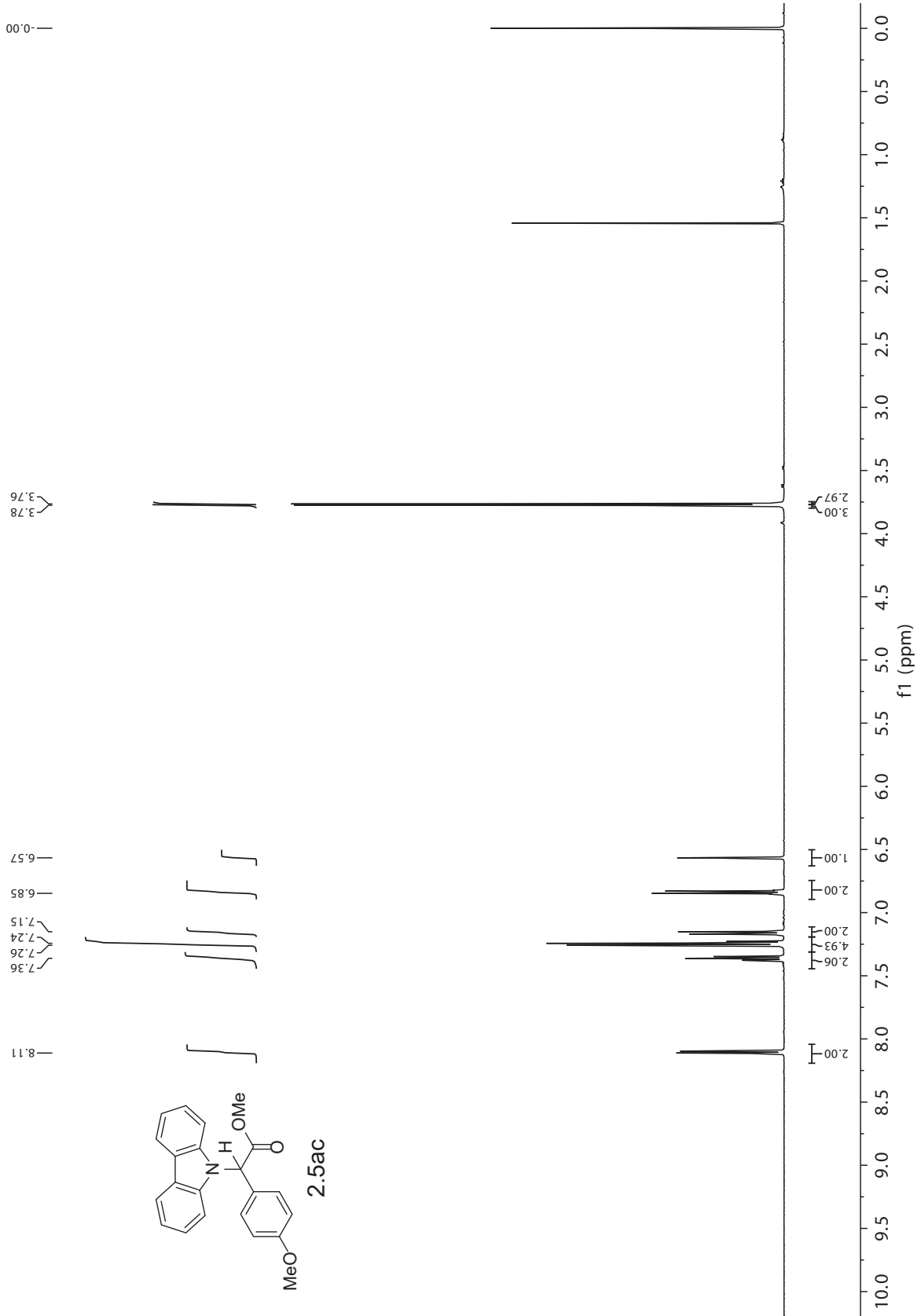


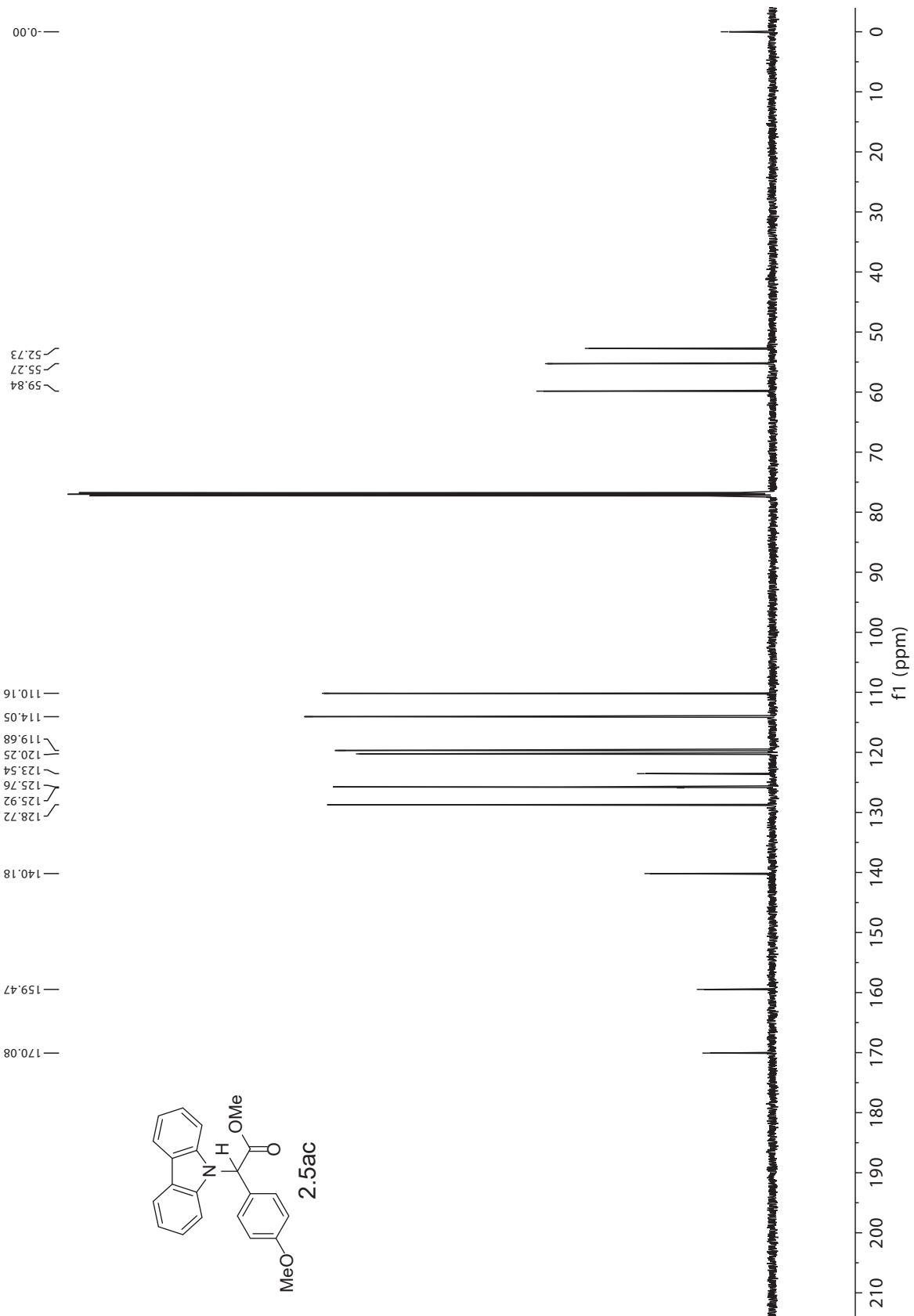


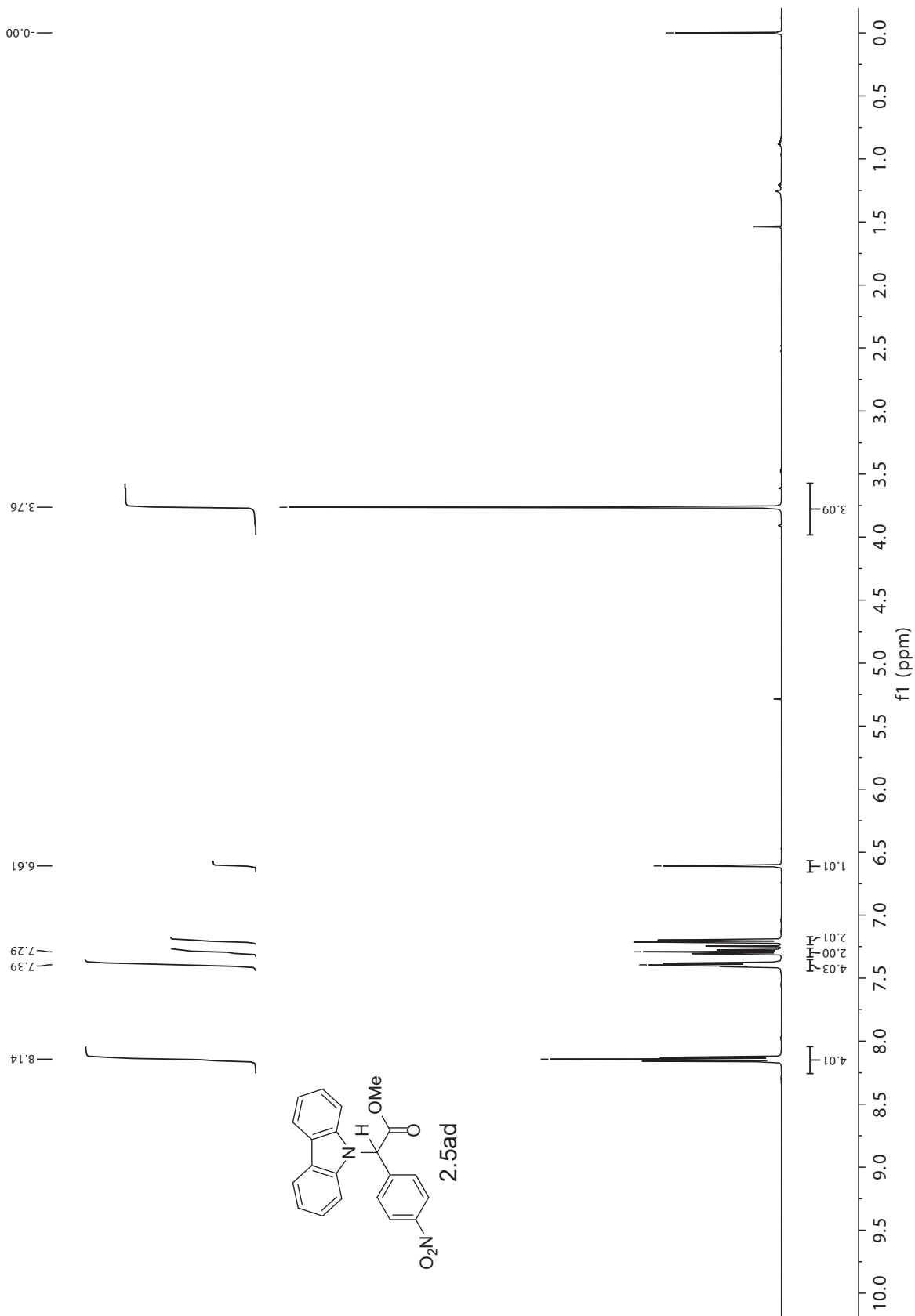


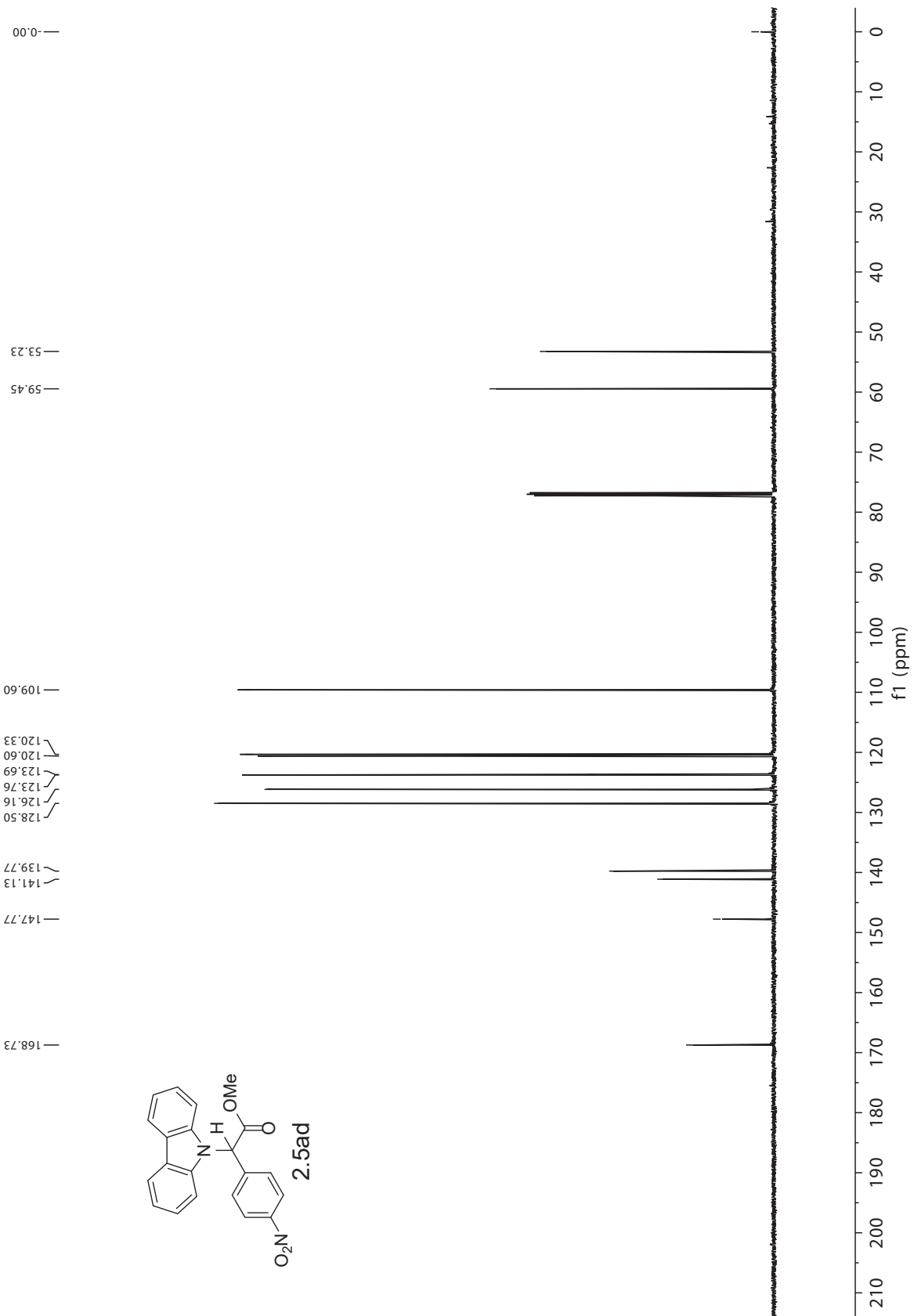


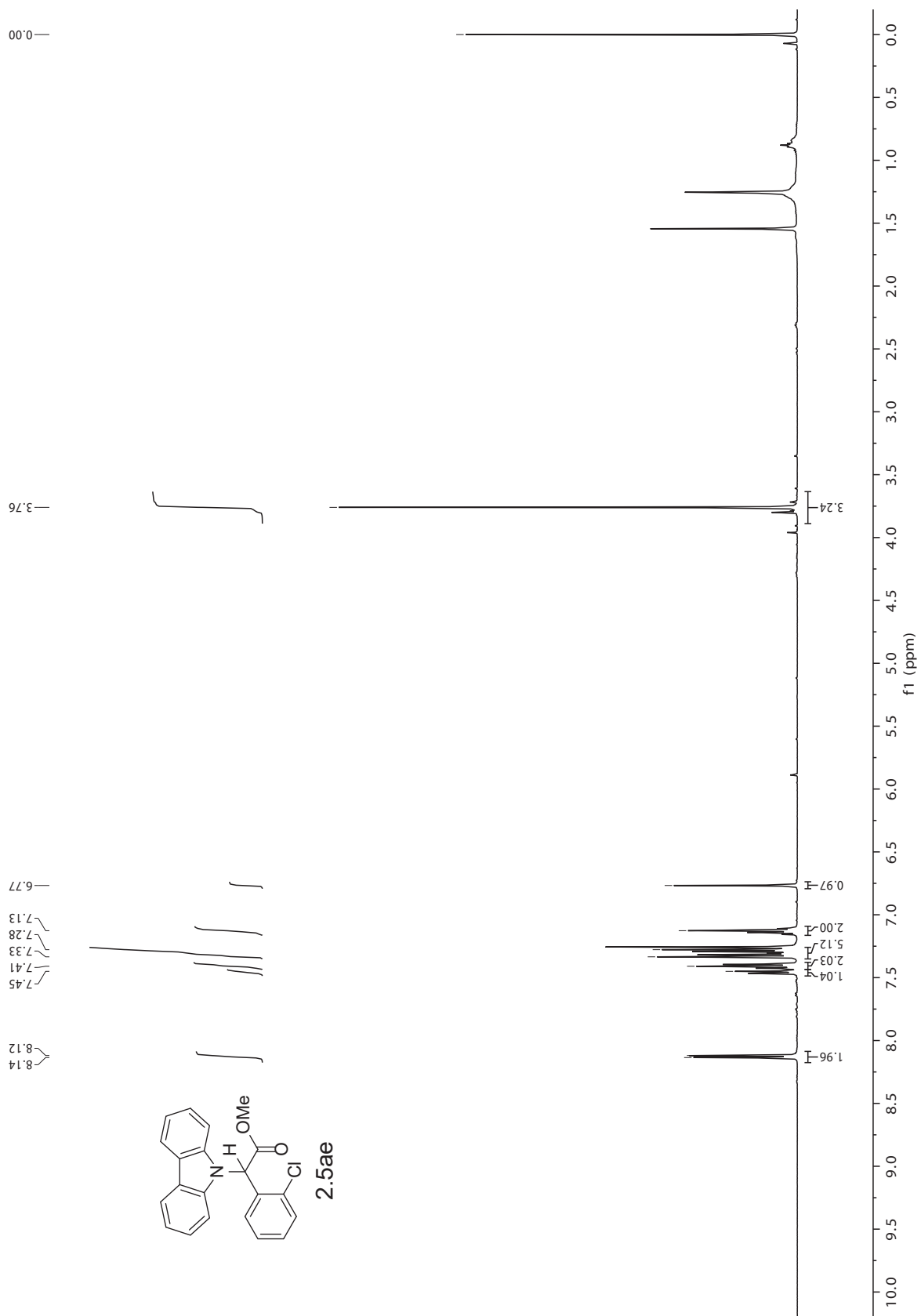


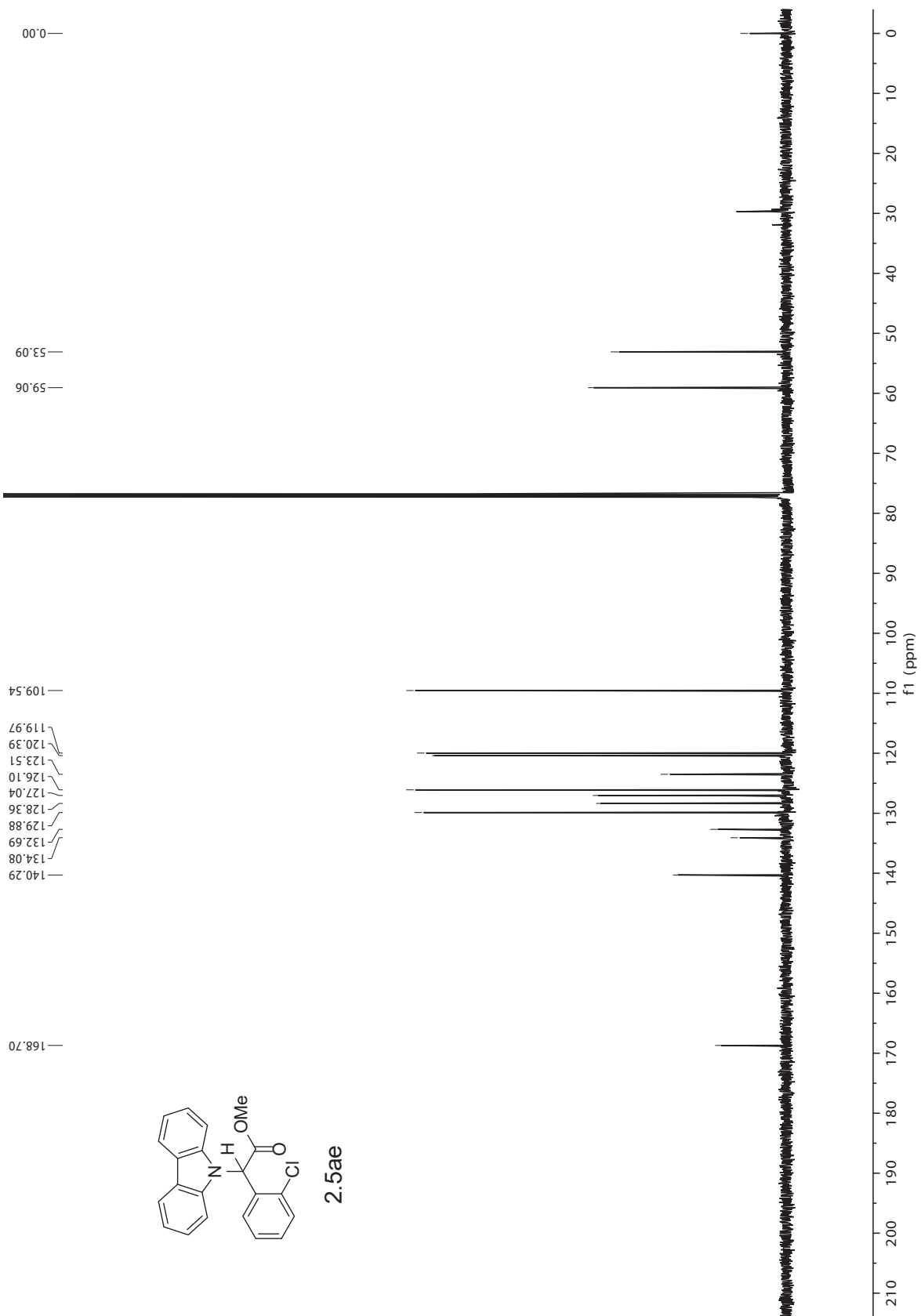


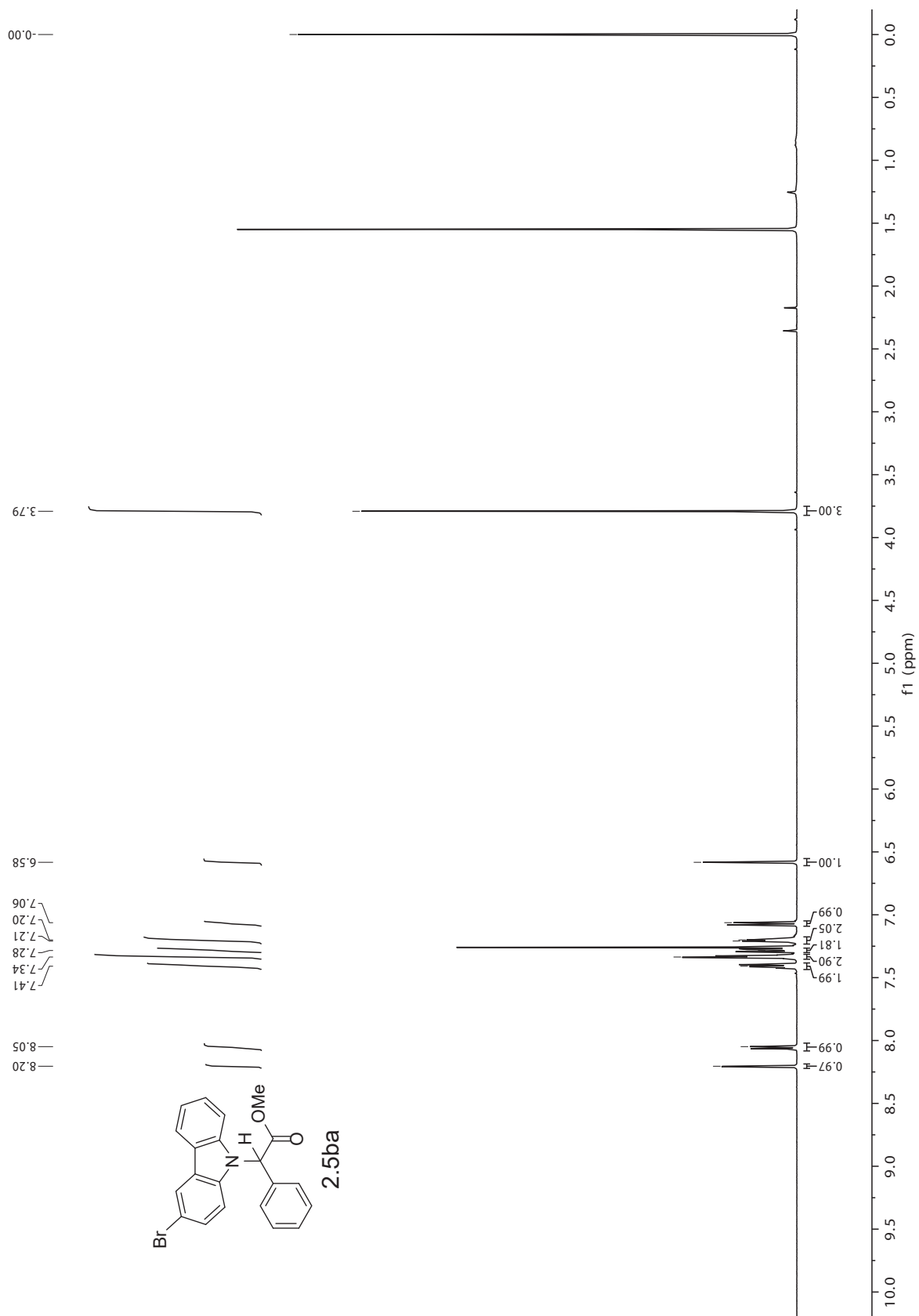


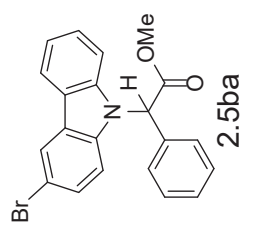
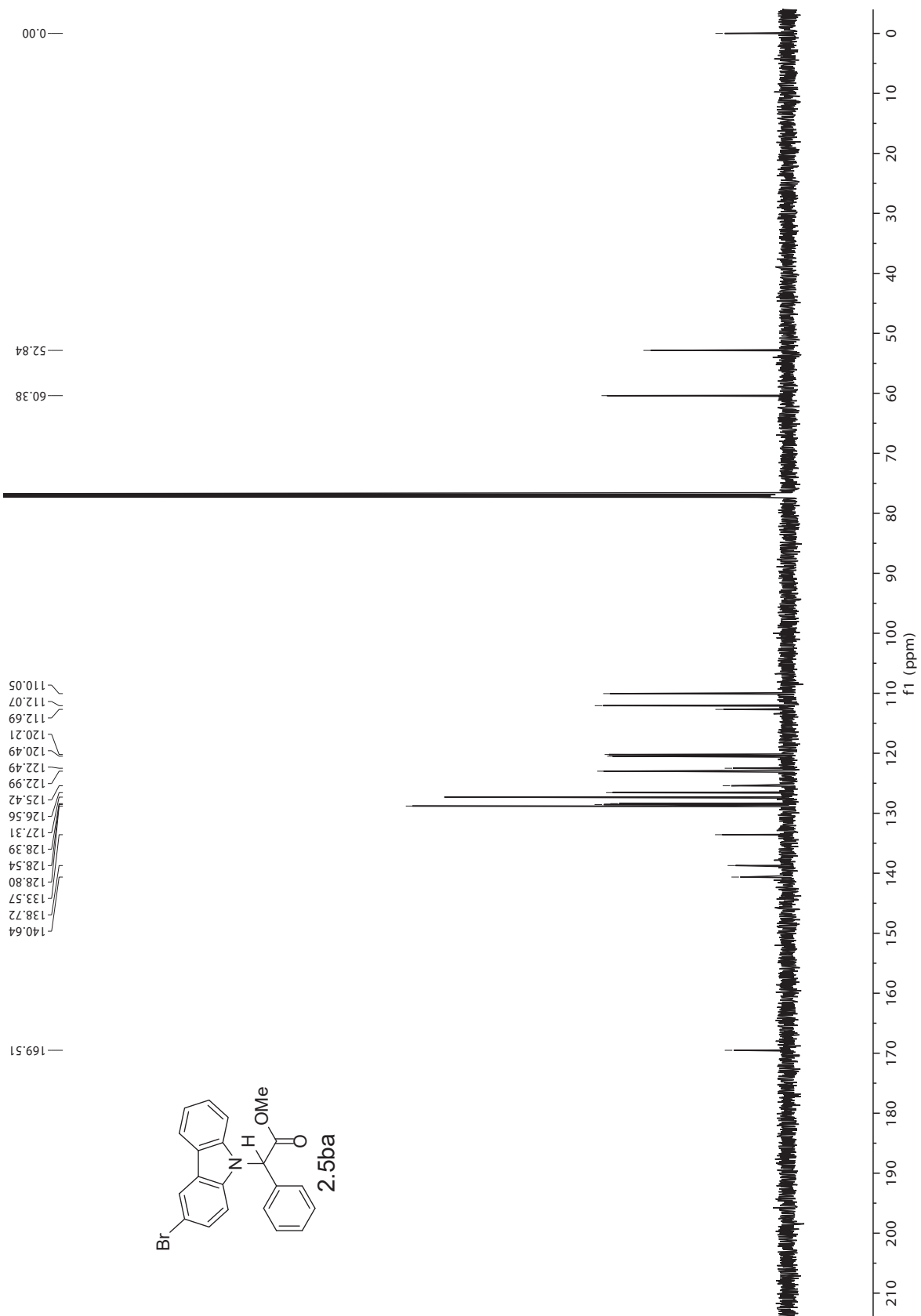


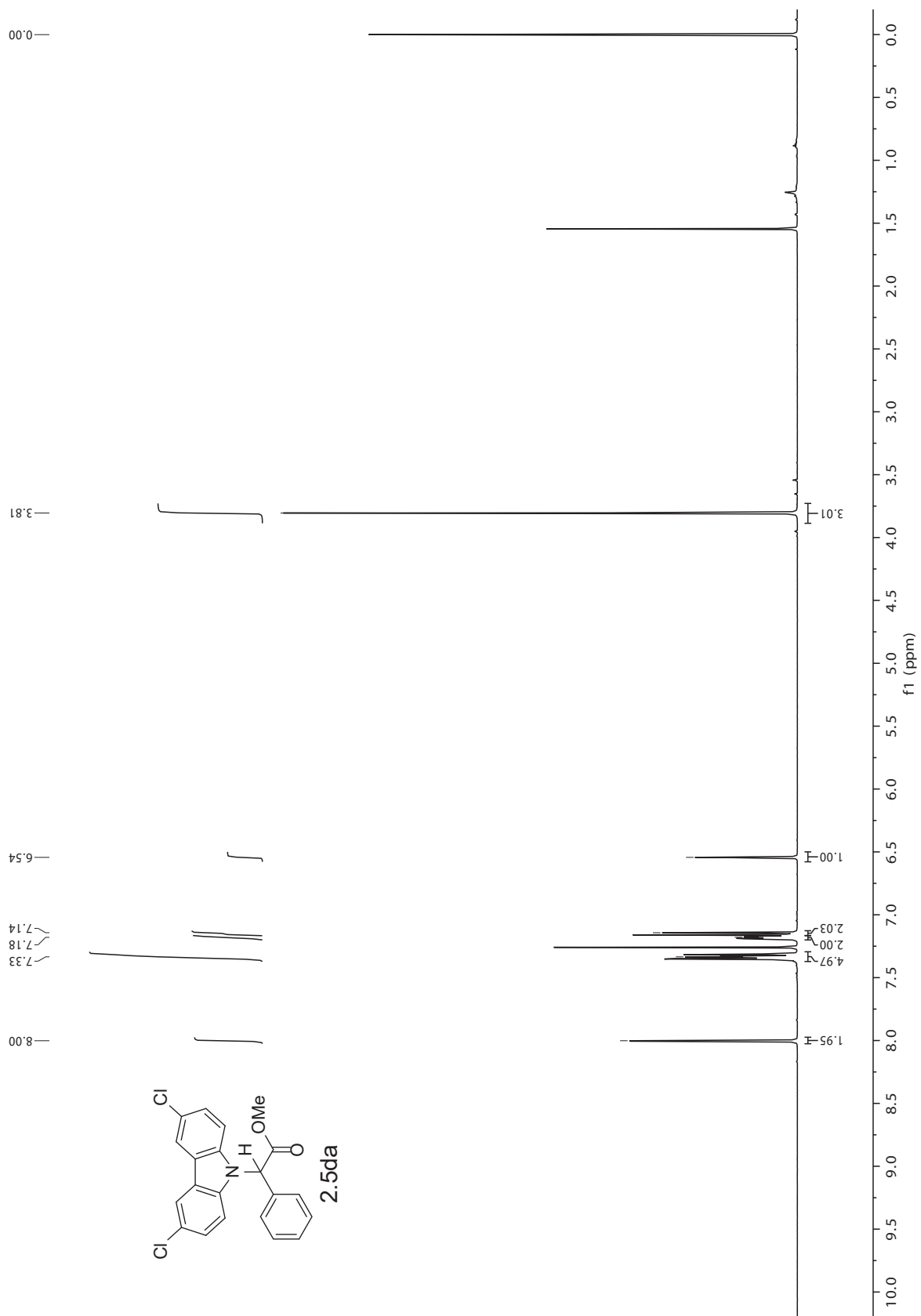


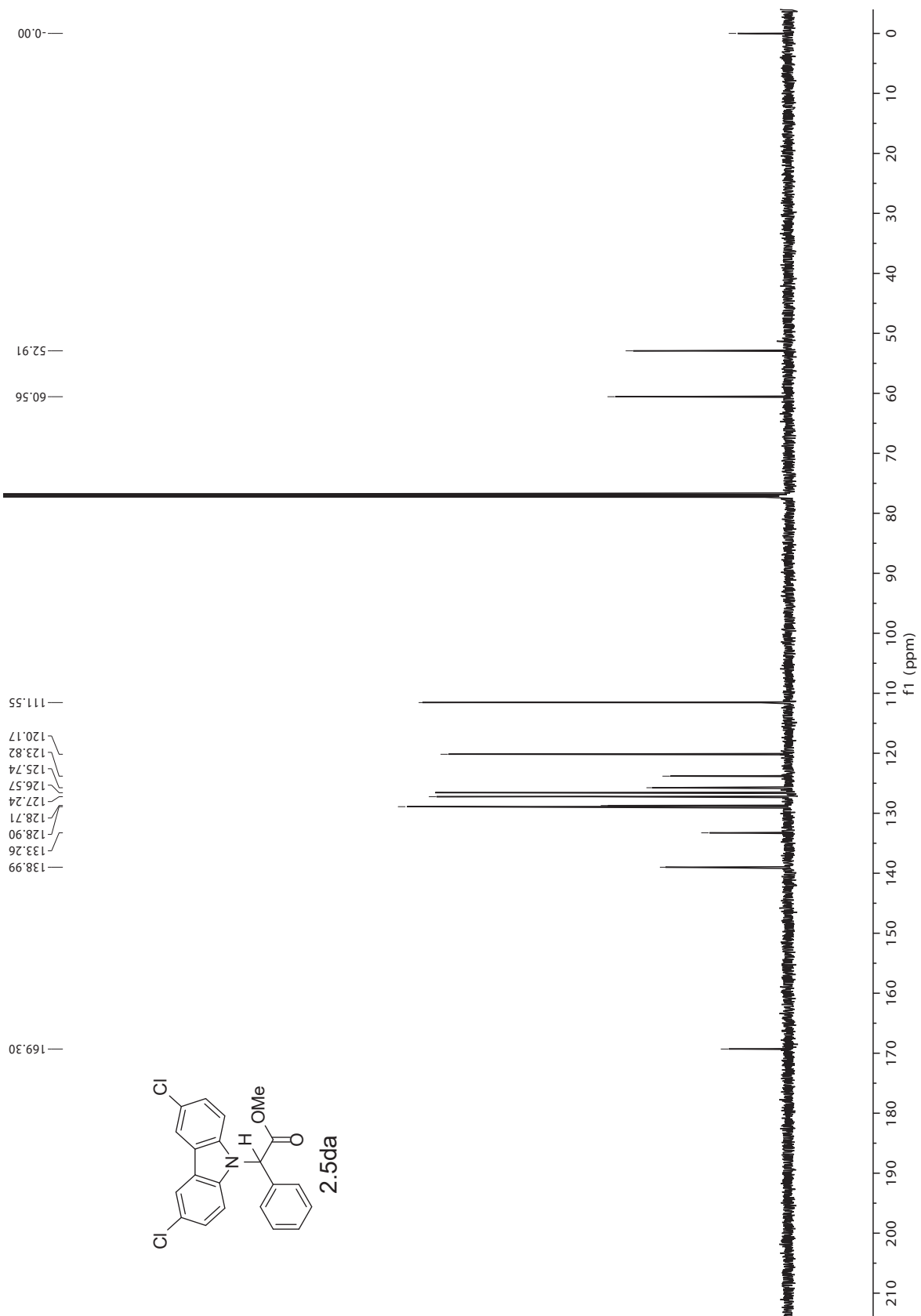


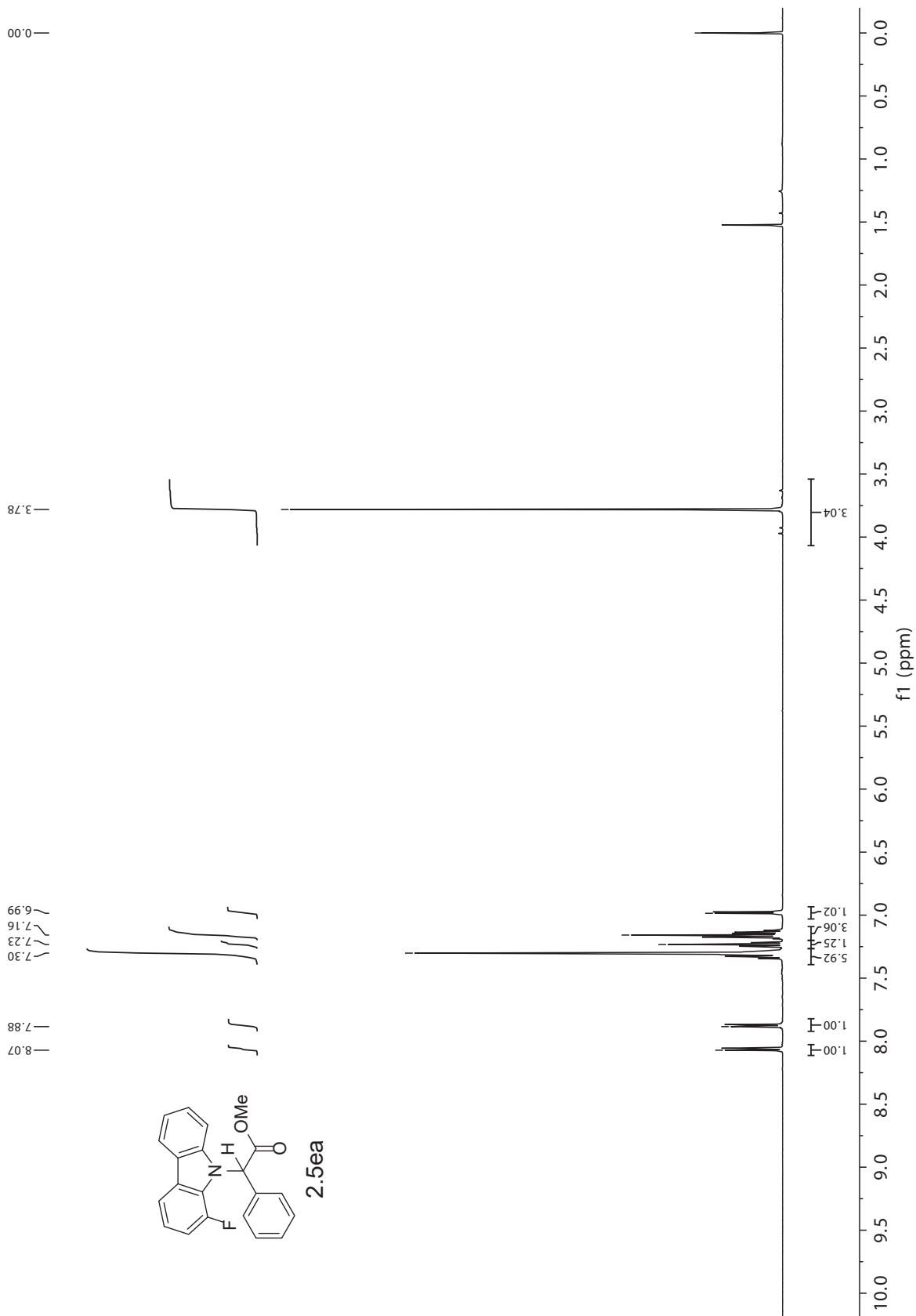


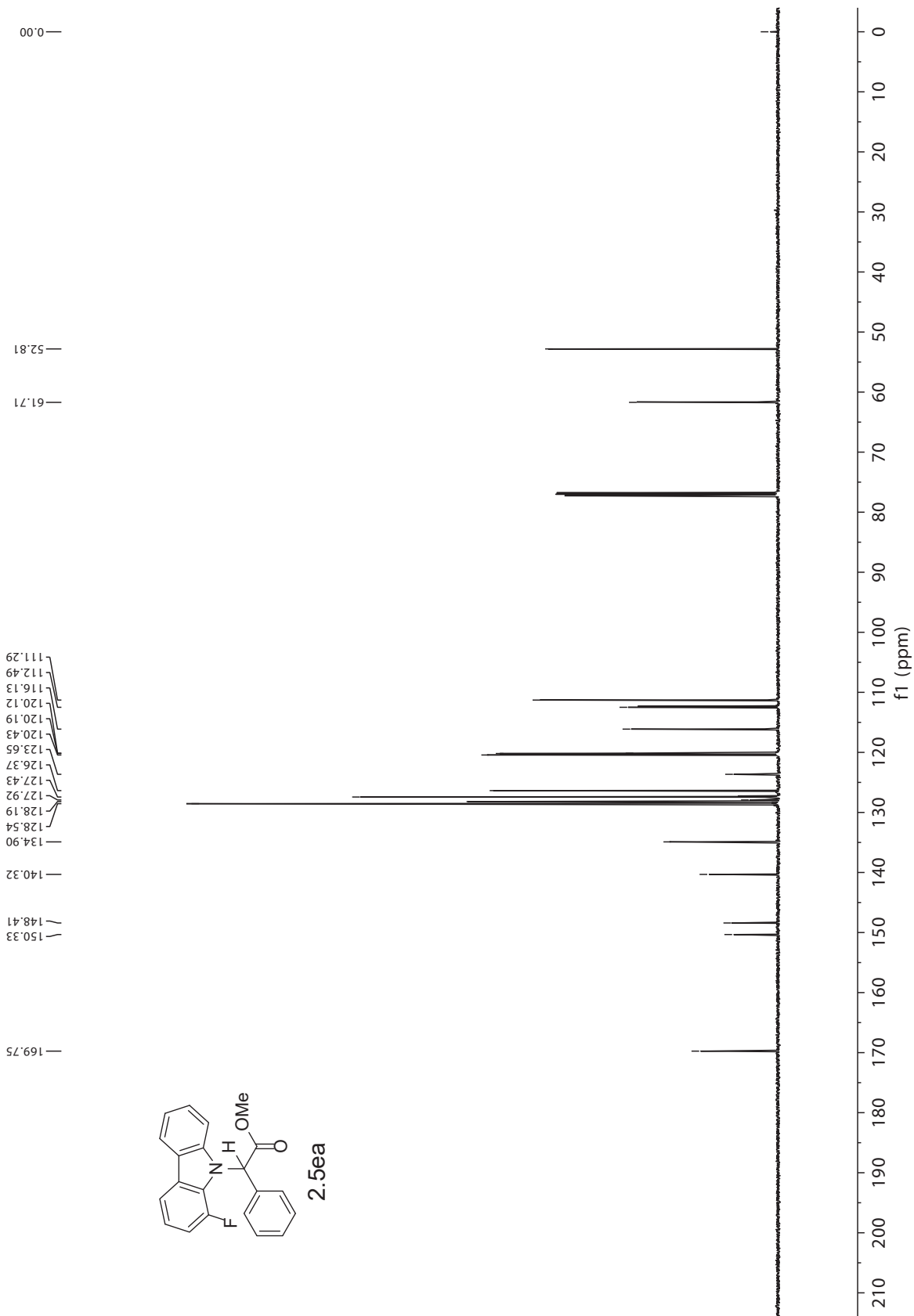


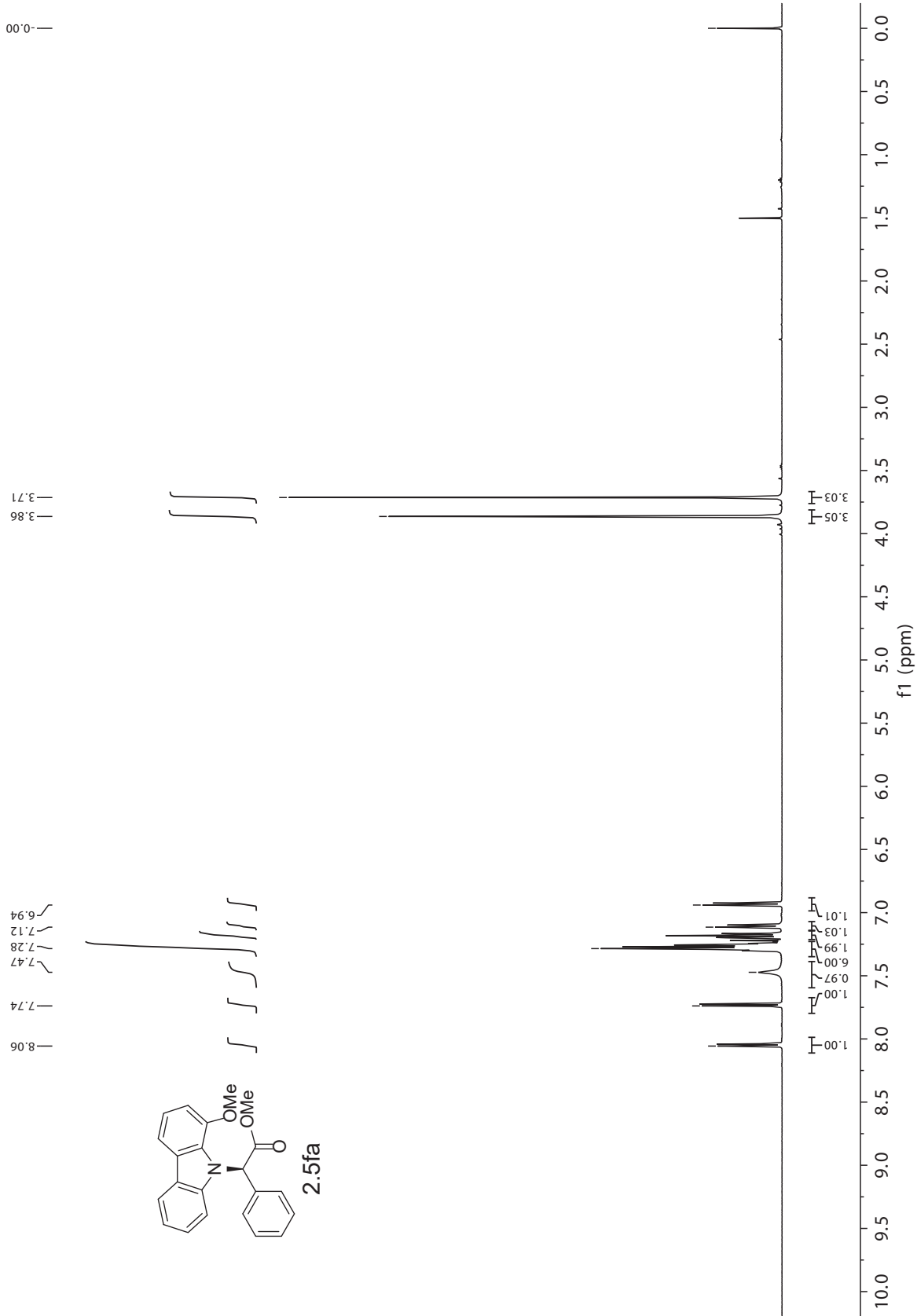


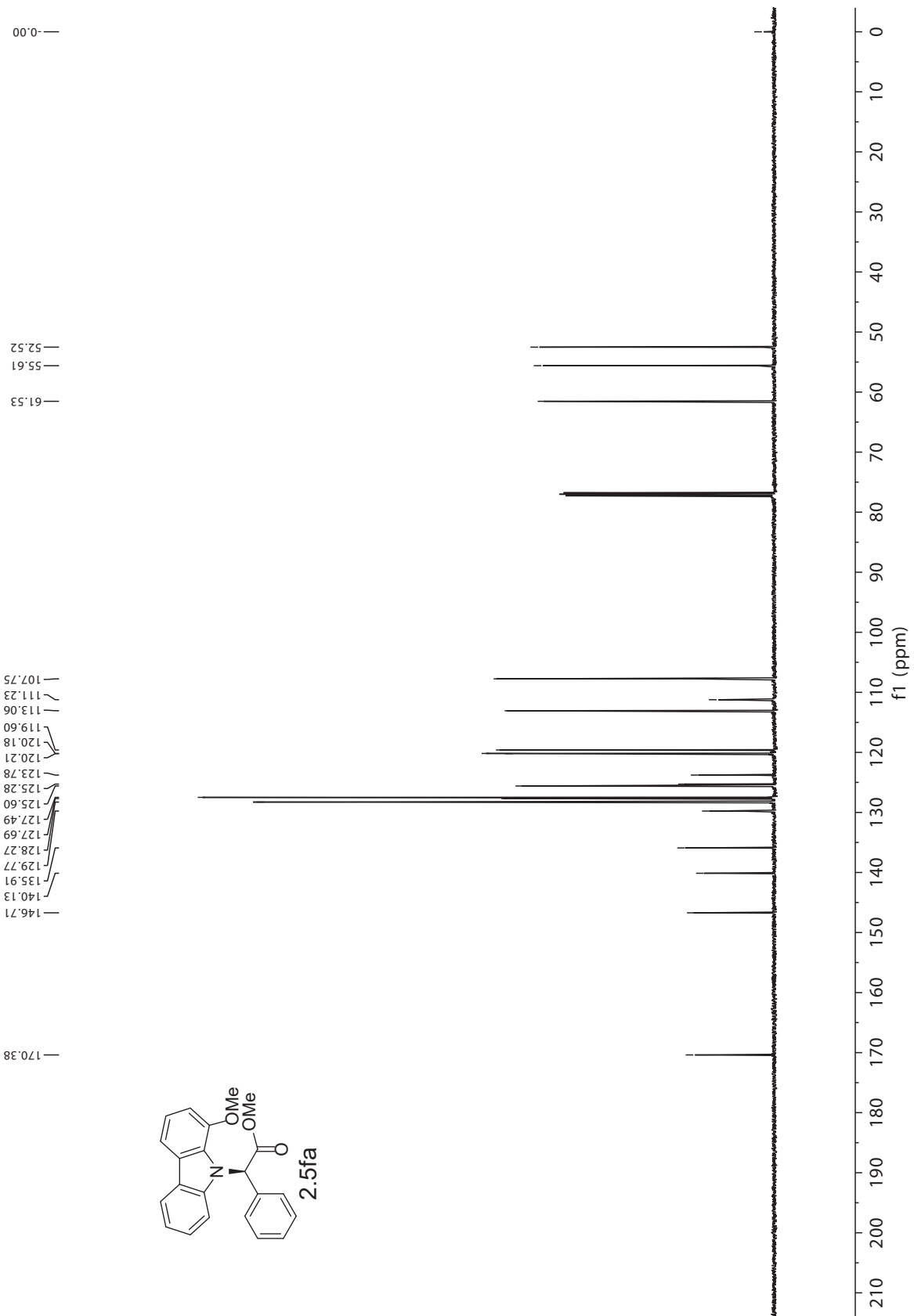


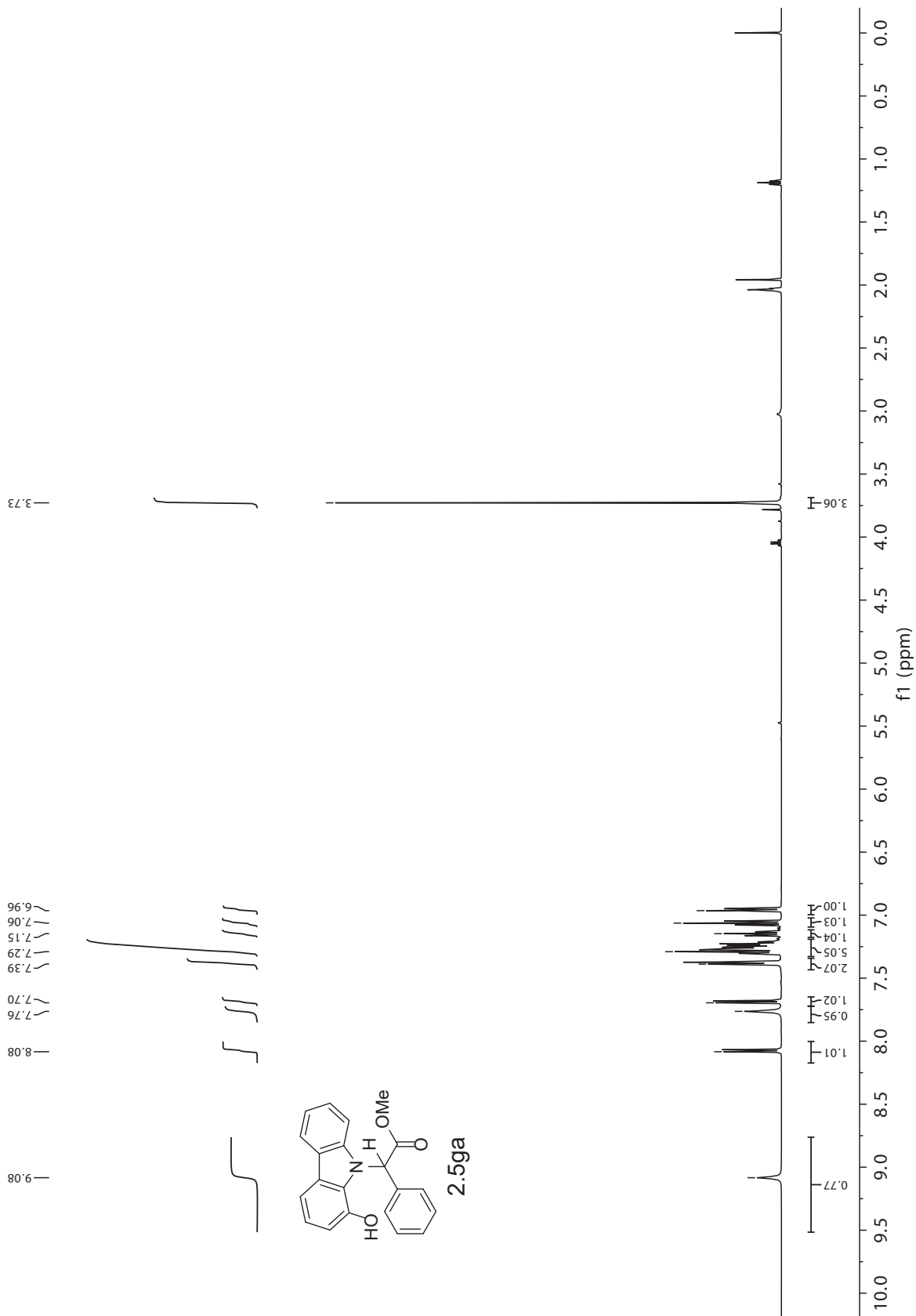


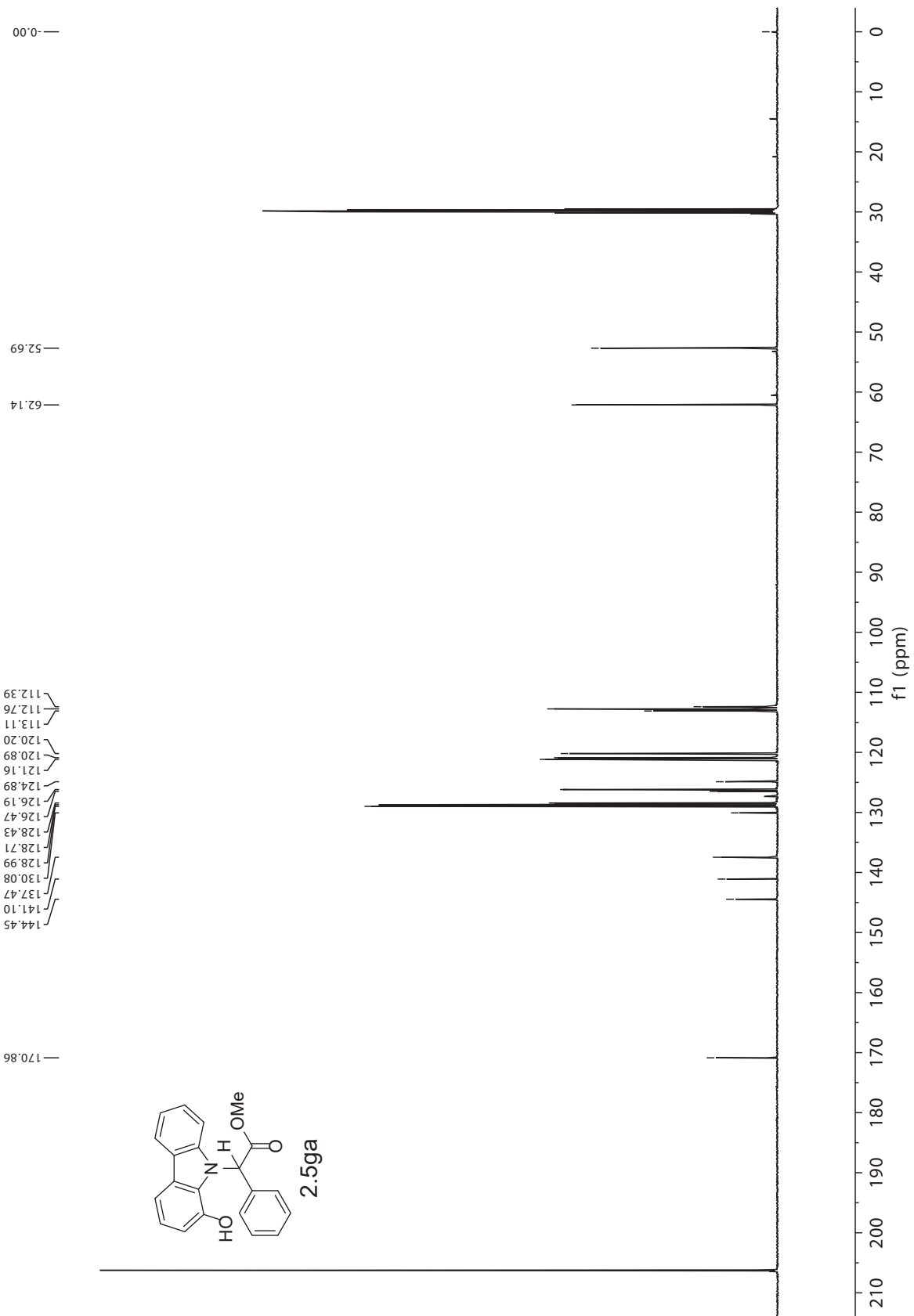


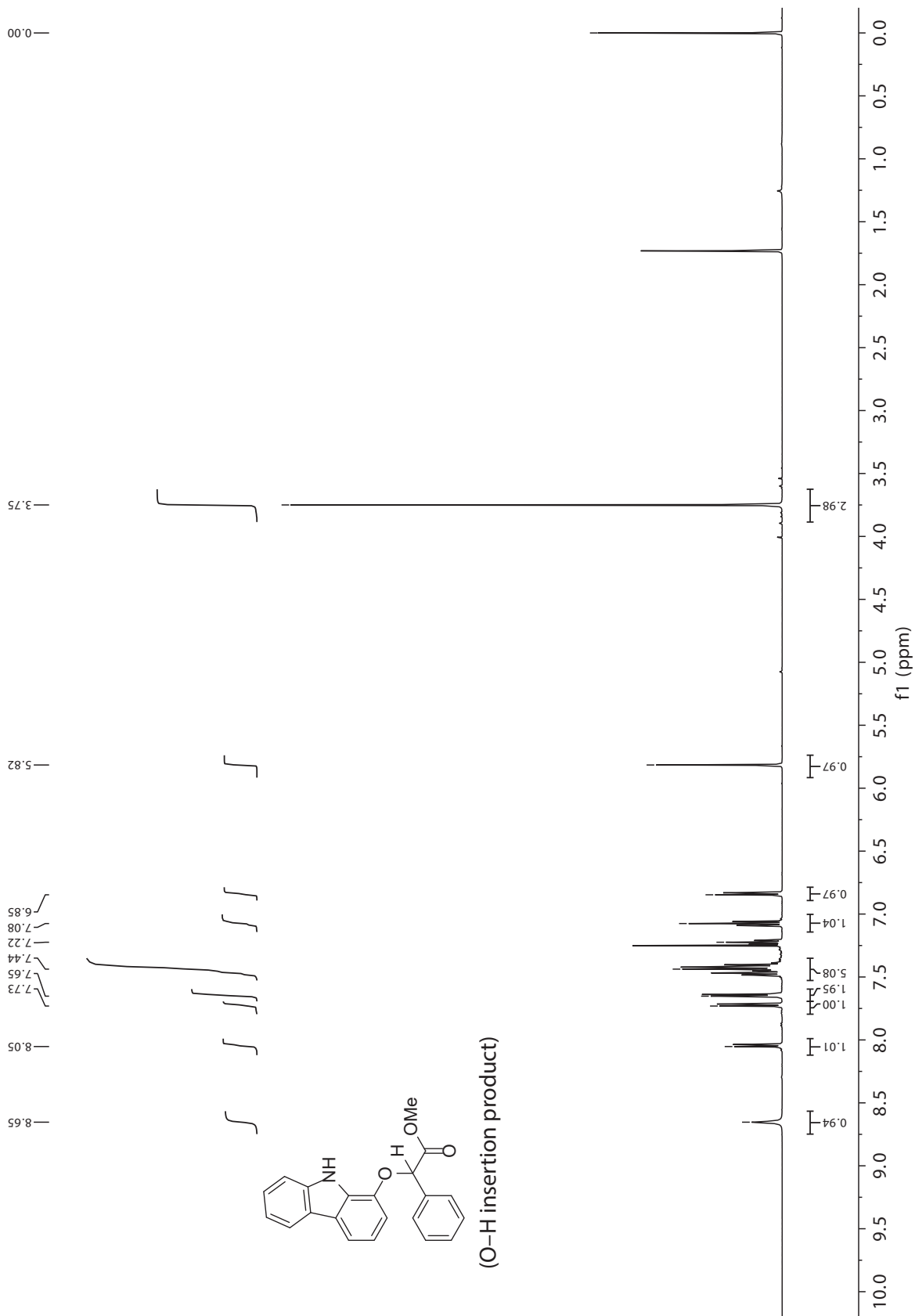


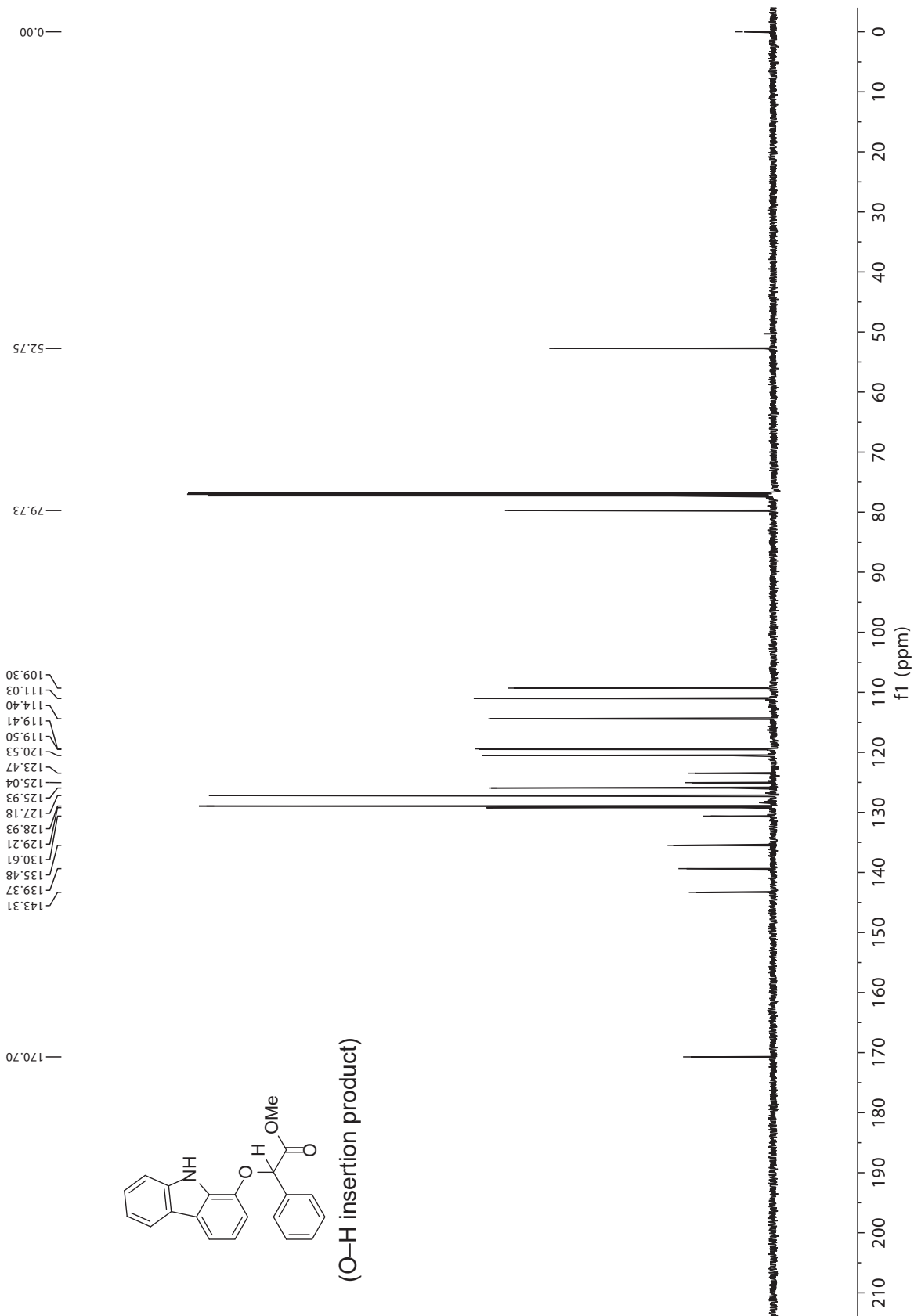


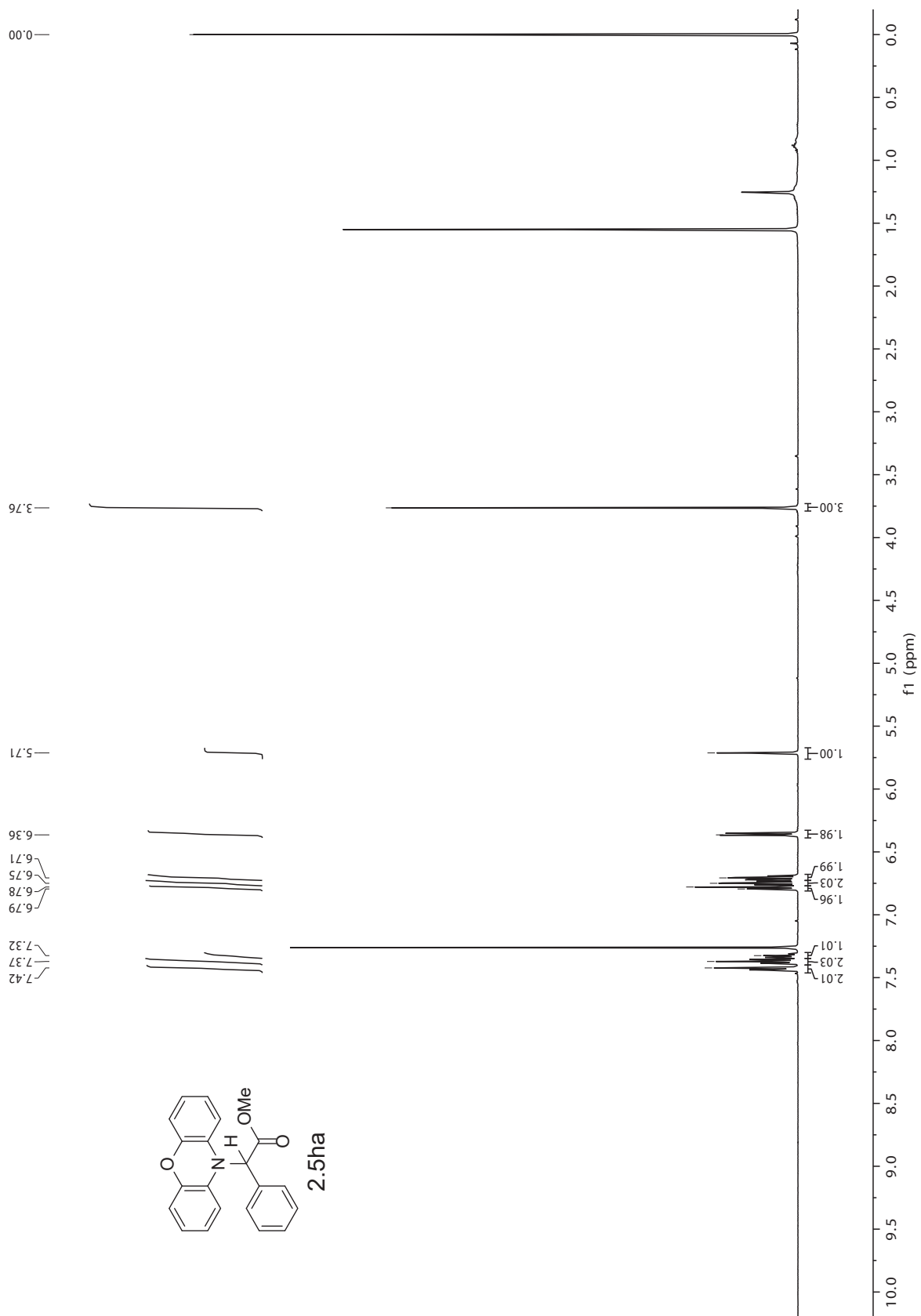


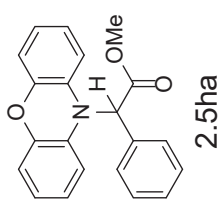
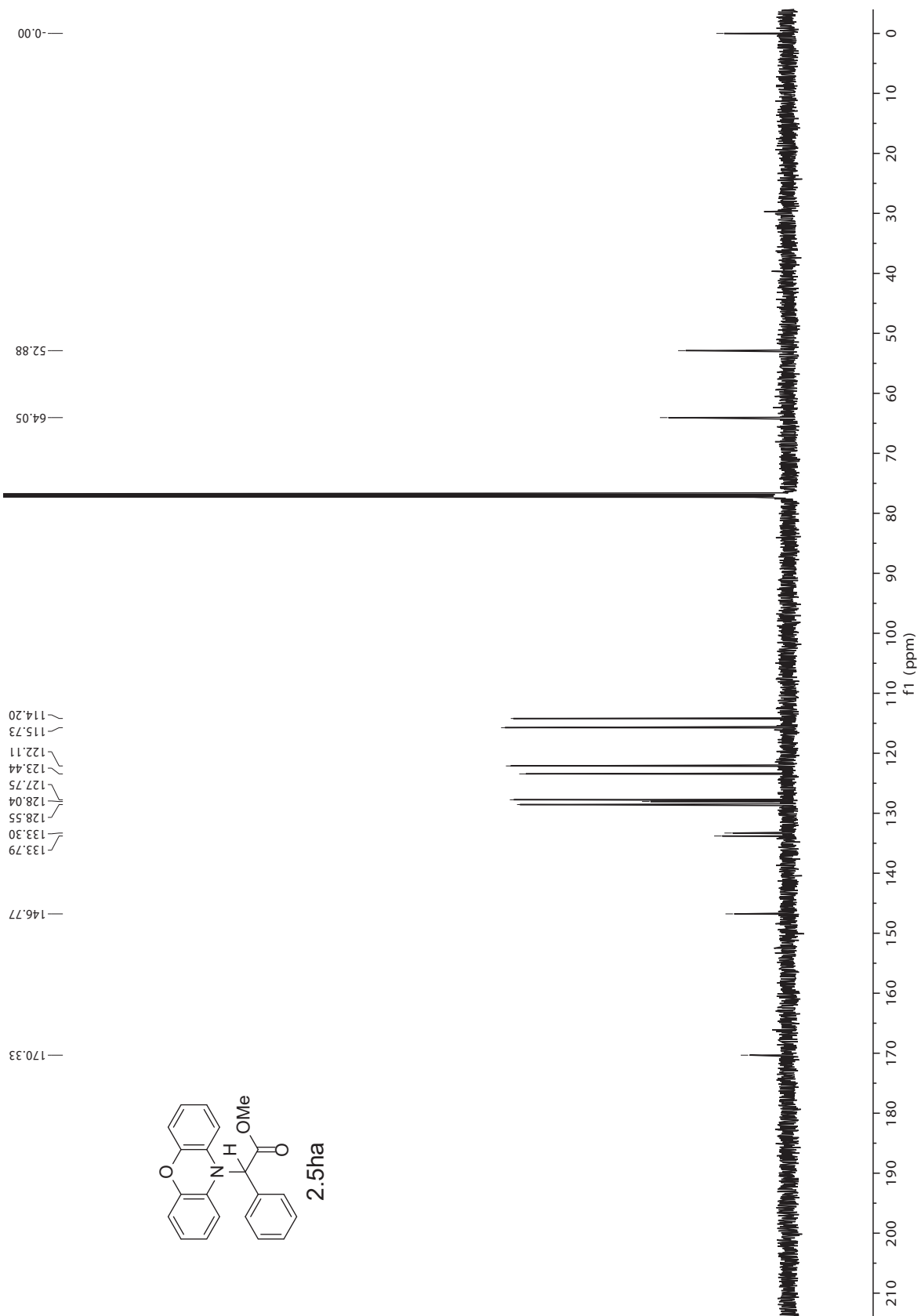


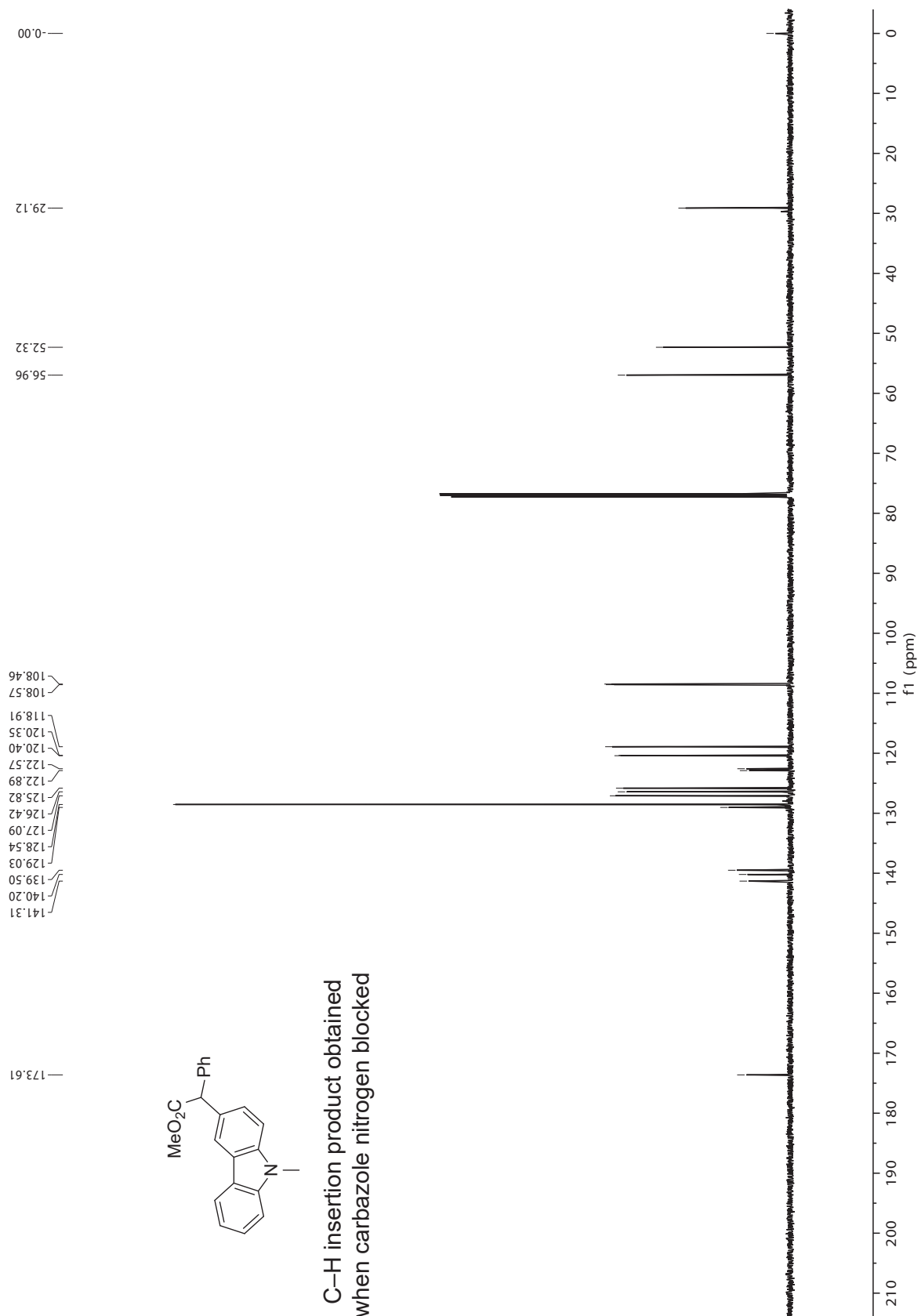


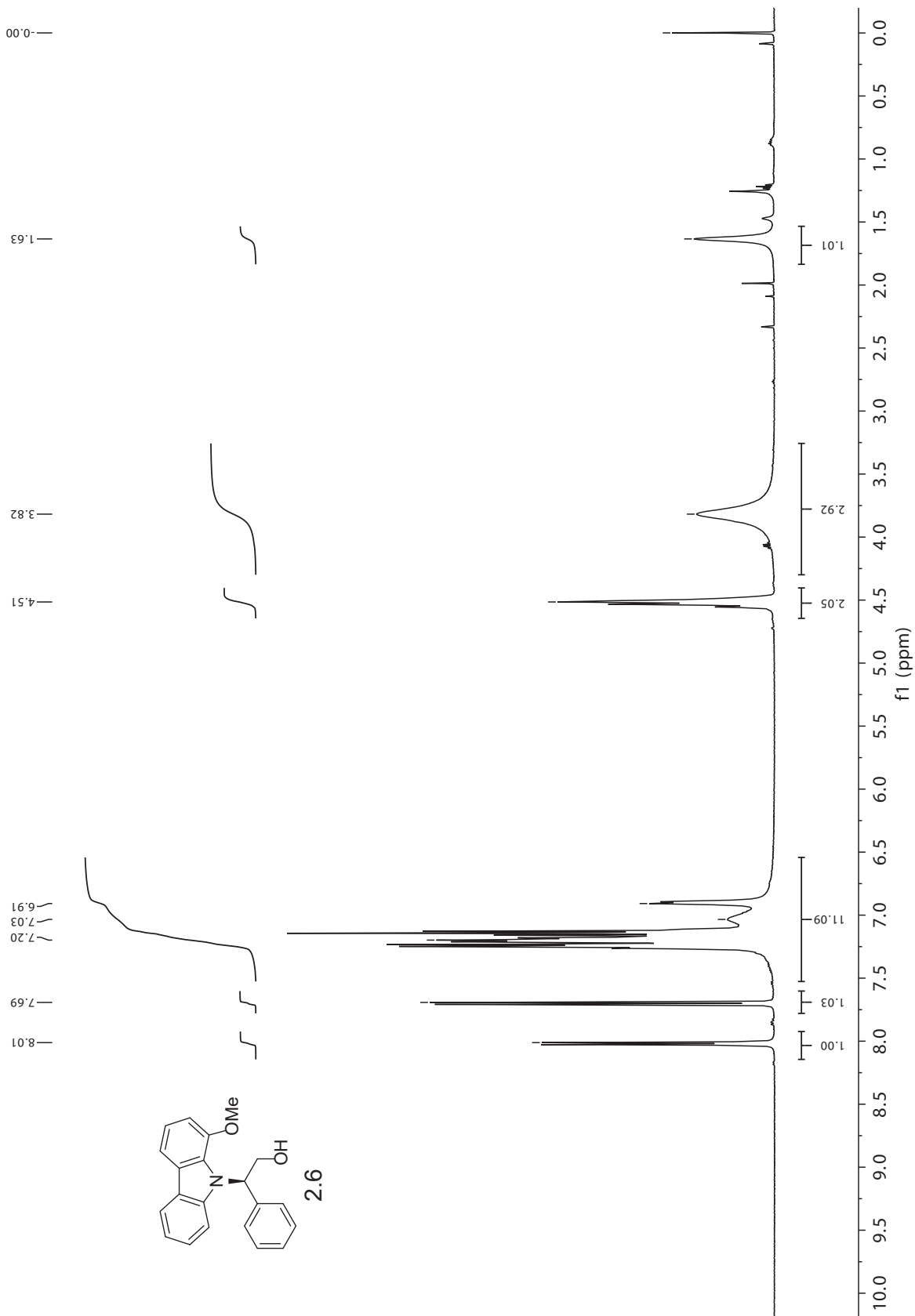


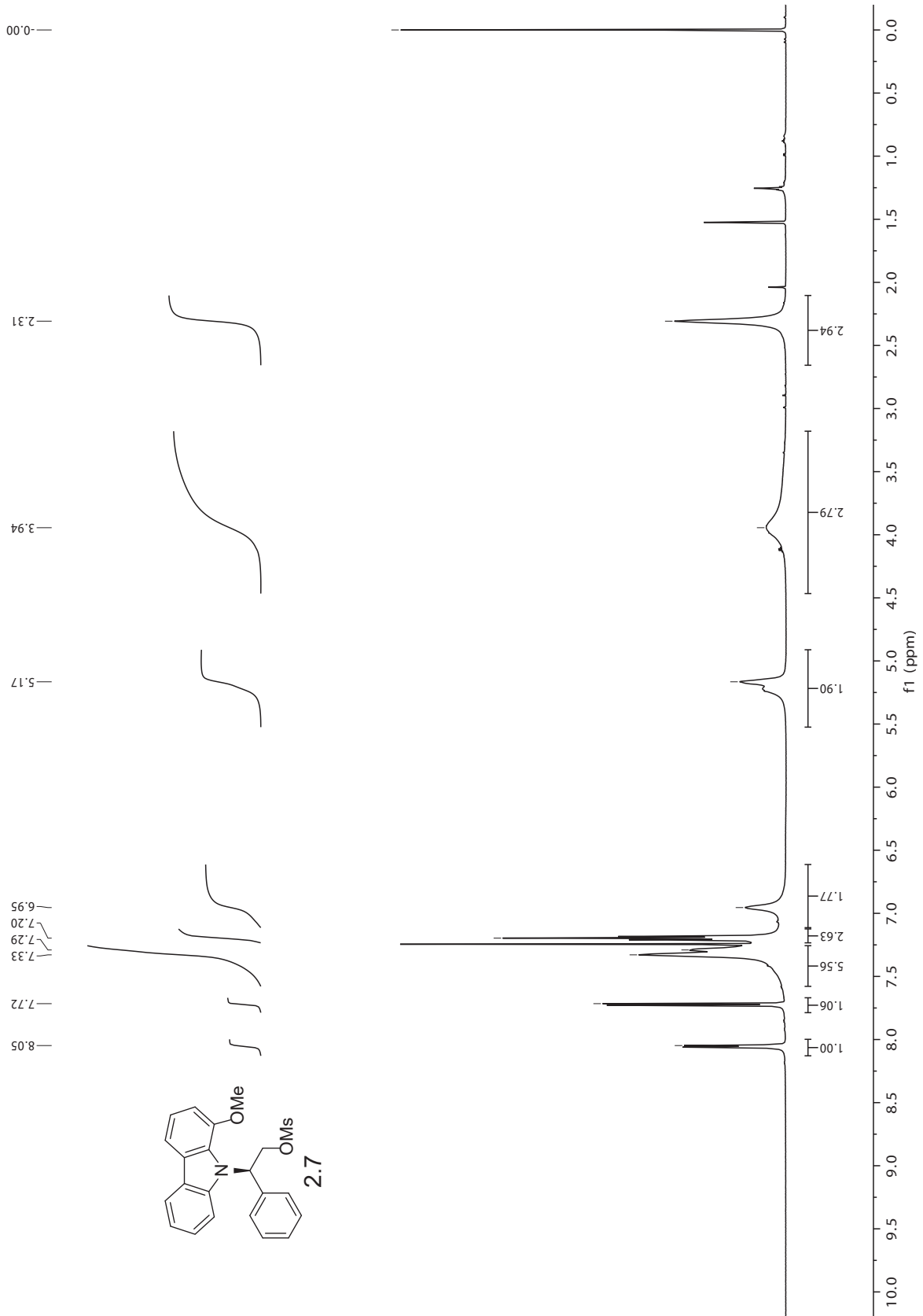


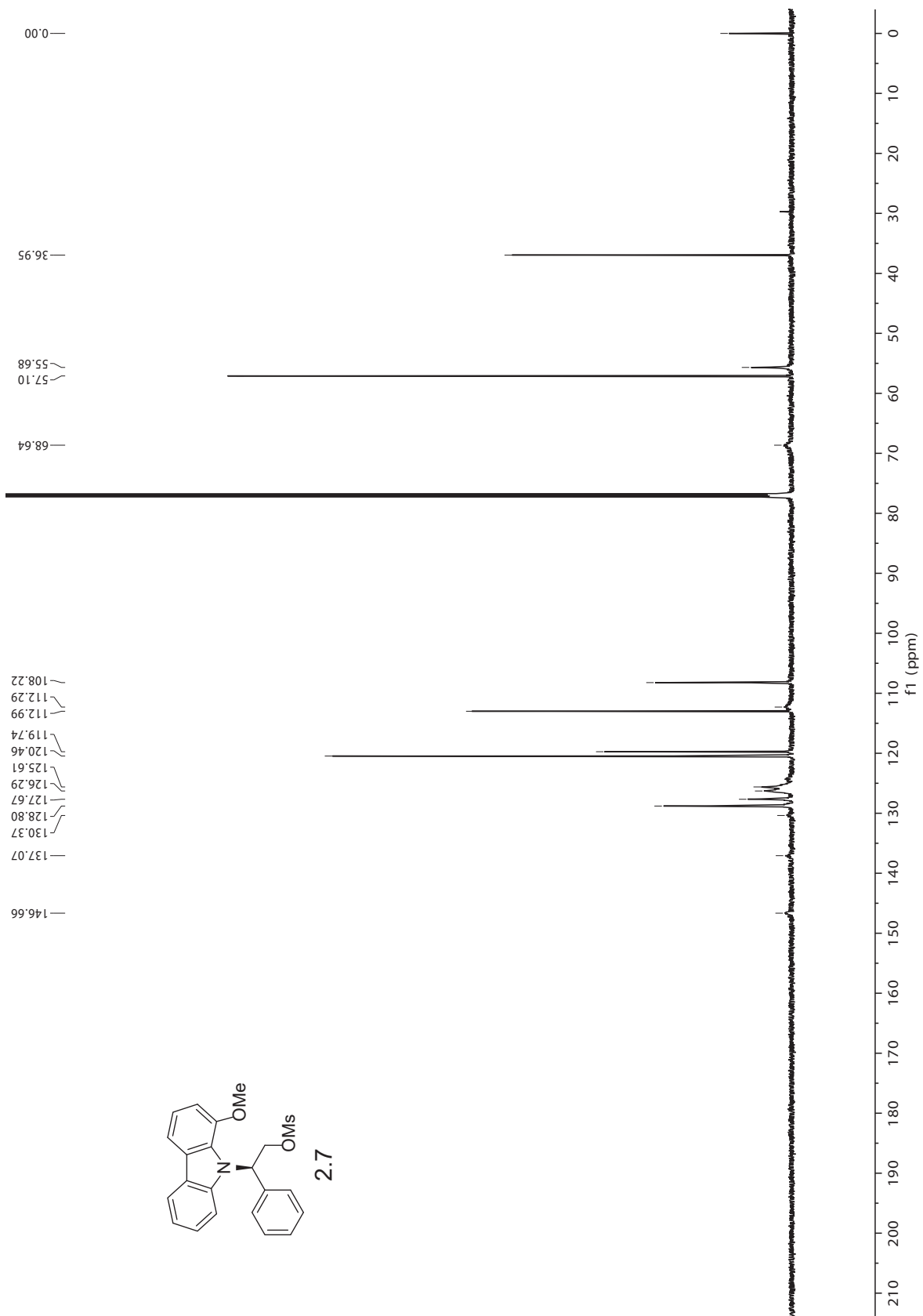


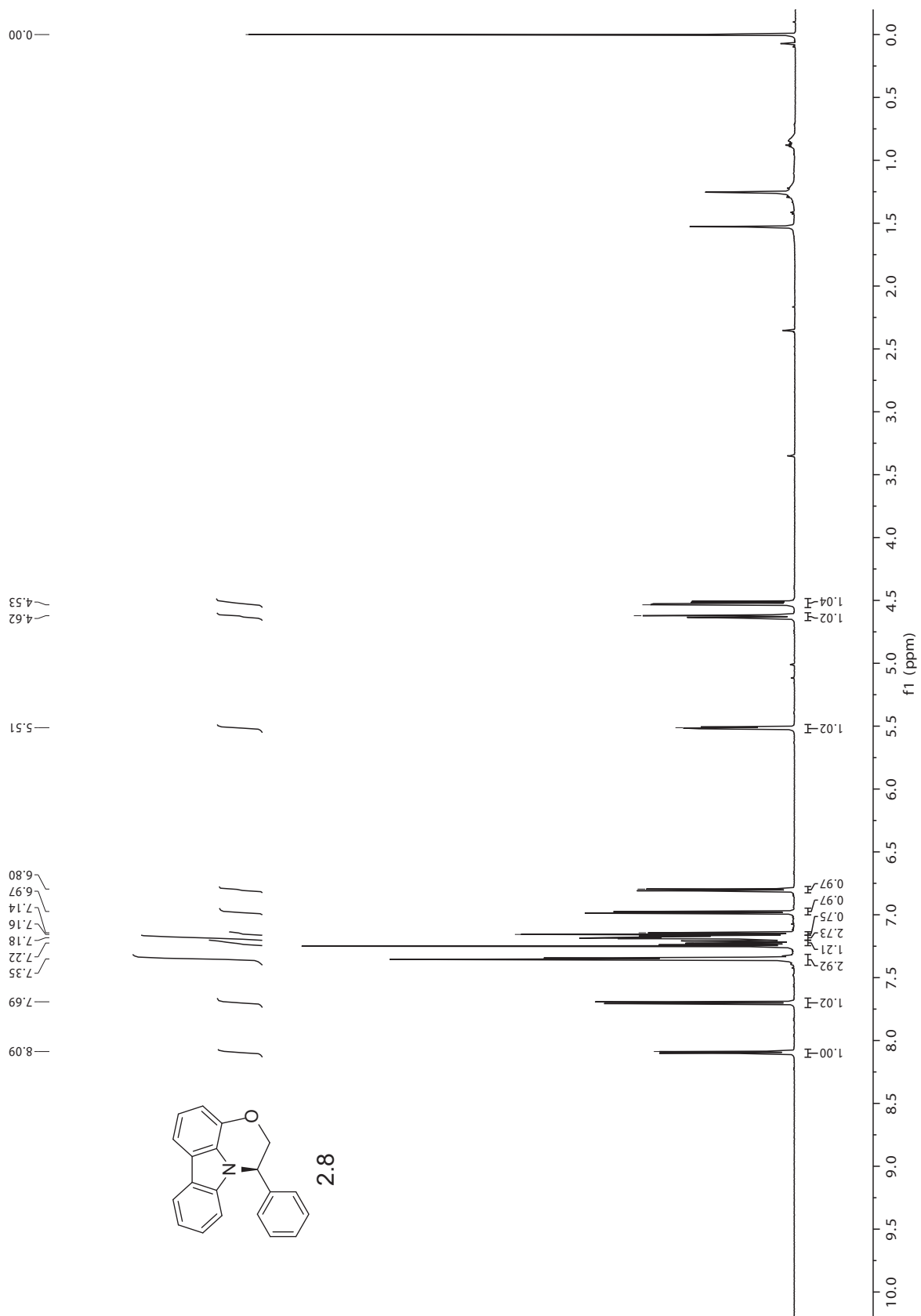


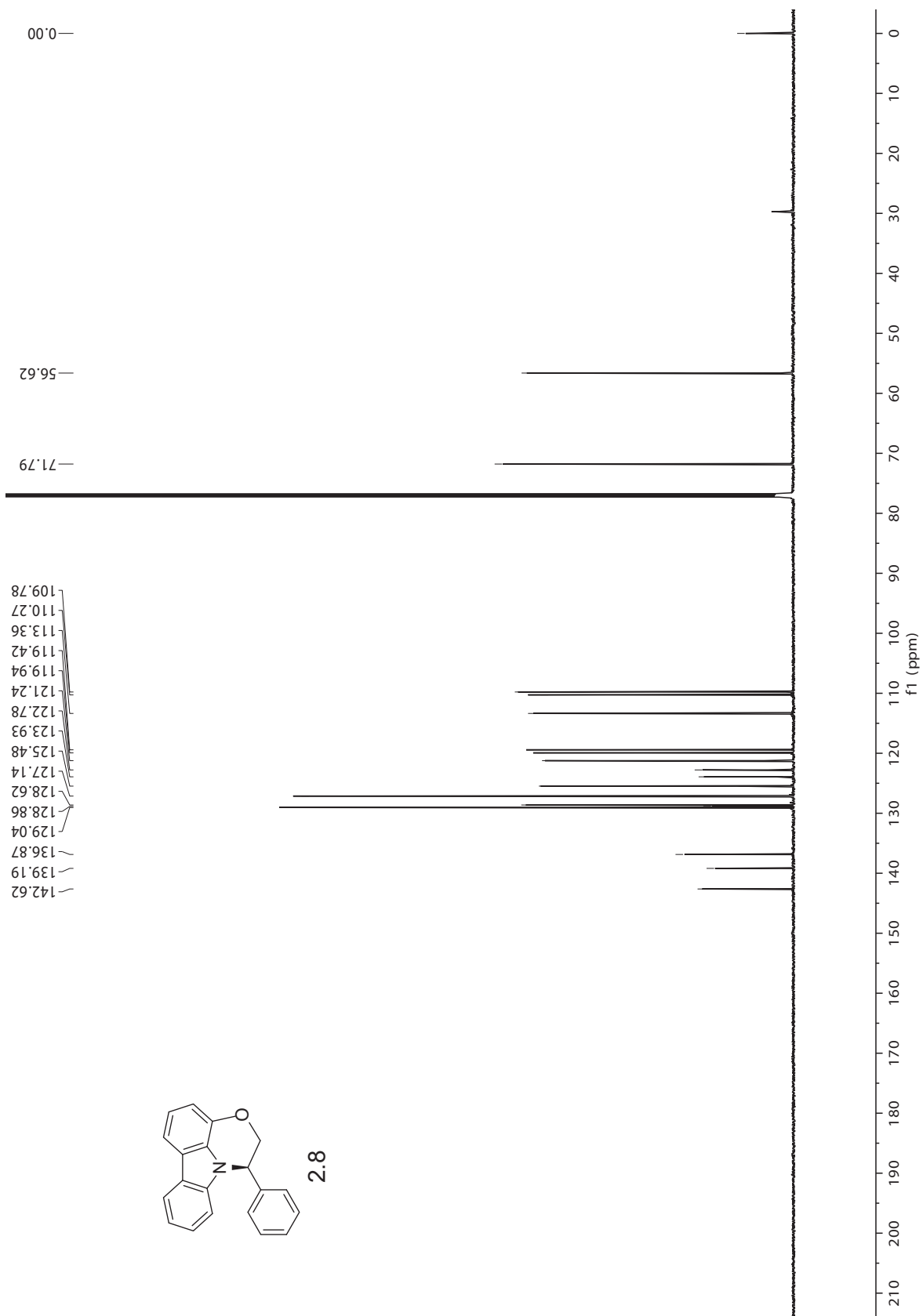


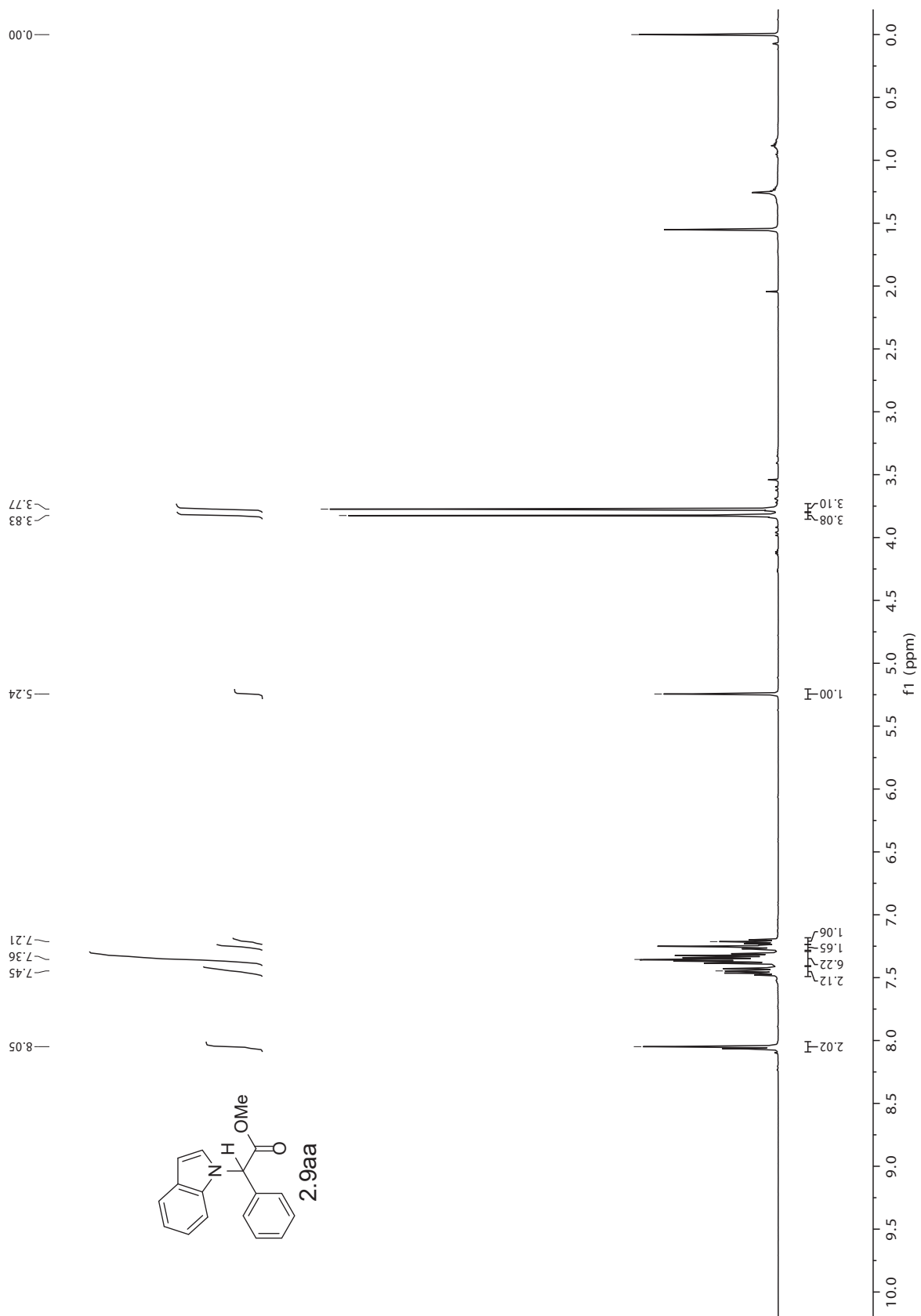


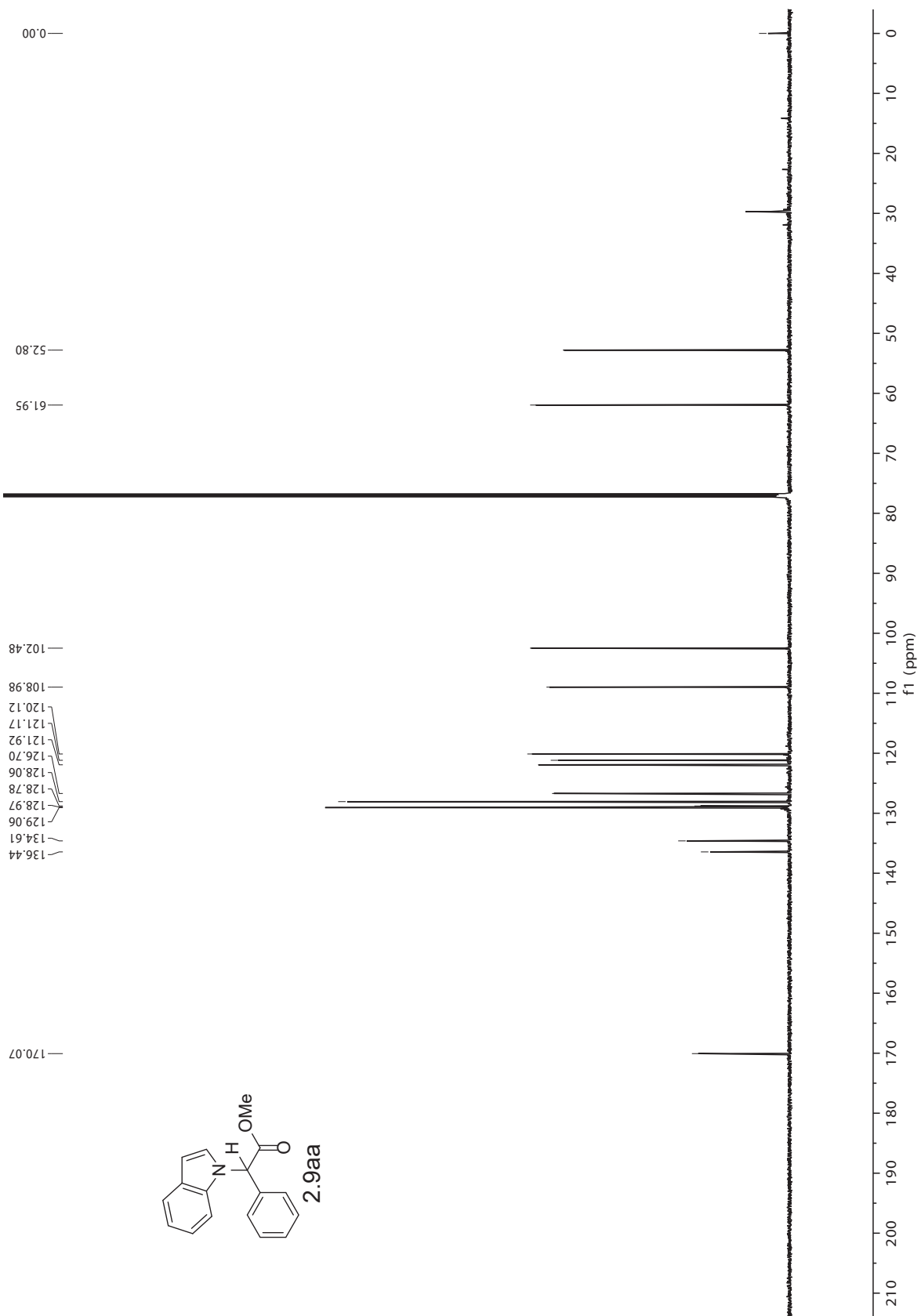


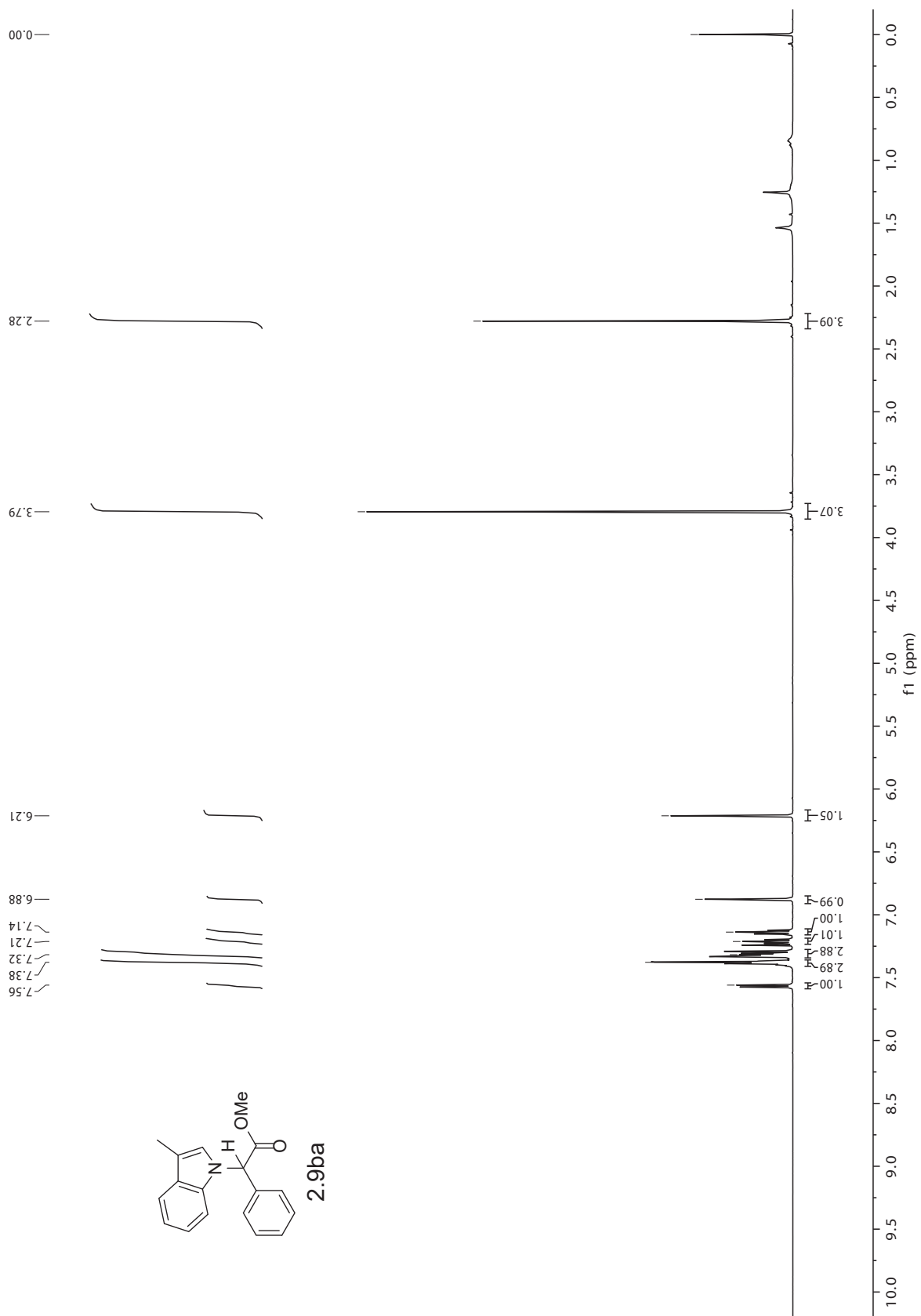


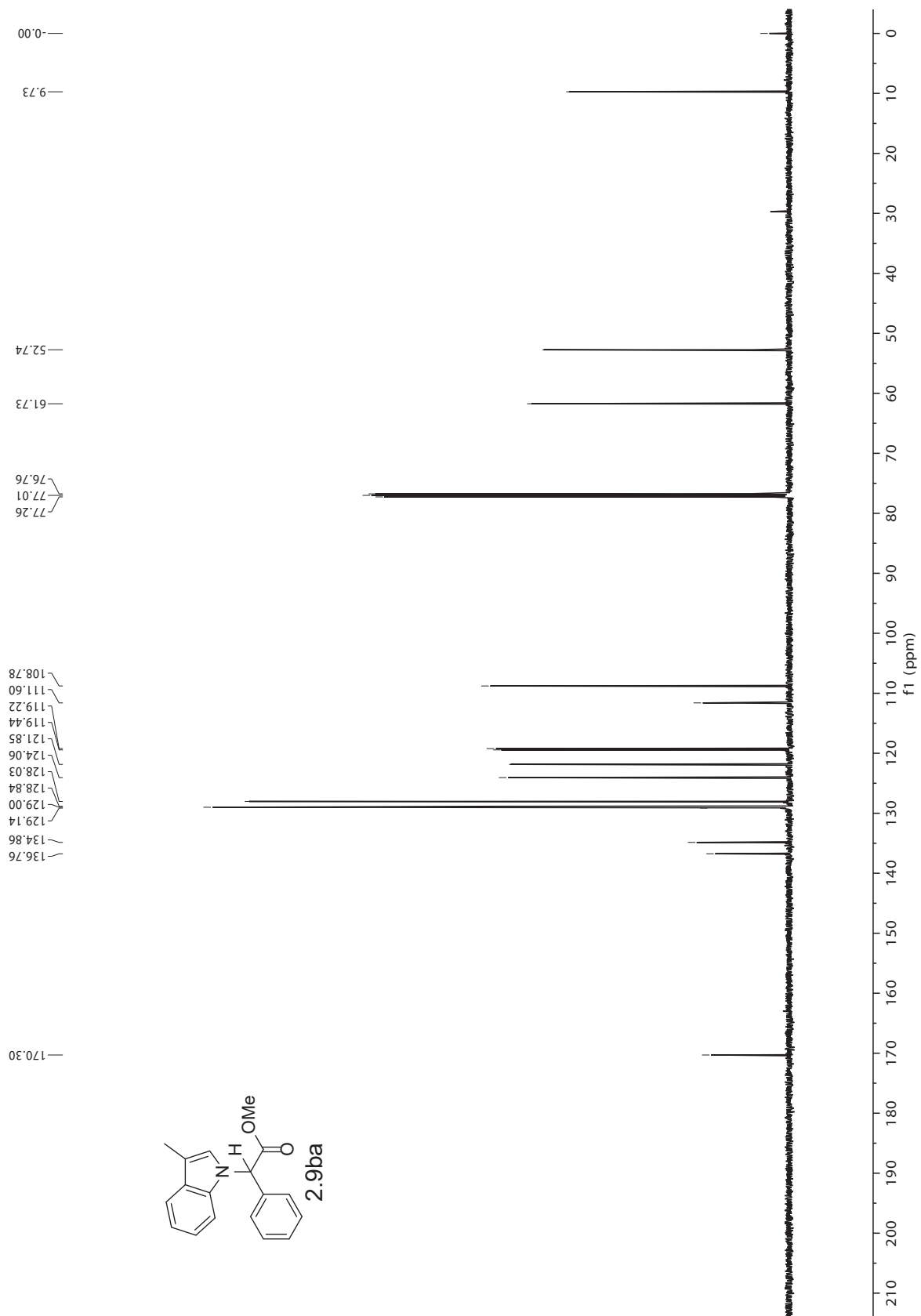


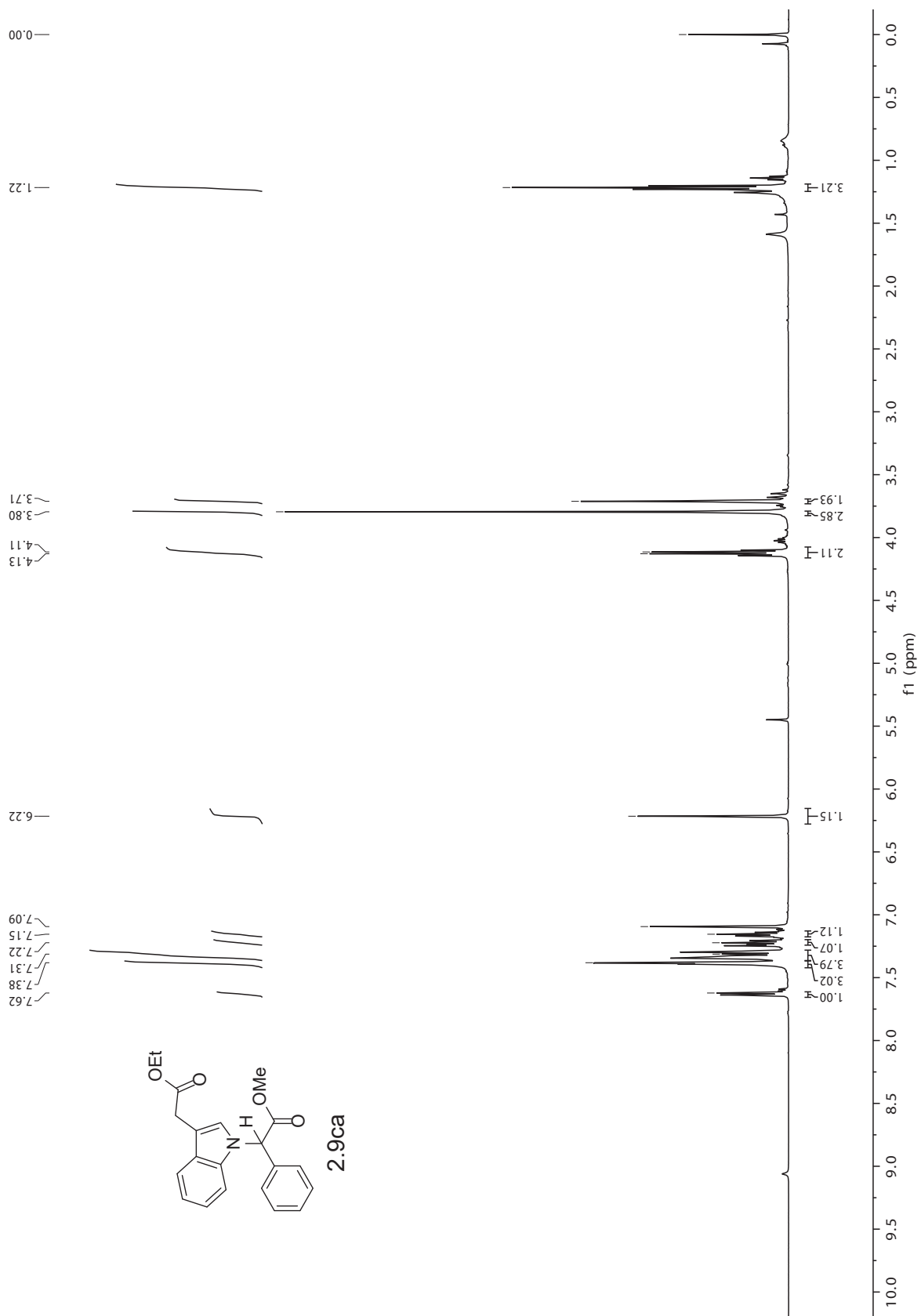


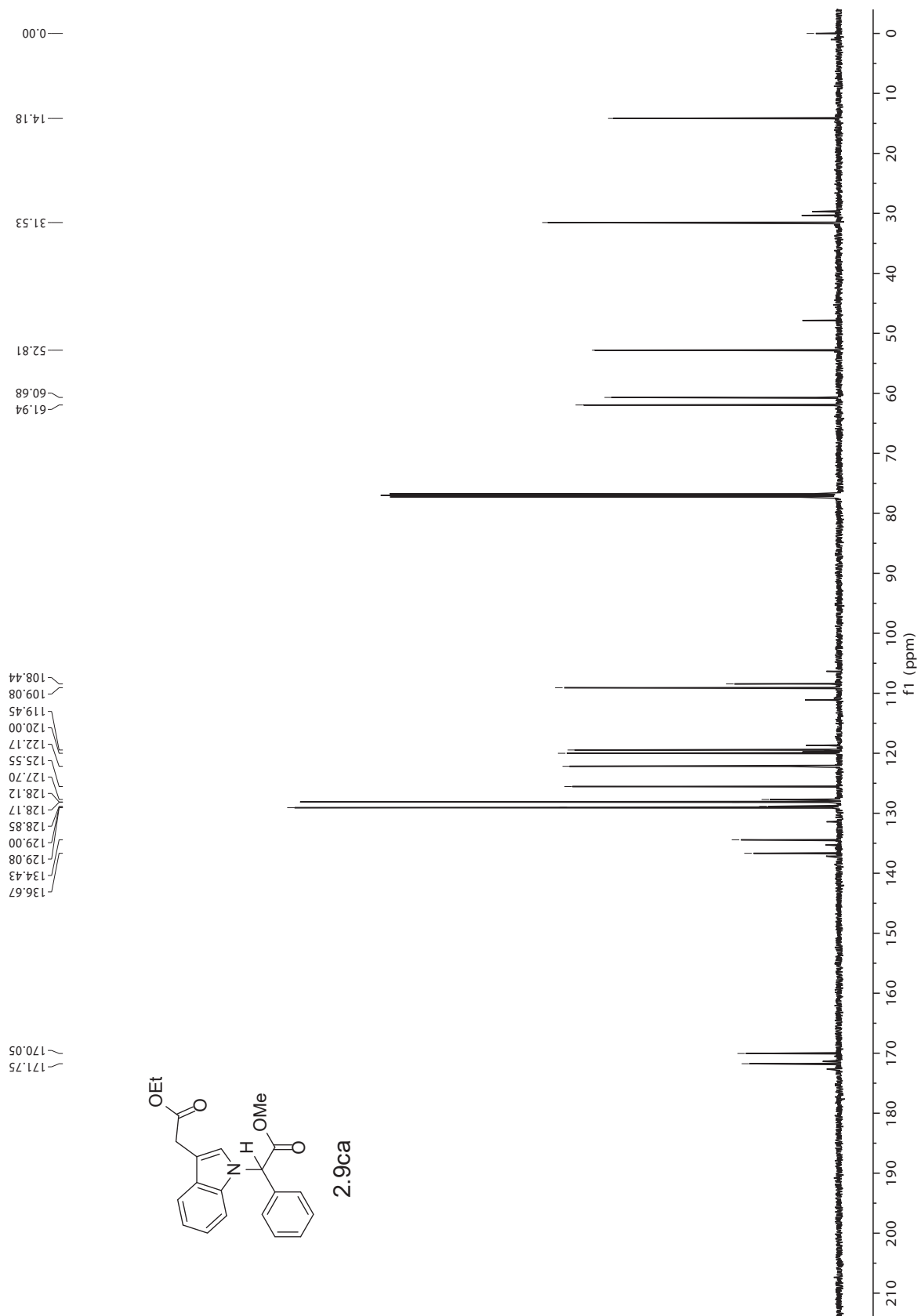


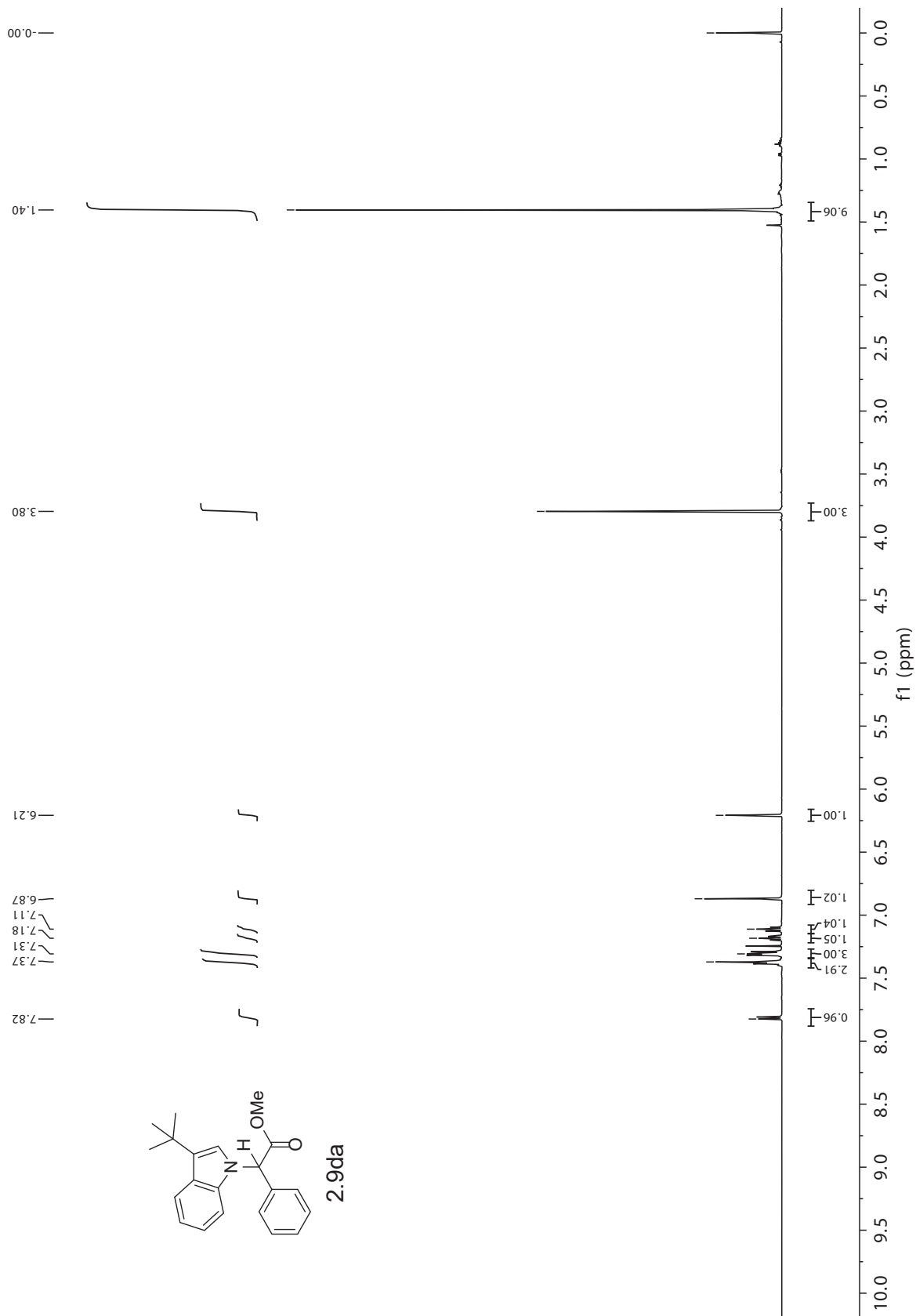


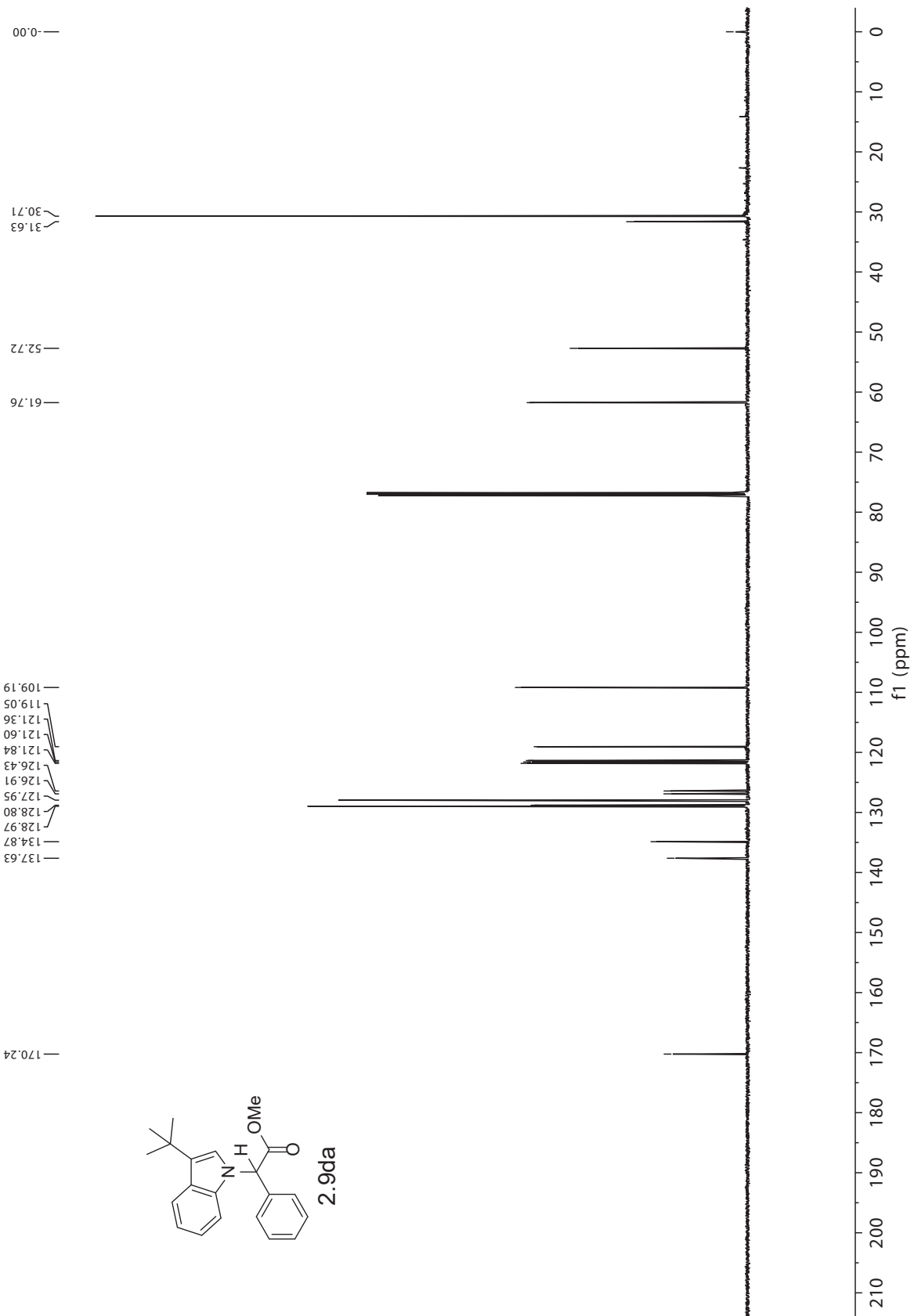


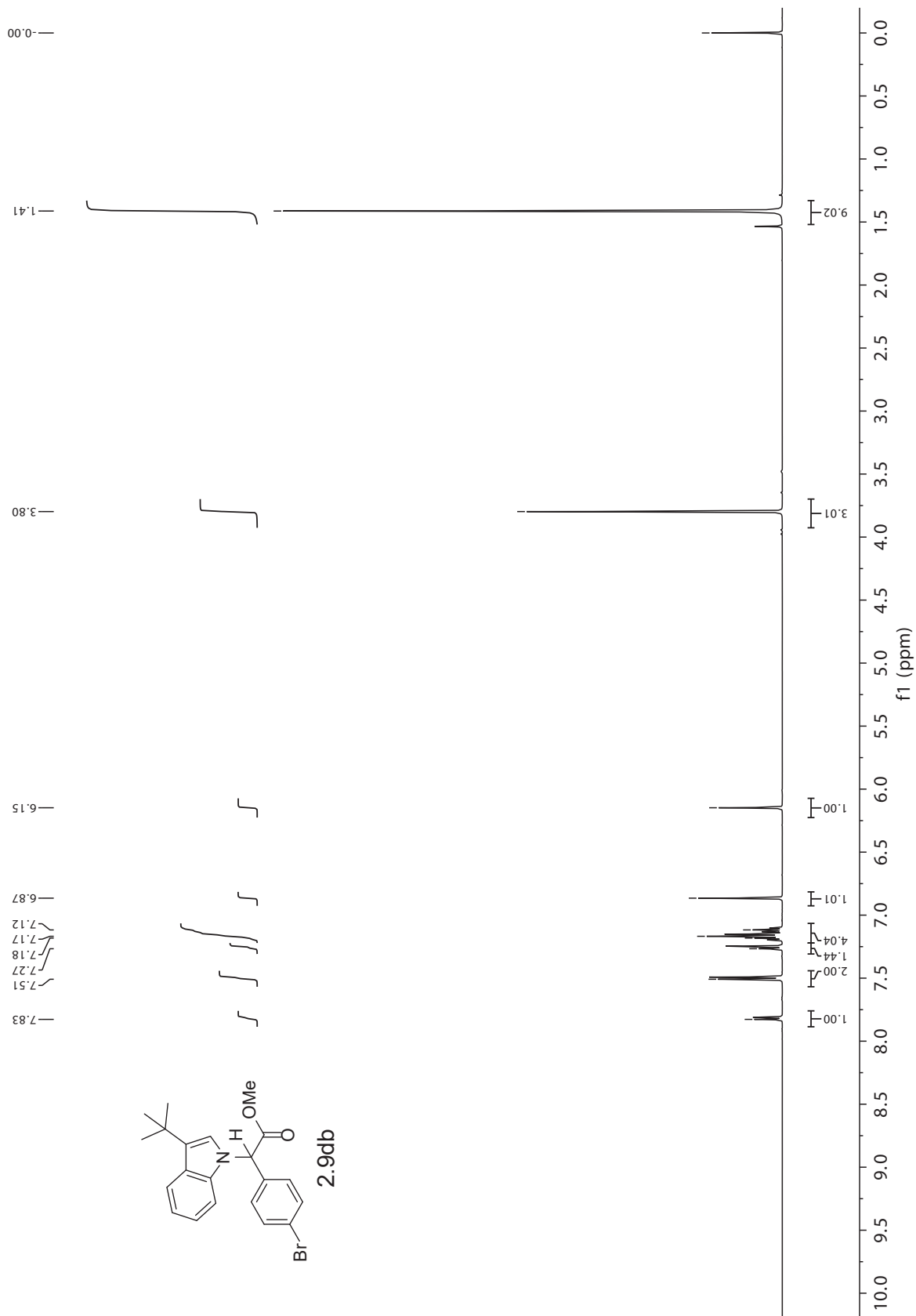


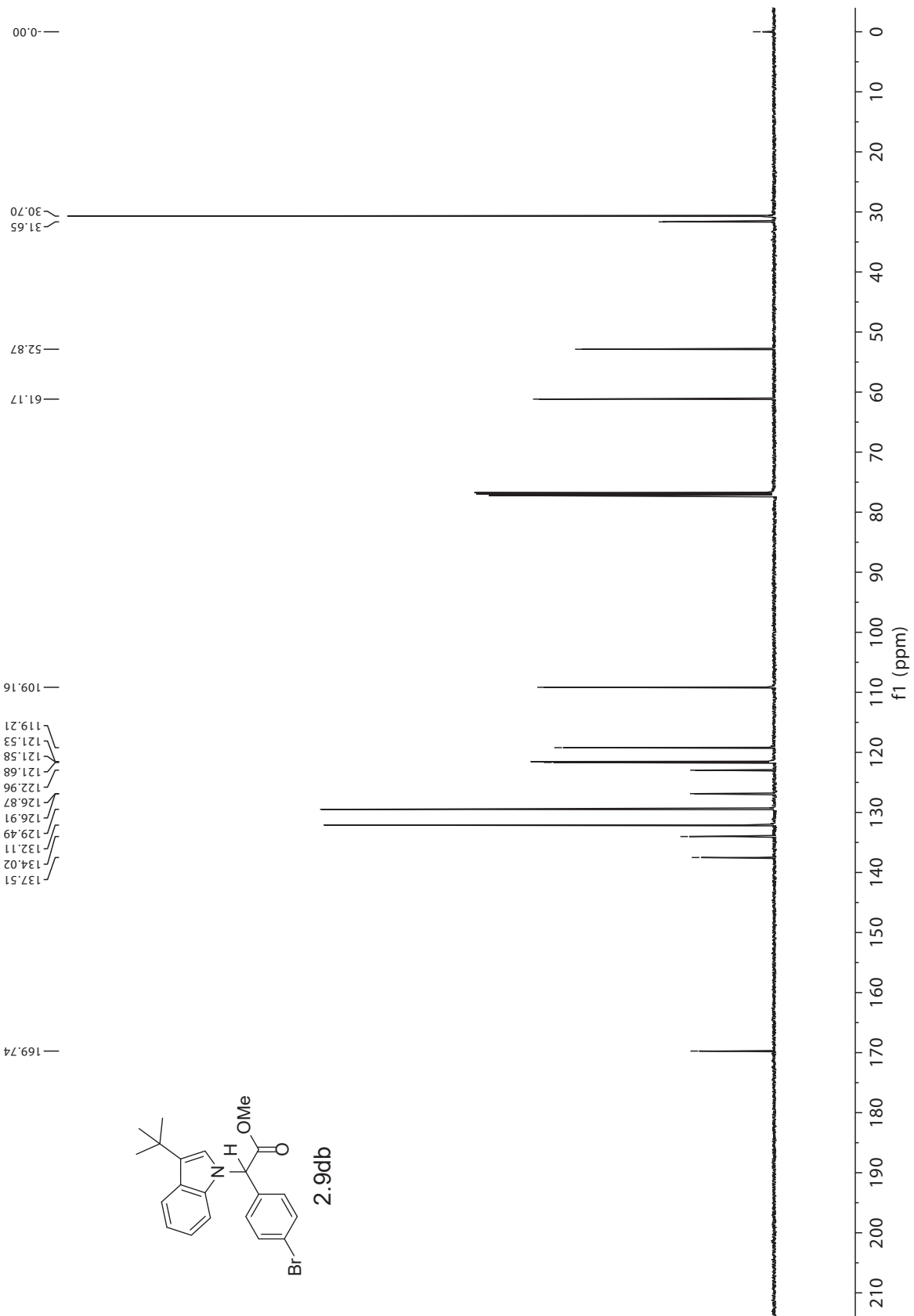


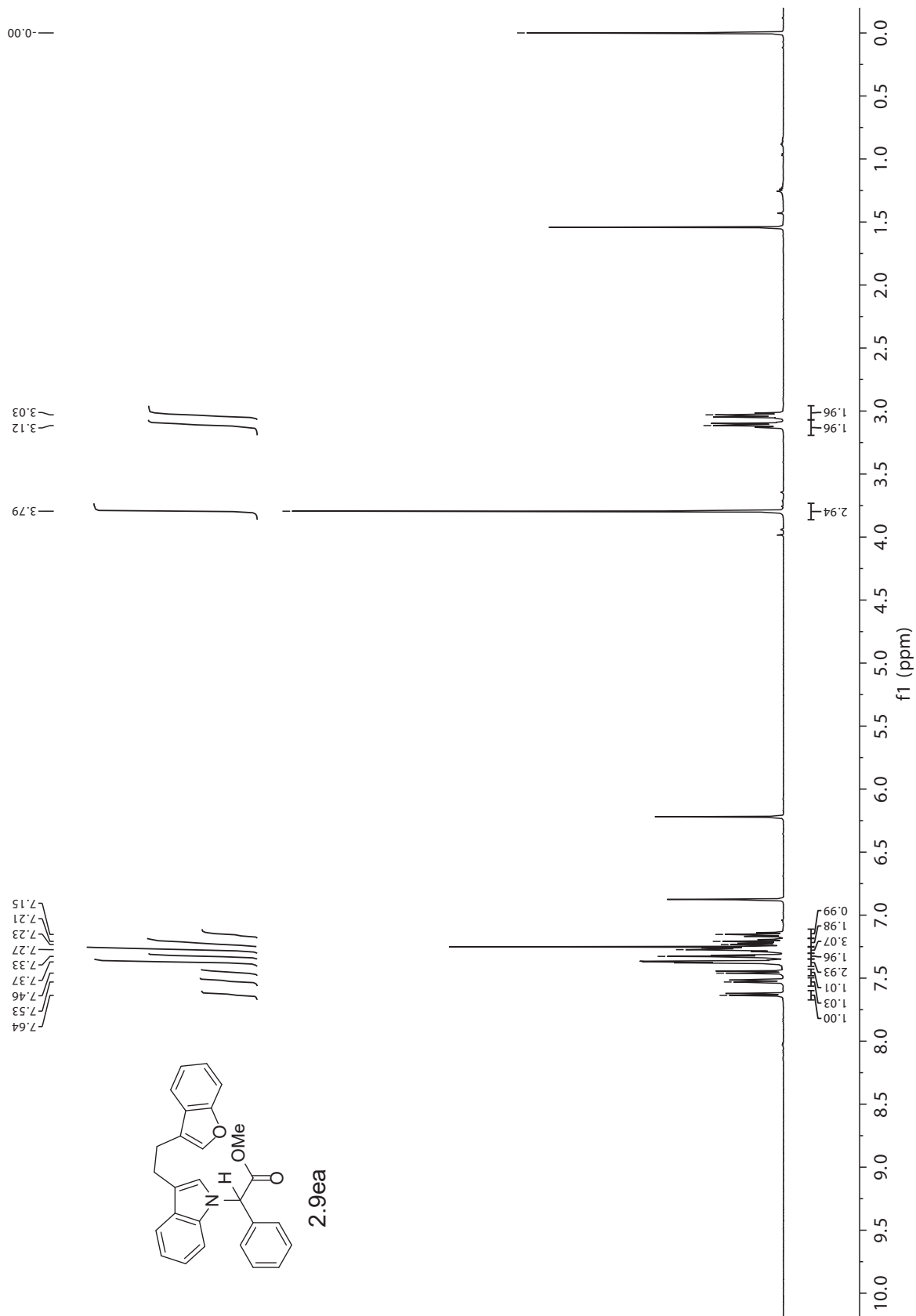


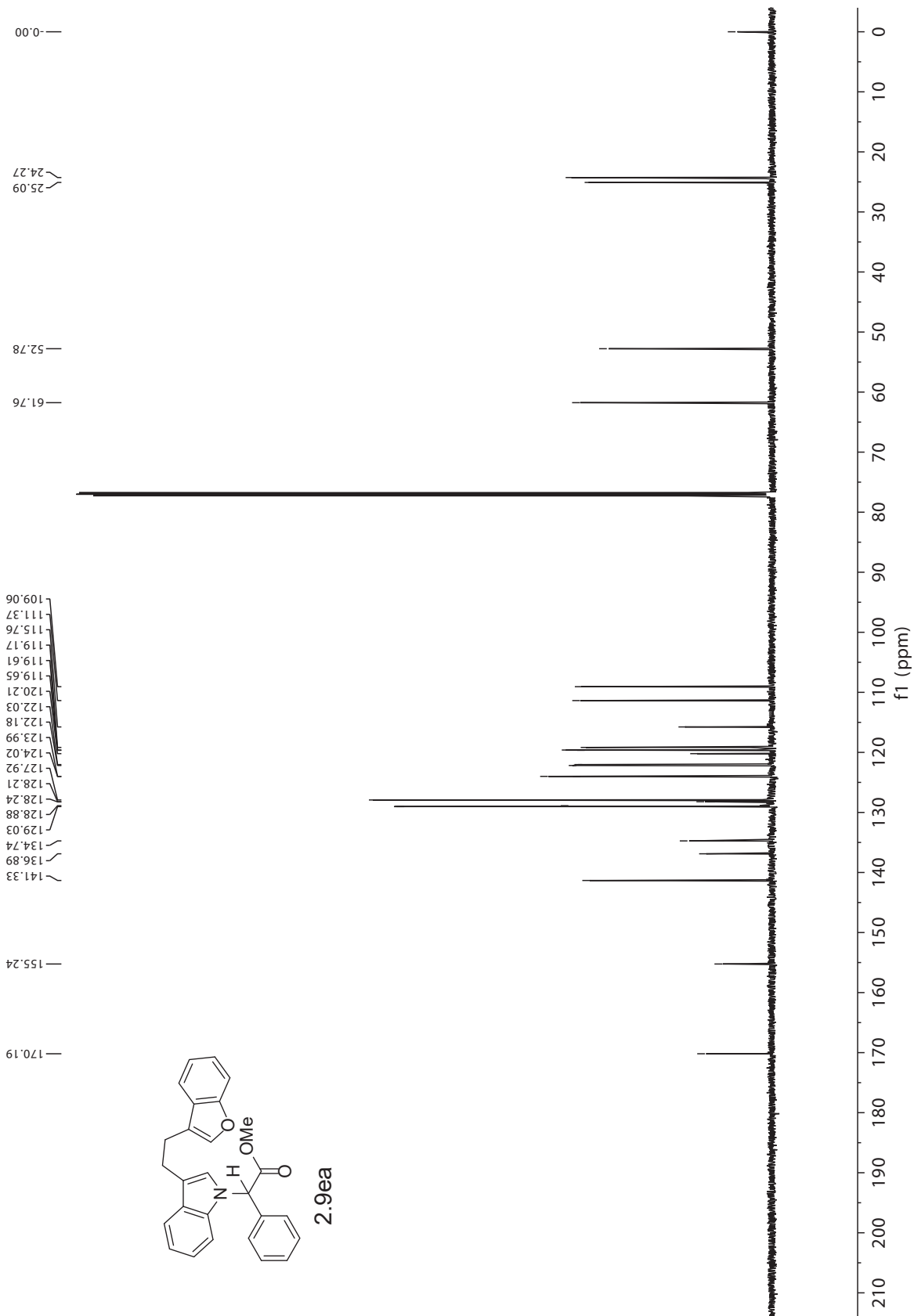


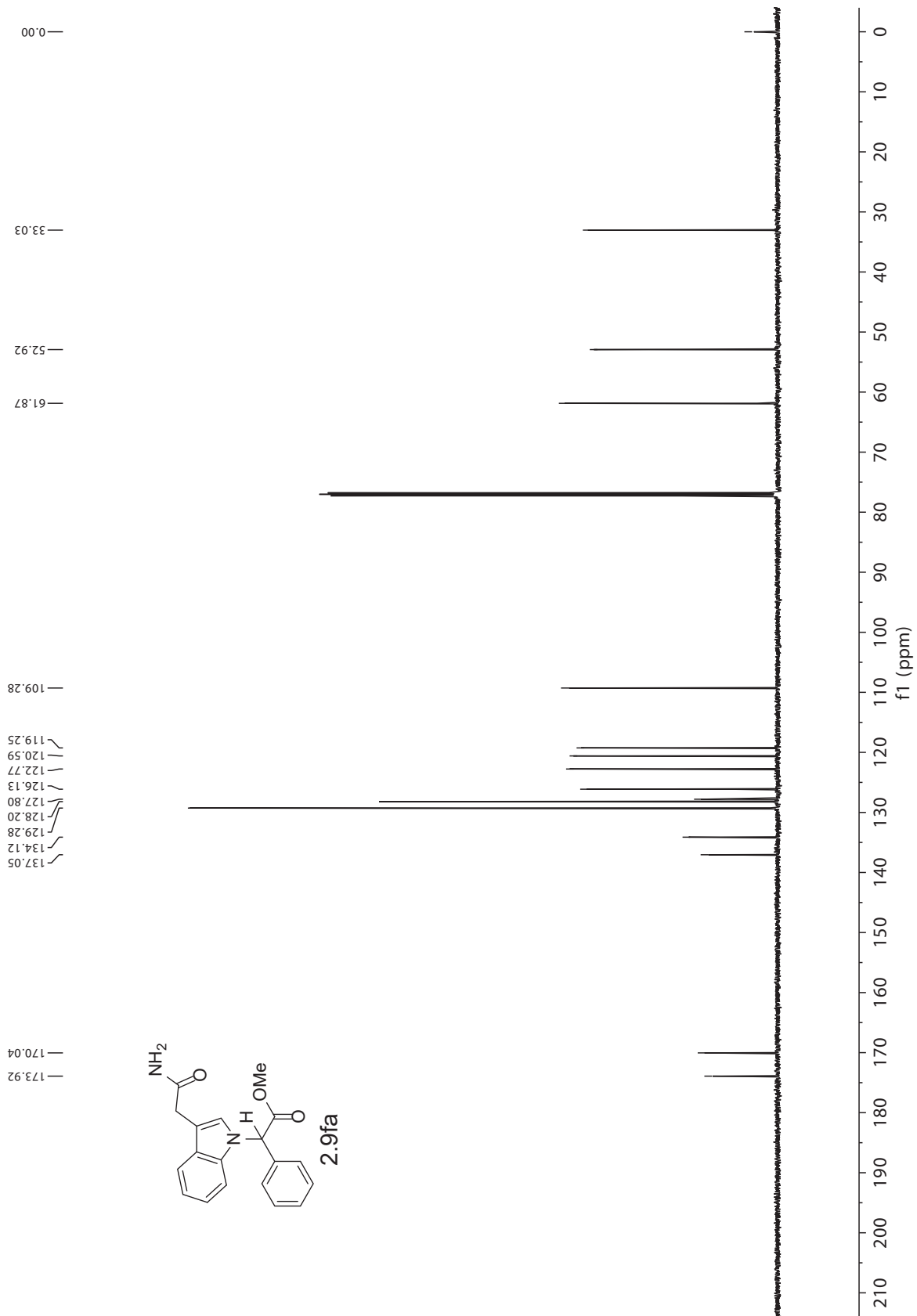


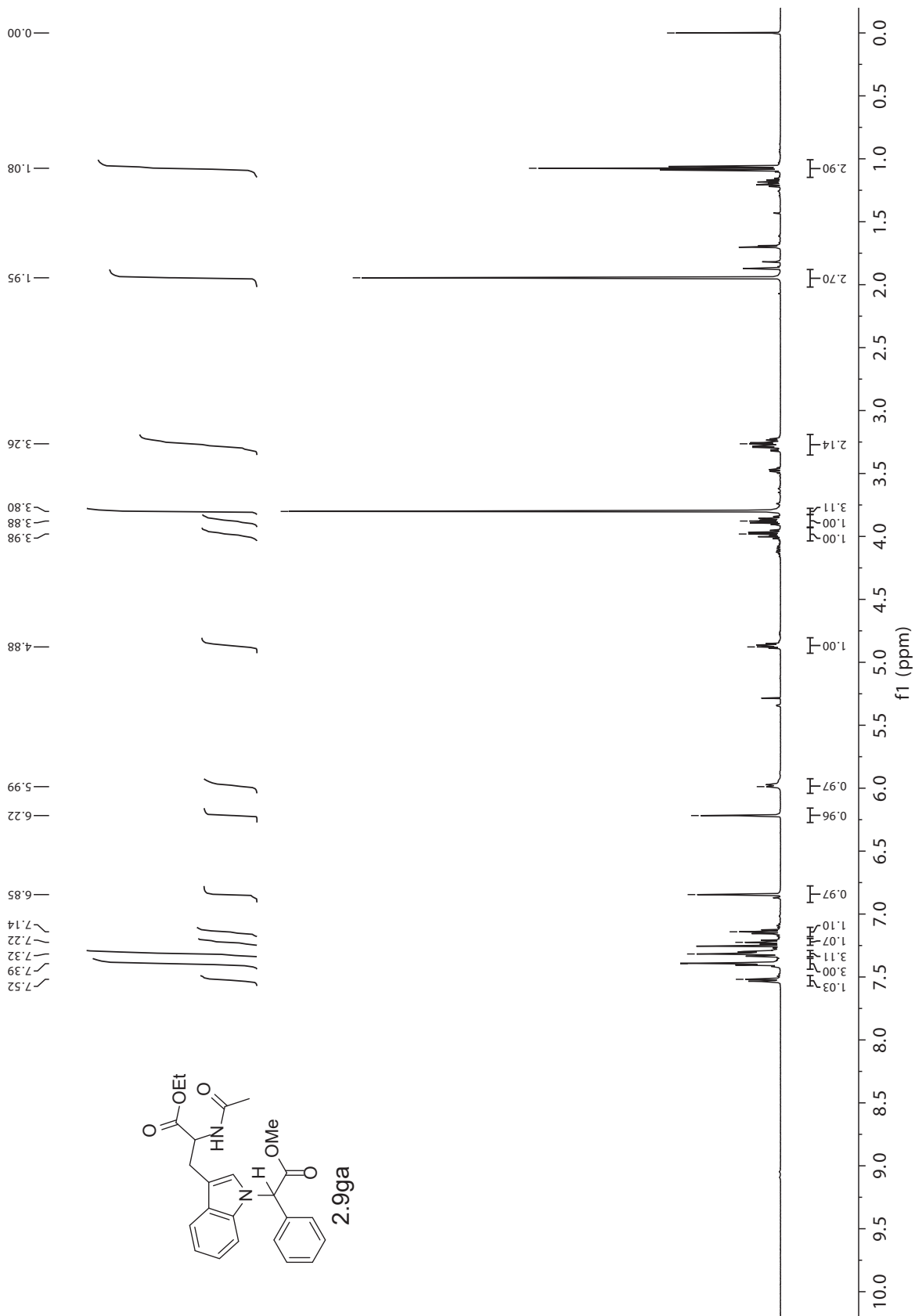


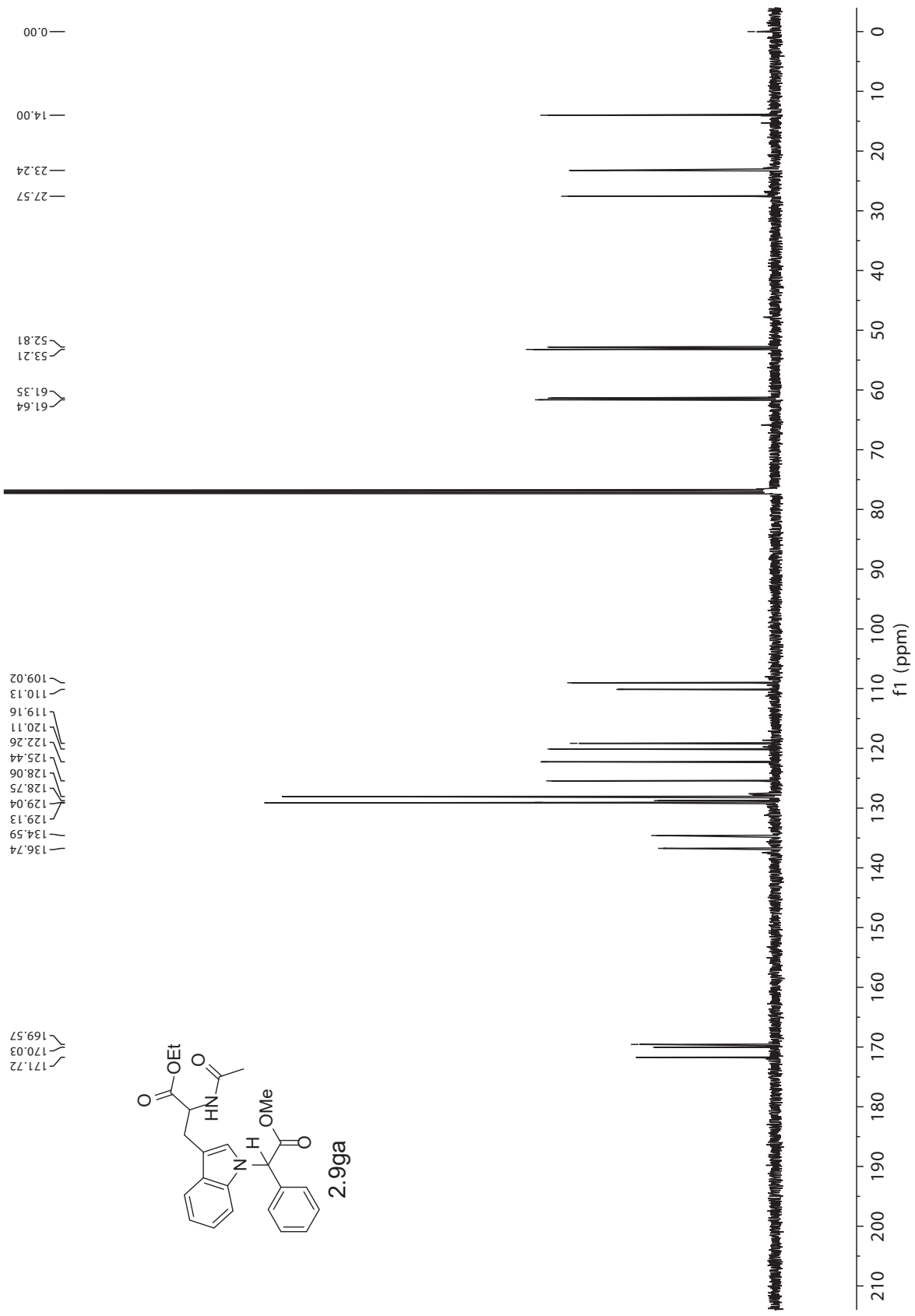


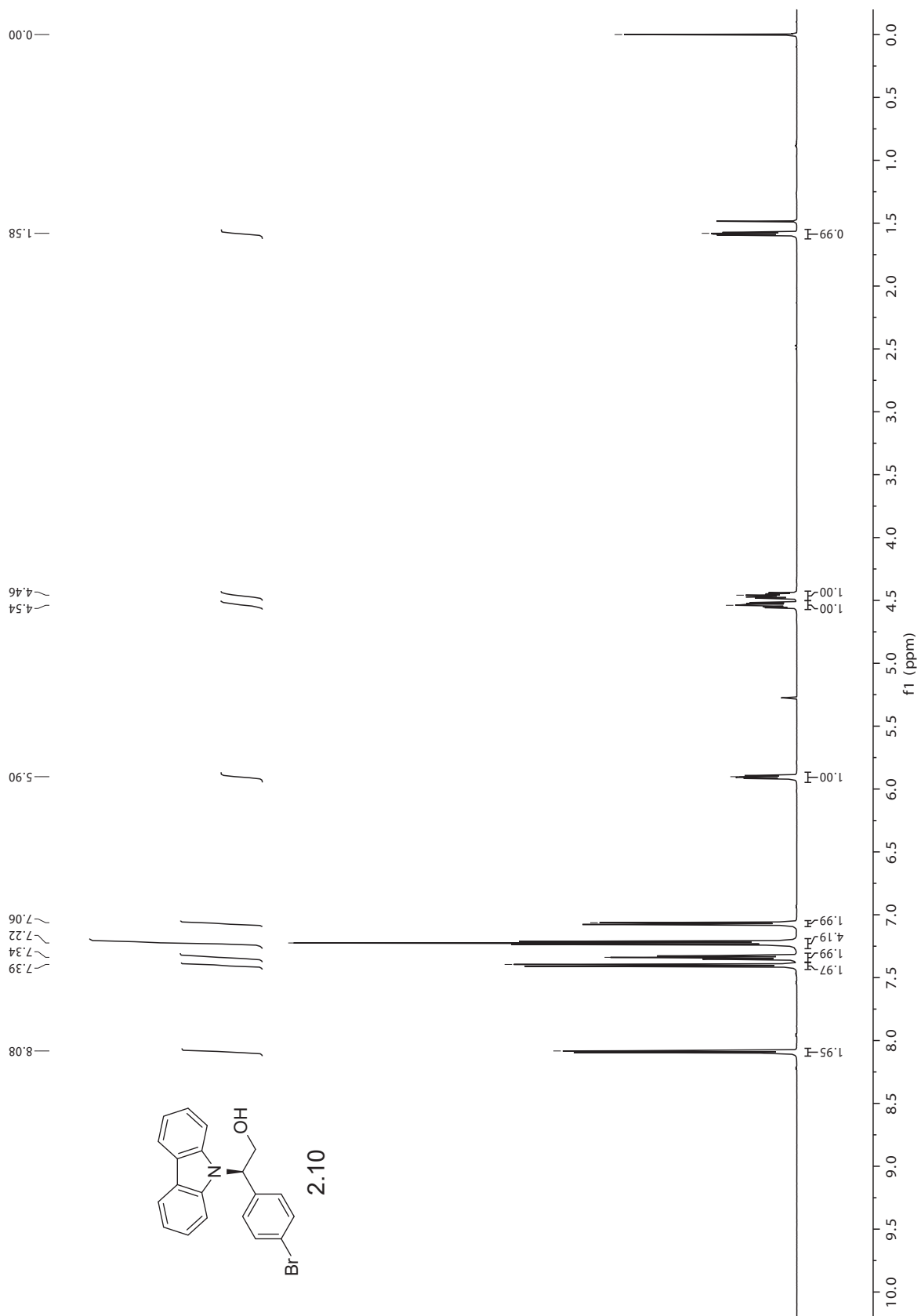


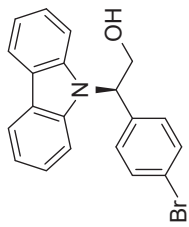




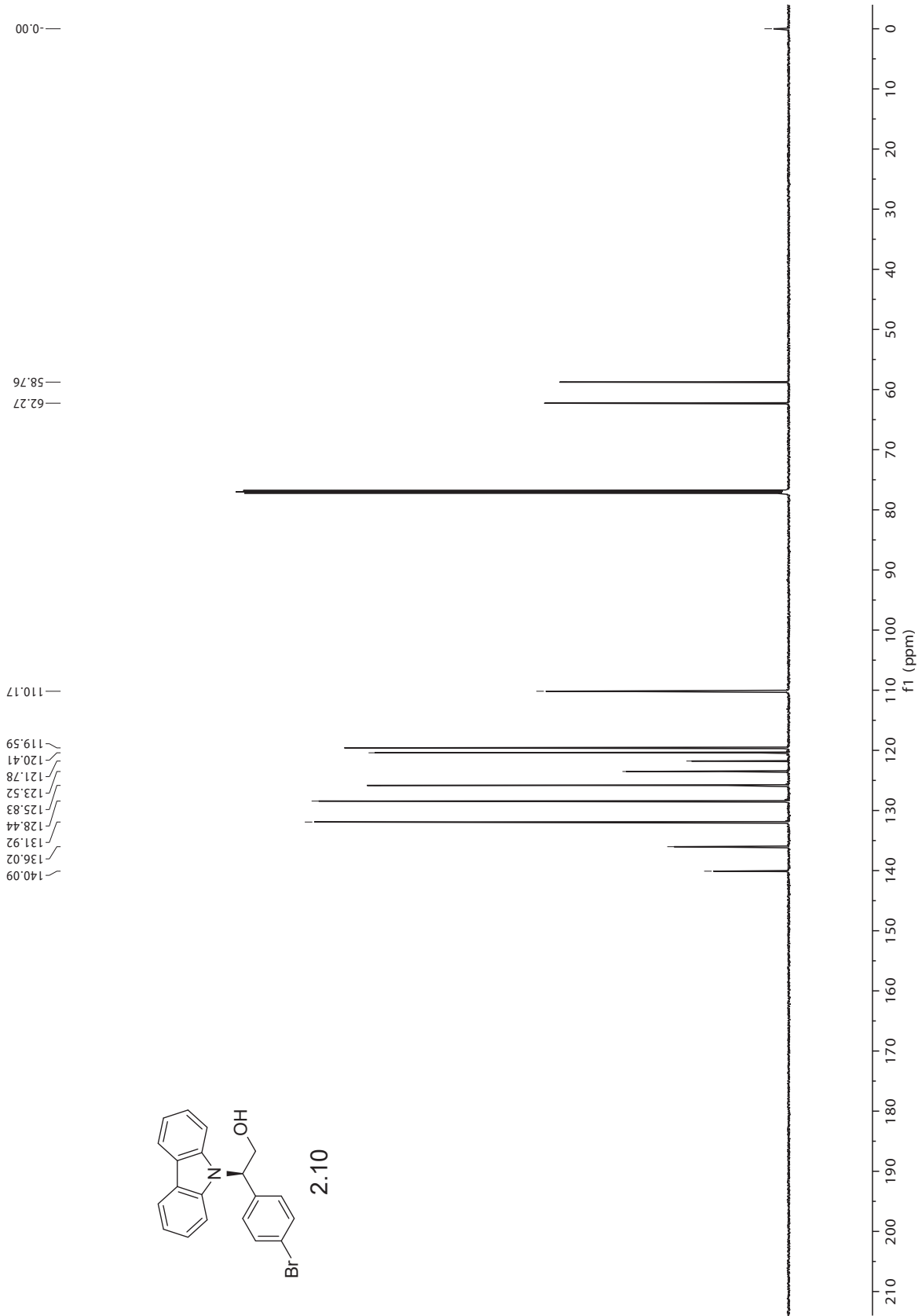


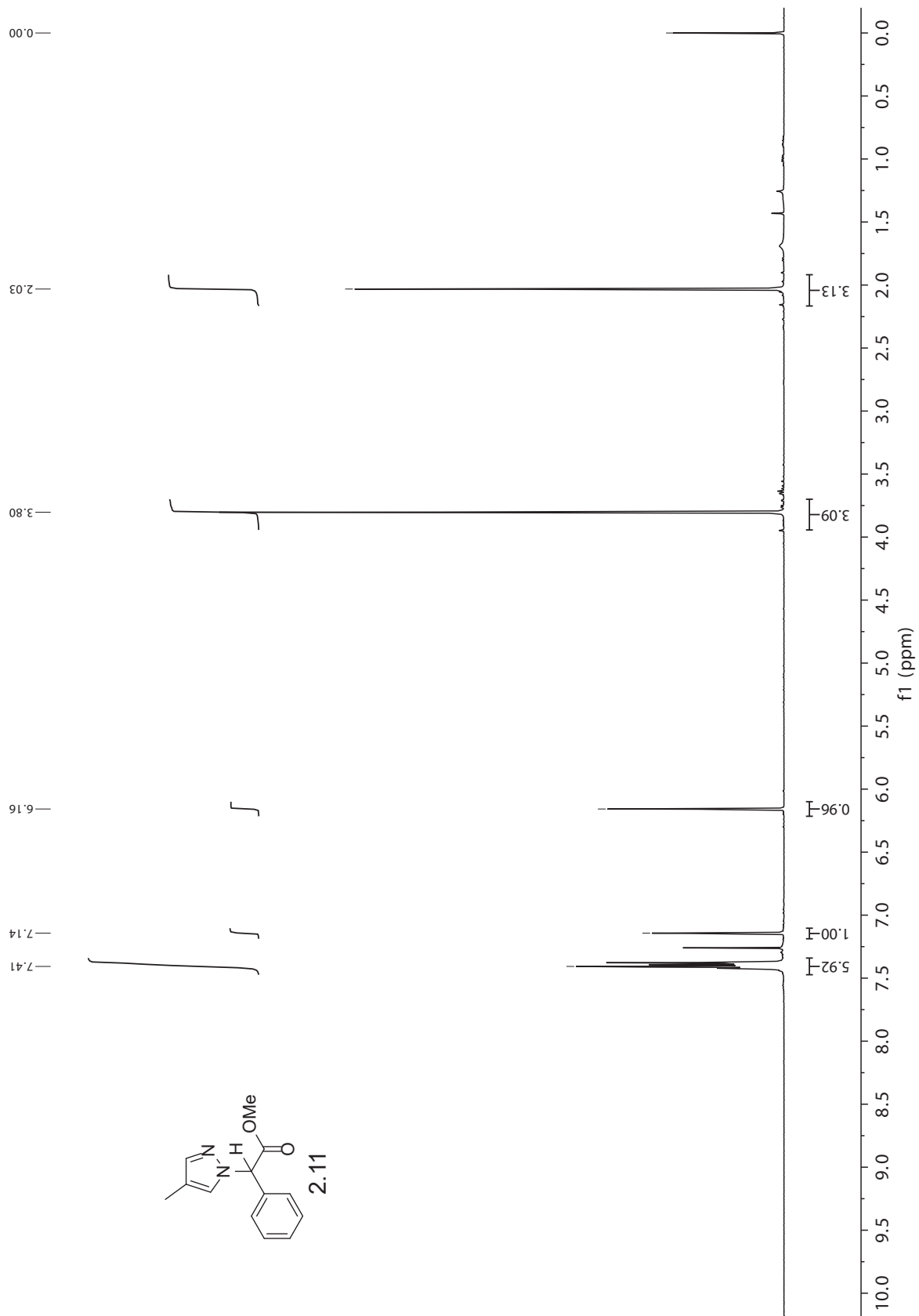


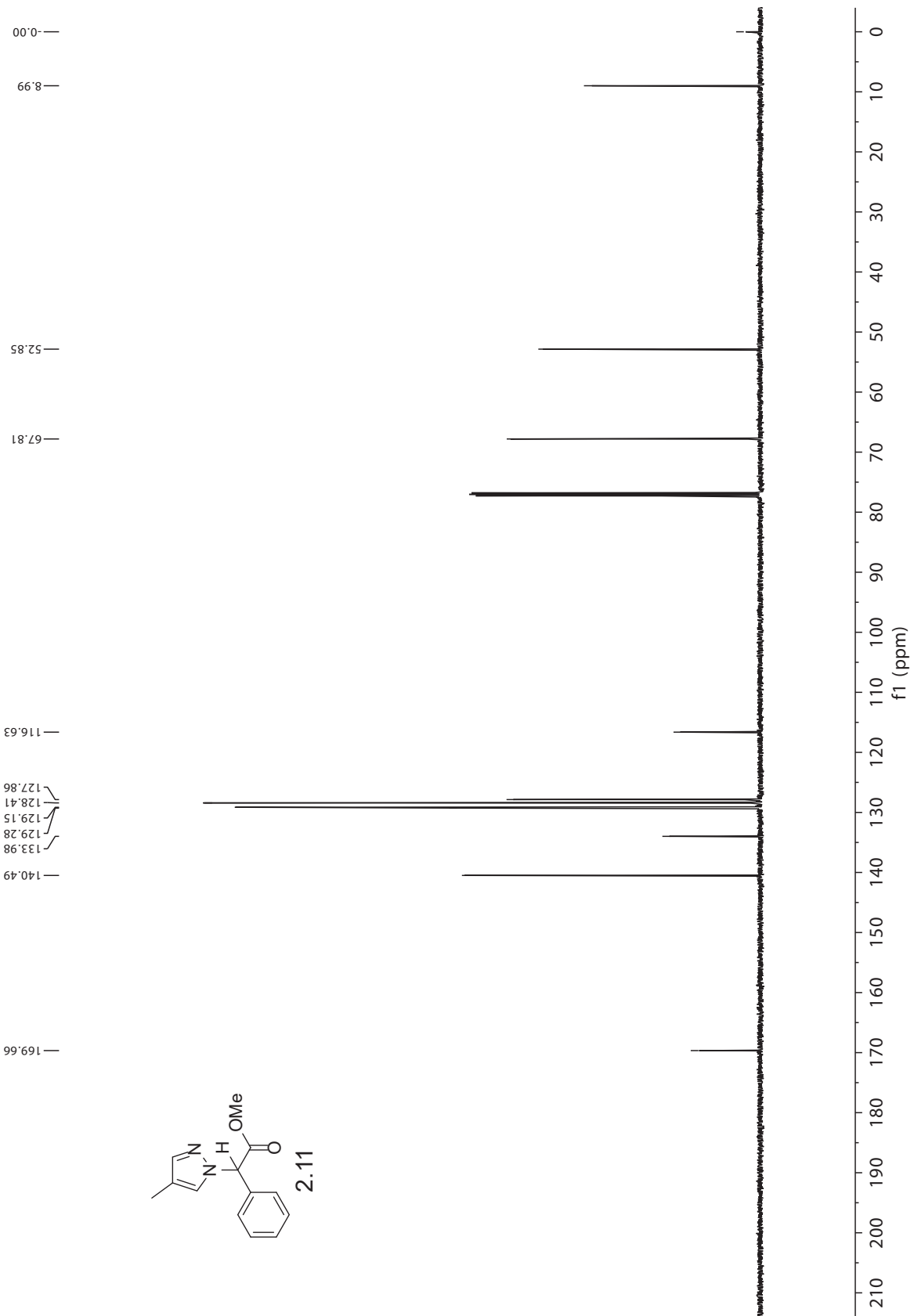


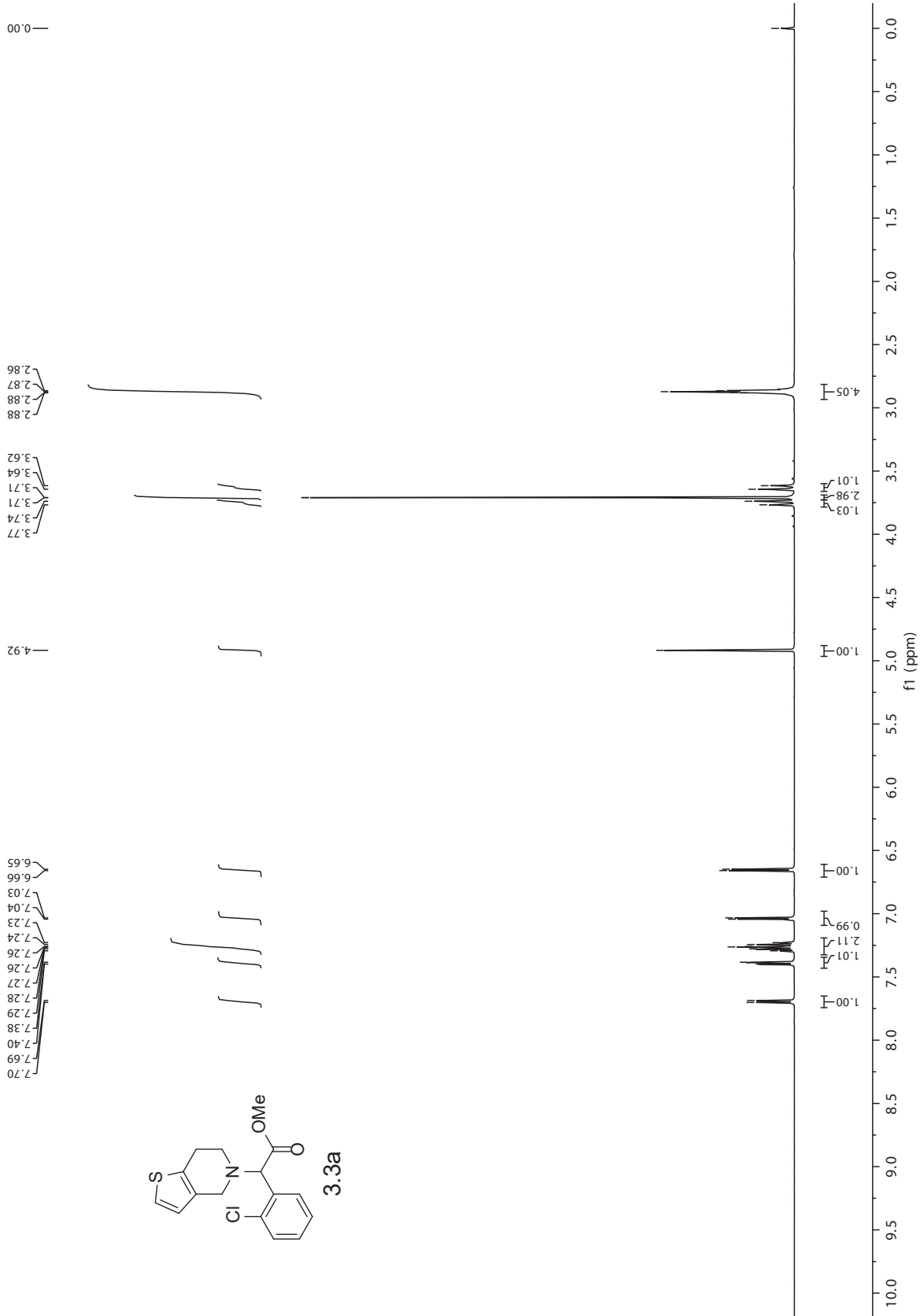


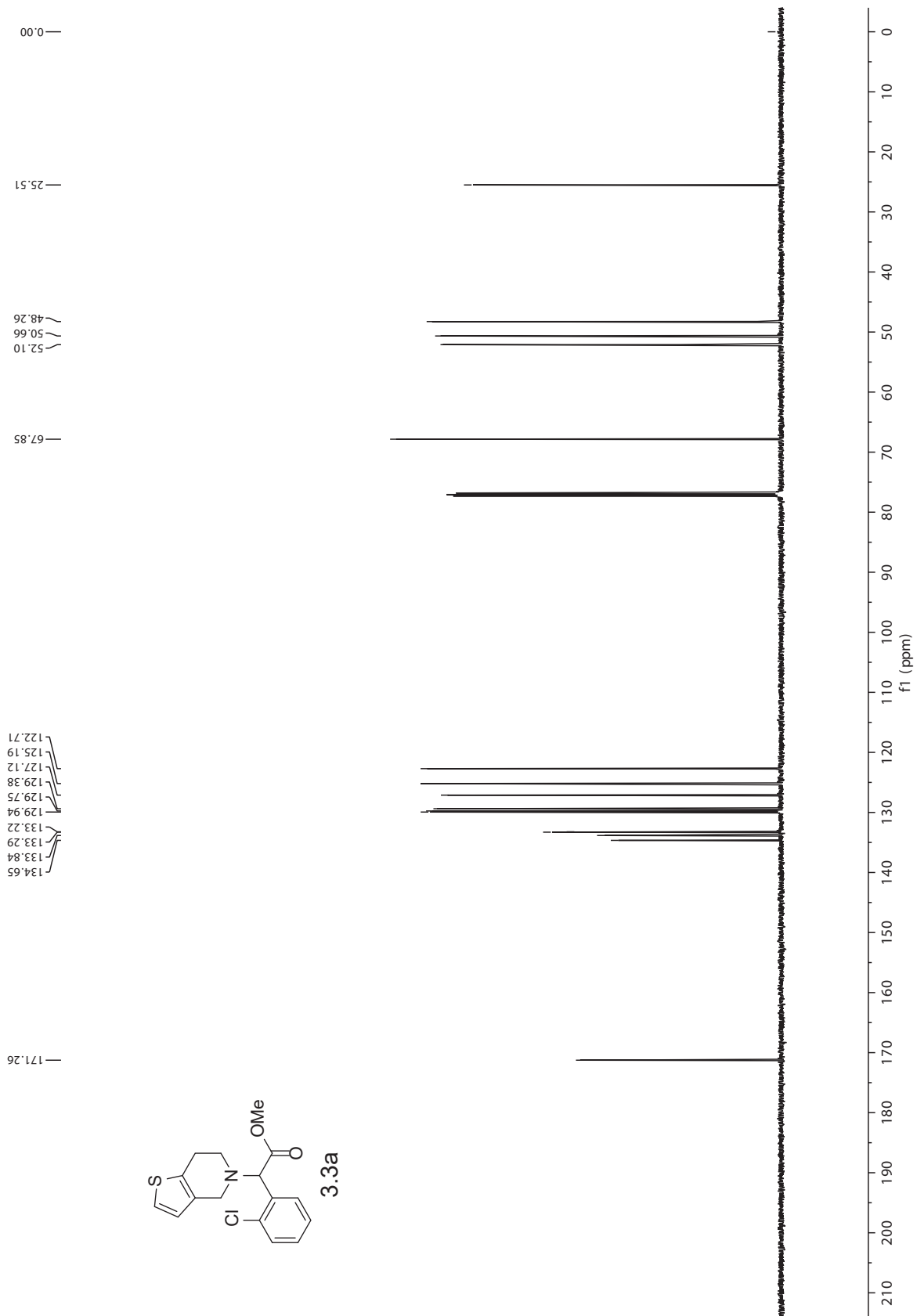
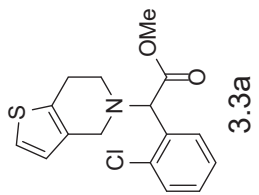
2.10

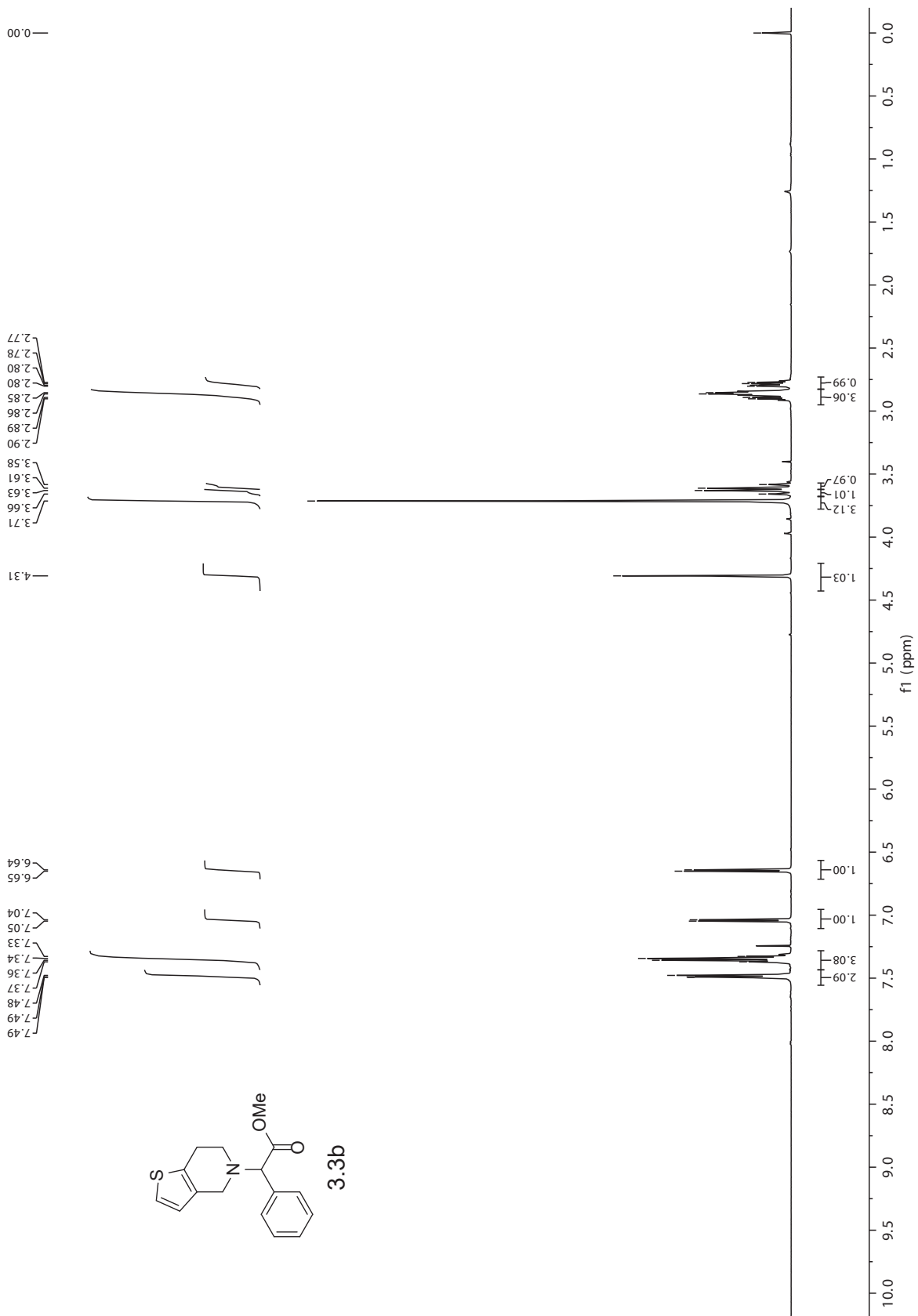


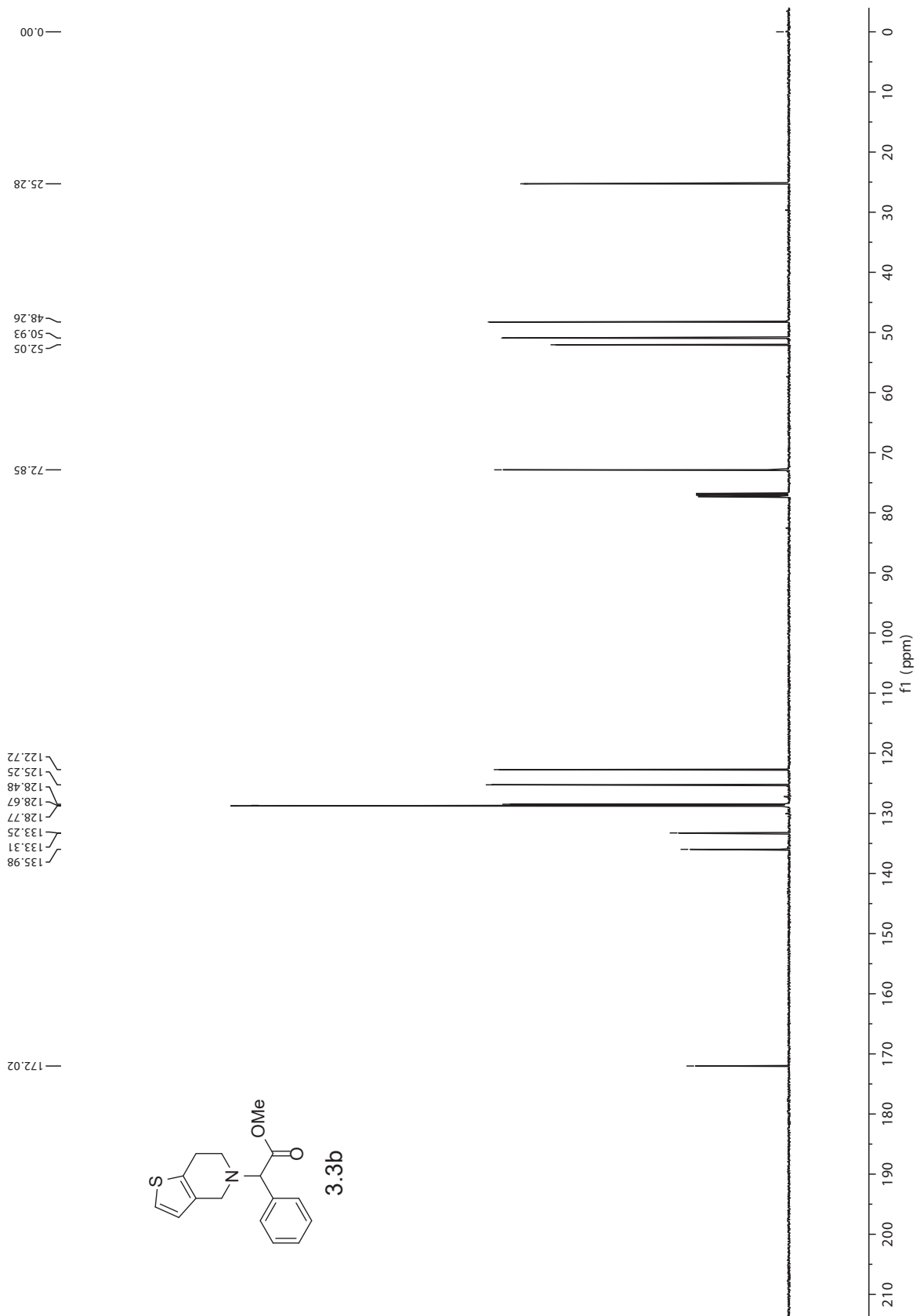


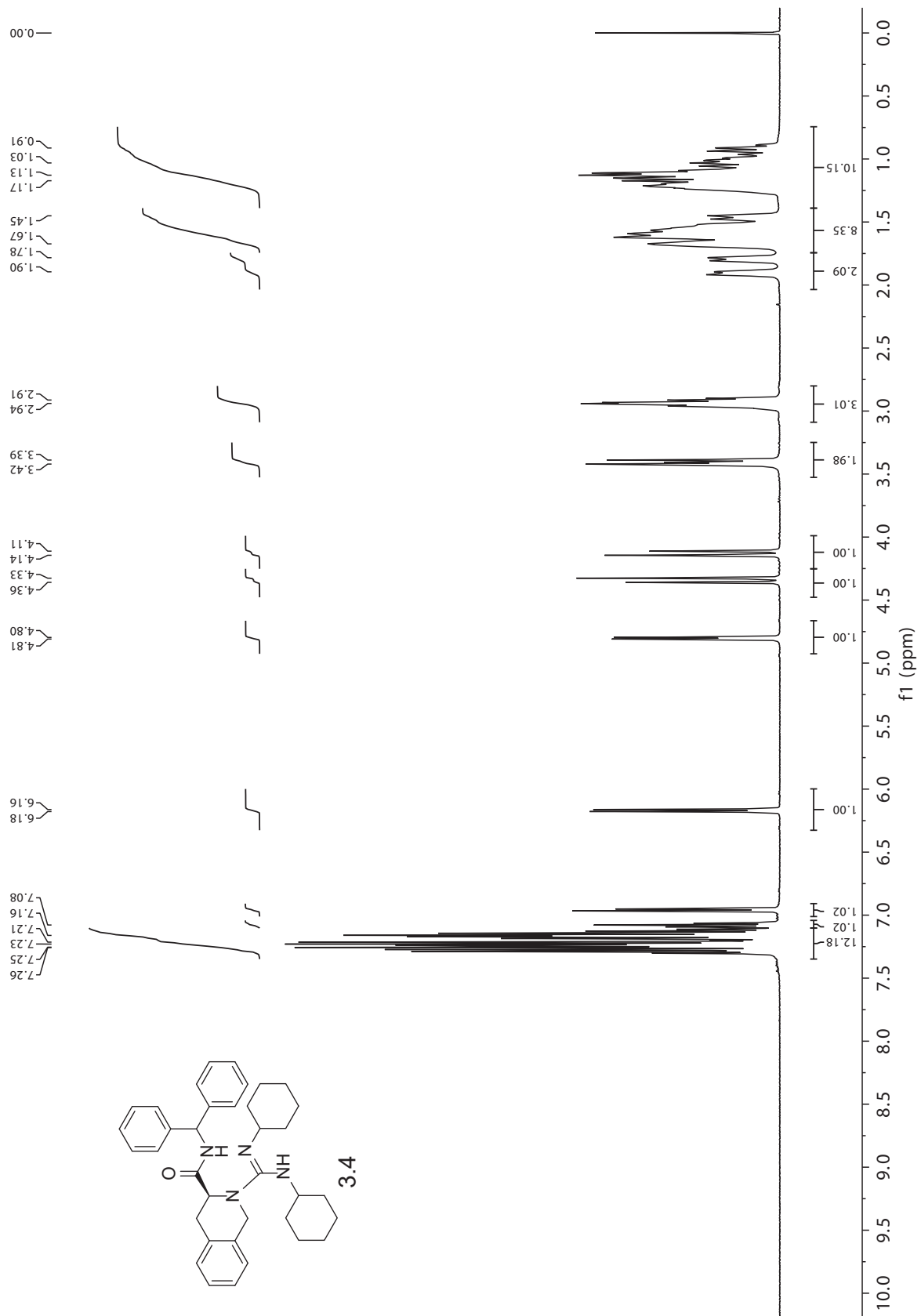


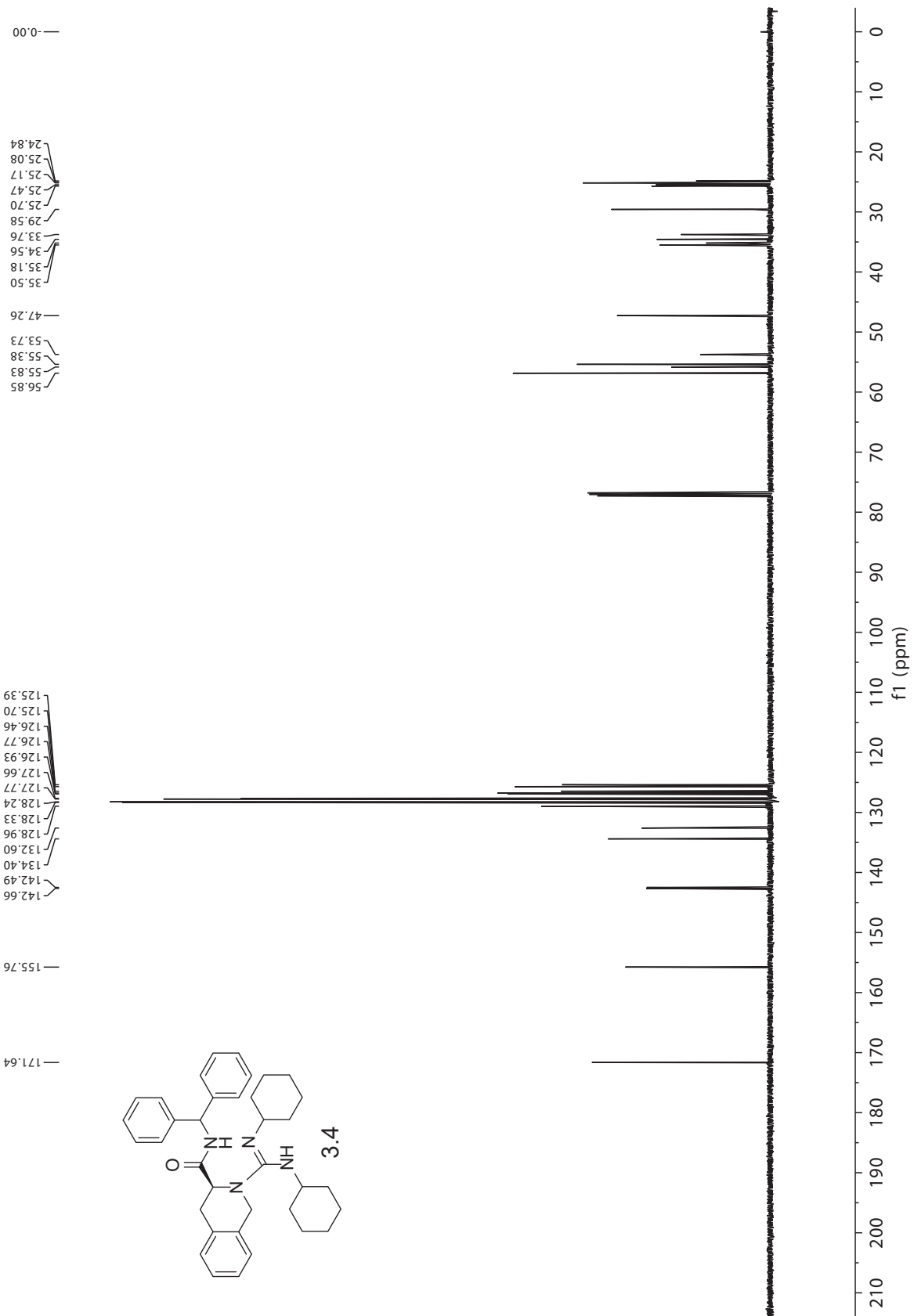


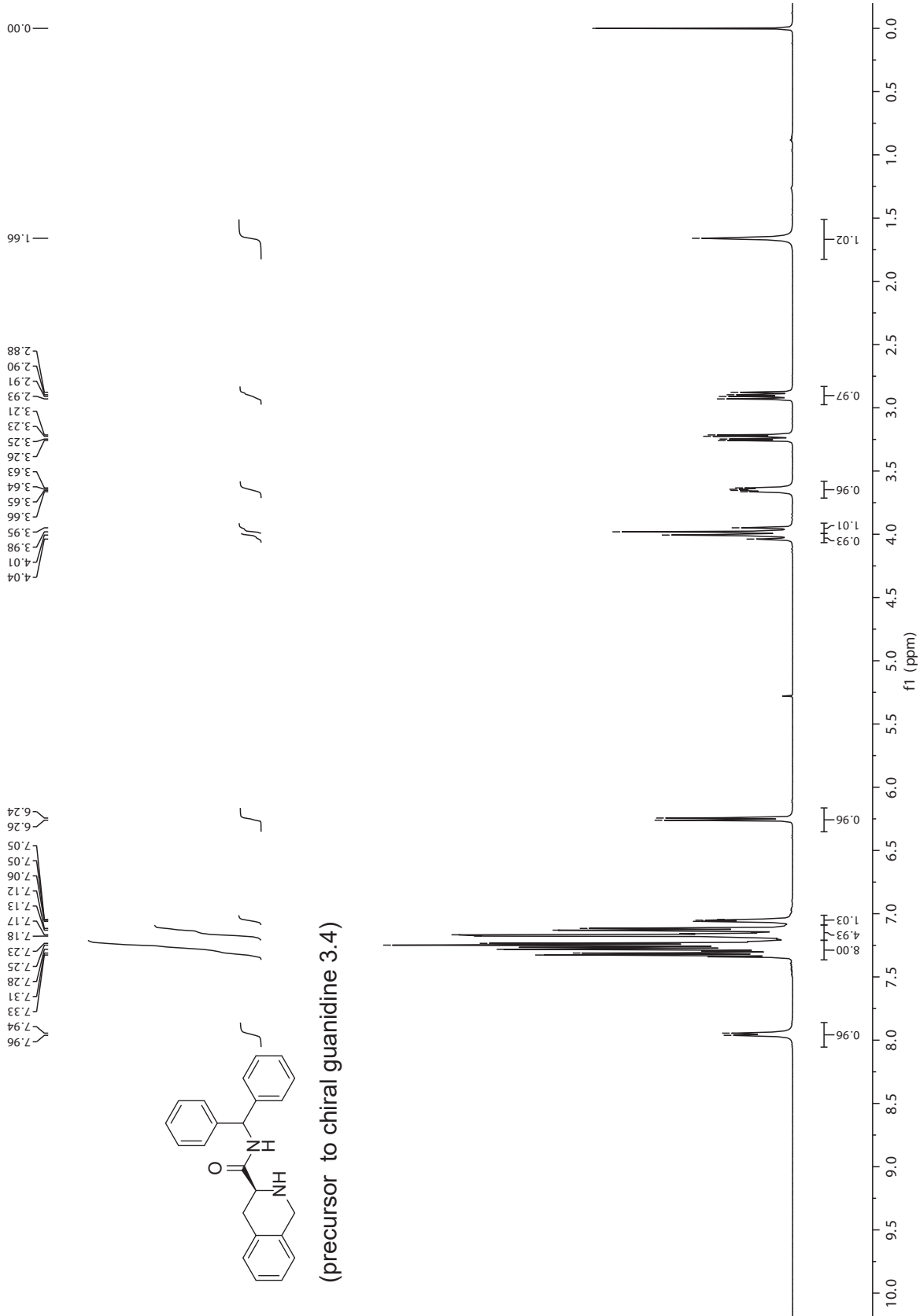


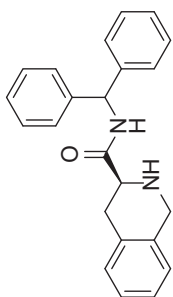




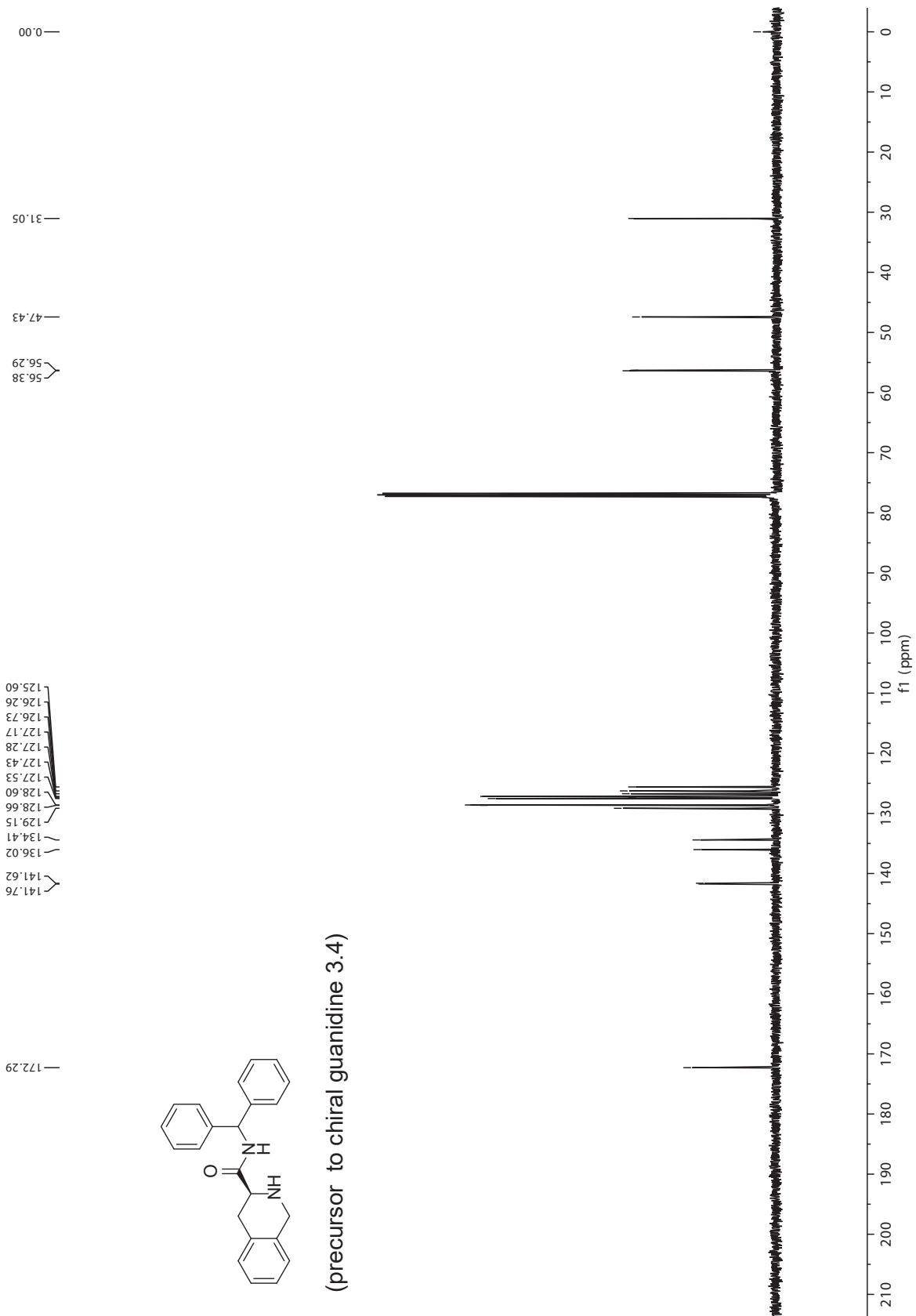


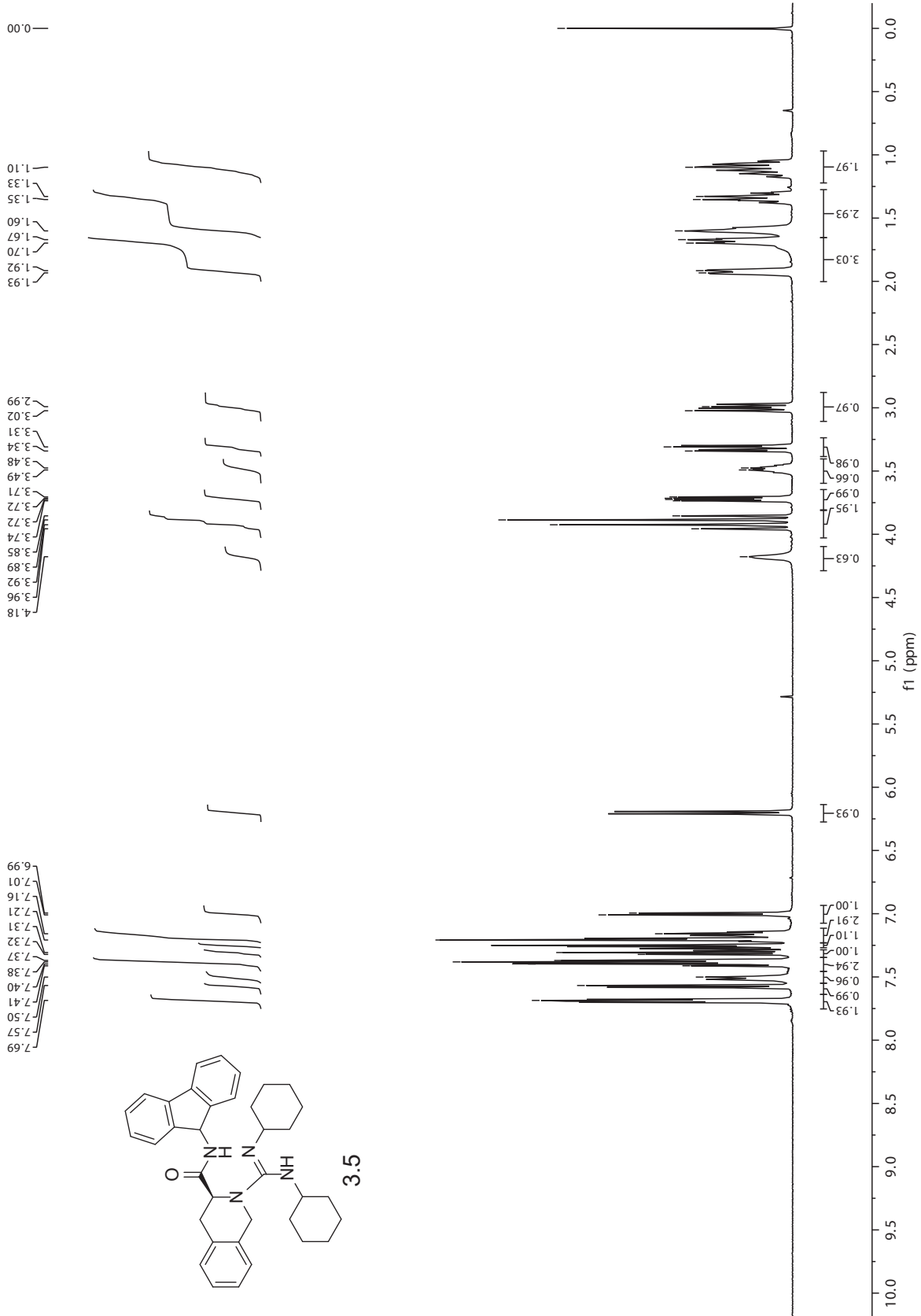


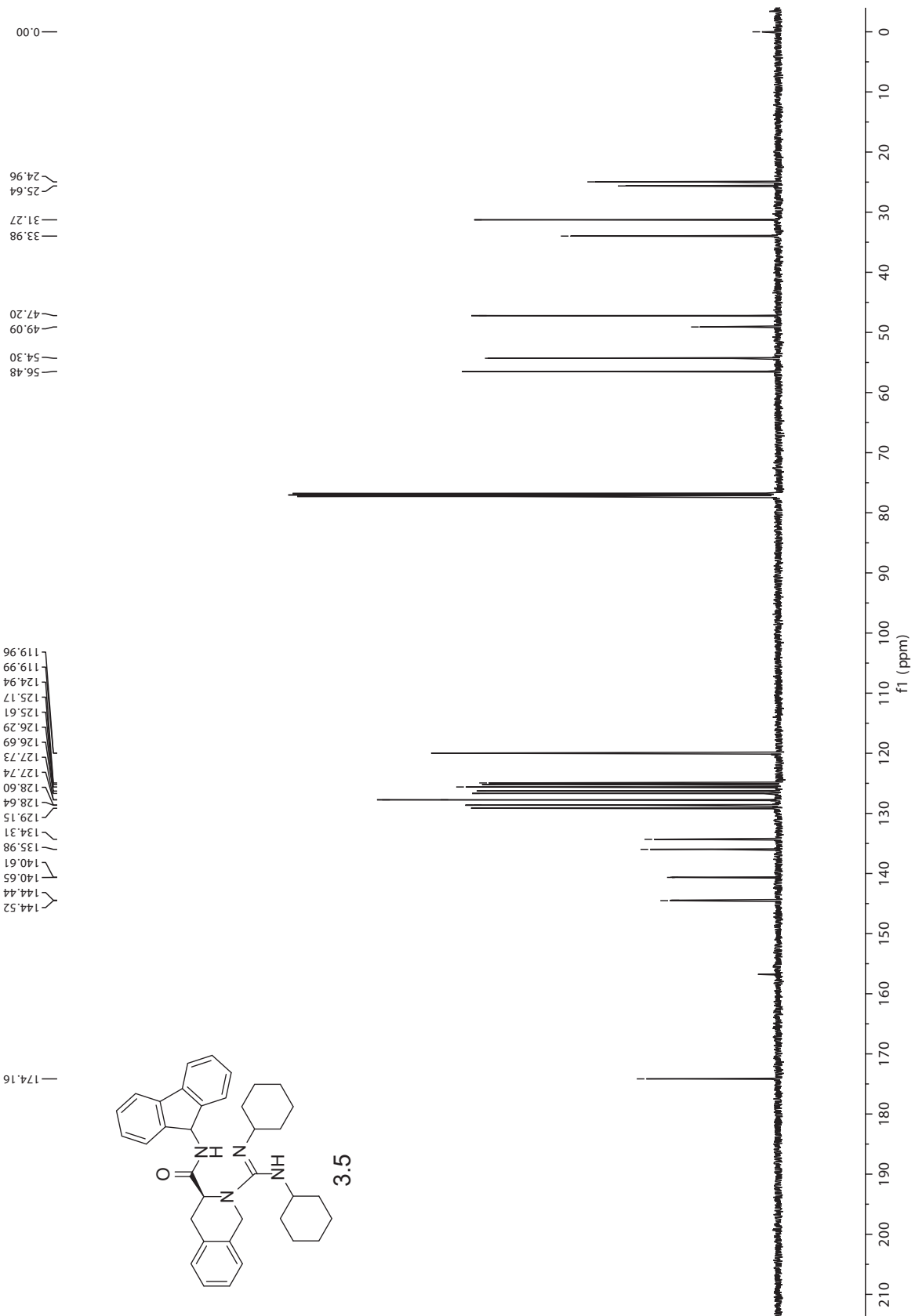


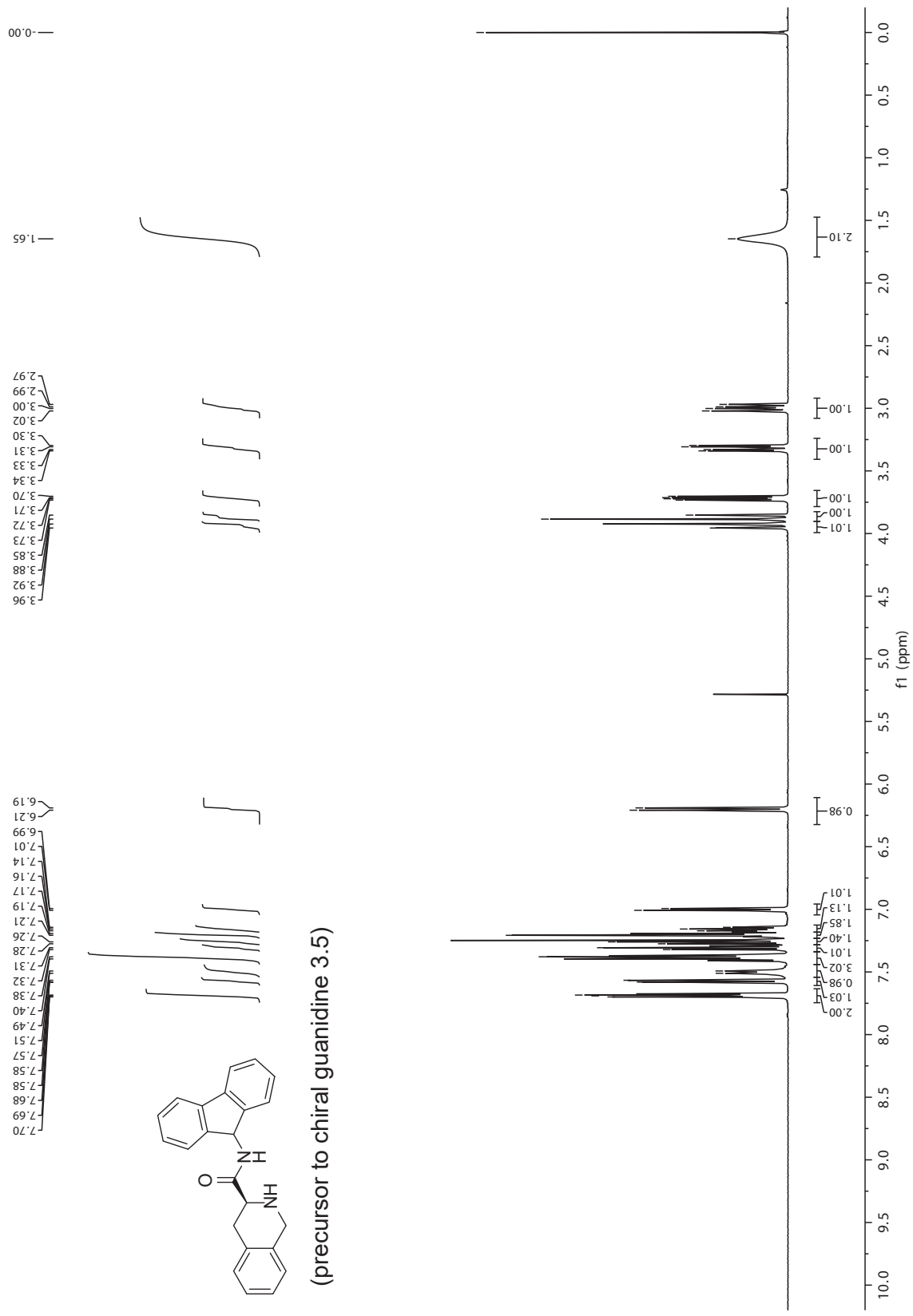


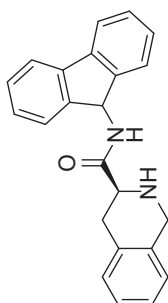
(precursor to chiral guanidine 3.4)



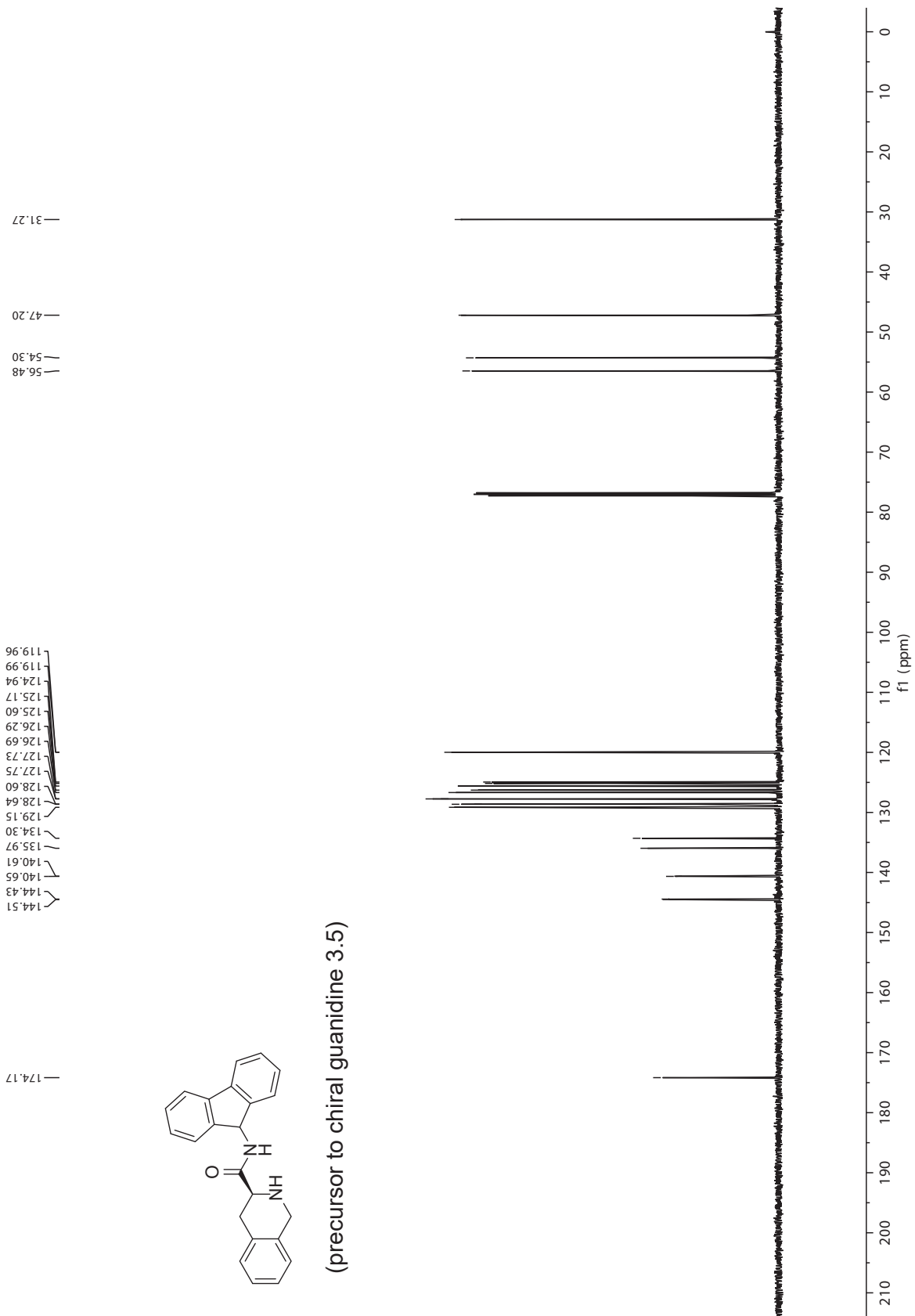


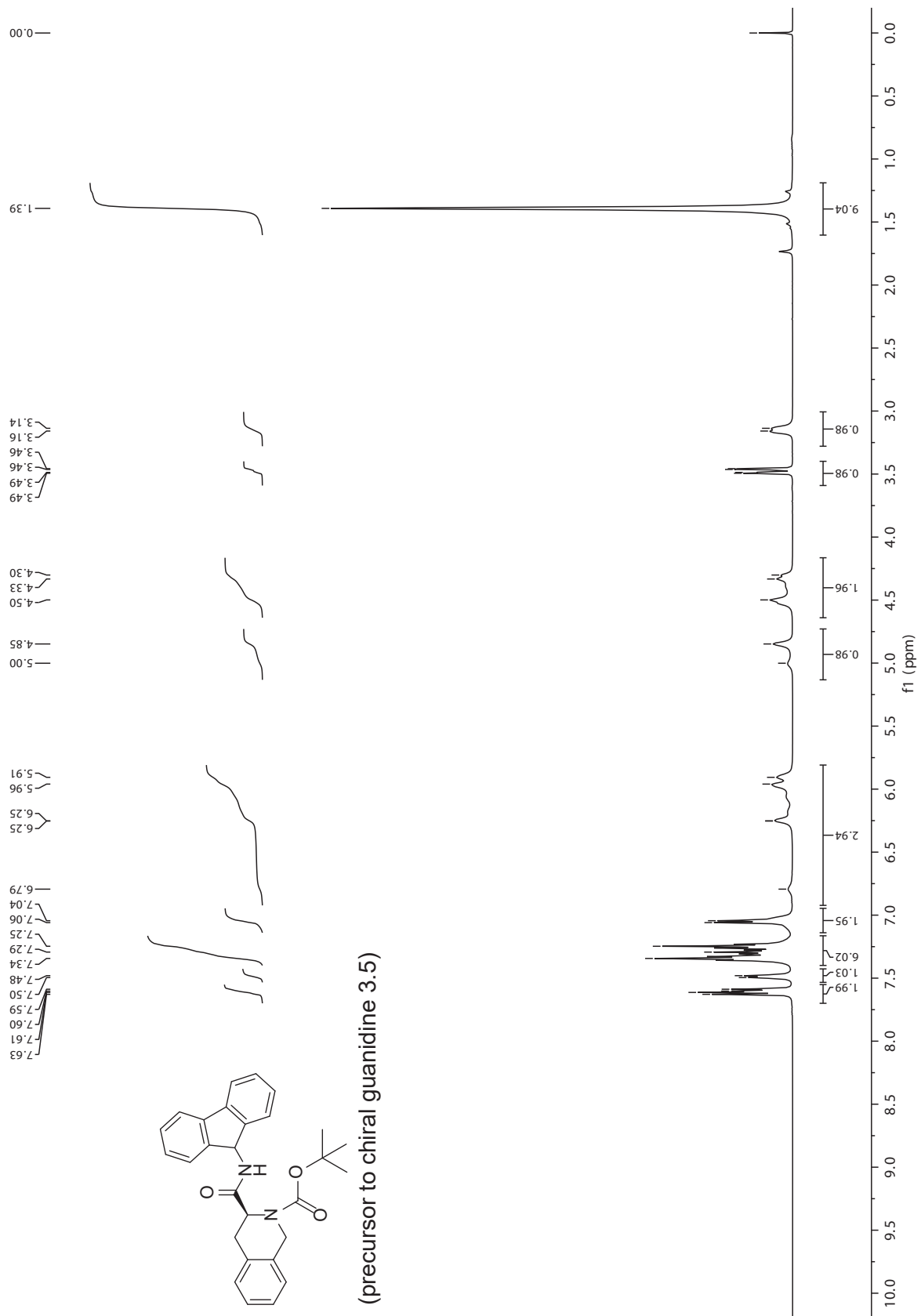


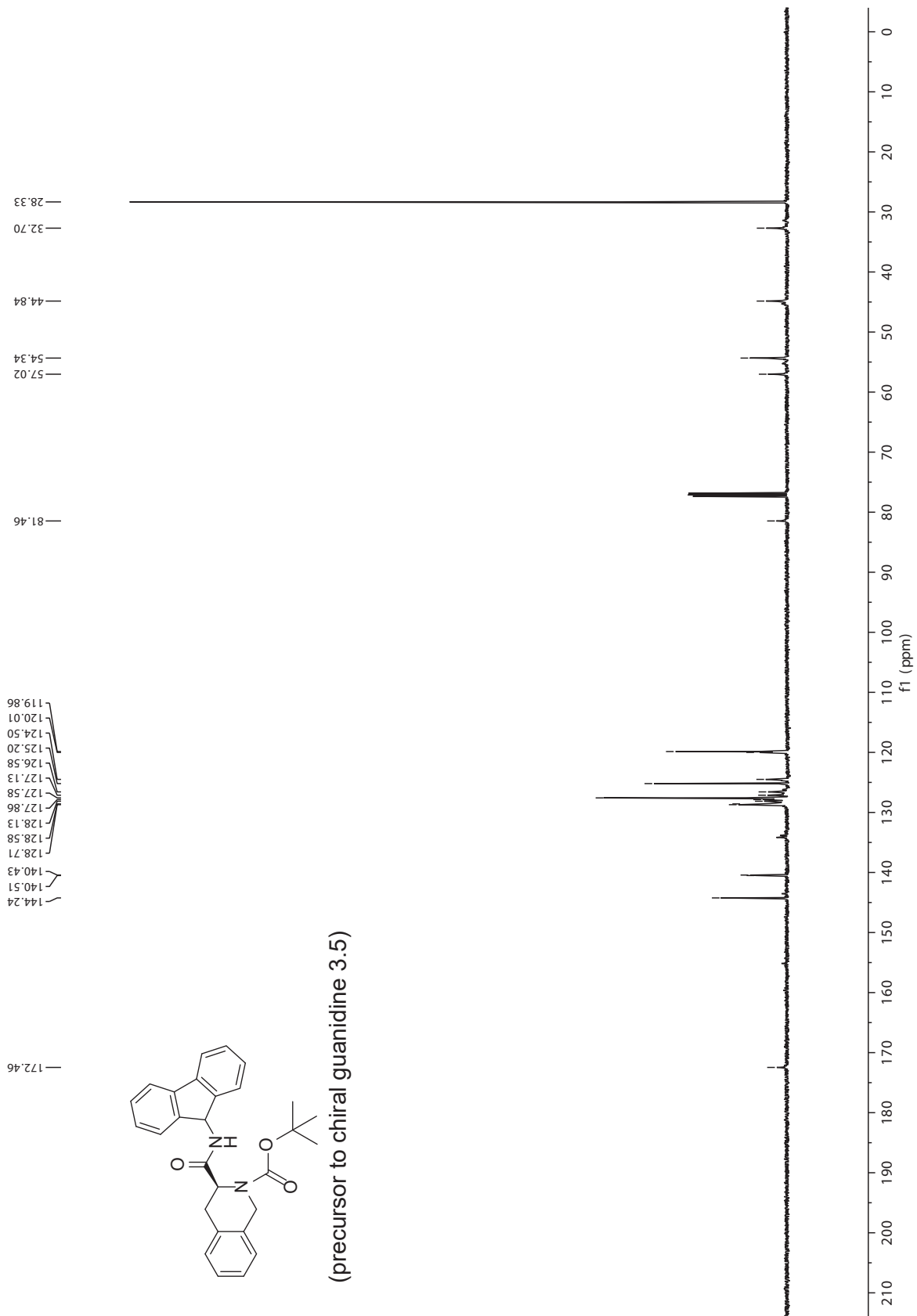


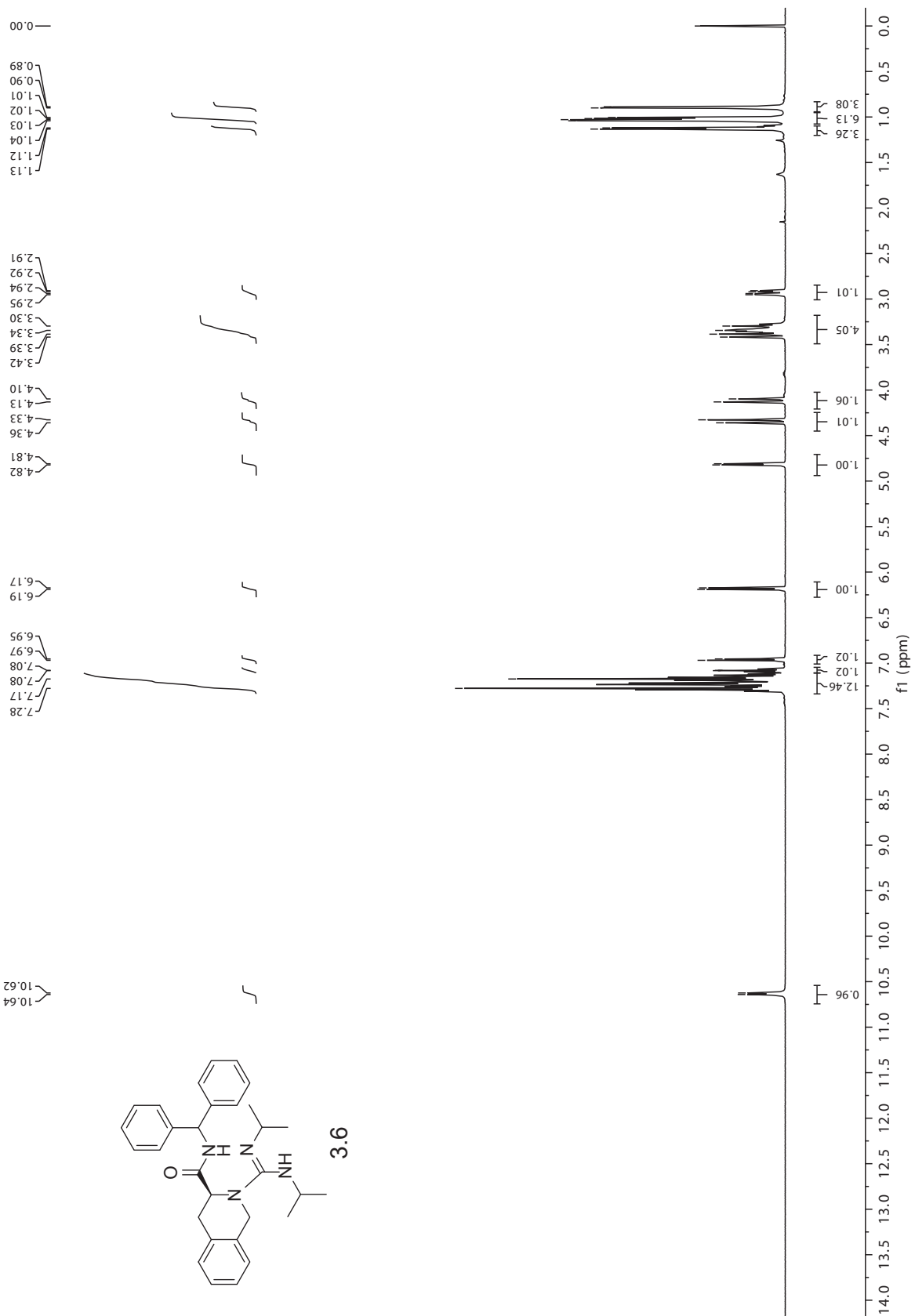


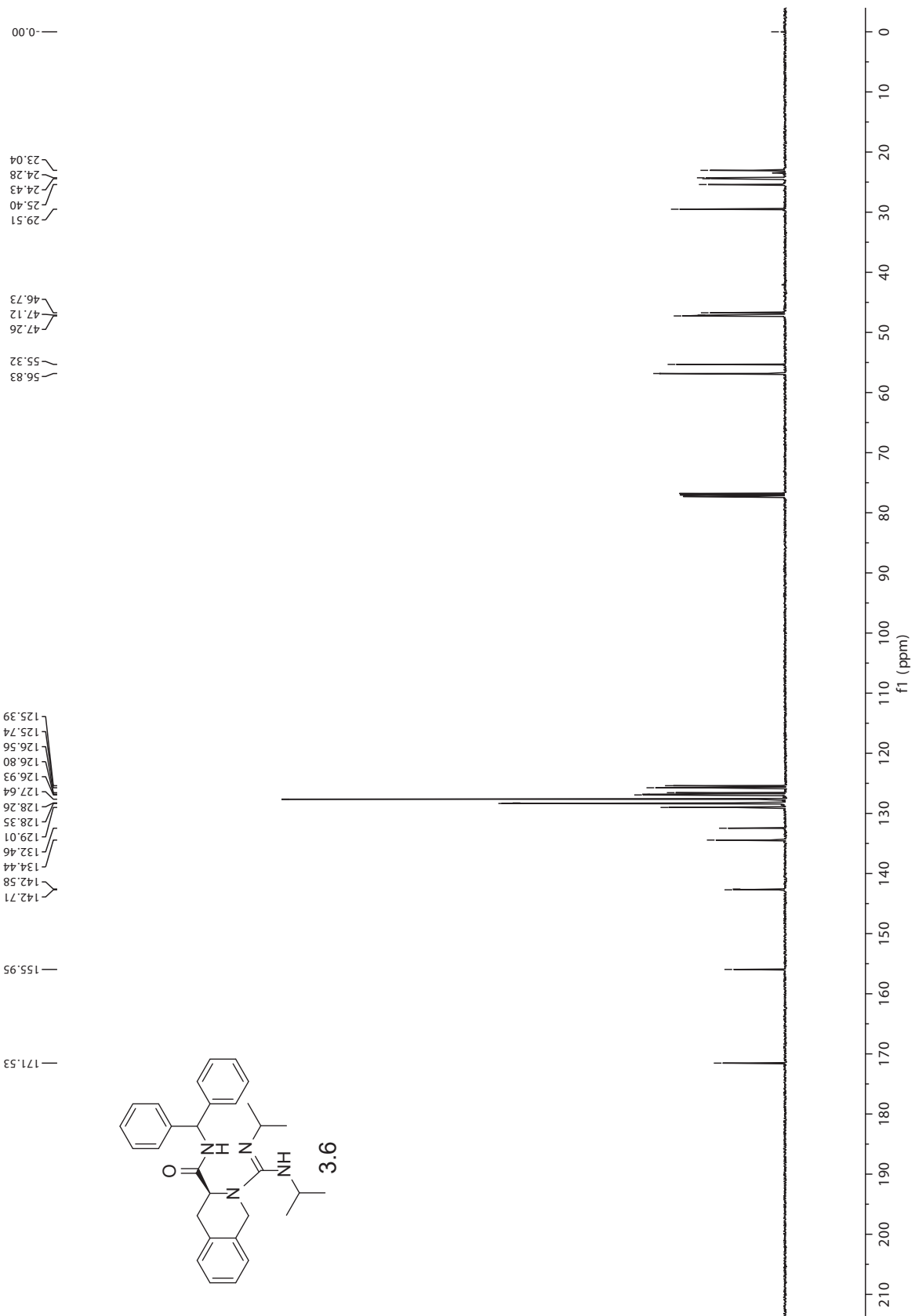
(precursor to chiral guanidine 3.5)

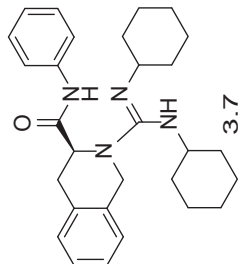
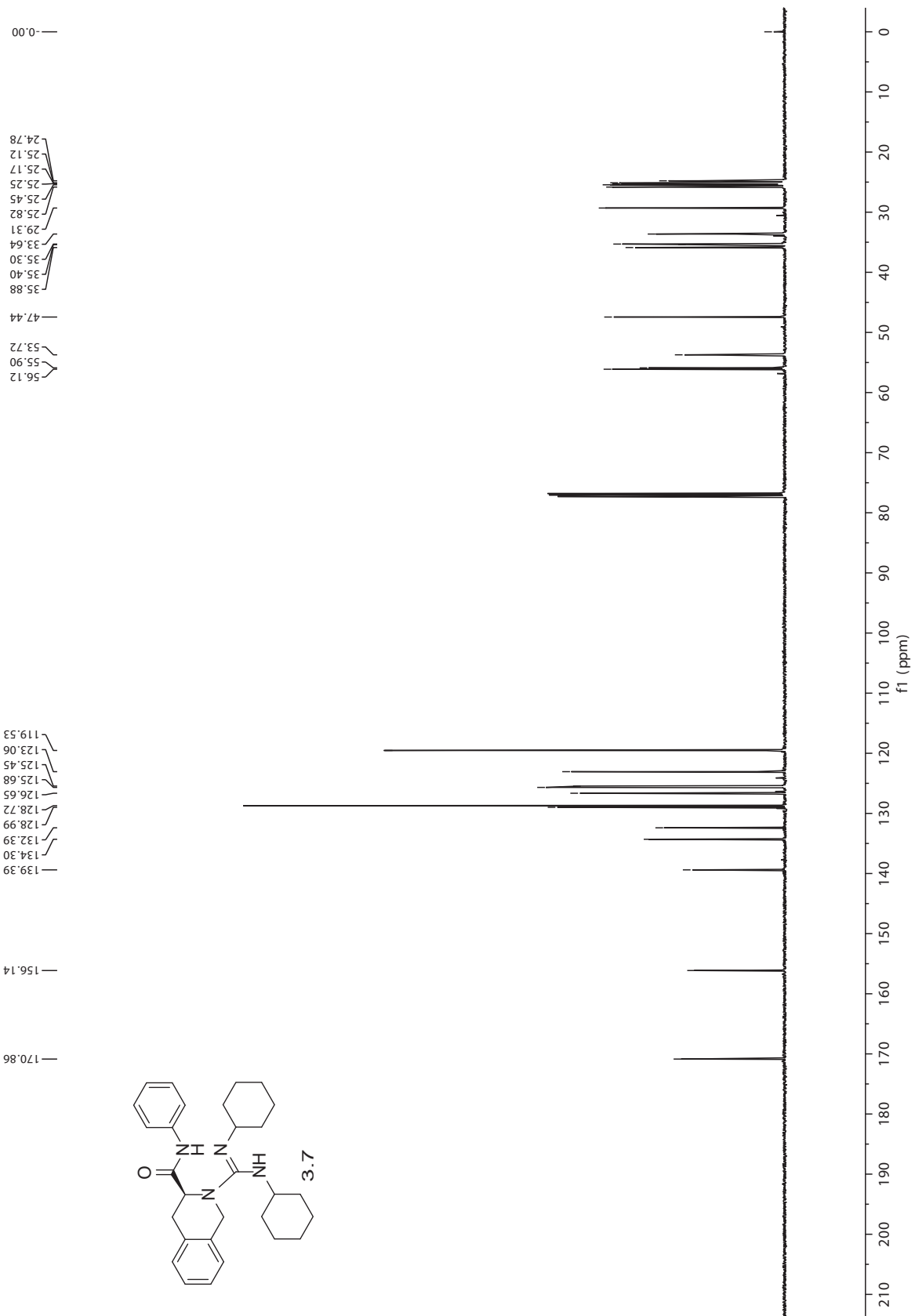


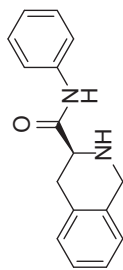




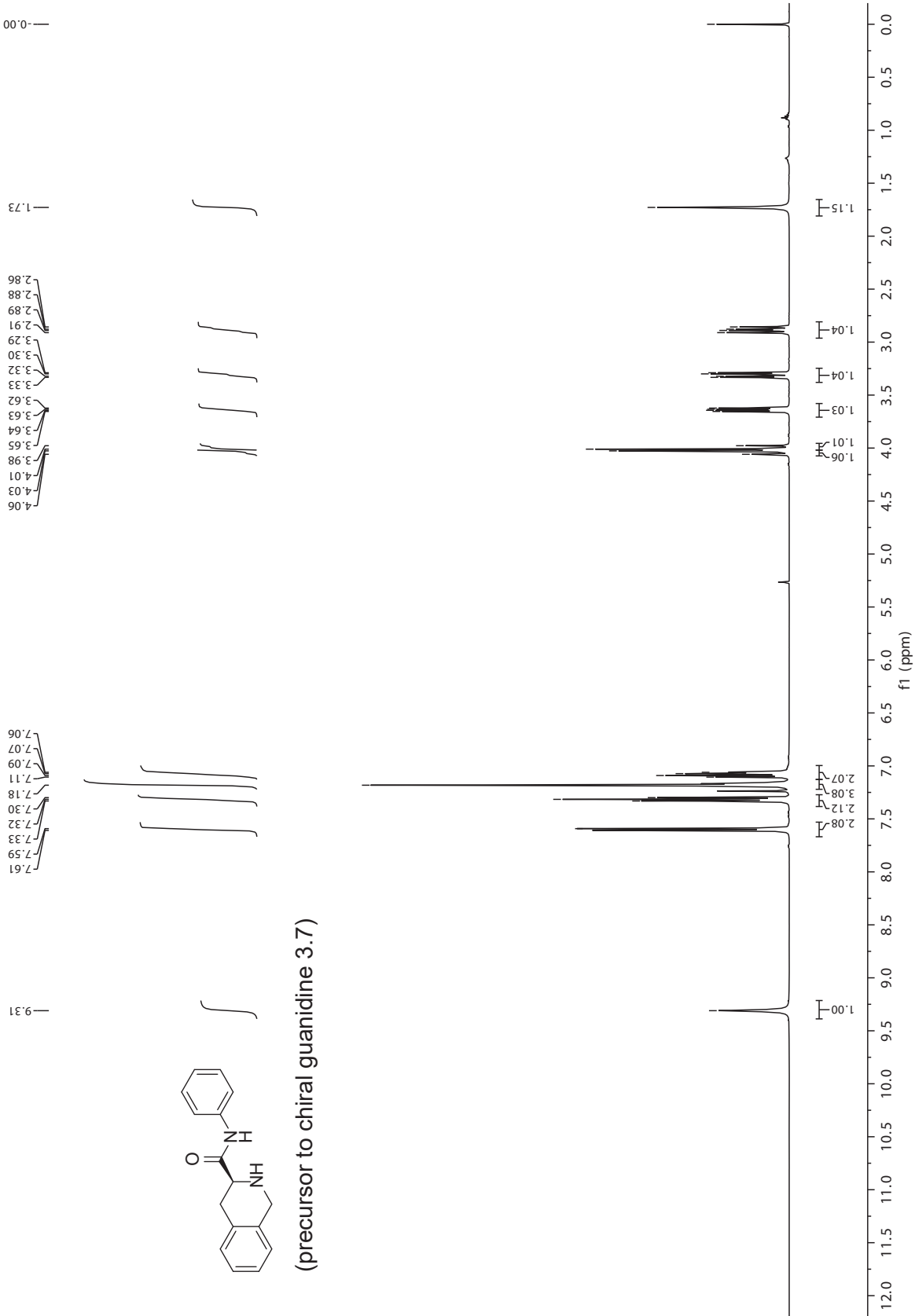


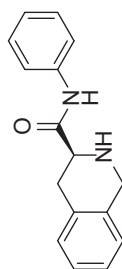




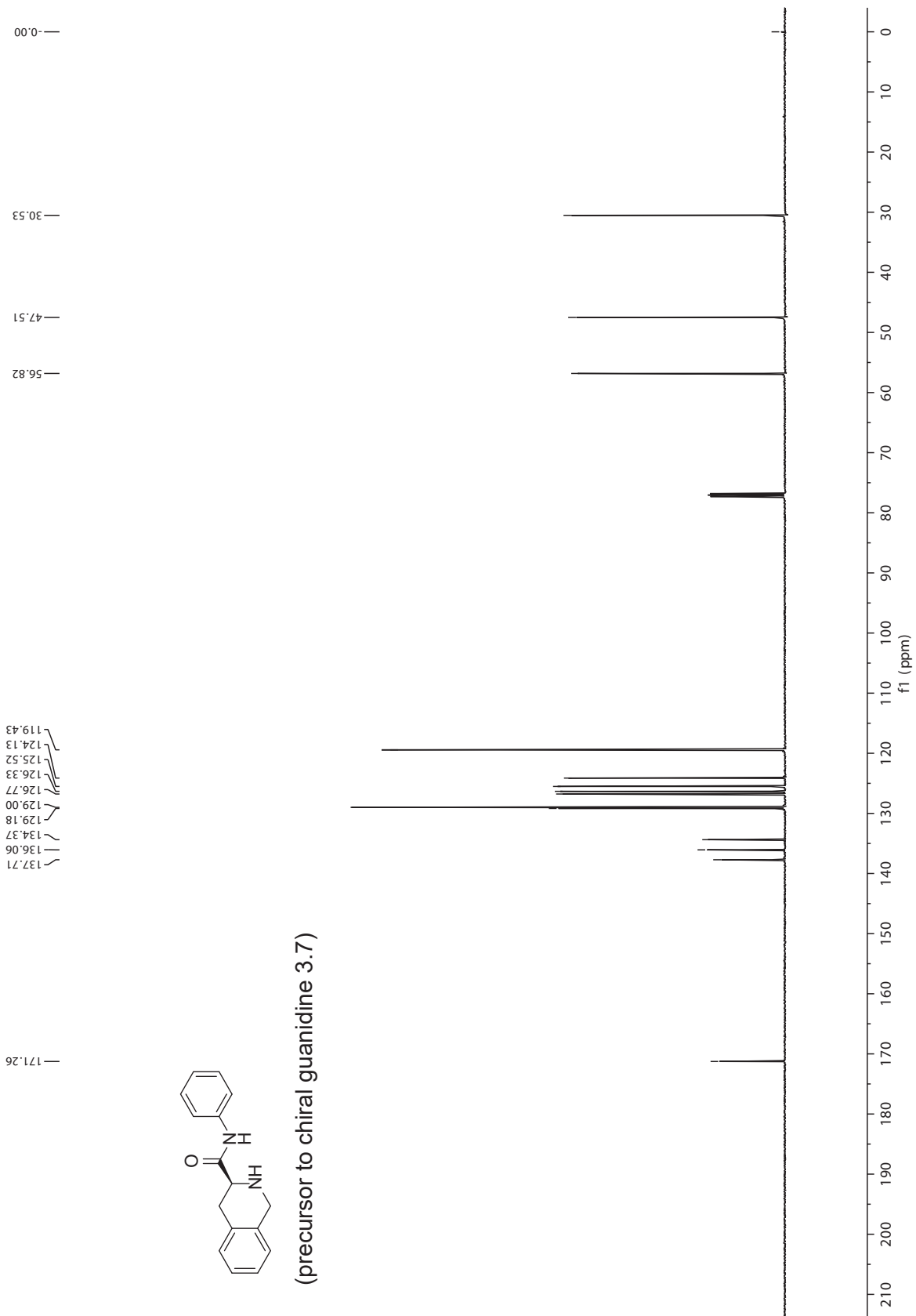


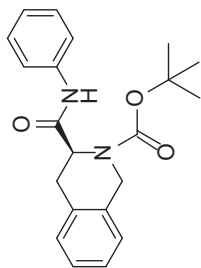
(precursor to chiral guanidine 3.7)



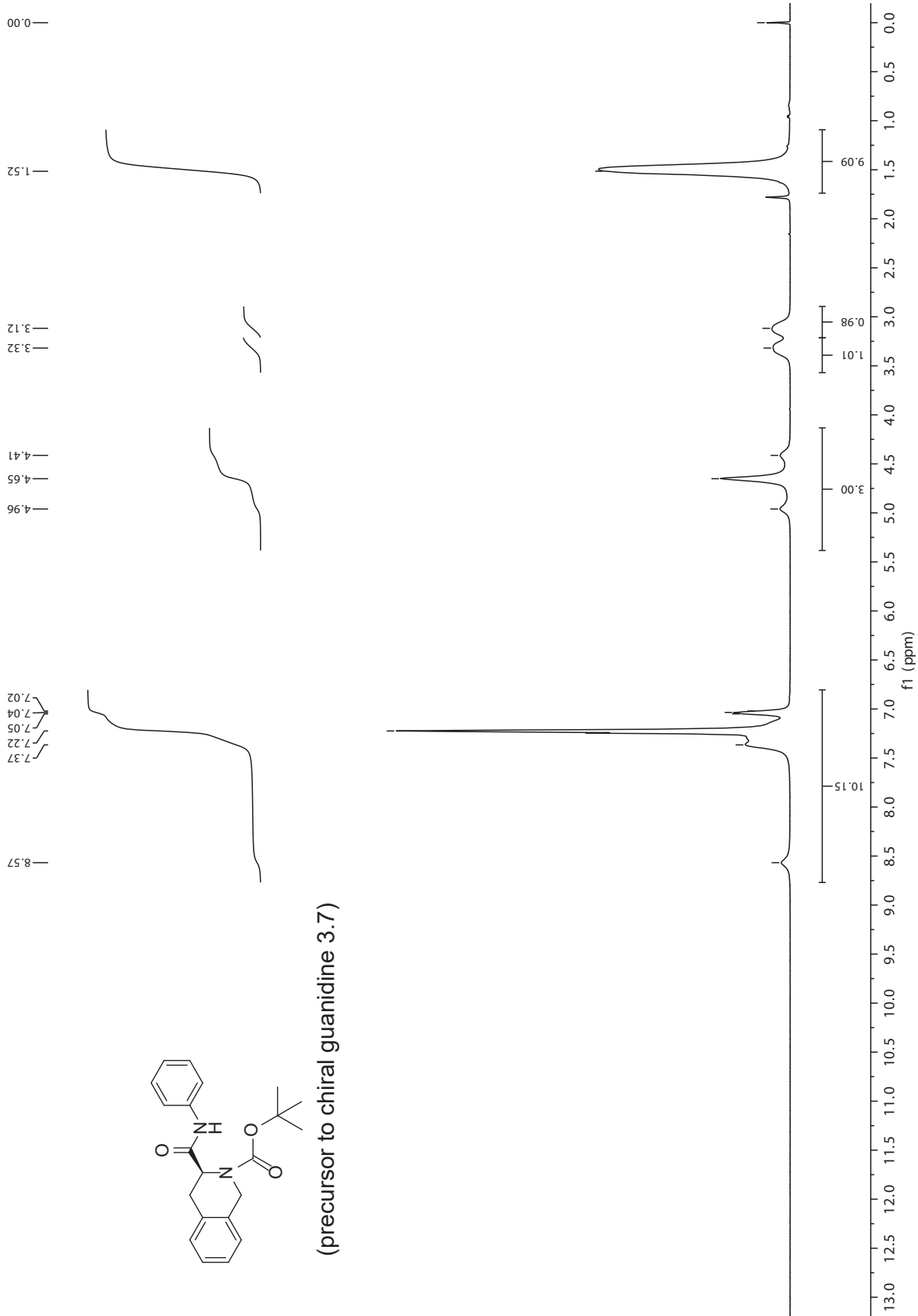


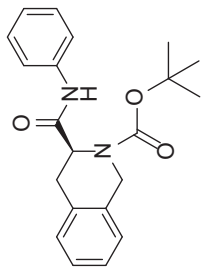
(precursor to chiral guanidine 3.7)



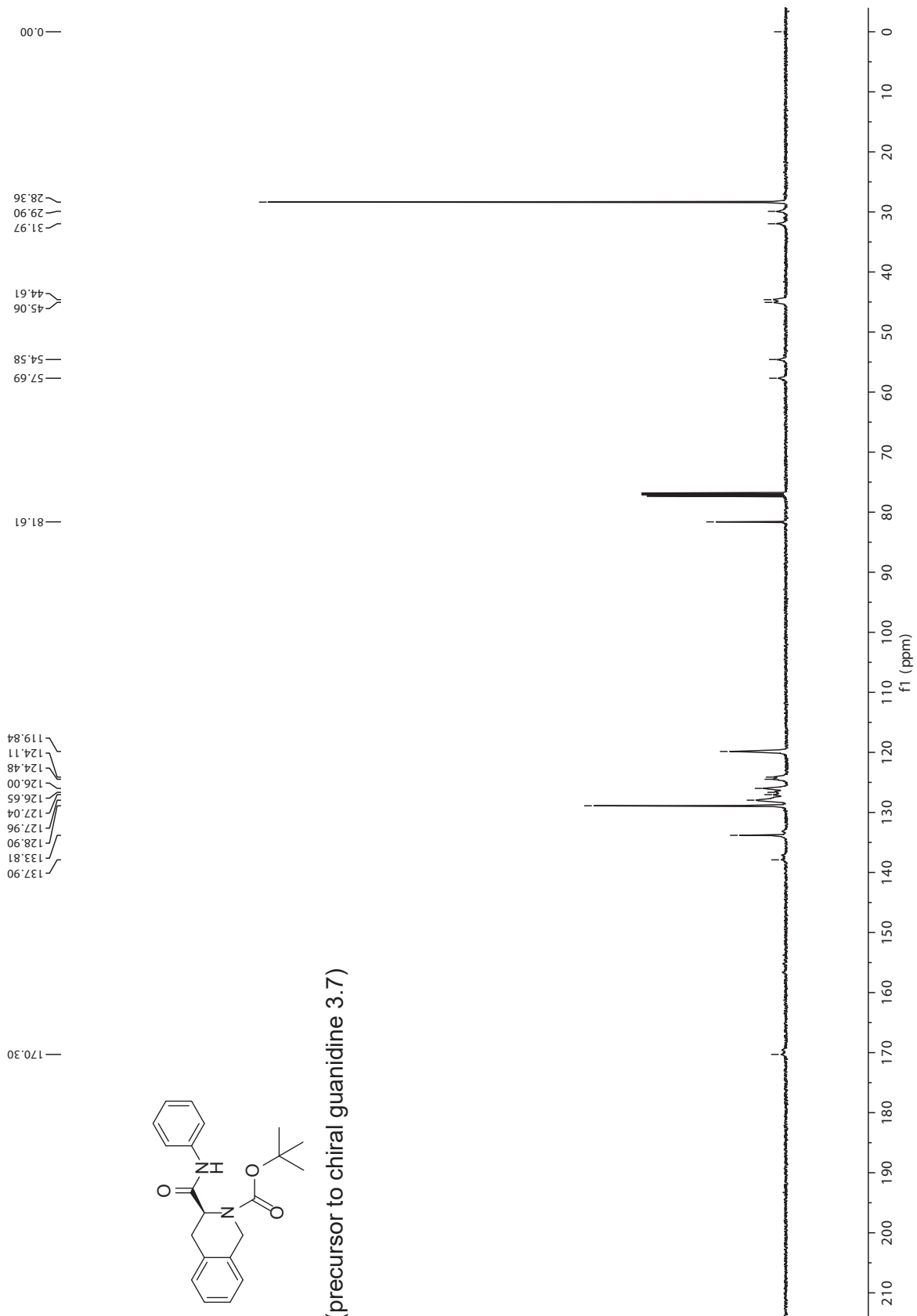


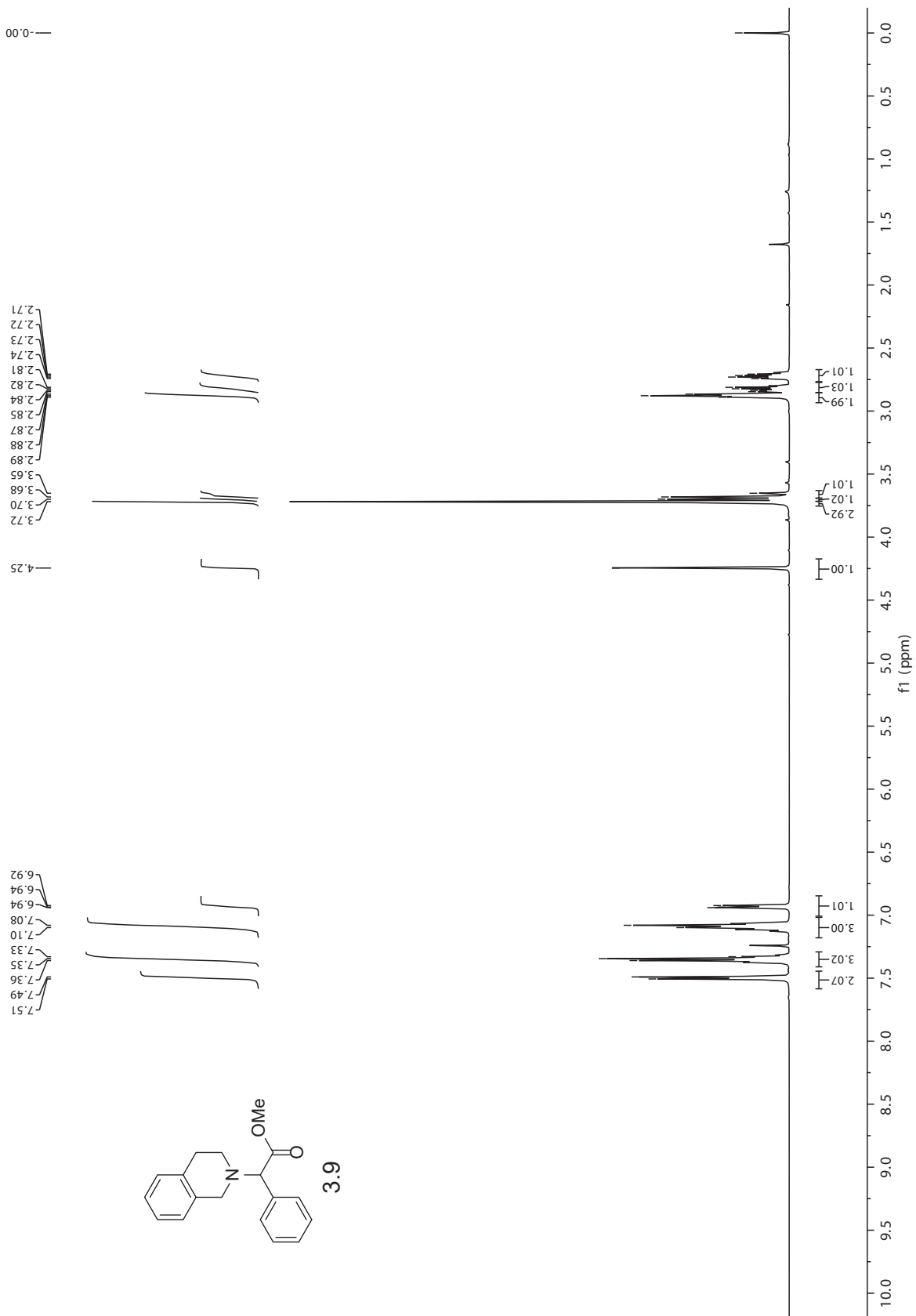
(precursor to chiral guanidine 3.7)

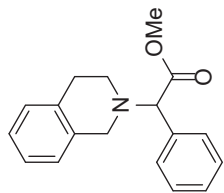




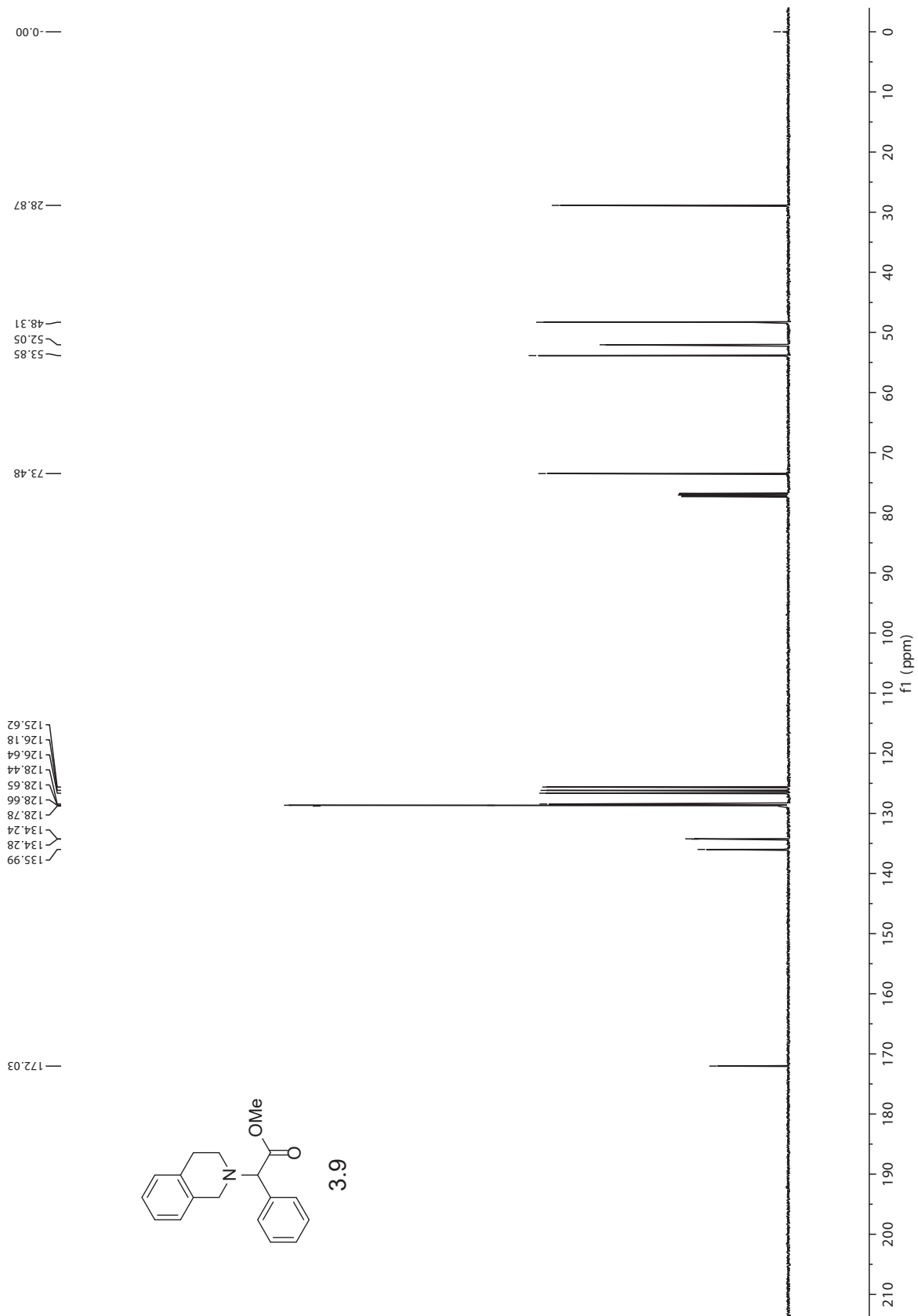
(precursor to chiral guanidine 3.7)

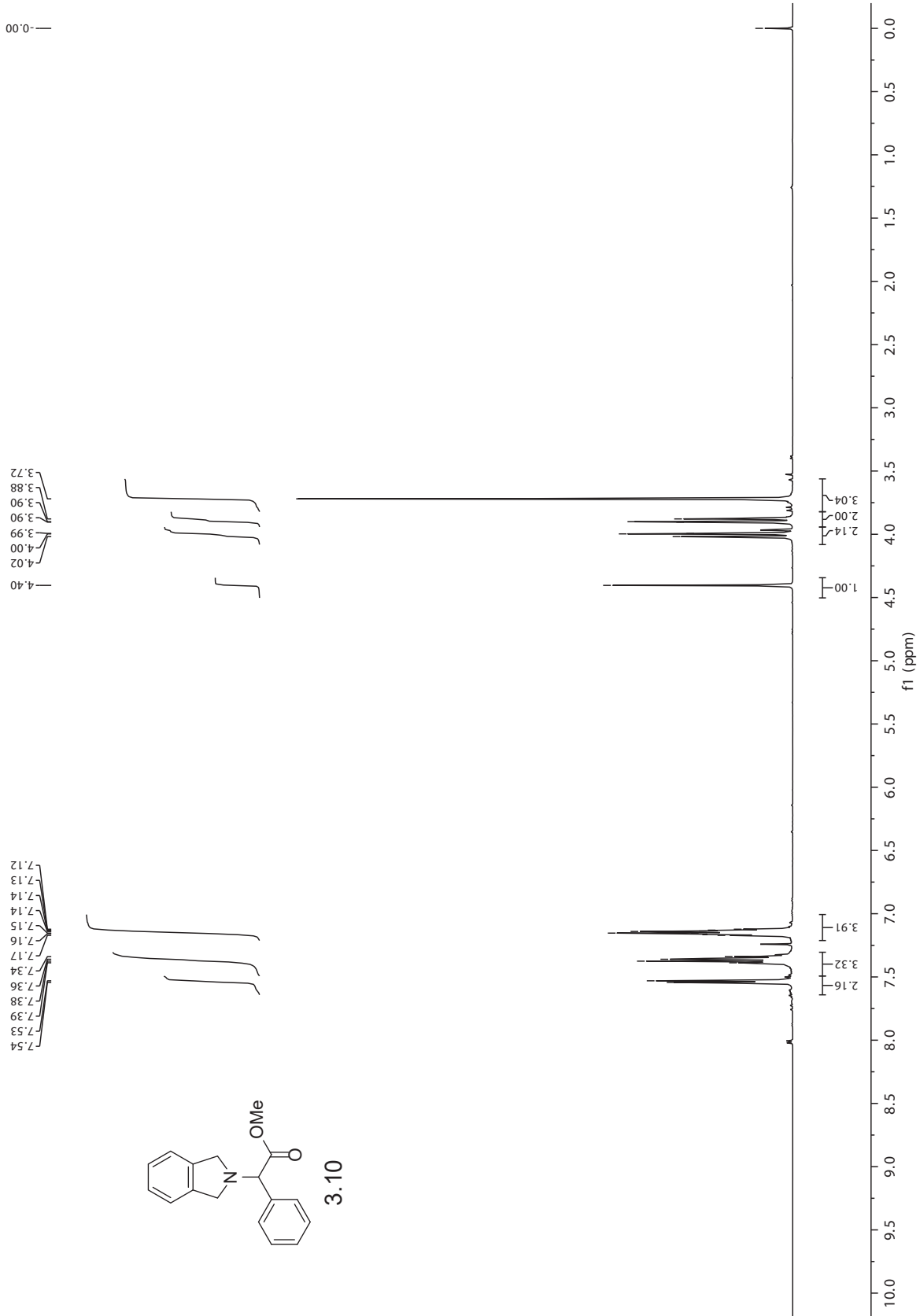


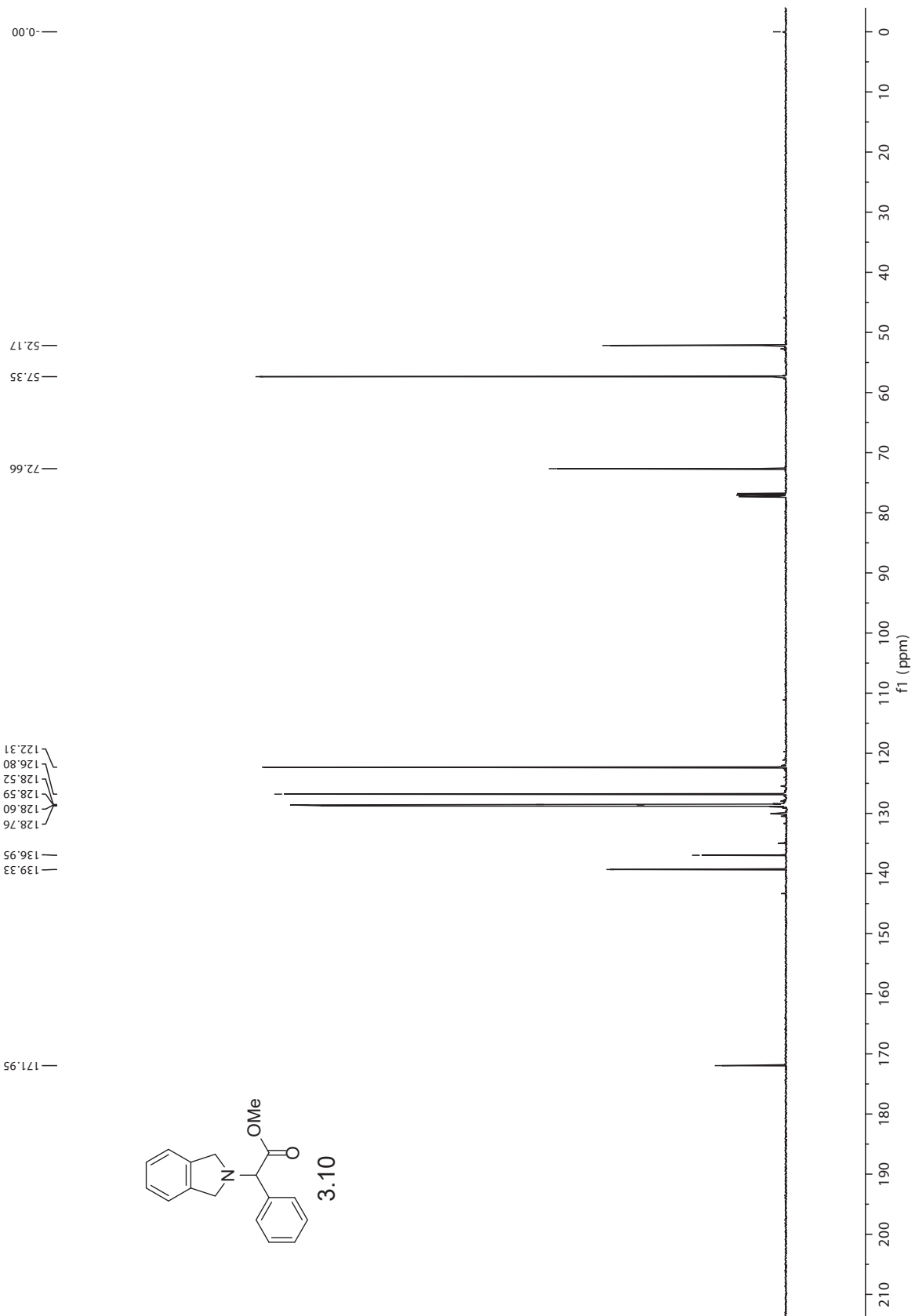


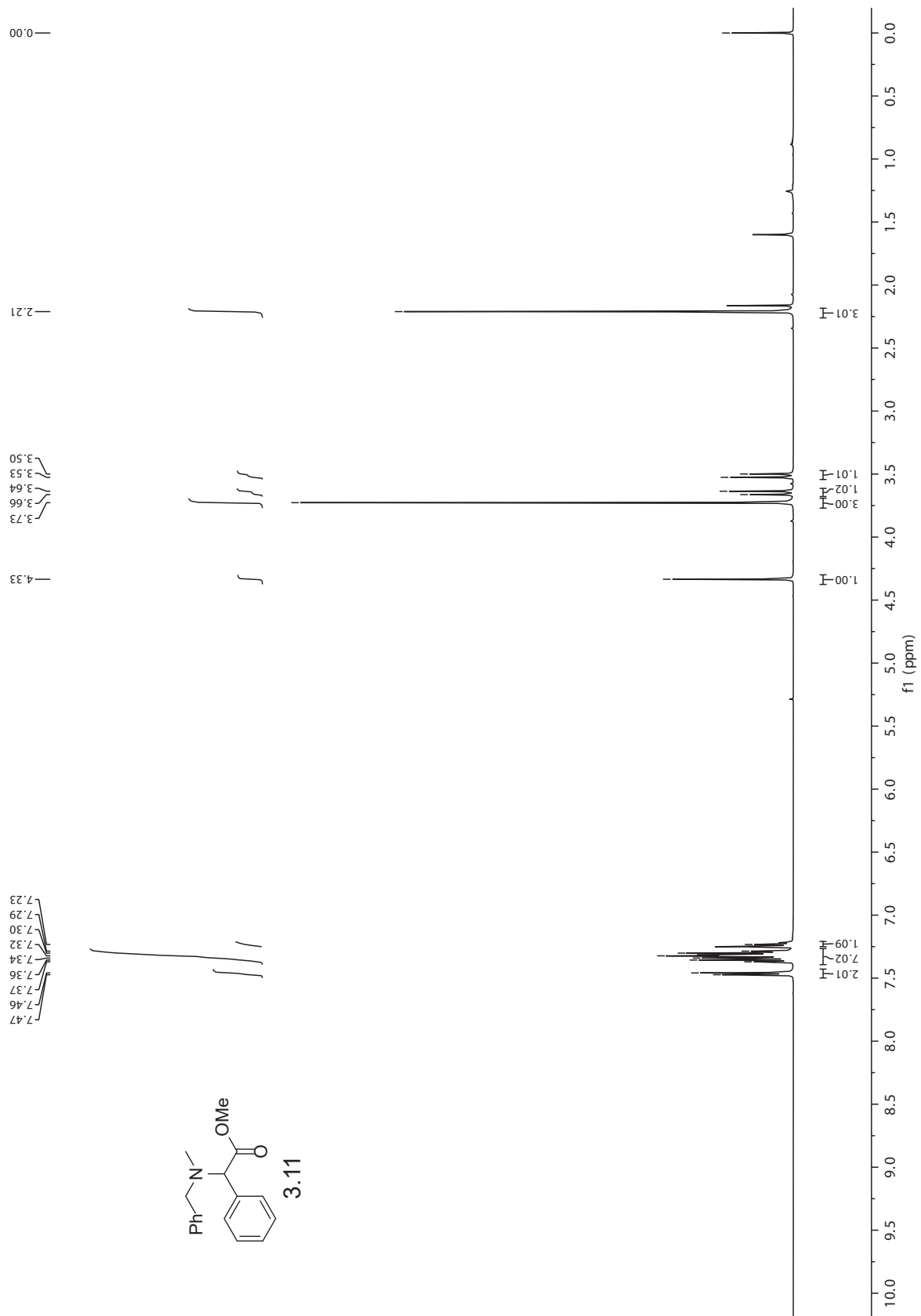


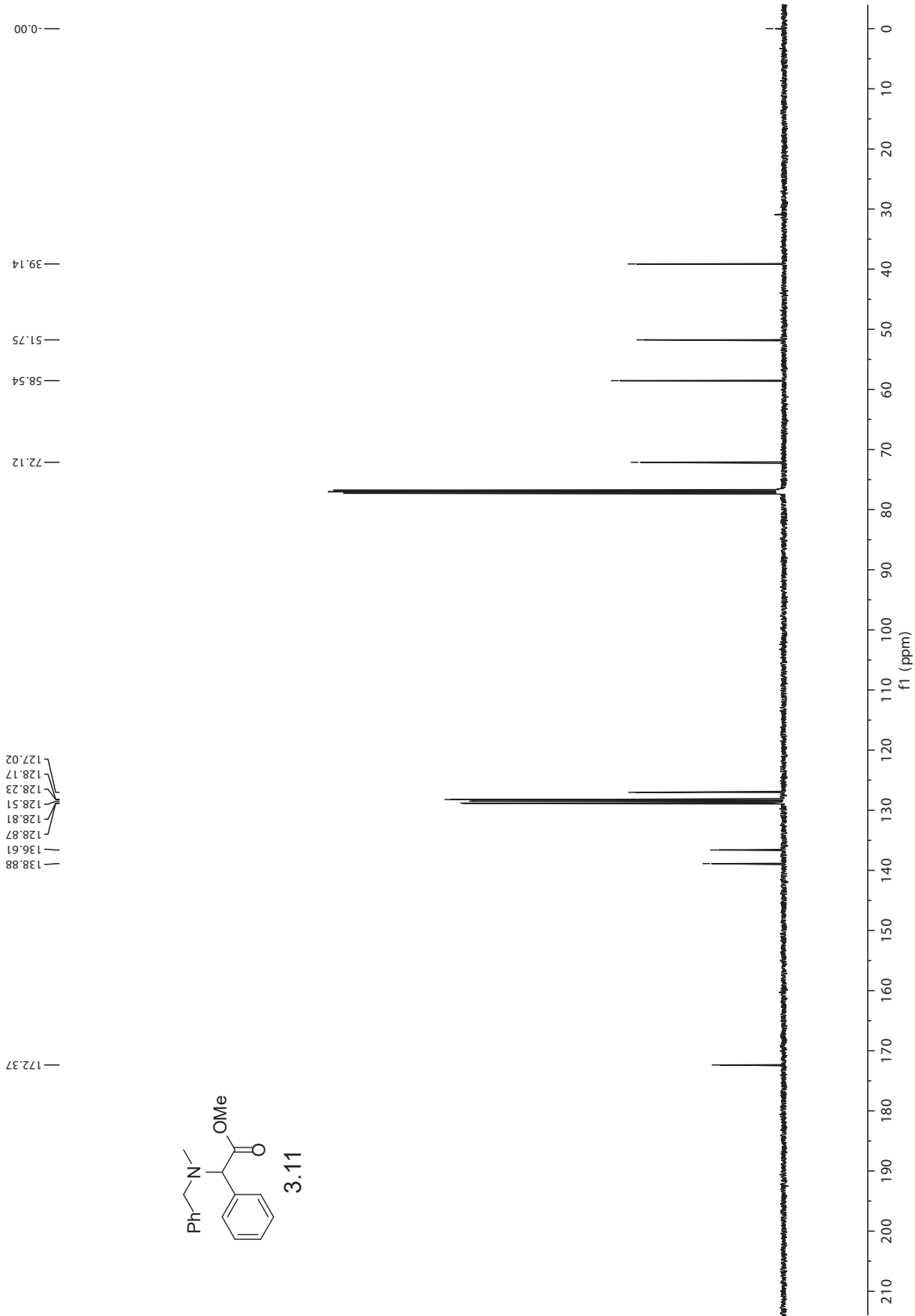
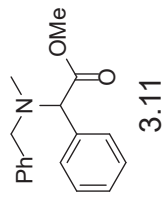
3.9

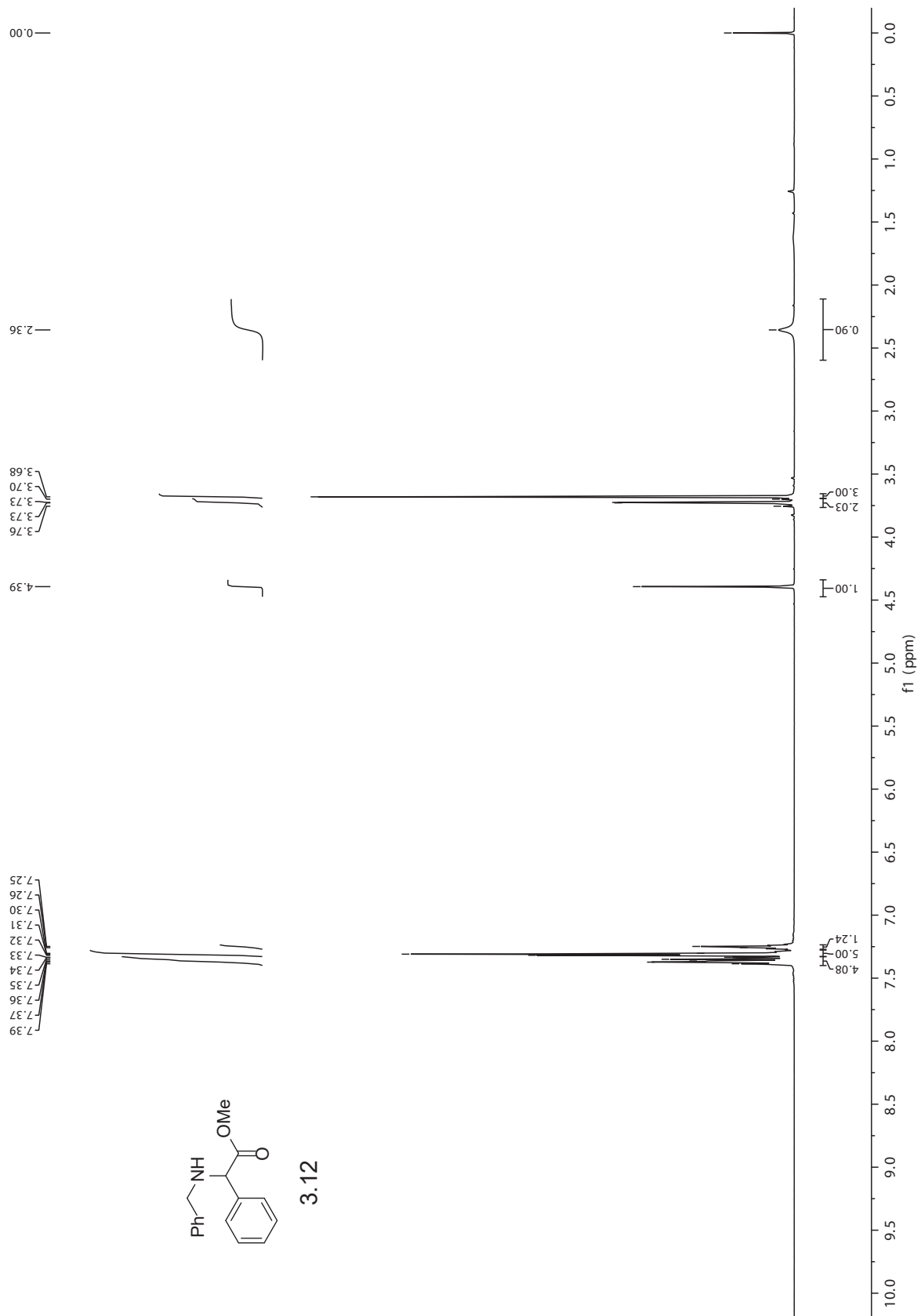


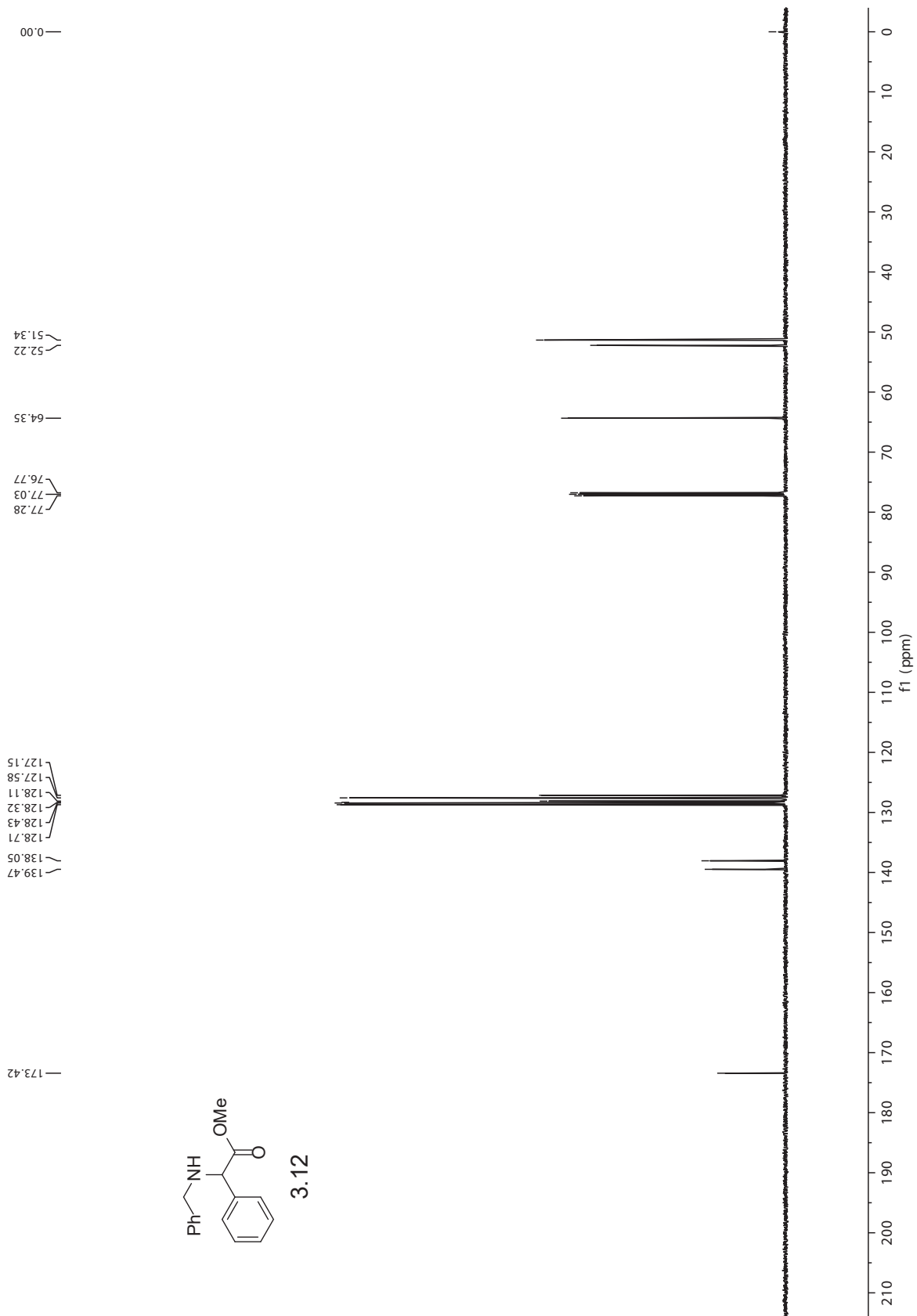
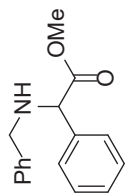


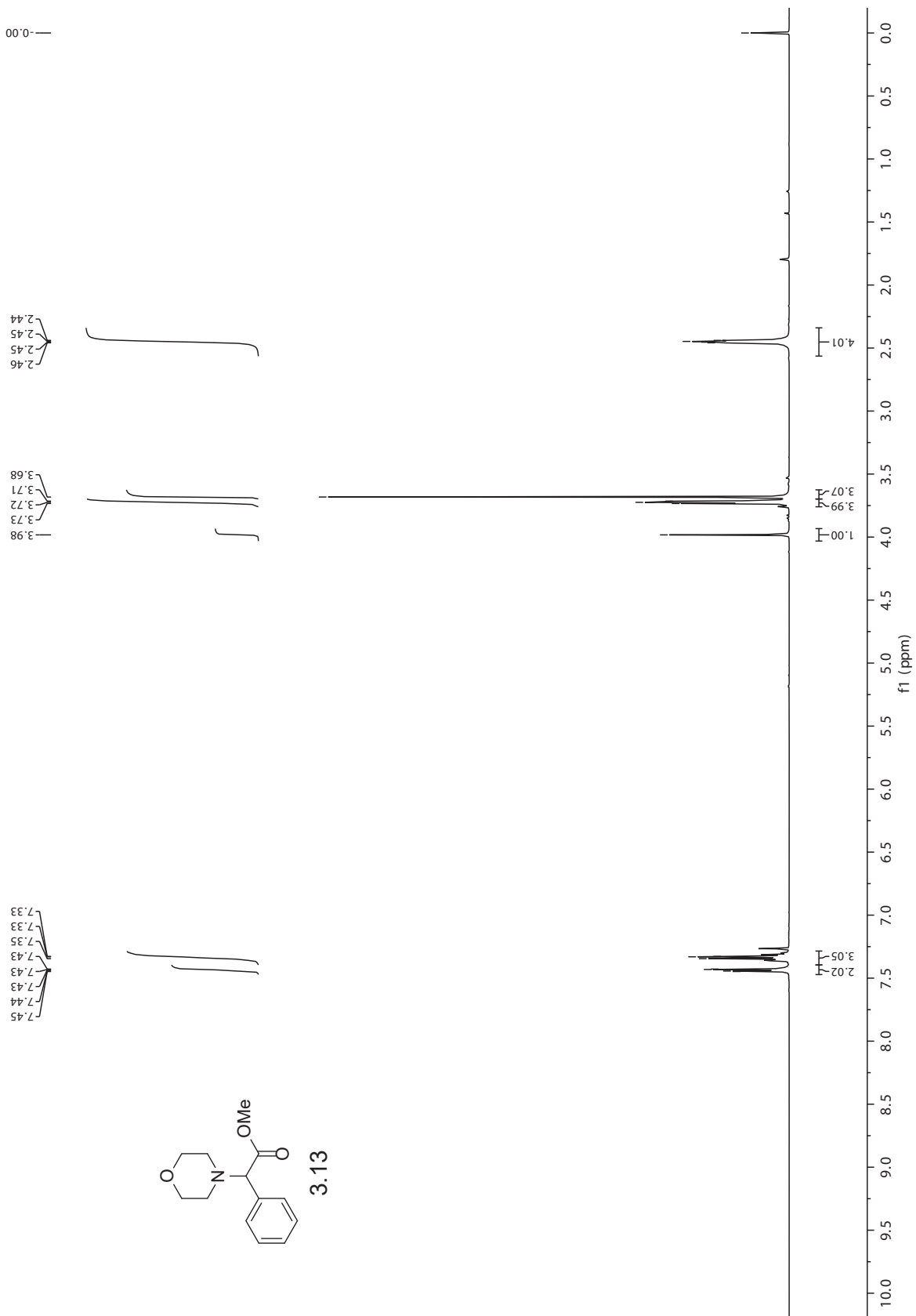


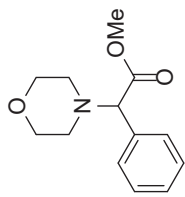




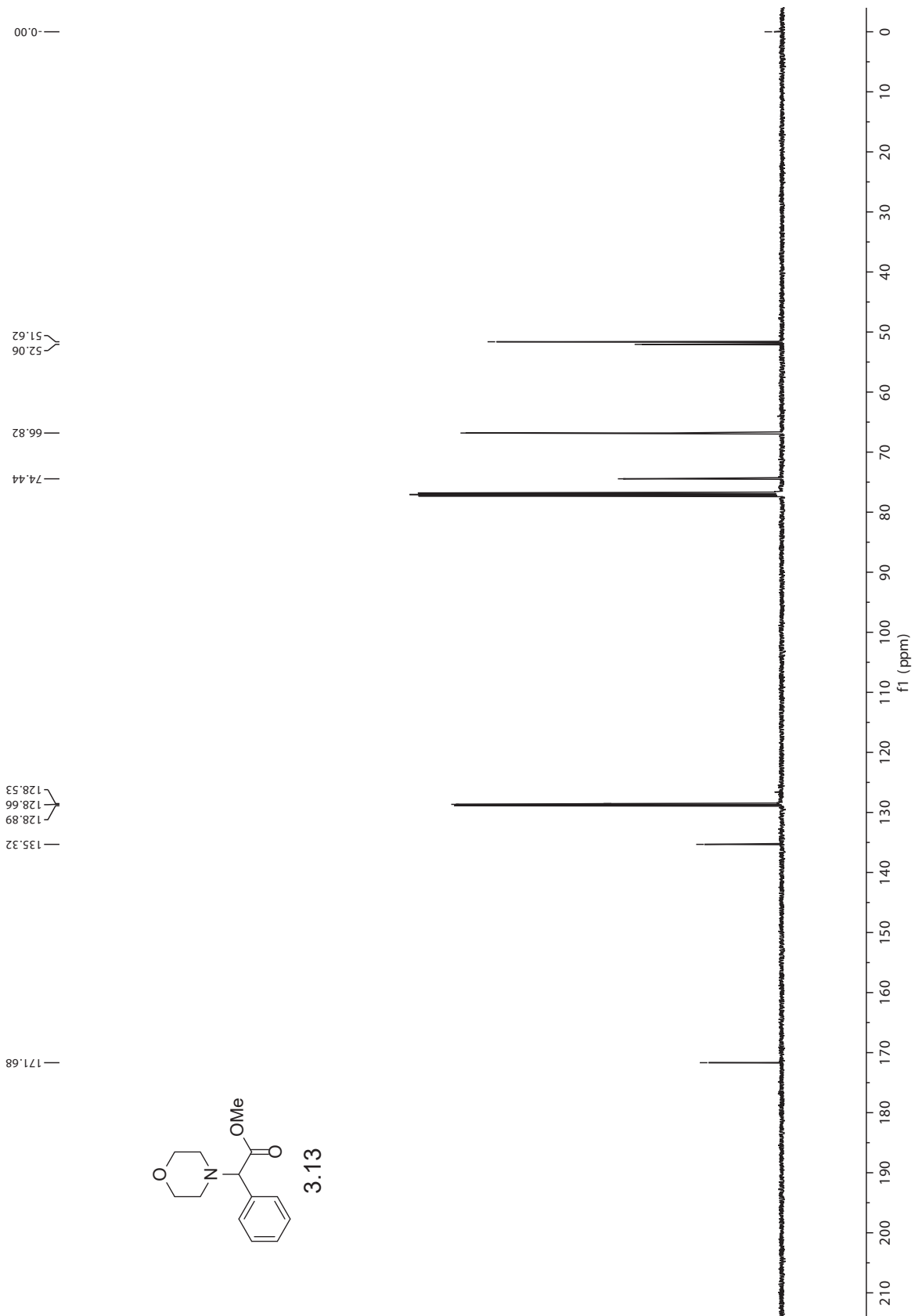


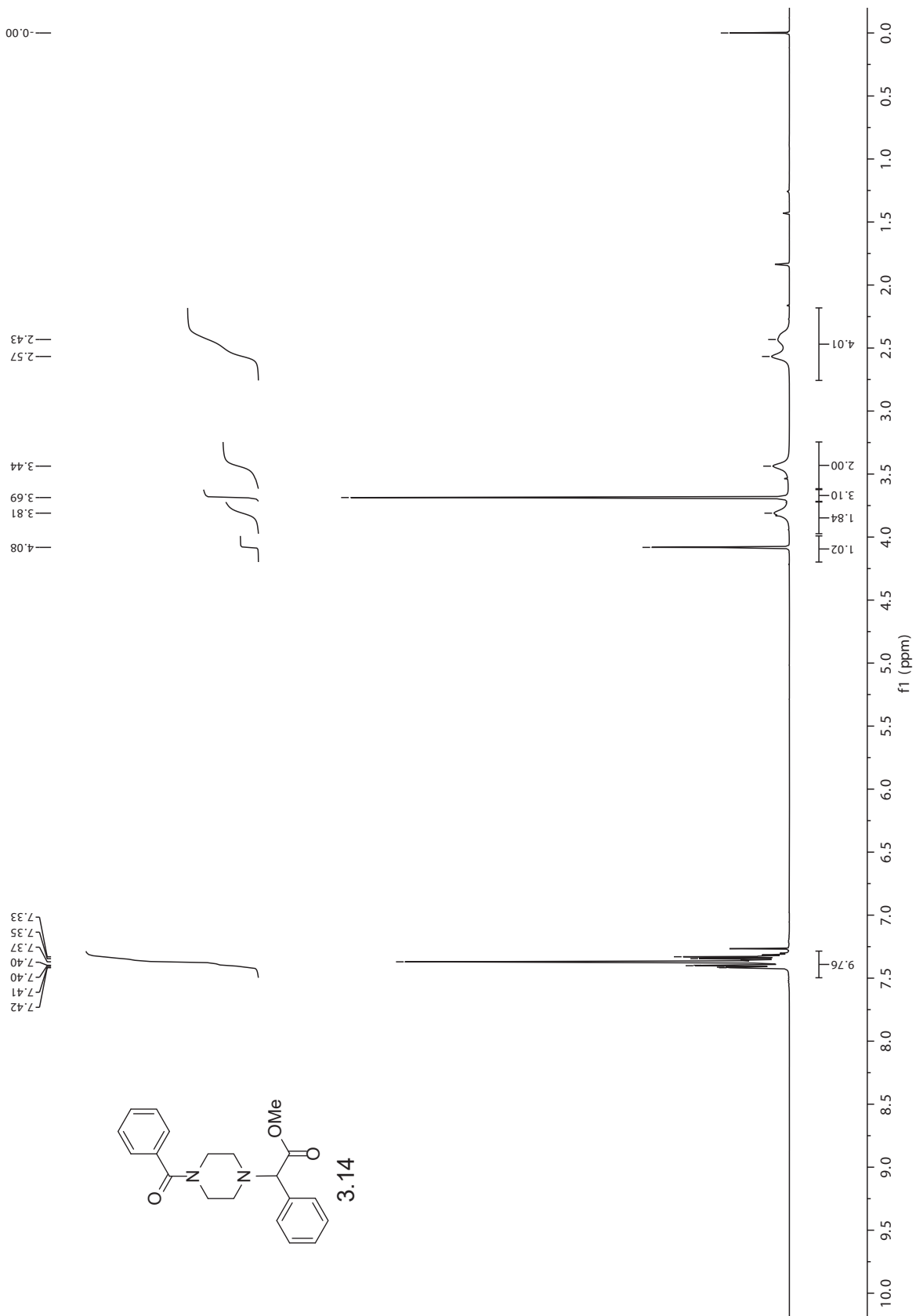


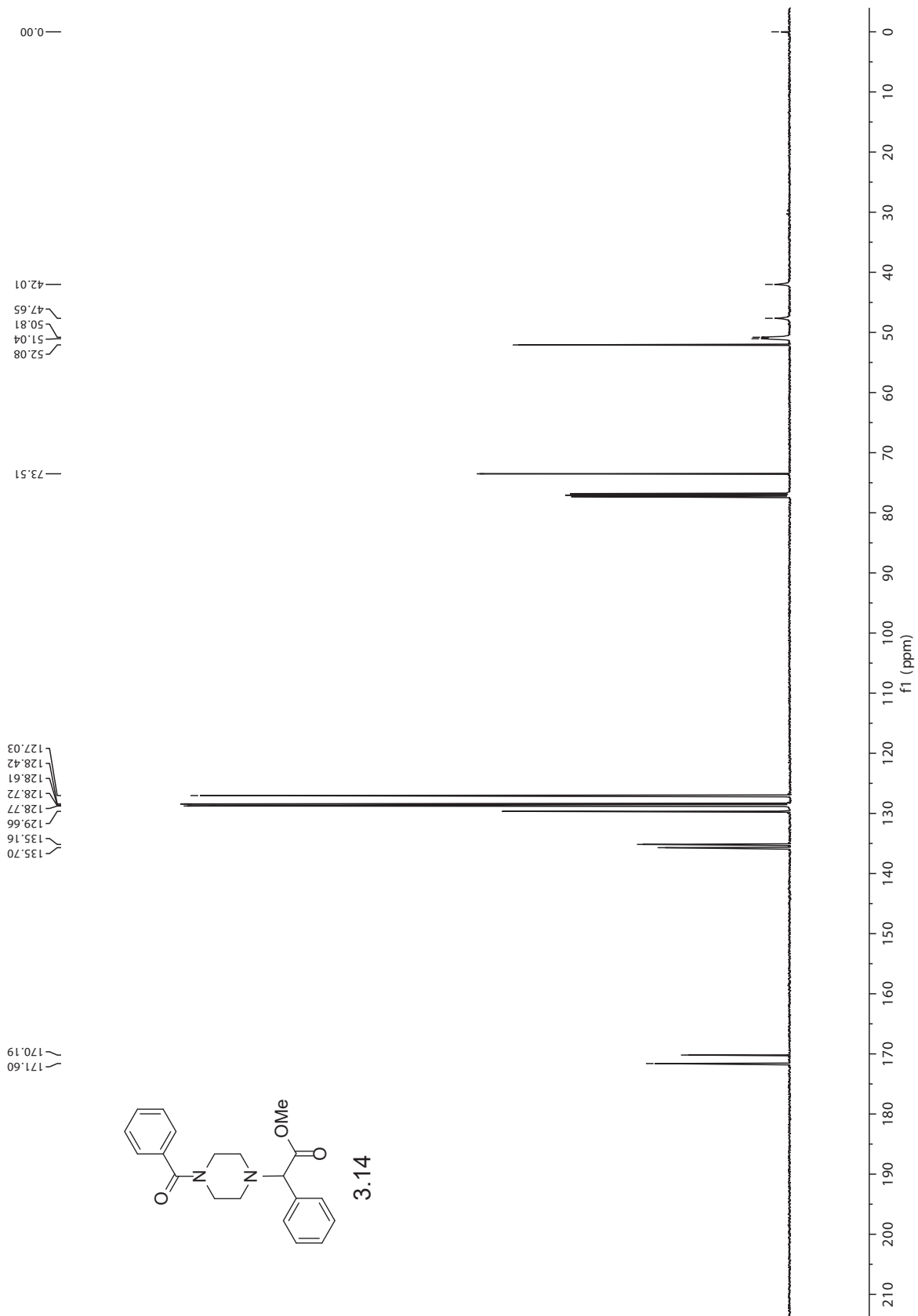


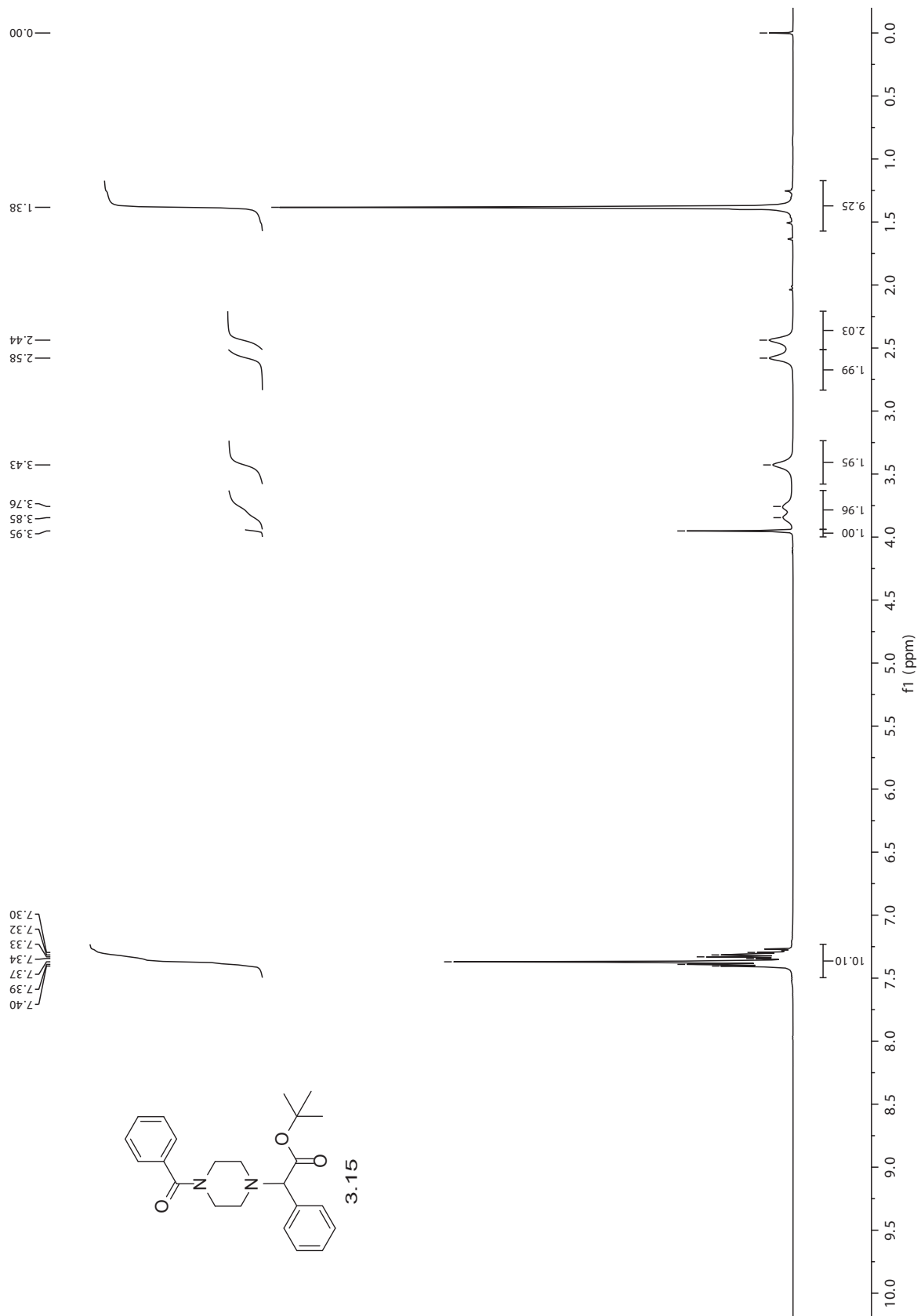


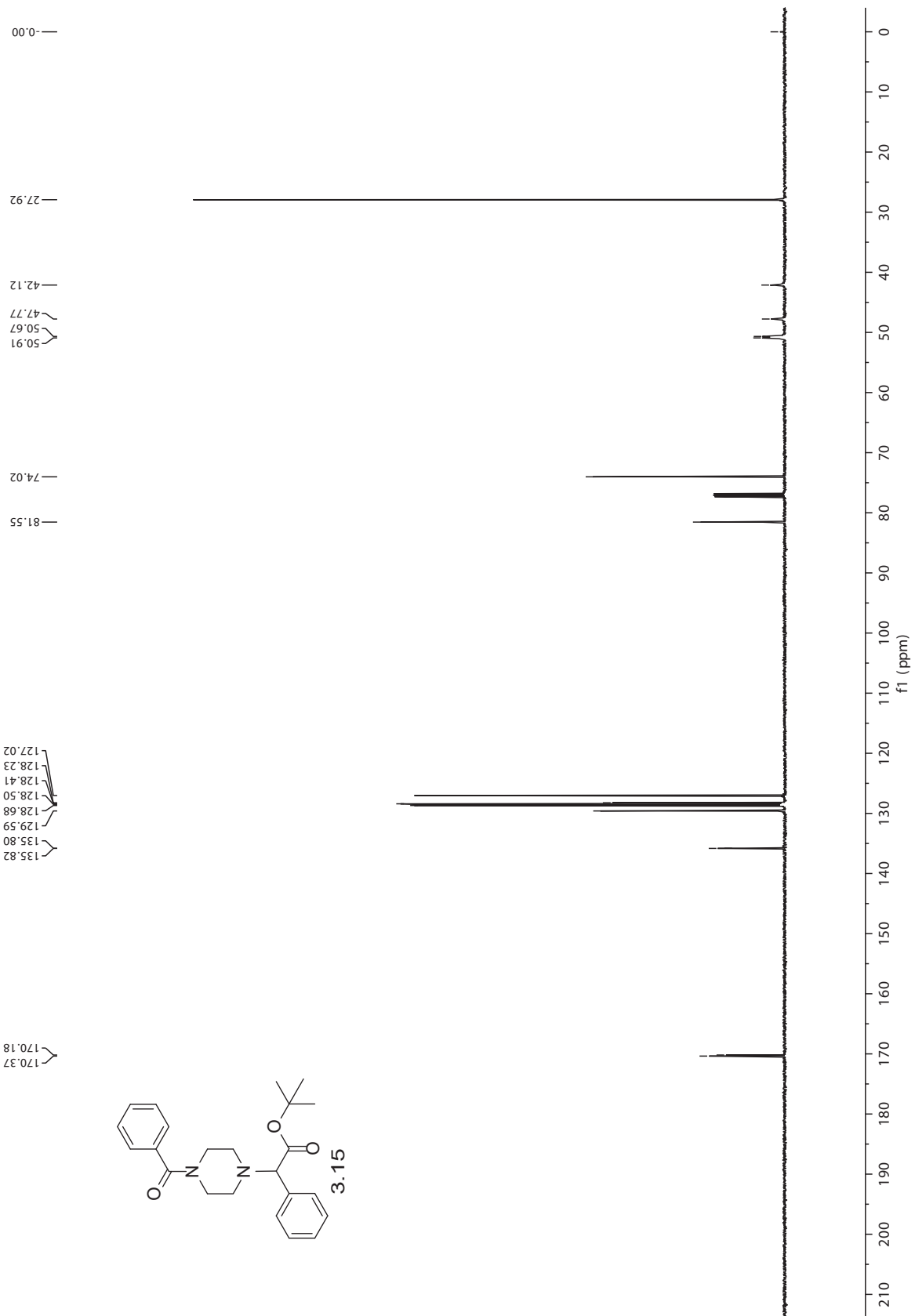
3.13

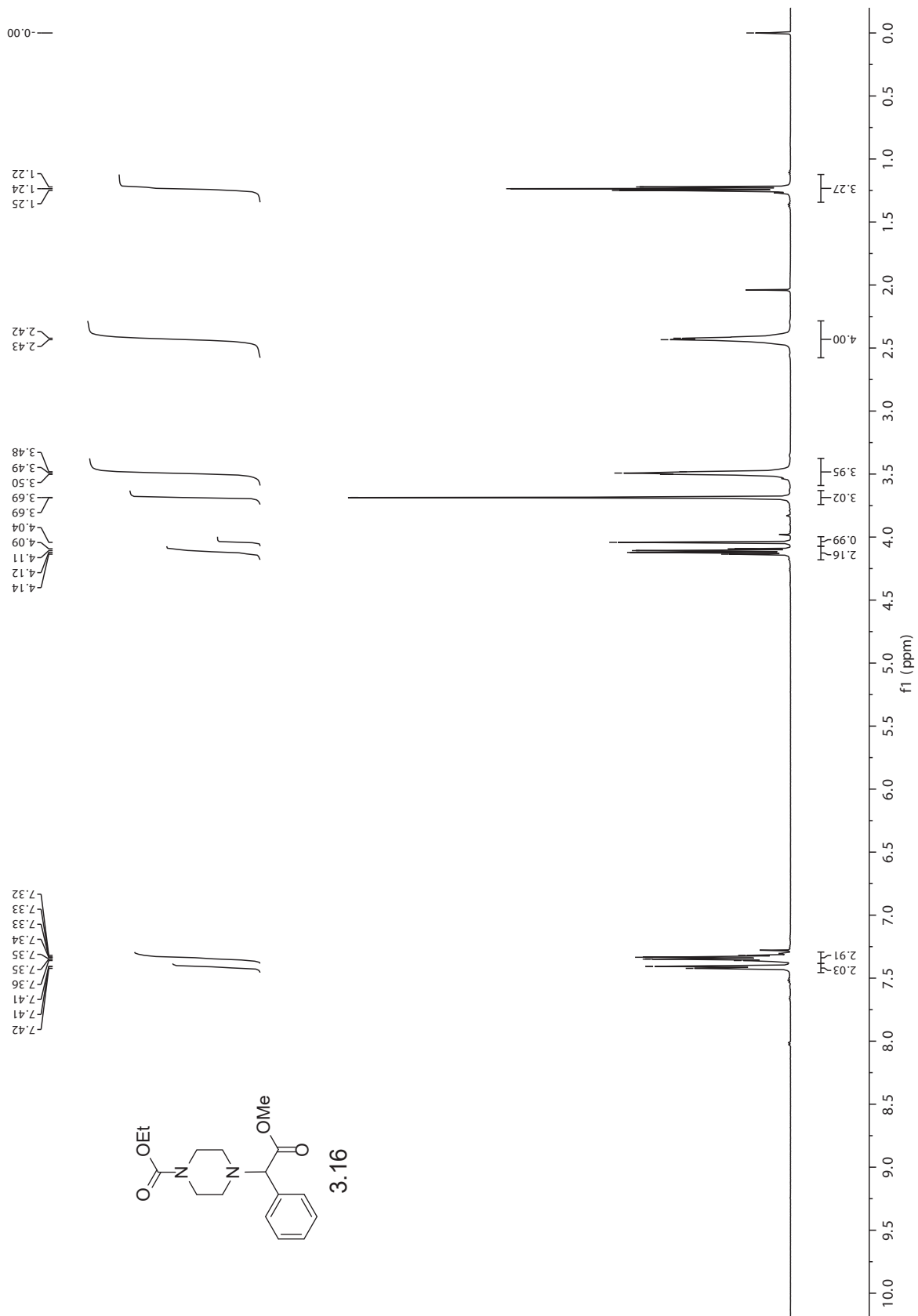


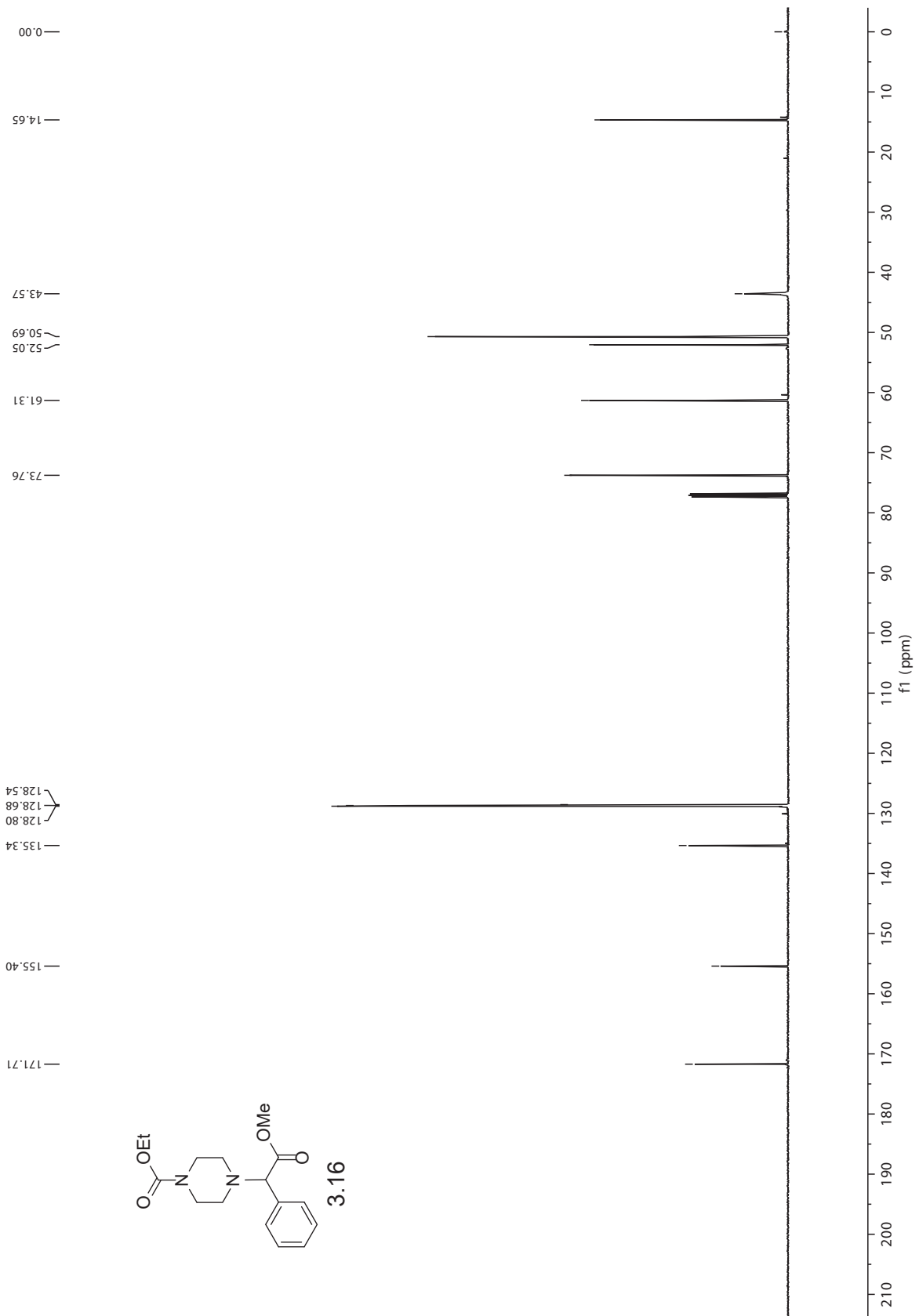


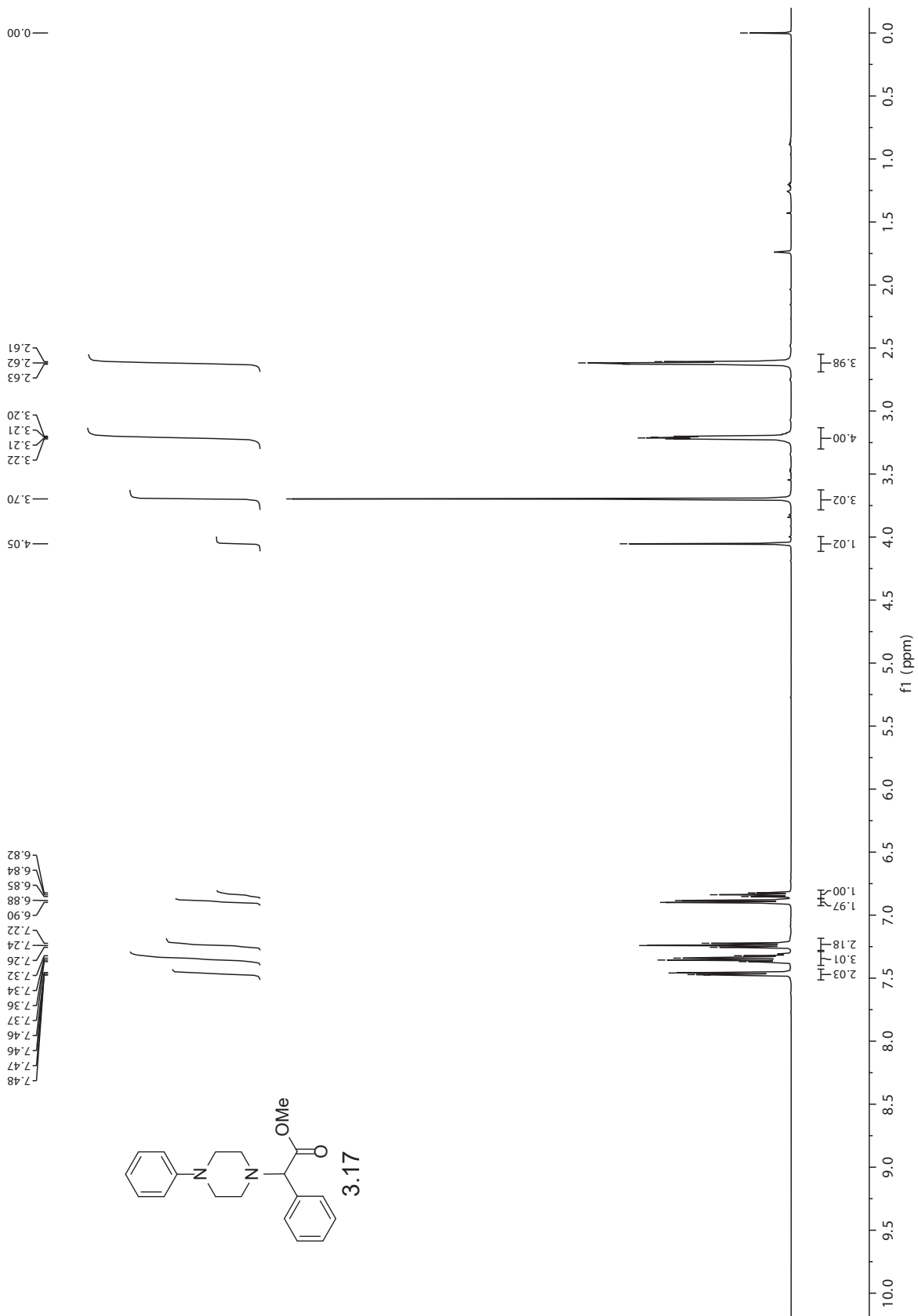


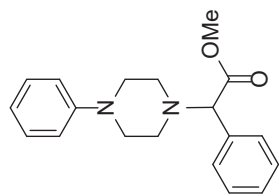




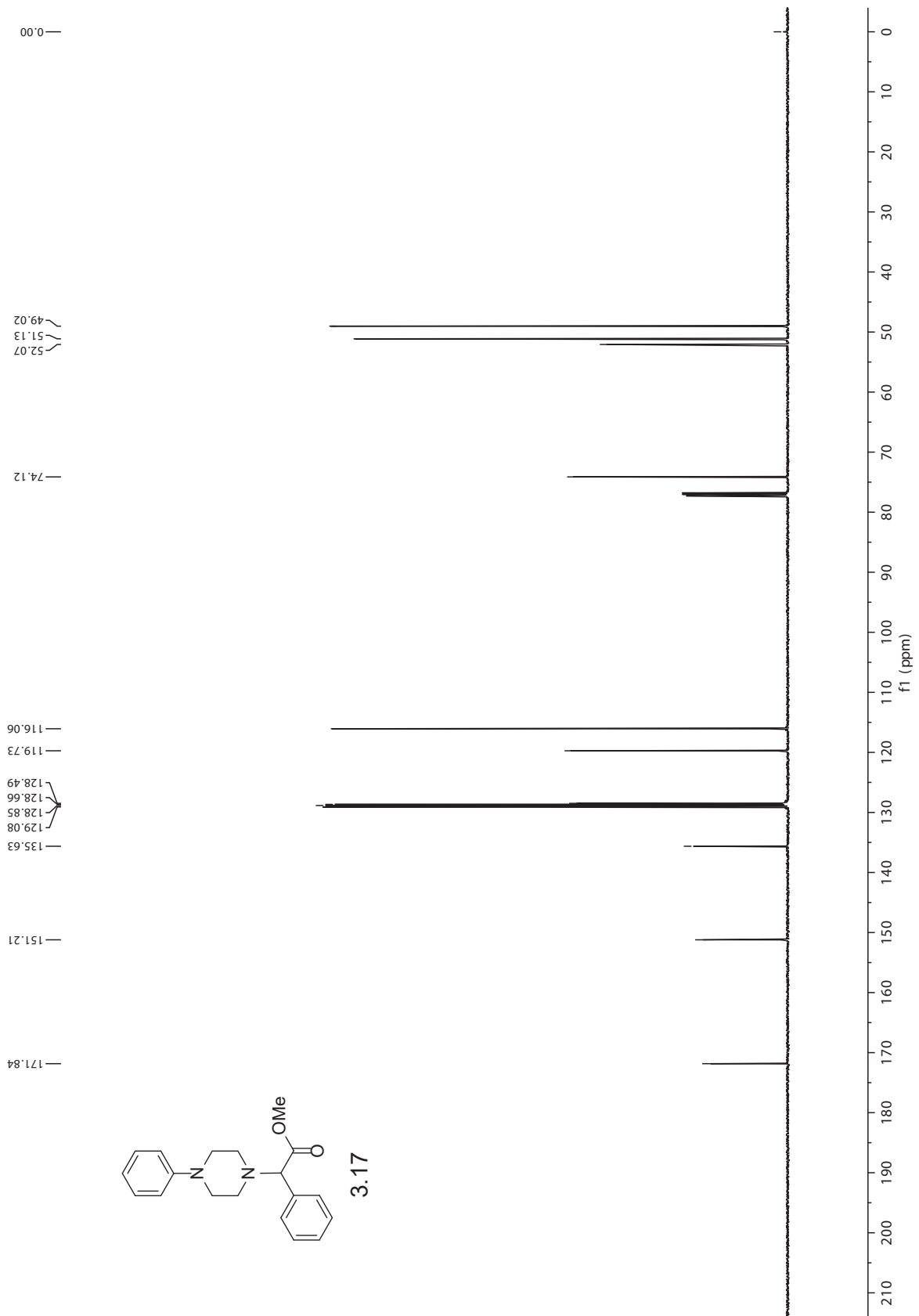


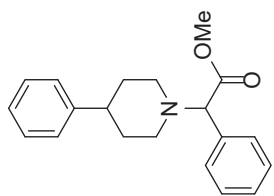






3.17





3.18

